

NASA TECHNICAL TRANSLATION

NASA TT F-15,017

STUDY ON THE PERFORMANCE OF BALL BEARINGS
AT HIGH dn VALUES

Y. Miyakawa, K. Seki, M. Yokoyama

(NASA-TT-F-15017) STUDY ON THE
PERFORMANCE OF BALL BEARINGS AT HIGH dn
VALUES (Scientific Translation Service)
170 p HC \$10.50 CSCL 131

N73-32364

G3/15 14823
Unclas

Translation of: "Koh dn chi ni okeru
gyokujikuju no seino ni kansuru ken'kyu",
National Aerospace Lab., Tokyo (Japan),
Report NAL-TR-284, May, 1972, 120 pp.



NATIONAL AERONAUTICS AND SPACE ADMINISTRATION
WASHINGTON, D.C. 20546
SEPTEMBER 1973

TABLE OF CONTENTS

CHAPTER 1. INTRODUCTION	1
CHAPTER 2. EXPERIMENTAL APPARATUS AND METHOD	3
2.1. Experimental Apparatus	3
2.2. Lubrication System	5
2.3. Lubricating Oil	7
2.4. Test Bearing	7
2.5. Experimental Method	7
CHAPTER 3. PRELIMINARY EXPERIMENT ON JET LUBRICATION	8
3.1. Oil Jet Velocity	8
3.2. Nozzle Position	10
3.3. Number of Nozzles	17
CHAPTER 4. DEEP-GROOVE BALL BEARING (#6206)	18
4.1. Introduction	18
4.2. Experimental Conditions	19
4.3. Test Bearing	19
4.4. Experimental Results	20
4.5. Bearing Temperature Rise	23
4.6. Amount of Heat Absorption by Lubricating Oil	27
4.7. Heat Exchange Efficiency of Lubricating Oil	36
4.8. Bearing Friction	41
4.9. Friction Characteristics of the High Speed Roller Bearing	42
4.10. Various Factors Affecting Friction Torque	46
4.11. Equation for Estimating the Bearing Temperature Rise	54
4.12. Allowable Limiting dn Value	61
4.13. Conclusions for Chapter 4	64
CHAPTER 5. EFFECT OF CAGE GUIDE TYPE WITH DEEP-GROOVE BALL BEARING (#6206)	67
5.1. Introduction	67
5.2. Experimental Conditions	68
5.3. Test Bearing	68
5.4. Experimental Results	69

5.5.	Allowable Limiting dn Value	72
5.6.	Bearing Temperature Rise	79
5.7.	Amount of Heat Absorption by Lubricating Oil	82
5.8.	Heat Exchange Efficiency of Lubricating Oil	88
5.9.	Bearing Friction	92
5.10.	Equation for Estimating Bearing Temperature Rise	97
5.11.	Conclusions to Chapter 5	101
CHAPTER 6.	ANGULAR CONTACT BALL BEARING (#17206)	104
6.1.	Introduction	104
6.2.	Experimental Conditions	105
6.3.	Test Bearing	105
6.4.	Experimental Results	106
6.5.	Allowable Limiting dn Value	106
6.6.	Bearing Temperature Rise	114
6.7.	Amount of Heat Absorption by Lubricating Oil	117
6.8.	Heat Exchange Efficiency of Lubricating Oil	124
6.9.	Bearing Friction	128
6.10.	Equation for Estimating Bearing Temperature Rise	131
6.11.	Conclusions for Chapter 6	134
CHAPTER 7.	ANGULAR CONTACT BALL BEARING (#30BNT)	137
7.1.	Introduction	137
7.2.	Experimental Conditions	138
7.3.	Test Bearing	138
7.4.	Experimental Results	138
7.5.	Allowable Limiting dn Value	141
7.6.	Bearing Temperature Rise	144
7.7.	Amount of Heat Absorption by Lubricating Oil	146
7.8.	Heat Exchange Efficiency of Lubricating Oil	150
7.9.	Bearing Friction	152
7.10.	Equation for Estimating Bearing Temperature Rise	154
7.11.	Conclusions for Chapter 7	157
CHAPTER 8.	SUMMARY	159

STUDY ON THE PERFORMANCE OF BALL BEARINGS
AT HIGH dn VALUES*

Yukio Miyakawa**, Katsumi Seki**, and
Masayuki Yokoyama**

CHAPTER 1. INTRODUCTION

Roller bearings are being used increasingly in high speed rotating machines such as gas turbines and superchargers. Wear and failure of roller bearings have become a very serious problem. The dn value (d is bore diameter of the bearing in mm, and n is shaft speed in rpm), which is commonly used as a criterion for the limiting speed of the roller bearing, is a comparative value of the peripheral speed of the roller bearing, and should be considered as a variation of the pV value (p is average bearing pressure, and V is the peripheral speed), which indicates the severity of the sliding friction portions inside the roller bearing [1]. Since the pV value of the slider bearing is affected by the method of lubrication, the dn value is also greatly affected by the lubrication method. Consequently, it is difficult to uniformly prescribe the limiting dn value for the lubrication /2***

* Received on March 4, 1972.

** Space Research Group.

*** Numbers in the margin indicate pagination in the original foreign text.

method which encompasses a broad range of techniques, such as forced lubrication and jet lubrication. Currently, used high dn values are in the neighborhood of 200×10^4 . In the near future, dn values of 300×10^4 or more will be required. The limiting dn value indicated by the bearing manufacturers is only an average value based on past experience for normal usage, and there is absolutely no fundamental reason why any roller bearing cannot be used at a higher dn value. In a series of high speed roller bearing experiments conducted at NACA [2], the temperature rise and failure limit under the same dn value widely fluctuated, depending on the lubrication conditions.

There are two factors limiting the speed of the roller bearing. One is the limit on lubrication: in other words, the limit imposed by the wear and failure upon piercing of the lubricant film. The other is the limit on the strength brought about by the shortening of bearing life by a centrifugal load of the roller body and the mechanical strength of the cage. With ever increasing roller bearing speeds, a clarification of this limiting speed becomes quite important from the application viewpoint.

Our study was conducted to clarify the limiting speed of ball bearings with jet lubrication and the various performance characteristics, such as the bearing temperature rise and friction torque. The bearing used in this experiment has a 30-mm inside diameter. Three kinds were used — deep-groove ball bearing (#6206) and angular contact ball bearings [#17206 (current number of #7206C) and #30BNT)]. The deep-groove ball bearing (#6206) is generally used for high speed applications. The angular contact ball bearing (#17206) is also widely used for high speed spindles in manufacturing machinery. The angular contact ball bearing (#30BNT) has the best performance expectations at high speeds.

In this paper, Chapter 2 discusses the high speed roller bearing test apparatus and an experimental method for performing experiments up to the dn value of 300×10^4 . Chapter 3 discusses a preliminary

experiment performed to determine the optimal condition for the nozzle position and oil jet velocity for jet lubrication. Next, the effect of cage guide type on the limiting dn value and the bearing performance at high dn values is investigated, for deep-groove ball bearing (#6206) equipped with an outer-race-riding cage (Chapter 4) and deep-groove ball bearing (#6206) equipped with an inner-race-riding cage (Chapter 5). The limiting dn value and the bearing performance are studied for angular contact ball bearing (#17206) in Chapter 6. The angular contact ball bearing (#30BNT) is discussed in Chapter 7. The results are compared with those of deep-groove ball bearing (#6206). Chapter 8 is the summary. As a result, it became clear that the wear and failure of high speed roller bearings always occurred at the sliding friction portion of the cage, and the problem of lubrication around the cage is the factor which determines the limiting dn value of roller bearings today. Consequently, it also became clear that the guide type, configuration, material, etc., of the cage has an extremely large influence on the limiting dn value and the bearing performance, and that certain considerations on the cage and the lubrication method should be made to raise the limiting dn value of the bearing. The angular contact ball bearing (#30BNT) has the best performance at high speeds, showing quite safe operation with no bearing failure at the dn value of 300×10^4 , and the peripheral speed of 157 m/s. Further, in the process of reaching the limiting speed, the way in which the bearing performance characteristics — such as the bearing outer race temperature rise and friction torque — are affected by such factors as speed, load, and oil flow, is studied and quantified.

CHAPTER 2. EXPERIMENTAL APPARATUS AND METHOD

2.1. Experimental Apparatus

The structure of a high speed roller bearing test equipment is shown in Figure 1. Figure 2 shows its exterior view. In order to study the roller bearing performance and its limiting speed at high dn values, bearing test equipment was made with the following

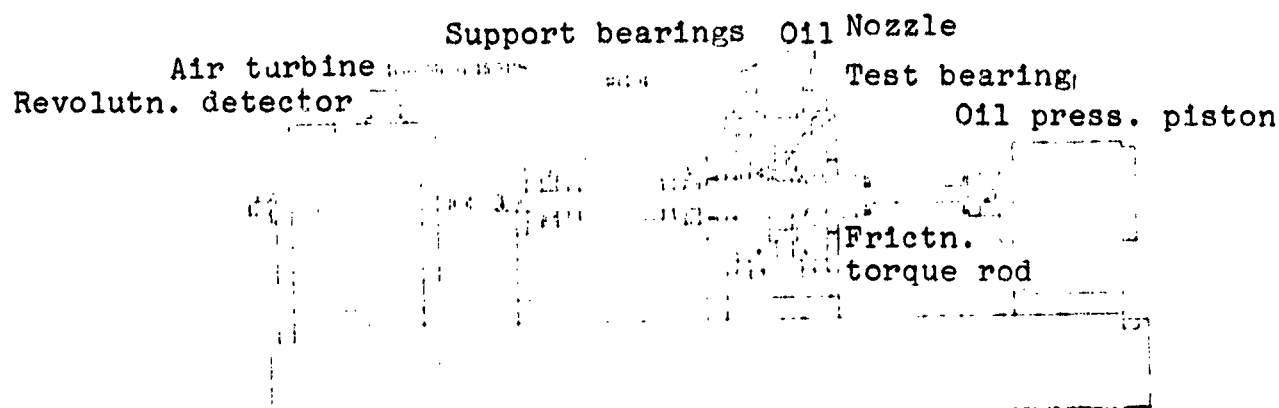


Figure 1. High speed roller bearing test equipment

considerations. A ball bearing with 30 mm inside diameter is used as a test bearing. To drive the test equipment, an air turbine with a maximum speed of 100,000 rpm and an output of 1.5 PS was made, so experiments with μ values of up to 300×10^4 are possible.

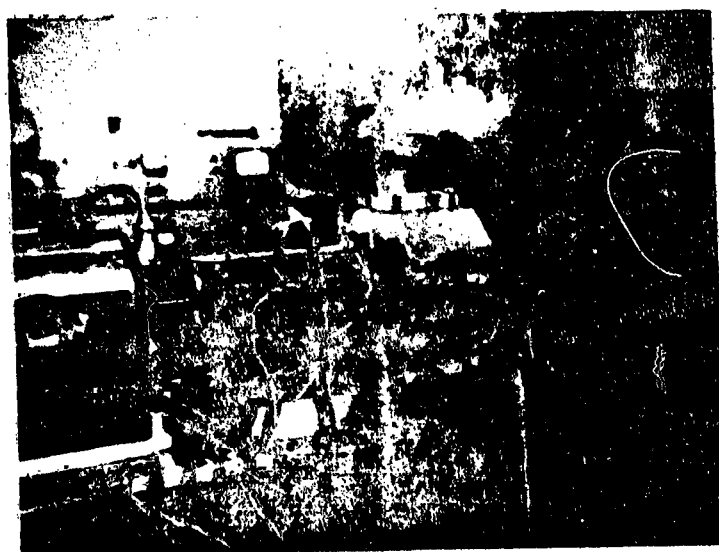


Figure 2. Exterior view of the test equipment

In the study of high speed roller bearings up to now, measurements of the bearing temperature rise were performed due to its ease. Measurements of friction torque often were not performed. As friction heat generated in the bearing is the cause of bearing temperature rise, it is necessary to correctly measure the friction simultaneously with the bearing temperature in order to examine the performance of high speed roller bearings. For this purpose, a 30-mm inside diameter test bearing is mounted on the

right edge of the shaft supported by the two support bearings (#6204) as shown in Figure 1. A thrust load is applied on the test bearing housing by an oil pressure piston on the right side. Since the test bearing housing is supported by a test bearing only, the outer-race friction torque of the test bearing can be derived from this torque. The housing torque is measured by continuously recording the changes which result when the spring-board covered with strain gages contacts a friction rod coming out of an oil pressure piston. In mounting the test bearing, the leading edge of the dial gage fixed on the shaft contacts the outer race face, while the thrust load from an oil pressure piston is maintained at 50 kg. The tilt of an outer-race is maintained at less than 2/100 mm.

The test shaft is driven by a 6 mm diameter drill rod inserted into an air turbine shaft. It is set up such that — when bearing failure takes place and the friction torque rapidly increases — a narrow portion of the rod between the air turbine and the test shaft will be cut off. Various couplings have been tried, but at high speeds this method was the best. There was no trouble at 100,000 rpm, either. All other methods resulted in large vibrations at high speeds. The shaft speed is measured by a pulse revolution-indicator using an electromagnetic revolution detector. /4

The temperature of the test bearing is recorded by a self-balancing thermometer which used a chromel-alumel thermocouple in contact with the bearing outer race.

2.2. Lubrication System

The air turbine, the support bearings, and the test bearing are each lubricated by an independent lubrication system. The oil supply is a jet oil supply in all cases. Figure 3 shows the lubrication system of the test bearing. Oil delivered by an oil supply pump flows through an oil filter, an oil cooler, a flow volume meter, an oil heater, and is fed to the test bearing. The oil flow is adjusted by the flow control valve. The inlet oil temperature of the test bearing can be maintained at any constant temperature by an oil

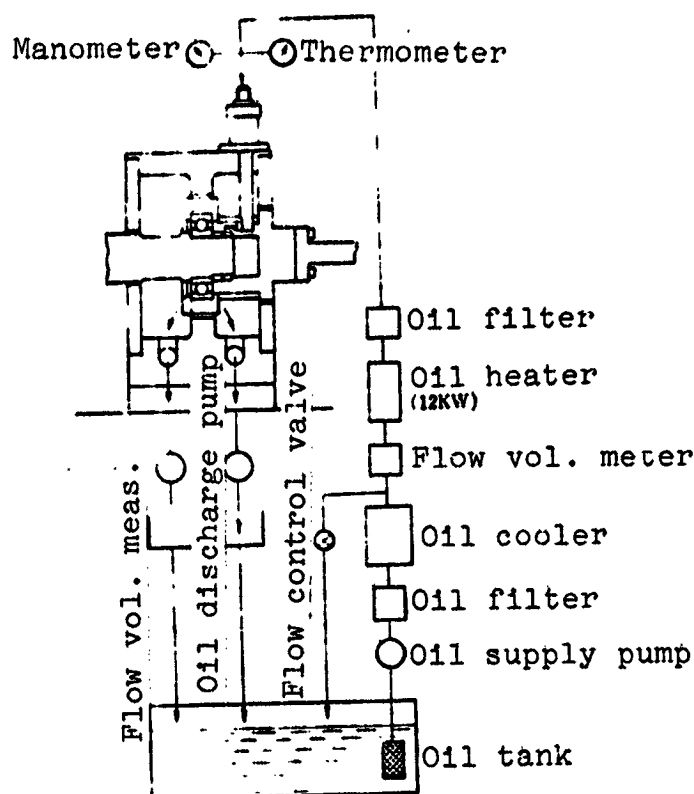


Figure 3. Lubrication system of the test bearing

cooler and an oil heater. Oil in the bearing is discharged by an oil discharge pump from the nozzle side, as well as from the transmission side. The discharged oil is measured on its way to an oil tank. The inlet oil temperature is measured at the nozzle inlet, while the outlet oil temperature at the nozzle side as well as at the transmitted side is measured near the bearing outer-race face of the housing using a chromel-alumel thermocouple. The bearing outer-race temperature is also recorded.

The lubrication systems for the air turbine and the support bearings also consist of a similar setup, except the oil heater is omitted, as there is no need to maintain constant inlet oil temperature.

In regard to the conditions of jet oil supply for the test bearing, the optimal conditions of jet velocity and the number of nozzles

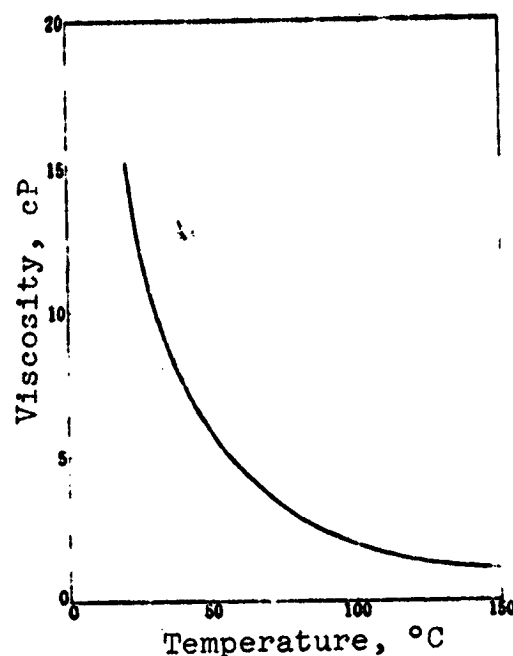


Figure 4. Viscosity-temperature curve of lubricating oil

are determined from a preliminary test, the details of which will be mentioned in the next chapter.

2.3 Lubricating Oil

The lubricating oil used is MIL-O-6081, 1010 class Esso turbo oil 10. The relation between its viscosity and temperature is shown in Figure 4.

2.4. Test Bearing

The test bearings used in this experiment are SP-class ball bearings #6026, #17206, and #30BNT. Their dimensions and other details will be mentioned in their respective chapters.

/5

2.5. Experimental Method

The bearing load is a thrust load only and, unless explicitly specified, it is constant at 50 kg. The inlet oil temperature is also maintained constant at 30° C, unless explicitly specified. In a normal experiment, the oil flow rate is varied from 0.22 to 3 kg/min, while thrust load and inlet oil temperature are kept constant at 50 kg and 30° C, respectively, and the bearing outer race temperature, outlet oil temperature, friction torque, and penetration ratio for each oil flow are measured as the speed is increased up to the allowable limit. In order to investigate the effects of thrust load and oil viscosity, thrust load and oil inlet temperature are varied from 25 kg to 200 kg and from 30° C to 90 - 120° C, respectively, and the experiments are conducted.

CHAPTER 3. PRELIMINARY EXPERIMENT ON JET LUBRICATION

As the oil jet velocity, the nozzle position, and the number of nozzles greatly affect the high speed performance of the bearing, with jet lubrication, the following preparatory experiment was conducted to determine the optimal condition.

3.1. Oil Jet Velocity

The slider bearing is a kind of viscous pump and produces an oil flow which is at least proportional to the velocity. It passes through the inside of the bearing. The roller bearing does not have this kind of an automatic pump action. Furthermore, at high speed, the roller bearing churns the surrounding air, causing wind pressure and rejecting the forced oil supply from the outside. Therefore, for high speed roller bearings, a special jet lubrication method of feeding oil into the bearing by oil jets at high velocity from the nozzle is used. If the oil jet velocity is low, oil will have difficulty getting into the bearing. Thus, for each oil flow, the jet velocity is changed by changing the nozzle bore diameter, and then the bearing performance is studied.

Figure 5 shows the relationship between jet velocity and temperature rise $T_B - T_I$ from the inlet oil temperature T_I (30°C constant) to the bearing outer-race temperature T_B and penetration ratio K , which is the ratio of oil flow transmitted through the bearing to the total oil flow, for oil flows of 0.22, 0.44, 0.72, and 1 kg/min. For the same oil flow rate, as the jet velocity increases, the bearing outer-race temperature rise rapidly decreases initially. Its percentage decrease becomes smaller above the jet velocity of 10 m/s, and then it becomes nearly constant above 20 m/s. This phenomenon is more pronounced when the oil flow is small. The penetration ratio increases with an increasing jet velocity for each oil flow. In contrast to the change in the bearing temperature rise, the penetration ratio rapidly increases initially with an increasing jet velocity,

but its percentage increase goes down and has a trend of becoming constant at about 10 m/s.

The above results indicate that as jet velocity increases, oil tends to penetrate into the bearing. The cooling action of the oil increases, and the bearing temperature rise decreases. Figure 6 shows the relation between heat absorption by oil (expressed in horsepower) obtained from the outlet oil temperature rise and jet velocity for each oil flow. With an increase in jet velocity, the horsepower absorption by oil rapidly increases, but its percentage increase becomes gradual in the neighborhood of 10 m/s jet velocity, and above 20 m/s it is nearly constant. The fact that the relations among jet velocity, bearing outer race temperature rise, and horsepower absorption by oil appear completely contradictory indicates that, when a large amount of oil is forcefully supplied as in jet lubrication, most of the oil acts as a coolant, and the greater the jet velocity, the greater the heat exchange efficiency of oil becomes.

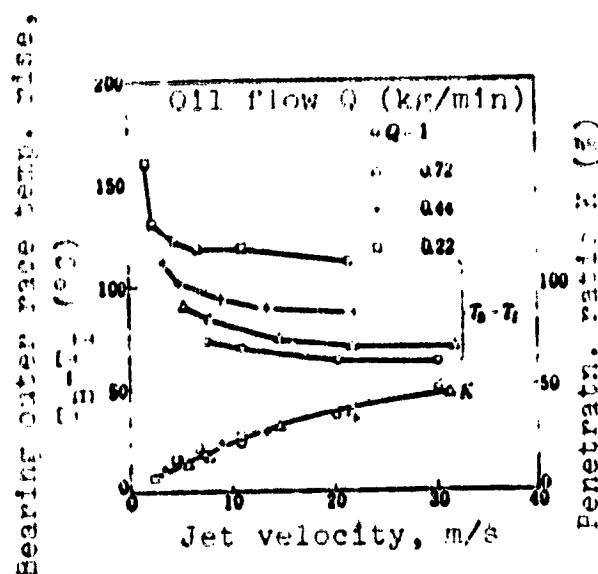


Figure 5. Bearing outer race temperature rise and penetration ratio versus jet velocity:

test bearing: #6206 (outer race-riding cage)
shaft speed: 60,000 rpm
thrust load: 50 kg
inlet oil temperature: 30° C

/6

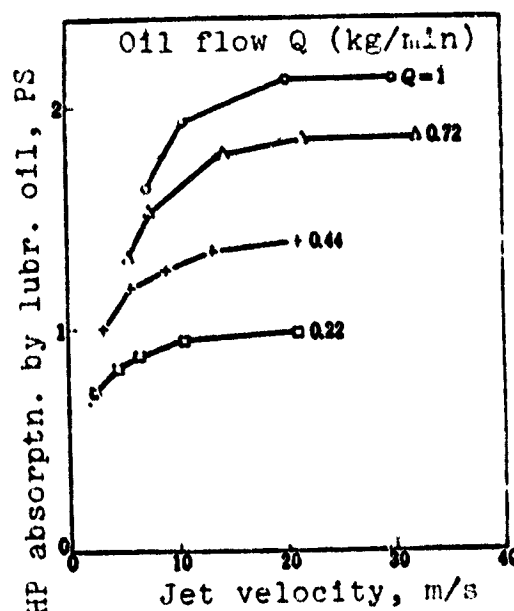


Figure 6. Horsepower absorption by lubricating oil and jet velocity:

test bearing: #6206 (outer-race-riding cage)
shaft speed: 60,000 rpm
thrust load: 50 kg
inlet oil temperature: 30° C

When the jet velocity is below 10 m/s, oil has difficulty getting inside the bearing at high speed and cooling by oil becomes insufficient. Consequently, the jet velocity should be at least above 10 m/s. However, as jet velocity increases, oil pressure at the nozzle correspondingly increases; thus, roughly 20 m/s is most appropriate for practical applications. Even when jet velocity is increased above this value, only the oil pressure at the nozzle significantly increases, and the corresponding benefits are small. If the jet velocity is set at 20 m/s, then at an inlet oil temperature of 30° C, the oil pressure at the nozzle inlet becomes about 4.5 kg/cm². In this experiment, the jet velocity is fixed at about 20 m/s at any oil flow rate, and the nozzle bore diameter is varied depending on oil flow, as shown in Table 1.

TABLE 1. AMOUNT OF SUPPLIED OIL AND NOZZLE DIAMETER

Amount of oil supplied (kg/min)	Nozzle diameter (mm)
3	1.8
1.8	1.4
1	1.1
0.72	0.9
0.44	0.7
0.22	0.5

3.2. Nozzle Position

As oil can easily enter inside the bearing if the nozzle is located close to the bearing, the distance between the leading edge of the nozzle and the inner race face is taken in this experiment to be 8 mm. Unless otherwise specified, the nozzle is placed at the center of the clearance between the cage and the inner race normal to the bearing face, regardless of the cage guide type. In addition, when the inner-race-riding cage is used, the nozzle is placed at the large clearance between the cage and the outer race, and the experiment is repeated, but, as will be mentioned later, the penetration ratio increases and the bearing temperature decreases, but failure tends to occur and the performance is not good.

When the thrust load is to be applied to the radial ball bearing, as in this experiment, the penetration ratio — that is, the ratio of oil transmitted through the bearing to the total oil flow — is expected to differ depending on whether the nozzle is placed on the thrust loaded side of the inner race or the unloaded side of the inner race, as shown in Figure 7. Because a large penetration ratio

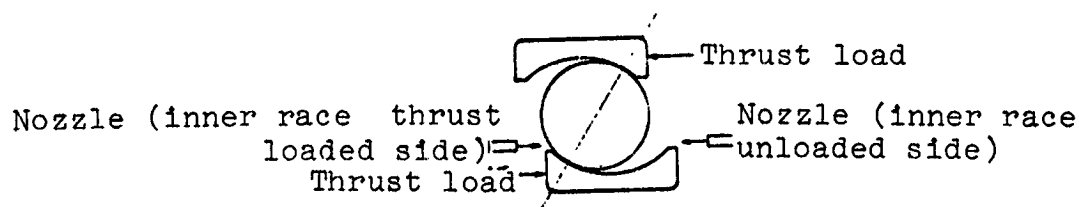


Figure 7: Thrust load and nozzle position:

is desirable for cooling of the bearing, how the penetration ratio changes, depending on the nozzle position, is studied in experiments and the optimal position is determined.

(a) #6206 (outer-race-riding cage)

17

Figure 8 shows the relation between penetration ratio and shaft speed for #6206 (outer-race-riding cage) when the nozzle is placed on the thrust loaded side or unloaded side of the inner race, with an oil flow $Q = 1$ kg/min. At low speeds, when the nozzle is placed on the unloaded side of the inner race, the penetration ratio is greater than when the nozzle is placed on the thrust loaded side of the inner race. But at high speeds, the difference becomes smaller, and on which side the nozzle is placed makes no difference. As the penetration ratio changes, the bearing temperature rise changes also. The bearing outer race temperature rise from an inlet oil temperature (30° C constant), as well as the temperature rise of deflected oil and transmitted oil as a function of speed, are shown in Figures 9 and 10. In Figure 9, in which the nozzle is placed on the thrust loaded side of the inner race, the bearing outer race temperature rise and transmitted oil temperature rise are nearly equal, but in Figure 10 — in which the nozzle is placed on the unloaded side of the inner

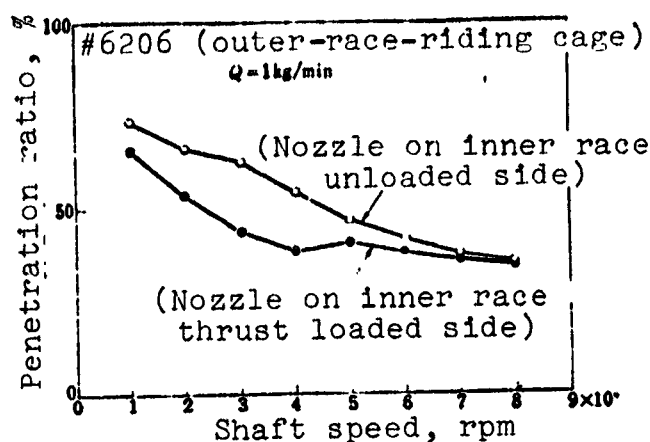


Figure 8. Penetration ratio and shaft speed

race, the bearing outer race temperature rise is significantly lower than the transmitted oil temperature rise above 60,000 rpm, despite the fact that the penetration ratios at high speed are nearly equal. Generally, the bearing outer race temperature rise is roughly equal to or slightly greater than the transmitted oil temperature rise at low speed, as shown in Figure 9, but as the speed becomes higher, the transmitted oil temperature rise is expected to be slightly greater, because the temperature of the cage and the roller body becomes higher than the bearing outer race temperature. The following explanation can be made regarding why this expectation was not fulfilled above 60,000 rpm, when the nozzle was placed on the unloaded side of the inner race.

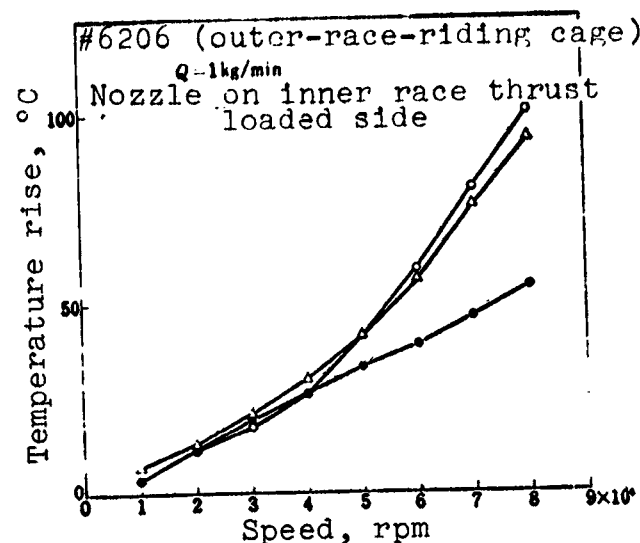


Figure 9. Bearing temperature rise and discharged oil temperature rise as a function of speed:

Δ — bearing outer race temperature rise; ● — deflected oil temperature rise; ○ — transmitted oil temperature rise

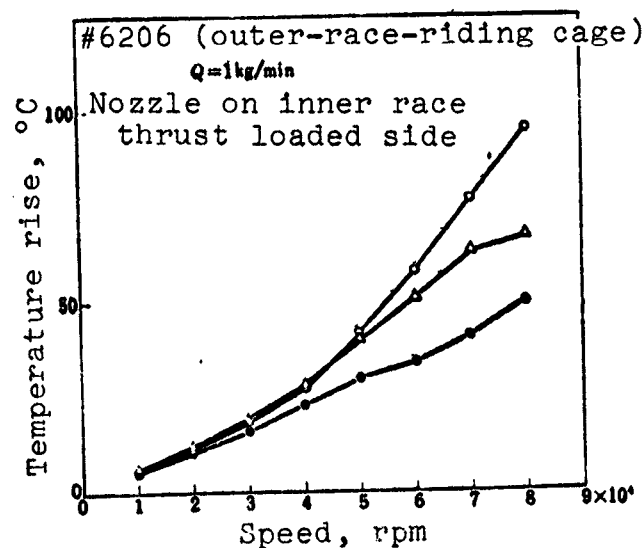


Figure 10. Bearing temperature rise and discharged oil temperature rise as a function of speed:

Δ — bearing outer race temperature rise; ● — deflected oil temperature rise; ○ — transmitted oil temperature rise

Looking at the structure of the test equipment in Figure 1, when the nozzle is placed on the unloaded side of the inner race, the nozzle enters inside the test bearing housing and the housing is cooled down by a large quantity of low-temperature deflected oil, causing a drop in the bearing outer race temperature. This is clear also from the fact that the transmitted oil temperature rise is nearly the same regardless of the side where the nozzle is placed. From the applications viewpoint, the nozzle can be placed on either side. It is more convenient to have the bearing outer race temperature rise be nearly equal to the transmitted oil temperature rise because the oil viscosity is used at an average bearing temperature in the analysis of bearing performance. It seems better to avoid structural influences. We decided to place the nozzle on the thrust loaded side of the inner race for #6206 (outer-race-riding cage).

(b) #6202 (inner-race-riding cage)

The penetration ratio and the temperature rise as a function of speed when the nozzle is placed on the thrust loaded side or unloaded side of the inner race are shown in Figures 11, 12, and 13. The trend is the same as for the previous #6206 (outer-race-riding cage). Consequently, the nozzle was placed on the thrust loaded side of the inner race for #6206 (inner-race-riding cage) for the same reason mentioned, even though, from the standpoint of penetration ratio, there is a slight advantage when the nozzle is placed on the unloaded side of the inner race.

(c) #17206

Figure 14 shows the penetration ratio as a function of speed when the nozzle is placed on the thrust loaded side or unloaded side of the inner race. The penetration ratio when the nozzle is placed on the thrust loaded side is drastically smaller than when the nozzle is placed on the unloaded side of the inner race. The reason there is such a large difference, depending on the nozzle position, compared to #6206 is that, as shown in Figure 15, the shoulder of one side of the outer race is removed for #17206. Then, when the nozzle

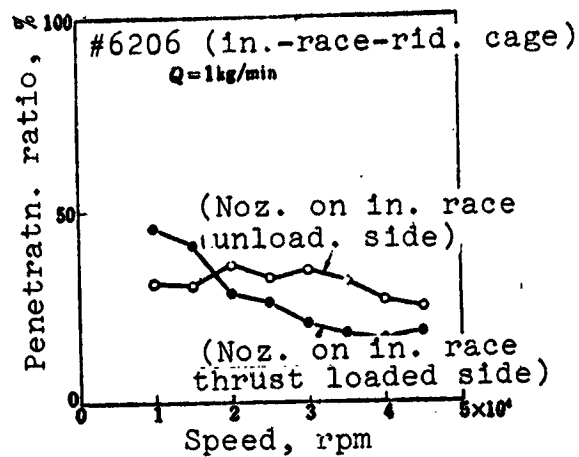


Figure 11. Penetration ratio and speed

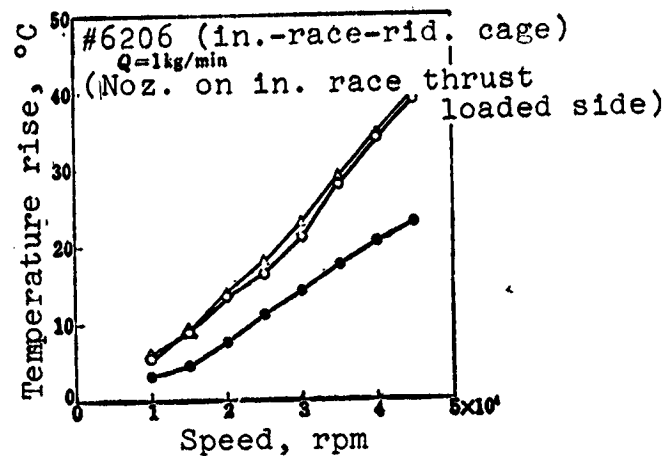


Figure 12. Bearing temperature rise and discharged oil temperature rise as a function of speed:

Δ — bearing outer race temperature rise; \bullet — deflected oil temperature rise; \circ — transmitted oil temperature rise

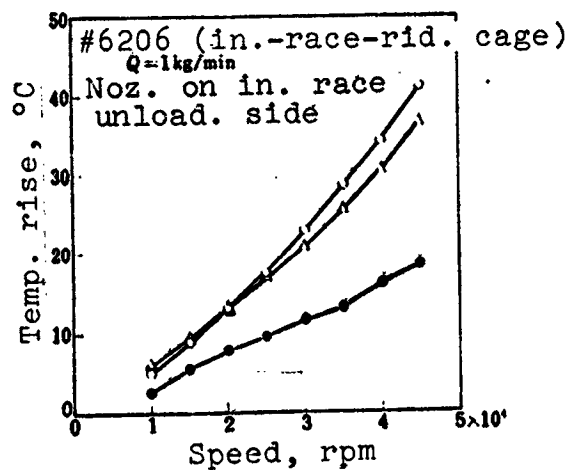


Figure 13. Bearing temperature rise and discharged oil temperature rise as a function of speed:

Δ — bearing outer race temperature rise; \bullet — deflected oil temperature rise; \circ — transmitted oil temperature rise

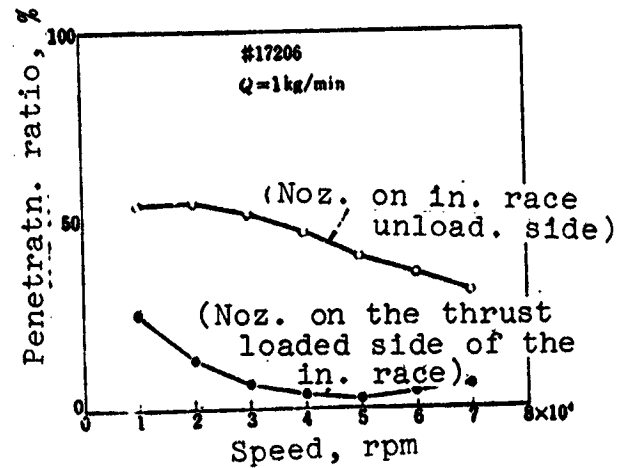
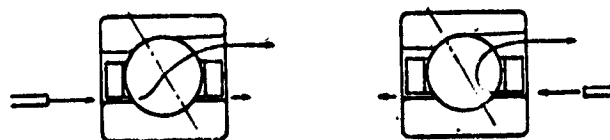


Figure 14. Penetration ratio and speed



Noz. on in. race unload. side) (Noz., in race thrust load. side)

Figure 15. Nozzle position and oil flow (#17206)

is placed on the thrust loaded side of the inner race, most of the oil flows backward to the nozzle side via the clearance space in the dropped shoulder of the outer race. The bearing outer race temperature rise and outlet oil temperature rise as a function of speed are shown in Figures 16 and 17. In Figure 16, in which the nozzle is placed on the thrust loaded side of the inner race, the bearing

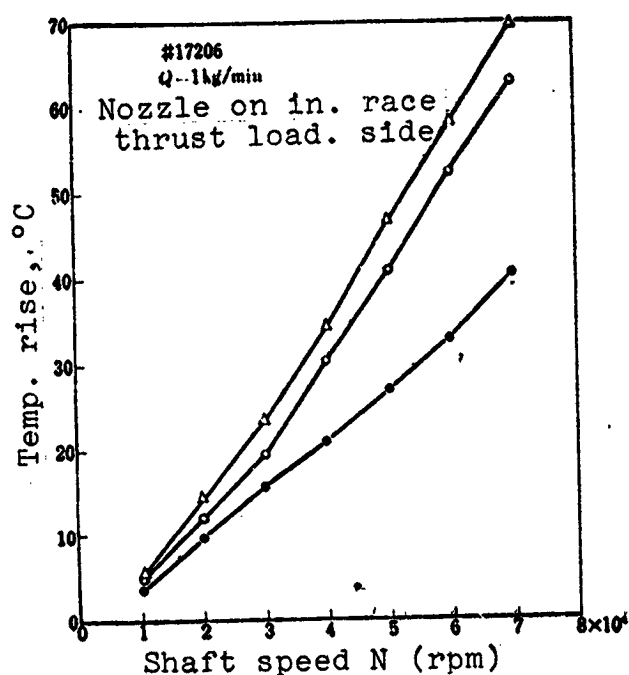


Figure 16. Bearing temperature rise and discharged oil temperature rise as a function of shaft speed:

Δ — bearing outer race temperature rise; ● — deflected oil temperature rise; ○ — transmitted oil temperature rise

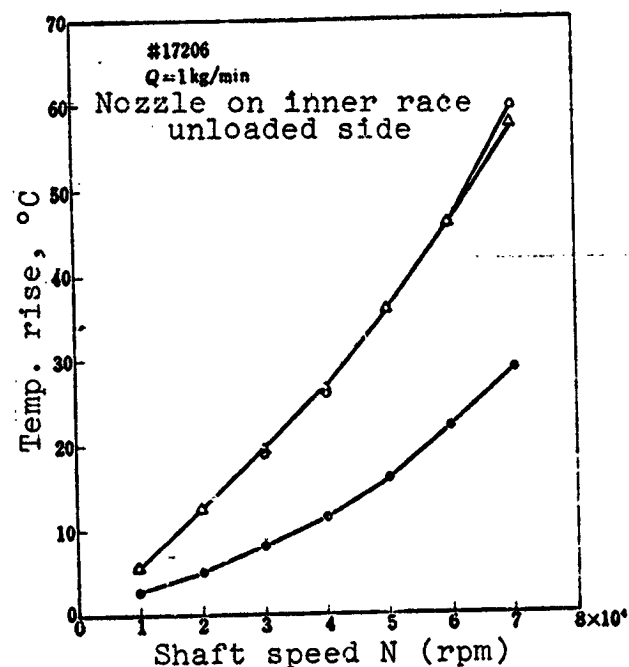


Figure 17. Bearing temperature rise and discharged oil temperature rise as a function of shaft speed:

Δ — bearing outer race temperature rise; ● — deflected oil temperature rise; ○ — transmitted oil temperature rise

outer race temperature rise is greater than the transmitted oil temperature rise. In Figure 17, in which the nozzle is placed on the unloaded side of the inner race, the temperature rise itself is lower than when the nozzle is placed on the thrust loaded side of the inner race, and the bearing outer race temperature rise and the transmitted oil temperature rise are roughly equal. The reason for this opposite behavior, compared to #6206, is that most of the oil flows through

the dropped shoulder of the outer race. As more than 90% of oil is deflected when the nozzle is placed on the thrust loaded side of the inner race, the average bearing temperature rise is assumed to be in between the bearing outer race temperature rise and the deflected oil temperature rise. When this average is taken, it roughly agrees with the bearing outer race temperature rise or the transmitted oil temperature rise when the nozzle is placed on the unloaded side of the inner race. As mentioned before, it is more convenient to have roughly equal bearing outer race temperature rise and transmitted oil temperature rise, because oil viscosity at the average bearing temperature is used in the analysis of bearing performance. Therefore, for #17206, the nozzle was placed on the unloaded side of the inner race, contrary to #6206.

(d) #30BNT

The penetration ratio as a function of speed when the nozzle is placed on the thrust loaded side or the unloaded side of the inner race is shown in Figure 18. The penetration ratio when the nozzle is placed on the thrust loaded side of the inner race is smaller below 70,000 rpm, but greater above 70,000* rpm, compared to when the nozzle is placed on the unloaded side of the inner race. At high speeds, there is a slight advantage in placing the nozzle on the thrust loaded side of the inner race. This is assumed to be due to the fact that the shoulder of the inner race is dropped for #30BNT, as shown in Figure 19, contrary to #17206. The bearing outer race temperature rise and the discharged oil temperature rise as a function of speed are shown in

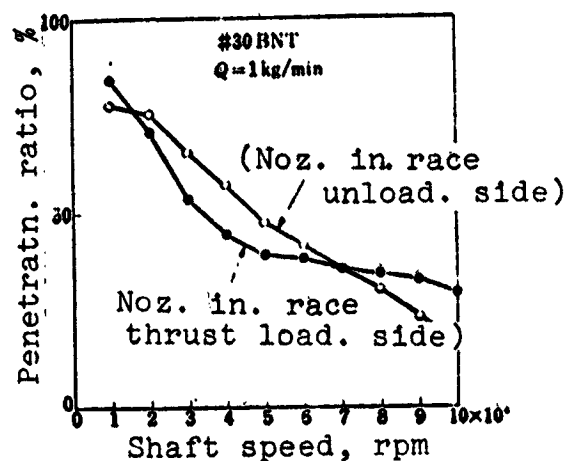


Figure 18. Penetration ratio and shaft speed

*Translator's Note: 7,000 rpm in foreign text.

Figures 20 and 21. They are the same as for #6206. Consequently, the nozzle is placed on the thrust loaded side of the inner race for #30BNT.

3.3. Number of Nozzles

If the number of jets is increased with the same total oil flow, there is the benefit

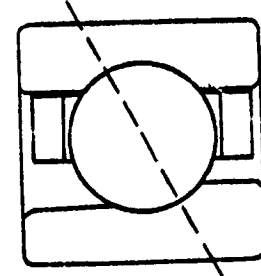


Figure 19. #30BNT

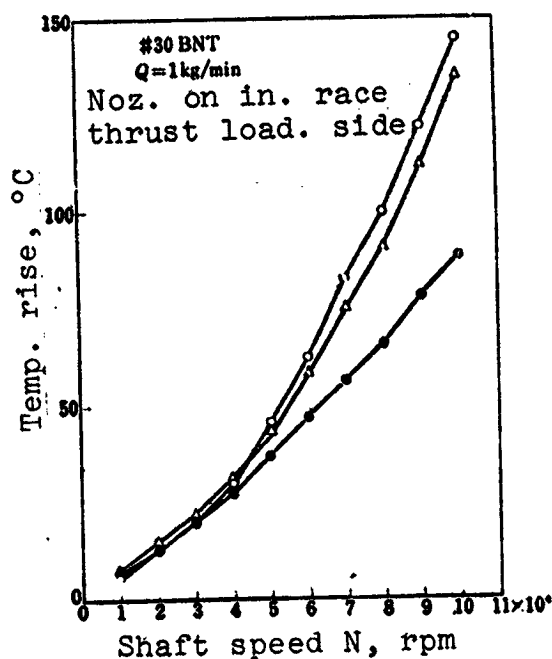


Figure 20. Bearing temperature rise and discharged oil temperature rise as a function of shaft speed:

Δ — bearing outer race temperature rise; \bullet — deflected oil temperature rise; \odot — transmitted oil temperature rise

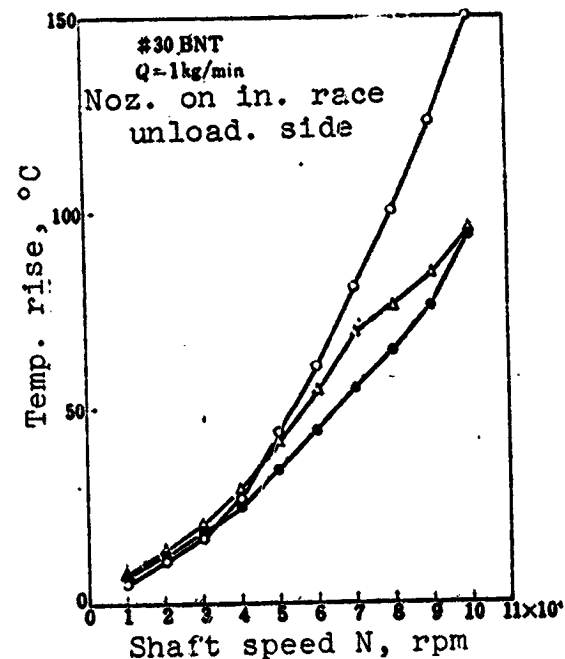


Figure 21. Bearing temperature rise and discharged oil temperature rise as a function of shaft speed:

Δ — bearing outer race temperature rise; \bullet — deflected oil temperature rise; \odot — transmitted oil temperature rise

of uniform temperature over the circumferential direction of the bearing. With jet oil feed, the area contacted by the jet is cooled by a large quantity of oil, but as oil violently scatters, the

temperature rises gradually in the direction of rotation. Figure 22 shows the temperature distribution in the circumferential direction of the bearing outer race when one or two nozzles are used with the same total oil flow. The temperature difference is $4 - 5^{\circ}\text{C}$ with a single nozzle, and 2°C with two nozzles. The small temperature difference is explained by the relatively small test bearing the load consisting of a thrust load only. Thus, unless explicitly specified, only a single nozzle is used in this experiment.

CHAPTER 4. DEEP-GROOVE BALL BEARING (#6206)

4.1. Introduction

As deep-groove ball bearings are commonly used for high speed applications, we conducted experiments on the deep-groove ball bearing first. As mentioned before, the sliding friction portion inside the bearing is expected to be the most vulnerable to failure at high speeds. As the sliding friction portions inside the roller bearing are primarily concentrated around the cage, it is expected that the cage guide type, configuration, etc., greatly affect the high speed performance. There are three kinds of cage guide types: roller-riding cage; inner-race-riding cage, and outer-race-riding cage. For high speed applications, the roller-riding cage type tends to generate vibrations and thus is not often used. Instead, the outer-race-riding cage or the inner-race-riding cage types are used. Anderson and others [3] investigated the effect of the cage guide type regarding the cylindrical roller bearing (#215), and reported that the performance of the outer-race-riding cage was better than the inner-race-riding

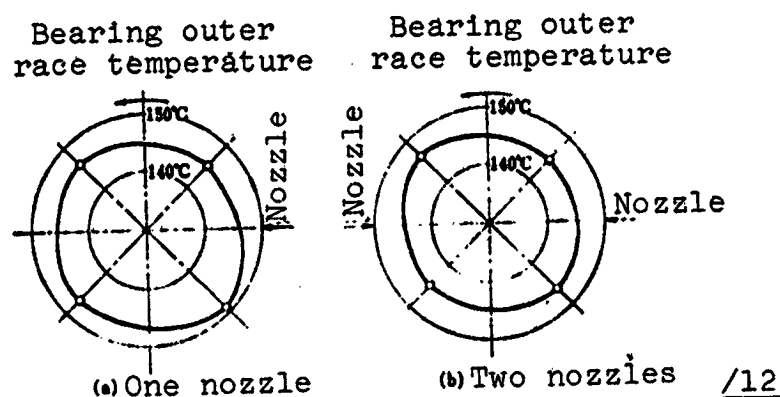


Figure 22. Number of nozzles and temperature distribution in the circumferential direction:

test bearing: #30BNT
oil flow: 1 kg/min
shaft speed: 90,000 rpm
thrust load: 50 kg
inlet oil temperature: 30°C

cage. However, in regard to which type is more advantageous at high speed, the experimental data are insufficient, and no clear conclusion has been reached.

The performance of #6206 equipped with the outer-race-riding cage is discussed first in this chapter, followed by #6206 equipped with the inner-race-riding cage in the next chapter, and these will be compared.

4.2. Experimental Conditions

Although mentioned already in Chapters 2 and 3, the conditions used in this experiment are briefly summarized. A single nozzle is placed on the thrust loaded side of the inner race. It is placed perpendicularly to the center of the clearance between the cage and the inner race. The distance between the leading edge of the nozzle and the inner race face is 8 mm. The jet velocity is constant at roughly 20 m/s, regardless of oil flow.

Also, unless explicitly specified, the thrust load is constant at 50 kg, and the inlet oil temperature is also constant at 30° C.

4.3. Test Bearing

The test bearing is a #6206 SP-class ball bearing. The cage is made of high-strength yellow brass and the cage guide type is the outer-race-riding cage. Around the outside perimeter of the cage, the special oil groove is set up as shown in Figure 23 to improve oil discharge.

The bearing dimensions are shown in Table 2. The radial clearance of the bearing is 25 - 35 μm , which is significantly larger than the normal bearing type. This is because, under high speed rotation, the temperature rise of the roller body will be significantly higher than that of the inner race and the outer race and the reduction in clearance is expected. The bearing fit is taken to be 10 - 15 μm .

TABLE 2. TEST BEARING #6206(SP)

Diameter of steel ball, mm	9.525 (3/8")
Number of steel ball	0
% of groove radius to steel ball	
Outer race, %	51.5 - 52.5
Inner race, %	50.5 - 51.5
Inside diameter of outer race, mm	52.8
Outside diameter of inner race, mm	40.4
Radial clearance, μm	25 - 35
Cage guide type	Outer-race-riding-cage
Guide clearance, mm	0.35 + 0 - 0.05
Pocket clearance, mm	0.195 + 0.05 - 0

4.4. Experimental Results

The bearing outer race temperature, the outlet oil temperature at the nozzle side as well as the bearing transmitted side, the friction torque, and the penetration ratio as a function of speed for each oil flow under the constant thrust load of 50

kg and an inlet oil temperature of 30° C are shown in Table 3. The maximum speed is limited to 60,000 rpm for oil flow rate of 0.22 kg/min, 70,000 rpm for 0.44 kg/min, and to 80,000 rpm for other oil flow rates, because at high speeds, conspicuous wear is sometimes generated on the cage. This limiting speed will be discussed later on, but here the experimental results within the region of safe bearing operating conditions below the limiting speed are shown.

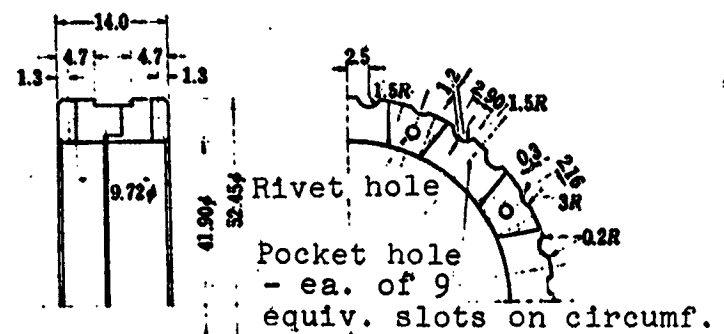


Figure 23. Configuration of cage

/13

TABLE 3. BEARING TEMPERATURE, OUTLET OIL TEMPERATURE, FRICTION TORQUE, PENETRATION RATIO, AND SHAFT SPEED
(30° C inlet oil temperature and 50 kg thrust load)

Q = 3 kg/min (room temperature 24° C)

Shaft speed, rpm	Bearing outer race temp., °C	Outlet oil temp. (nozzle side), °C	Outlet oil temp. (trans. side), °C	Friction torque, kg·cm	Penetrn. ratio, %
10,000	33	32	32	1.23	53.1
20,000	37	35.5	35.5	1.68	45.0
30,000	41.5	39	39	2.12	40.1
40,000	46.5	42	43	2.57	36.4
50,000	54.5	46.5	51	3.00	31.2
60,000	64.5	51	52.5	3.41	29.2
70,000	73	54.5	74	3.78	28.8
80,000	84	59	90	4.00	26.6

Q = 1.8 kg/min (room temperature 24° C)

Shaft speed, rpm	Bearing outer race temp., °C	Outlet oil temp. (nozzle side), °C	Outlet oil temp. (trans. side), °C	Friction torque, kg·cm	Penetrn. ratio, %
10,000	34.5	33	33	1.13	60.0
20,000	39.5	38	38	1.50	54.2
30,000	44.5	42.5	42	1.86	45.0
40,000	51.5	48	47	2.20	35.2
50,000	60.5	53	57.5	2.57	32.4
60,000	73	58.5	73.5	2.89	29.5
70,000	85.5	62	90	3.17	30.0
80,000	100	69	106	3.35	28.0

(Table continued on following page)

TABLE 3 (continued)

 $Q = 1 \text{ kg/min}$ (room temperature 25°C)

Shaft speed, rpm	Bearing outer race temp., $^\circ\text{C}$	Outlet oil temp. (nozzle side), $^\circ\text{C}$	Outlet oil temp. (trans. side), $^\circ\text{C}$	Friction torque kg·cm	Penetrn. ratio, %
10,000	38	34.5	34.5	1.03	65.7
20,000	43.5	42	41.5	1.35	56.4
30,000	51	49	47.5	1.64	46.3
40,000	59	55.5	54.5	1.85	35.1
50,000	71.5	62.5	69.5	2.13	31.5
60,000	85	67.5	88.5	2.39	32.5
70,000	102	73	108.5	2.62	33.9
80,000	120.5	80	130	2.82	33.3

 $Q = 0.72 \text{ kg/min}$ (room temperature 23°C)

Shaft speed, rpm	Bearing outer race temp., $^\circ\text{C}$	Outlet oil temp. (nozzle side), $^\circ\text{C}$	Outlet oil temp. (trans. side), $^\circ\text{C}$	Friction torque kg·cm	Penetrn. ratio, %
10,000	37.5	36	36	0.97	69.5
20,000	46	45	44	1.24	62.7
30,000	55	52.5	51	1.48	53.7
40,000	64.5	61	58	1.65	42.0
50,000	76.5	70.5	70.5	1.87	41.1
60,000	94	80	88	2.11	42.4
70,000	112	89.5	110.5	2.30	40.0
80,000	131	101	135	2.48	37.0

 $Q = 0.44 \text{ kg/min}$ (room temperature 25°C)

Shaft speed, rpm	Bearing outer race temp., $^\circ\text{C}$	Outlet oil temp. (nozzle side), $^\circ\text{C}$	Outlet oil temp. (trans. side), $^\circ\text{C}$	Friction torque kg·cm	Penetrn. ratio, %
10,000	39.5	38.5	37	0.90	71.8
20,000	50	50	47.5	1.15	58.5
30,000	62.5	61.5	58	1.34	50.7
40,000	74	72	67	1.48	40.3
50,000	89.5	84.5	87.5	1.67	38.2
60,000	110	97.5	115	1.87	41.7
70,000	134	107	139	1.95	35.4

(Table concluded on following page)

TABLE 3 (concluded)
Q = 0.22 kg/min (room temperature 24° C)

Shaft speed, rpm	Bearing outer race temp., °C	Outlet oil temp. (nozzle side), °C	Outlet oil temp. (trans. side), °C	Friction torque, kg·cm	Room temp., °C
10,000	44	43	41.5	0.82	70.7
20,000	59.5	59.5	57	0.97	54.0
30,000	74.5	73	70.5	1.13	44.4
40,000	90	87.5	84.5	1.21	37.8
50,000	111	106	110.5	1.32	40.5
60,000	138.5	127	140.5	1.42	41.8

The above experimental results, together with the results obtained by changing the thrust load and the inlet oil temperature, are analyzed next in order to study the high speed performance of the deep-groove ball bearing.

4.5. Bearing Temperature Rise.

Figure 24 shows the temperature rise $T_B - T_I$ from the inlet oil temperature T_I (30° C) to the bearing outer race temperature T_B as a function of speed from the data in Table 3. With an increasing speed, the bearing temperature rise increases. On the other hand, with an increasing oil flow, the bearing temperature rise decreases. This bearing outer race temperature rise $T_B - T_I$ as a function of speed N and oil flow Q is shown in Figures 25 and 26, respectively. In Figure 25, the relation between $T_B - T_I$ and N changes at 40,000 rpm. In the high speed region above 40,000 rpm, it can be expressed as:

$$(T_B - T_I) \propto N^{0.4-1.1} \quad (1)$$

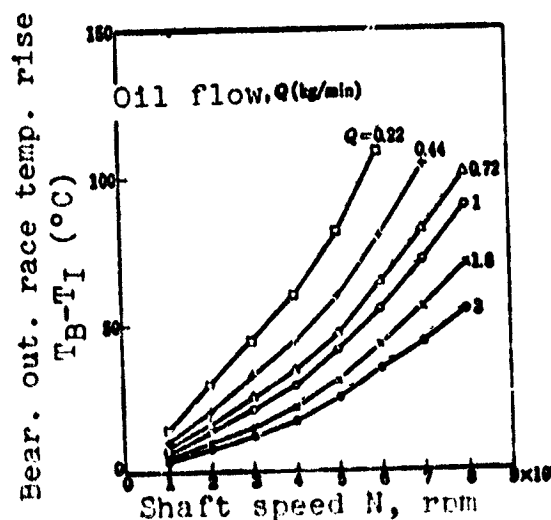


Figure 24. Bearing temperature rise and shaft speed

From Figure 26, $T_B - T_I$ and Q are related by

$$(T_B - T_I) \propto Q^{-0.41 \sim -0.50} \quad (2)$$

The smaller exponents of N and Q correspond to the larger value of $T_B - T_I$.

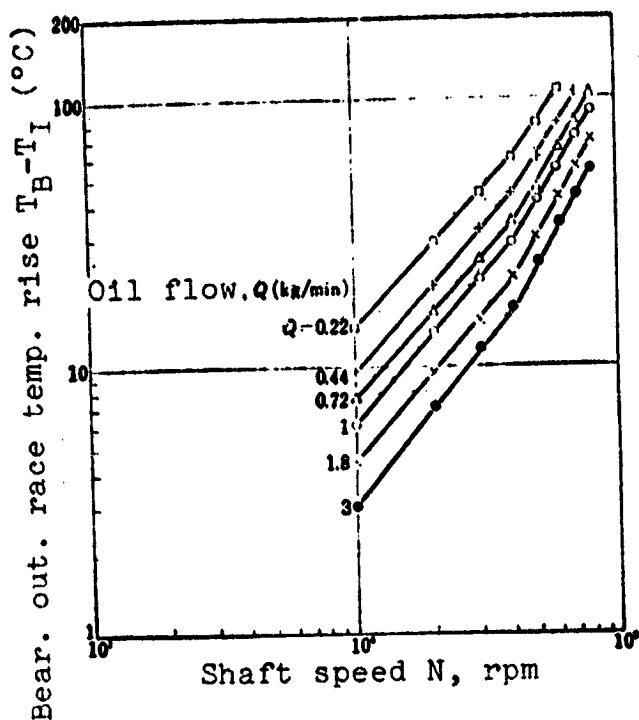


Figure 25. Bearing temperature rise and shaft speed

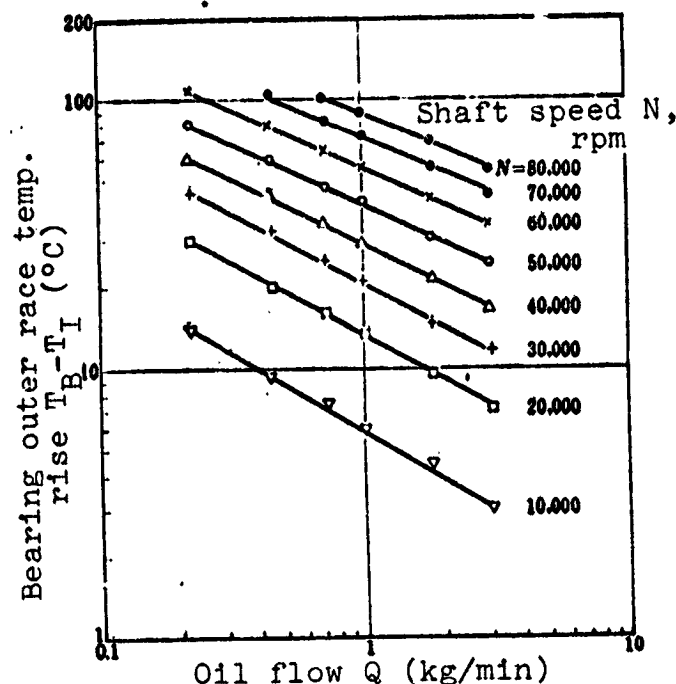


Figure 26. Bearing temperature rise and oil flow

From Equation (1), the bearing temperature rise increases in proportion to $N^{1.44-1.7}$. Thus, unless significant cooling is performed, the bearing failure due to overheating is expected later at high speeds. As is clear from the exponent of Q in Equation (2) for the temperature rise versus oil flow, sufficient cooling cannot be accomplished unless the forced-feed oil flow rate is significantly increased, even though oil acts as a coolant in the jet oil supply of high speed roller bearings. As for the exponents of N and Q in Equations (1) and (2), Soda and others [4] performed an experiment with the ball bearing #6315, and obtained the exponents of 1 for N and -0.45 for Q . In an experiment with the cylindrical roller bearing #215 by Macks and others [2], the exponent of N was 1.2, and the

exponent of Q was -0.36 . These exponents differ widely, depending on the bearing type, test condition, cooling conditions, viscosity-temperature characteristic of lubricating oil, dn value, etc. The details on these exponents will be discussed in the section on friction torque.

The above results are for the case of the constant thrust load of 50 kg, shown in Table 3. Figure 27 shows a sample of the temperature rise $T_B - T_I$ from the oil inlet temperature (30°C) to the bearing outer race temperature T_B as a function of thrust load. The range of the thrust load is 25 - 200 kg. The bearing temperature rise increases with increasing thrust load. This relation between the bearing outer race temperature rise $T_B - T_I$ and the thrust load P in the high speed region can be approximated by

$$(T_B - T_I) \propto P^{0.18-0.17} \quad (3)$$

As the shaft speed increases and $T_B - T_I$ becomes greater, the exponent of P becomes smaller.

As is clear from the comparison of an exponent of N in Equation (1) and an exponent of P in Equation (3), the bearing temperature rise of the high speed roller bearing is affected more by the shaft speed than the load. It is known that the bearing temperature rise is determined by the bearing friction, and that this friction consists

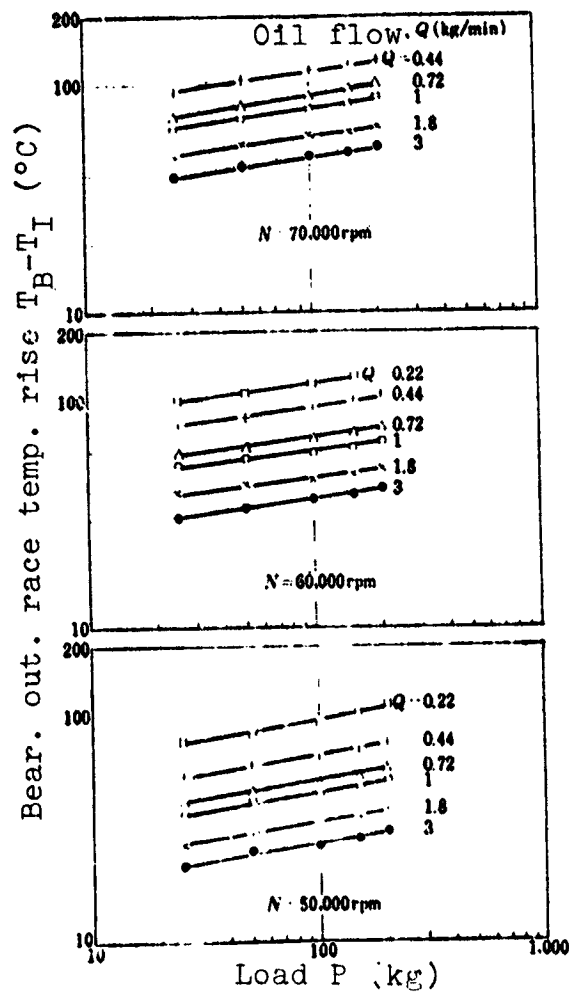


Figure 27. Bearing temperature rise and load

of a velocity term which depends on the viscosity and the velocity, and a non-velocity term which depends on the load. It thus indicated that most of the bearing temperature rise of the high speed roller bearing is based on the velocity term of friction, and the percentage of non-velocity term due to load is extremely small. This point will be discussed in greater detail in the section on friction torque.

The above results are for the case of the constant inlet oil temperature of 30° C. In practical applications, it is frequently difficult to maintain a constant inlet oil temperature. If inlet oil temperature is changed, average viscosity of the bearing and inlet viscosity of supplied oil will certainly be changed. Figure 28 shows a sample of the relation between the viscosity at the inlet oil temperature Z_I and the bearing outer race temperature rise at the inlet oil temperature when the inlet oil temperature is varied from 30° C to 120° C. The relationship between the bearing outer race temperature rise $T_B - T_I$ and Z_I can be approximated by

$$(T_B - T_I) \propto Z_I^{0.25-0.3} \quad (4)$$

The greater the shaft speed and $T_B - T_I$, the smaller becomes the exponent of Z_I . Below 30,000 rpm and with a higher inlet oil temperature, there is a deviation from this relationship because of the small temperature rise based on rotation and the resulting large error. As the region of the high dn values is the subject of this experiment, Equation (4) is appropriate. In general, the smaller the viscosity at the inlet oil temperature, Z_I , the lower is the bearing temperature rise $T_B - T_I$. However, the absolute value of T_B is large when T_I is large, as shown in Figure 29. If Z_I is too low, the bearing temperature rise is low, but the formation of oil film becomes difficult; thus there must be a lower limit on Z_I . This point will be discussed in greater detail in the section on friction torque.

/17

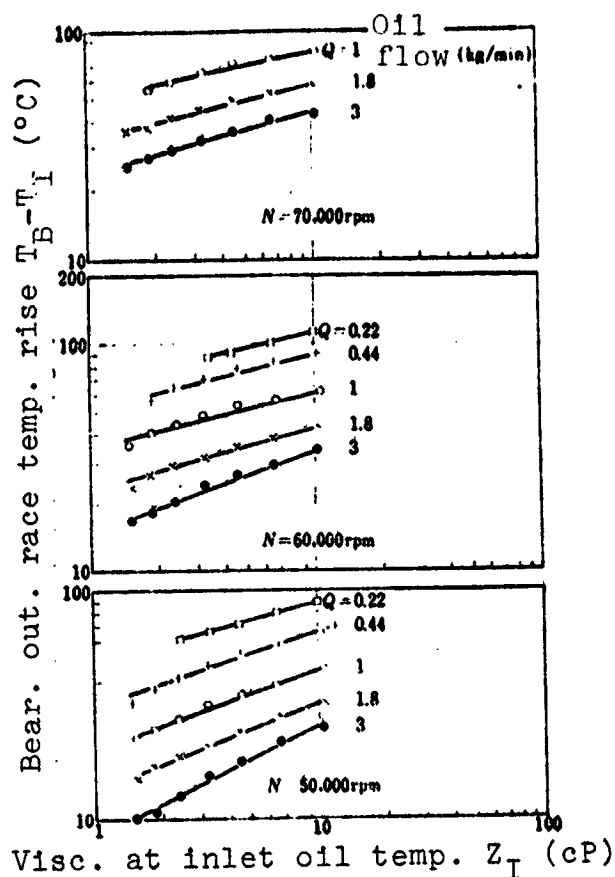


Figure 28. Bearing temperature rise and viscosity at inlet oil temperature

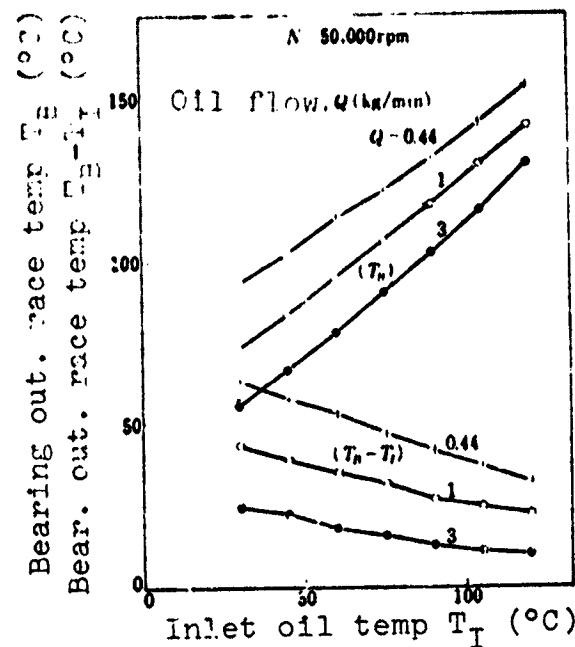


Figure 29. Bearing outer race temperature and temperature rise as a function of inlet oil temperature

Summarizing the bearing outer race temperature rise in the high speed region, it can be approximated by

$$(T_B - T_I) \propto Z_I^{0.28-0.5} P^{0.15-0.17} N^{1.44-1.7} Q^{-0.41-0.58} \quad (5)$$

The smaller exponent of each factor corresponds to the larger value of $T_B - T_I$. The above equation approximately holds in the following range: 40,000 - 80,000 rpm speed, 0.22 - 3 kg/min oil flow, 25 - 200 kg thrust load, and 30 - 120° C inlet oil temperature.

4.6. Amount of Heat Absorption by Lubricating Oil

The fact that the bearing temperature rise of the high speed roller bearing is roughly inversely proportional to $(\text{oil flow})^{1/2}$ indicates that, for jet lubrication using a large quantity of oil, oil acts as a coolant. Therefore, by obtaining the amount of heat

transfer to the oil due to the outlet oil temperature rise, the cooling effect can be analyzed. Table 4 shows the quantity of heat absorption by the deflected oil and transmitted oil, as well as the total heat absorption by oil calculated from the data in Table 3. Figure 30 shows the total horsepower absorption by oil H_0 as a function of speed from the results in Table 4. The total horsepower

TABLE 4. HORSEPOWER ABSORPTION BY OIL AND SHAFT SPEED
(30° C inlet oil temperature and 50 kg thrust load)

Oil flow $Q = 3 \text{ kg/min}$			
Shaft speed, rpm	Horsepower absorption by oil (nozzle side), PS	Horsepower absorption by oil (trans. side), PS	Total horsepower absorption by oil, PS
20,000	0.44	0.36	0.80
30,000	0.78	0.52	1.30
40,000	1.10	0.68	1.78
50,000	1.63	0.94	2.57
60,000	1.96	1.36	3.32
70,000	2.54	1.85	4.39
80,000	3.00	2.25	5.25

$Q = 1.8 \text{ kg/min}$			
Shaft speed, rpm	Horsepower absorption by oil (nozzle side), PS	Horsepower absorption by oil (trans. side), PS	Total horsepower absorption by oil, PS
20,000	0.32	0.38	0.70
30,000	0.57	0.48	1.05
40,000	1.00	0.52	1.52
50,000	1.35	0.77	2.12
60,000	1.73	1.11	2.84
70,000	1.97	1.59	3.56
80,000	2.41	1.80	4.21

(Table continued on following page)

TABLE 4 (continued)

 $Q = 1 \text{ kg/min}$

Shaft speed, rpm	Horsepower absorption by oil (nozzle side), PS	Horsepower absorption by oil (trans. side), PS	Total horsepower absorption by oil, PS
20,000	0.25	0.31	0.56
30,000	0.49	0.39	0.88
40,000	0.79	0.41	1.20
50,000	1.08	0.60	1.68
60,000	1.21	1.03	2.24
70,000	1.39	1.31	2.70
80,000	1.59	1.58	3.17

 $Q = 0.72 \text{ kg/min}$

Shaft speed, rpm	Horsepower absorption by oil (nozzle side), PS	Horsepower absorption by oil (trans. side), PS	Total horsepower absorption by oil, PS
20,000	0.19	0.30	0.49
30,000	0.36	0.39	0.75
40,000	0.61	0.40	1.01
50,000	0.82	0.57	1.39
60,000	0.99	0.85	1.84
70,000	1.23	1.11	2.34
80,000	1.46	1.32	2.79

 $Q = 0.44 \text{ kg/min}$

Shaft speed, rpm	Horsepower absorption by oil (nozzle side), PS	Horsepower absorption by oil (trans. side), PS	Total horsepower absorption by oil, PS
20,000	0.13	0.22	0.40
30,000	0.32	0.30	0.62
40,000	0.53	0.32	0.85
50,000	0.70	0.46	1.16
60,000	0.85	0.73	1.58
70,000	1.05	0.81	1.86

(Table concluded on following page)

TABLE 4 (concluded)

$$Q = 0.22 \text{ kg/min}$$

Shaft speed, rpm	Horsepower absorption by oil (nozzle side), PS	Horsepower absorption by oil (trans. side), PS	Total horsepower absorption by oil, PS
20,000	0.14	0.15	0.29
30,000	0.25	0.19	0.44
40,000	0.38	0.22	0.60
50,000	0.48	0.35	0.83
60,000	0.61	0.50	1.11

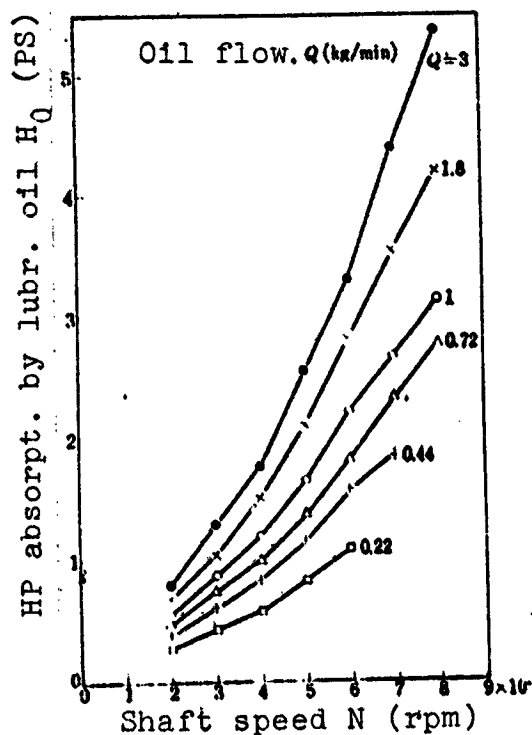


Figure 30. Horsepower absorption by oil and shaft speed

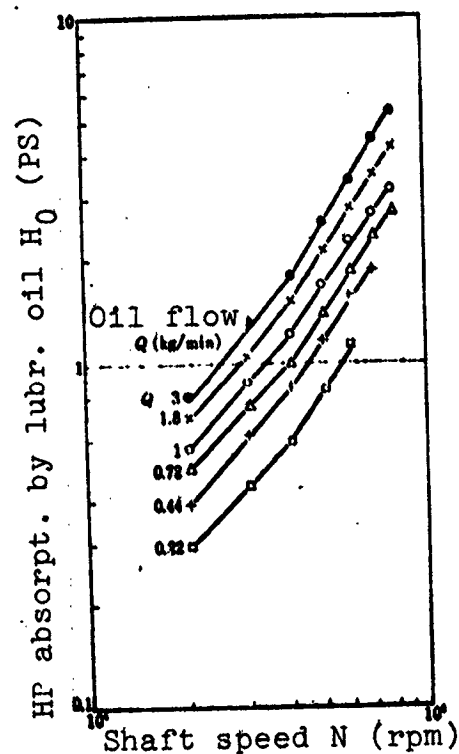


Figure 31. Horsepower absorption by oil and shaft speed

absorption by oil increases with an increasing speed. It also increases with an increasing oil flow. As the bearing temperature rise goes down with an increasing oil flow, most of the oil must act as a coolant. Figures 31 and 32 show the total horsepower absorption by oil as a function of shaft speed N and oil flow Q , respectively. In Figure 31, the relation between H_0 and N changes at 40,000 rpm,

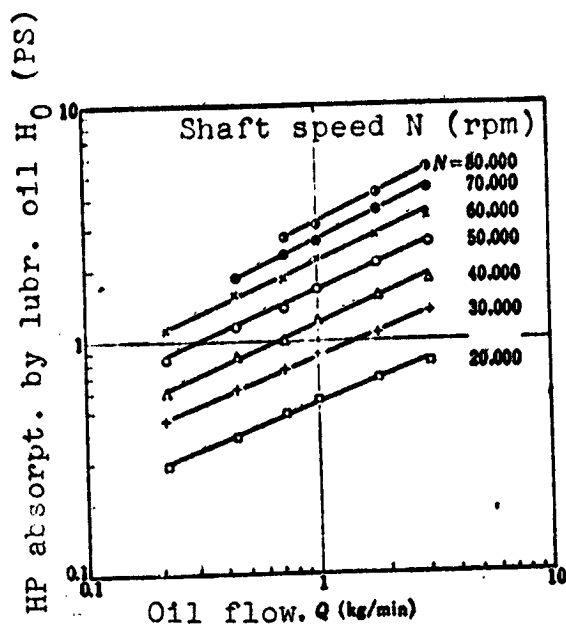


Figure 32. Horsepower absorption by oil and oil flow

just as for the case of the bearing temperature rise. In the high speed region above 40,000 rpm, it can be expressed as

$$H_0 \propto N^{1.47-1.58} \quad (6)$$

The smaller exponent of N corresponds to the larger value of $T_B - T_I$.

From Figure 32, the relationship between H_0 and Q can be expressed by

$$H_0 \propto Q^{0.47-0.58} \quad (7)$$

The larger exponent of Q corresponds to the larger value of $T_B - T_I$.

The above results are for the constant thrust load of 50 kg. In Figure 33, the relation between the total horsepower absorption by oil H_0 and the thrust load P is shown. From this, it can be approximated by

$$H_0 \propto P^{0.13-0.14} \quad (8)$$

The greater the speed and $T_B - T_I$, the smaller is the exponent of P.

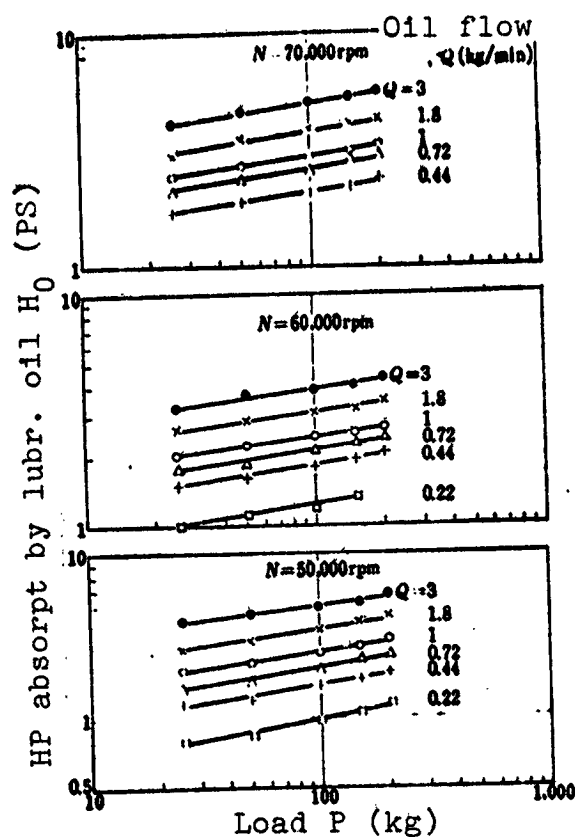


Figure 33. Horsepower absorption by oil and load

The above results are for the constant inlet oil temperature of 30° C. Figure 34 shows a sample of the relationship between the inlet oil temperature and the total horsepower absorption by oil when the inlet oil temperature is varied from 30° C to 120° C. As the inlet oil temperature increases, the total horsepower absorption by oil decreases because friction torque decreases also. This point will be discussed in the section on friction torque. Figure 35 shows the relation between the oil viscosity at inlet oil temperature Z_I and the

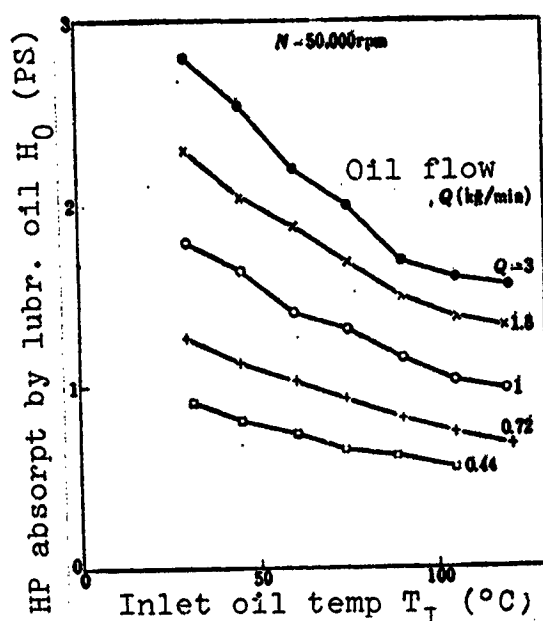


Figure 34. Horsepower absorption by oil and inlet oil temperature

total horsepower absorption by oil. The relation between the total horsepower absorption by oil H_0 and Z_I can be approximated by

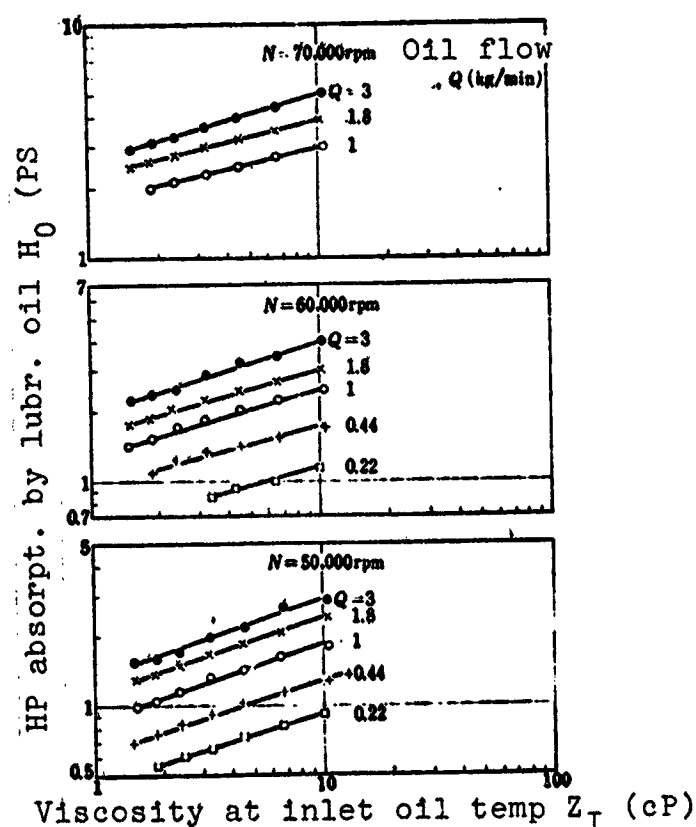


Figure 35. Horsepower absorption by oil and viscosity at inlet oil temperature

$$H_0 \propto Z_I^{0.24-0.4}$$

(9)

As the shaft speed and $T_B - T_I$ increase, the exponent of Z_I also decreases.

Summarizing the above, the total horsepower absorption by oil H_0 in the high speed region can be approximated by

$$H_0 \propto Z_I^{0.24-0.4} P^{0.12-0.18} N^{1.43-1.68} Q^{0.47-0.59} \quad (10)$$

The smaller exponents of Z_I , P , and N and the larger exponent of Q correspond to the larger value of $T_B - T_I$.

Compared to Equation (5) for the bearing temperature rise, the exponents of Z_I , P , and N are similar. The sign of the exponent of Q is reversed, and the smaller exponent of Q in the bearing temperature rise and the larger exponent of Q in the total horsepower absorption by oil, correspond to the larger value of $T_B - T_I$, indicating that, under such a jet lubrication, most of the friction generated heat is carried away by oil. /22

Let us examine further the action of oil as a coolant in the high speed roller bearing. Table 3 shows the ratio of oil flow transmitted through the bearing to the total supplied oil flow, that is, the penetration ratio. It decreases with increasing speed. As shown also by Noto's [5] experiment, at a high speed the surrounding air and oil are churned, and oil has difficulty entering inside the bearing. Also in Table 3, as oil flow rate increases, the penetration ratio becomes smaller, especially at low speeds. As the jet velocity is fixed at a roughly constant value for each oil flow in this experiment, the jet flow diameter must increase when the oil flow increases. It is assumed that oil has difficulty entering because the clearance (diametral clearance of 1.5 mm) between the cage and the inner race is small, and thus the penetration ratio decreases. With the larger type bearing and a larger clearance between the cage and the inner race, different results from Table 3 can be expected. In any event, the penetration ratio is around 25 - 40% in all cases at high speed. As the transmitted oil is assumed to have more effective heat exchange inside the bearing, its temperature rise is greater than that of the deflected oil as shown in Table 3. The temperature of the transmitted oil in high speed rotation is either equal to or even higher than the bearing outer race temperature. This is reasonable, in view of the fact that the temperature of the cage and the

roller body is significantly higher than the outer race temperature. Overall, the amount of heat carried away by the deflected oil is generally greater, as shown in Table 4, because its oil flow rate is greater than that of the transmitted oil, as shown in Table 3, even though the temperature rise of the deflected oil is smaller. Figures 36, 37, 38, 39, 40, and 41 show the penetration ratio K , the horsepower absorption by the deflected oil H_R , the horsepower absorption by the transmitted oil H_P , and the total horsepower absorption by oil H_0 as a function of speed N for each oil flow rate from the data in Tables 3 and 4. The horsepower absorption by the deflected oil is generally greater, but at high speed with a penetration ratio of roughly 30%, the horsepower absorption by the transmitted oil is, in some cases, nearly equivalent to that of the deflected oil.

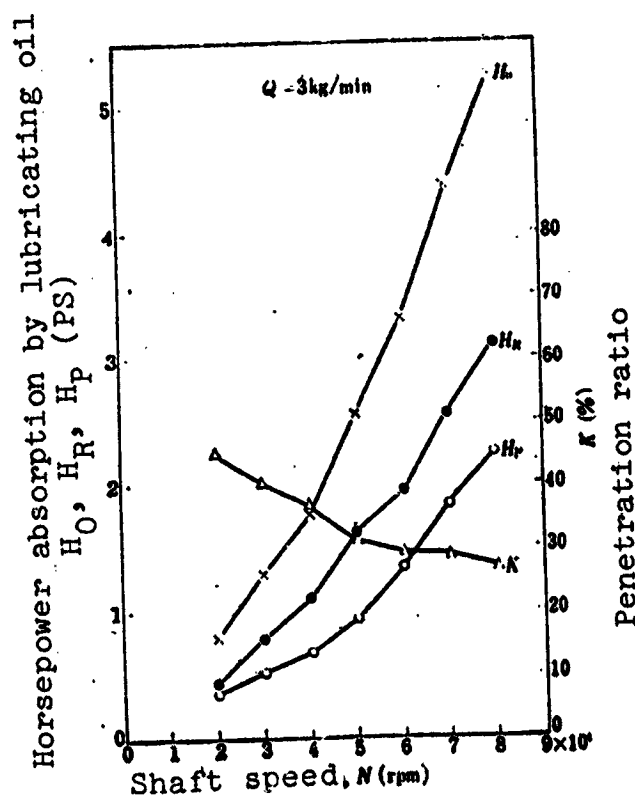


Figure 36. Horsepower absorption by oil and penetration ratio as a function of shaft speed:

X — total horsepower absorption; ● — horsepower absorption by the deflected oil; ○ — horsepower absorption by the transmitted oil; Δ — penetration ratio

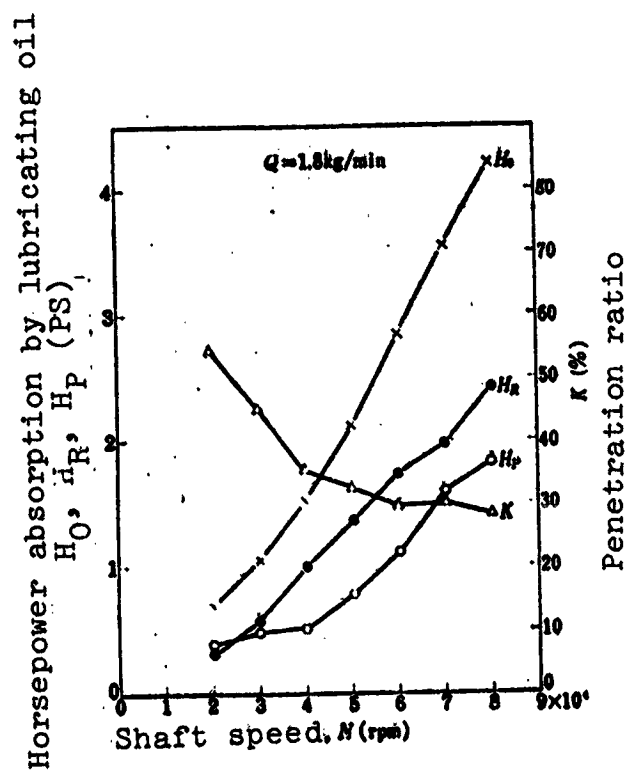


Figure 37. Horsepower absorption by oil and penetration ratio as a function of shaft speed

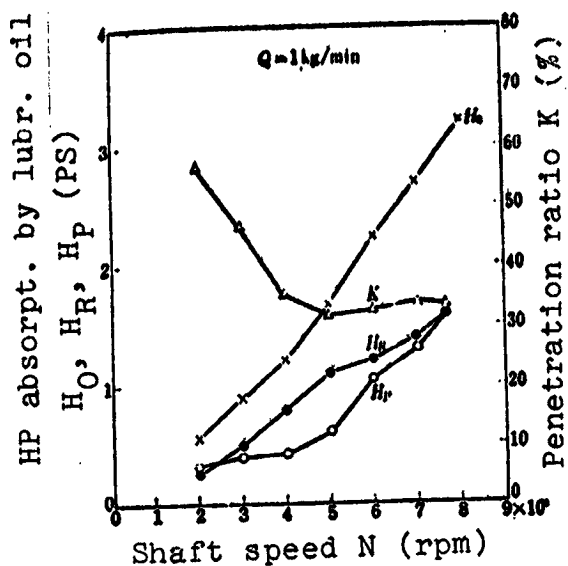


Figure 38. Horsepower absorption by oil and penetration ratio as a function of shaft speed

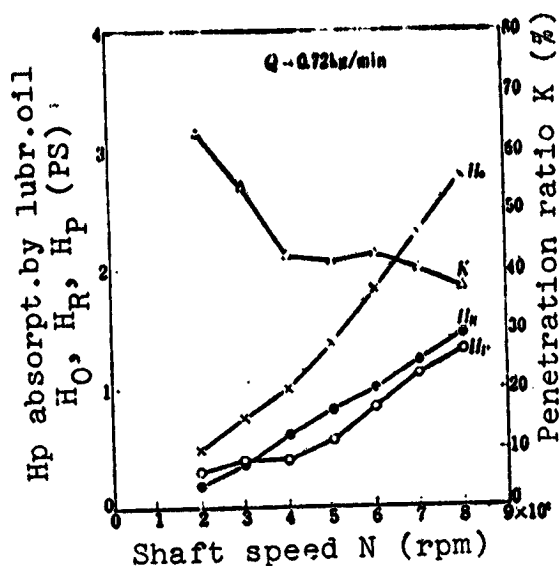


Figure 39. Horsepower absorption by oil and penetration ratio as a function of shaft speed

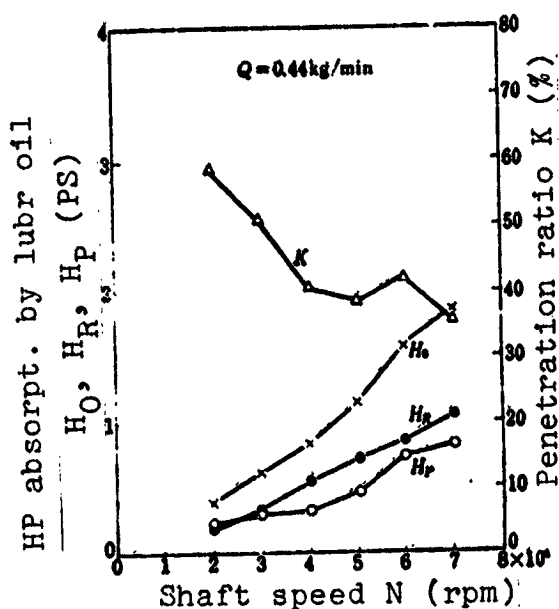


Figure 40. Horsepower absorption by oil and penetration ratio as a function of shaft speed

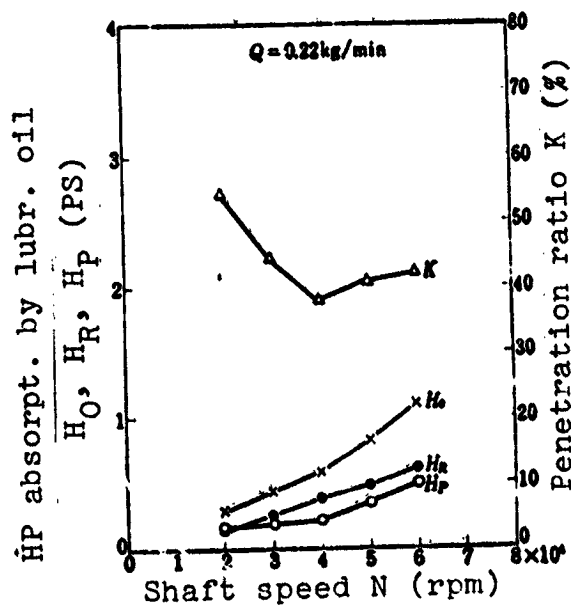


Figure 41. Horsepower absorption by oil and penetration ratio as a function of shaft speed

4.7. Heat Exchange Efficiency of Lubricating Oil

We have examined how oil acts as a coolant in the high speed roller bearing, and how the horsepower absorption by the transmitted oil and the deflected oil reacts to the change in the penetration ratio in the high speed region. Next, we shall examine it in more detail from the viewpoint of heat exchange between the bearing and oil. /23

When the bearing reaches a normal condition, the amount of heat generated by the bearing friction will be equal to the amount of heat radiated from the bearing. There are two kinds of heat radiated from the bearing; one is the heat radiated into the surrounding air by convection, radiation, or heat conduction of the bearing box and the shaft, and the other is the heat carried away by oil while lubricating oil is passing inside the bearing. In jet lubrication using a large quantity of oil, the former can be safely ignored. Consequently, if we let friction generated heat per unit time in the bearing be H , then the following relation holds:

$$H = C_p Q (T_L - T_I) \quad (11)$$

where C_p is the specific heat of the lubrication oil, Q is the lubrication oil flow rate per unit time, T_L is the outlet temperature of the lubrication oil, and T_I is the inlet temperature of the lubrication oil. /24

If we let h be overall thermal conductivity of the bearing, then from Equation (11), we have [6]

$$\left. \begin{aligned} h &= \frac{H}{T_B - T_a} = \eta_o C_p Q \\ \eta_o &= \eta_I \eta_S \\ \eta_I &= \frac{T_B - T_I}{T_B - T_a} \\ \eta_S &= \frac{T_L - T_I}{T_B - T_I} \end{aligned} \right\} \quad (12)$$

where T_B is the bearing outer race temperature, T_a is the outside air temperature, η_E is the heat exchange efficiency of lubricating oil, and η_I is the efficiency due to the difference between the inlet oil temperature and the outside air temperature.

As oil is discharged from both faces of the bearing in a jet lubrication, η_E in Equation (12) can be expressed by the following, taking into consideration the transmitted and deflected flows of lubricating oil inside the bearing:

$$\left. \begin{aligned} \eta_E &= K \left(\frac{T_{LP} - T_I}{T_B - T_I} - \frac{T_{LR} - T_I}{T_B - T_I} \right) + \frac{T_{LR} - T_I}{T_B - T_I} \\ &= K(\eta_P - \eta_R) + \eta_R \\ \eta_P &= \frac{T_{LP} - T_I}{T_B - T_I} \\ \eta_R &= \frac{T_{LR} - T_I}{T_B - T_I} \end{aligned} \right\} \quad (13)$$

where T_{LP} is the outlet oil temperature of lubricating oil on the transmitted side, T_{LR} is the outlet oil temperature of lubricating oil on the deflected side, K is the penetration ratio, η_P is the heat exchange efficiency of the transmitted oil, and η_R is the heat exchange efficiency of the deflected oil.

From Equation (12), $\eta_I \eta_E C_p Q$ should be increased to increase the effect of cooling by oil and to lower the bearing temperature rise. Although there is no problem in increasing η_I by lowering the inlet oil temperature, there is a limit. As the specific heat of lubricating oil is constant at approximately 0.4 - 0.6 kcal/kg · °C. it is better to increase Q . But, as will be mentioned later, an increase in Q results in a decrease in η_E , so that h does not increase exactly as shown by an exponent of Q in Equation (2). The most effective way would be to increase Q and, at the same time, increase η_E .

Table 5 shows the heat exchange efficiencies of lubricating oil, η_E , η_R , and η_P , calculated by Equation (13), using the data in Table

TABLE 5. HEAT EXCHANGE EFFICIENCIES OF OIL η_R , η_P , η_E ,
AND SHAFT SPEED
(30° C inlet oil temperature and 50 kg thrust load)

Shaft speed rpm	η_R %					
	Oil flow rate kg/min					
	3	1.8	1	0.72	0.44	0.2
20,000	78.5	84.2	88.9	93.8	100	100
30,000	78.2	86.2	90.5	90	96.9	96.6
40,000	72.7	83.7	87.9	89.9	95.4	95.8
50,000	67.4	75.4	78.3	87.1	91.5	93.8
60,000	60.9	66.3	68.2	78	84.4	89.4
70,000	56.3	57.6	59.7	72.5	74.0	
80,000	53.7	55.7	55.2	70.3		

Shaft speed rpm	η_P %					
	Oil flow rate kg/min					
	3	1.8	1	0.72	0.44	0.22
20,000	78.5	84.2	85.2	87.5	87.5	91.5
30,000	78.2	82.7	83.3	84	86.2	91
40,000	78.8	79.1	84.5	81.2	84.1	90.8
50,000	85.7	90.2	95.2	87.1	96.6	99.4
60,000	100	101.2	106.4	90.6	106	101.8
70,000	101	108	109	98.2	104.8	
80,000	111	108.5	110.5	104		

Shaft speed rpm	η_E %					
	Oil flow rate kg/min					
	3	1.8	1	0.72	0.44	0.22
20,000	78.5	84.2	86.8	89.8	92.7	95.4
30,000	78.2	84.6	87.2	86.8	91.5	94.1
40,000	74.9	82.1	86.7	86.2	90.8	93.9
50,000	73.1	80.2	83.6	87.1	93.5	96.1
60,000	72.3	78.6	80.6	83.4	93.7	94.6
70,000	68.9	72.7	76.4	82.8	84.9	
80,000	68.9	70.5	73.6	82.8		

3. Figures 42, 43, 44, 45, 46, and 47 show the penetration ratio K and the heat exchange efficiencies of oil η_E , η_R , and η_P as a function of speed N from the data in Tables 3 and 5. Whereas the heat exchange efficiency of the deflected oil η_R decreases with an

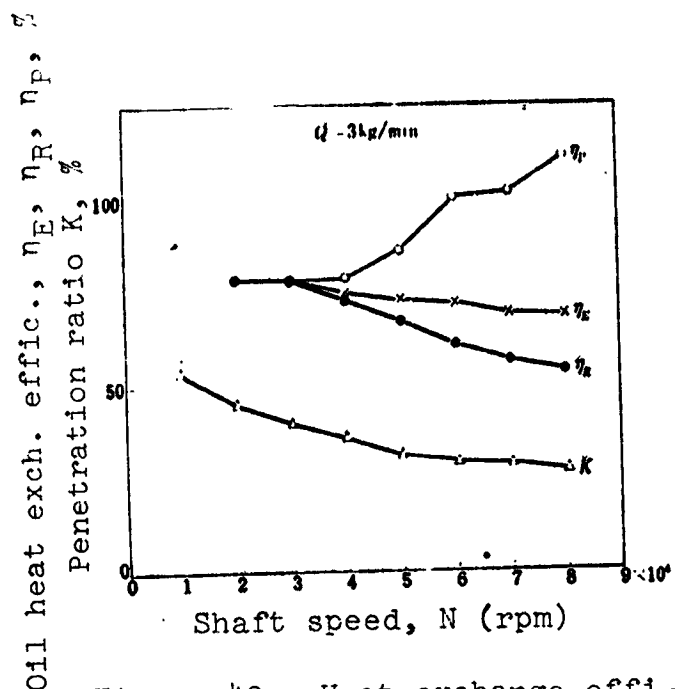


Figure 42. Heat exchange efficiency of oil and penetration ratio versus shaft speed

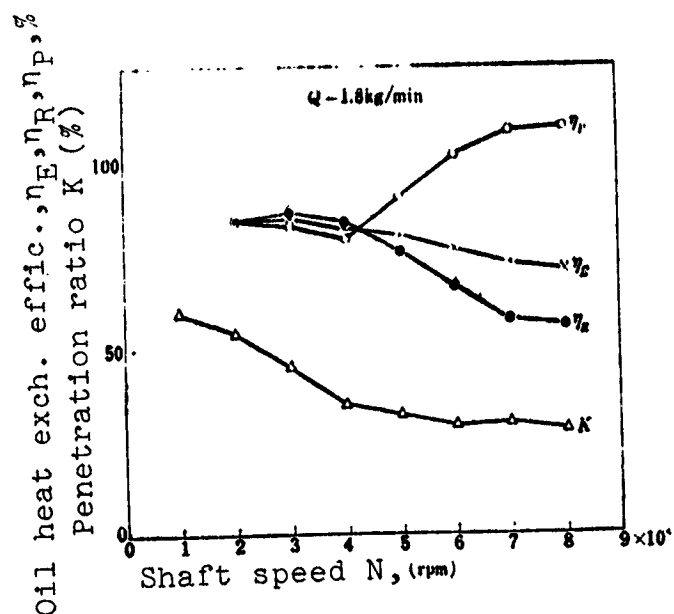


Figure 43. Heat exchange efficiency of oil and penetration ratio versus shaft speed

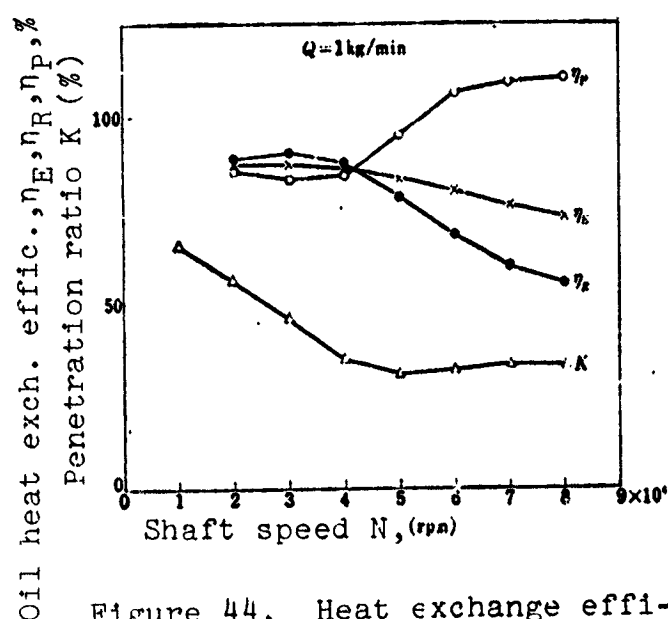


Figure 44. Heat exchange efficiency of oil and penetration ratio versus shaft speed

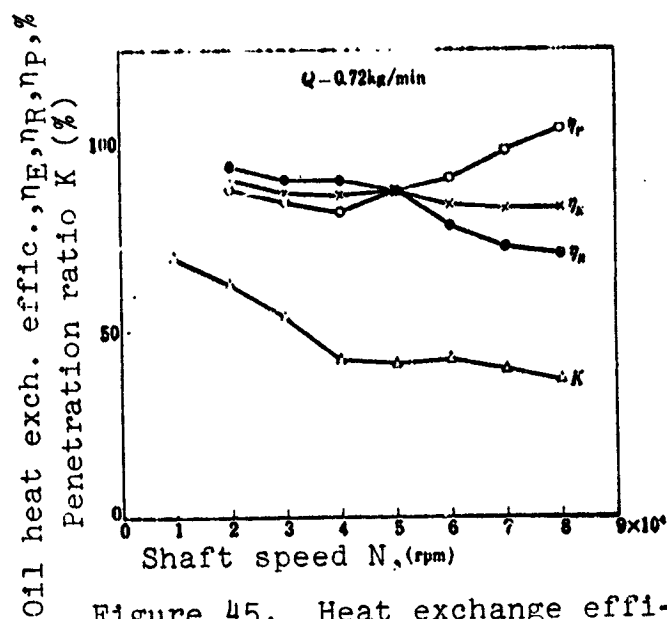


Figure 45. Heat exchange efficiency of oil and penetration ratio versus shaft speed

increasing speed, the heat exchange efficiency of the transmitted oil η_P rapidly increases with increasing speed, reaching 100% or more for each oil flow at high speed. η_P of more than 100% means that at high speed, the temperature of the cage and the roller body

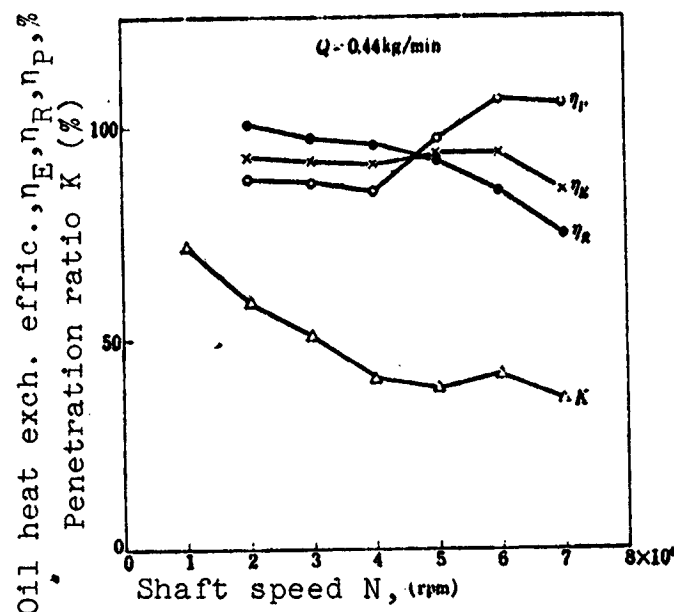


Figure 46. Heat exchange efficiency of oil and penetration ratio versus shaft speed

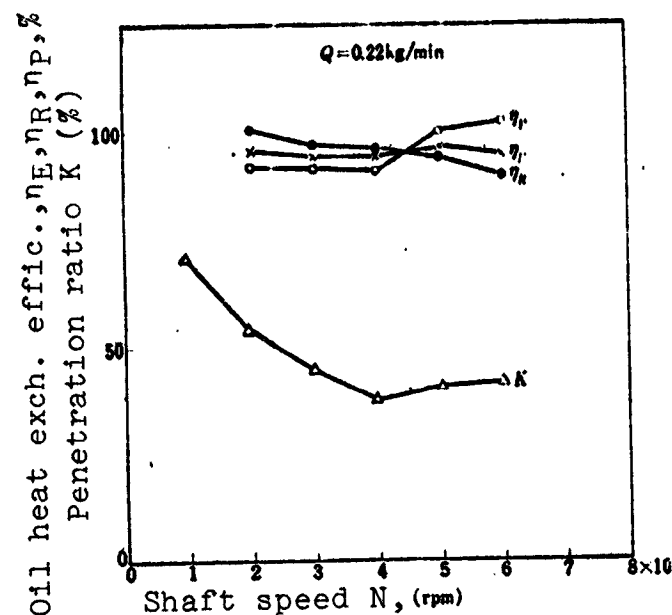


Figure 47. Heat exchange efficiency of oil and penetration ratio versus shaft speed

is higher than the bearing outer race temperature and the transmitted oil temperature becomes higher than the bearing outer race temperature. Thus, at high speed, η_P is extremely large compared to η_R , and the cooling effect of the transmitted oil is quite large. Because the penetration ratio decreases to roughly 30%, and the amount of the transmitted oil decreases at high speed, the total heat exchange efficiency of lubricating oil η_E increases by only 10 - 30% over η_R . Therefore, it is still possible to increase η_E by increasing the penetration ratio. As shown in Figures 42 - 47, as oil flow decreases, η_R increases, and with oil flow of 0.22 kg/min, η_R is nearly equivalent to η_P . As a result, η_E increases with a decreasing oil flow. It shows that, when oil flow is large, the percentage of oil flow actually performing effective heat exchange by contacting the bearing surface is small, and this percentage increases with a decreasing oil flow.

As can be seen in Figures 42 - 47, η_E varies with speed and oil flow. An approximate relationship between the average value of η_E and oil flow Q in the high speed region is shown in Figure 48. As mentioned before, η_E increases with decreasing oil flow. From Figure 48, the relation between η_E (%) and oil flow Q (kg/min) can be expressed by

$$\eta_E = 82Q^{-0.18} \quad (14)$$

In order to reduce the bearing temperature rise of the high-speed roller bearing, the oil flow must be increased. On the other hand, since increased oil flow causes a decrease in η_E , η_E must also be increased by increasing the penetration ratio. The preliminary experiment concerning a jet lubrication, such as the oil jet velocity, in the previous chapter

was conducted from such a viewpoint. The penetration ratio is an important factor affecting the heat exchange efficiency of oil and the bearing temperature. The greater the penetration ratio, the greater becomes the heat exchange efficiency, and the smaller becomes the bearing temperature rise. Although the penetration ratio affects the bearing temperature rise, it is not necessarily related to the limiting speed, as will be mentioned in the next chapter.

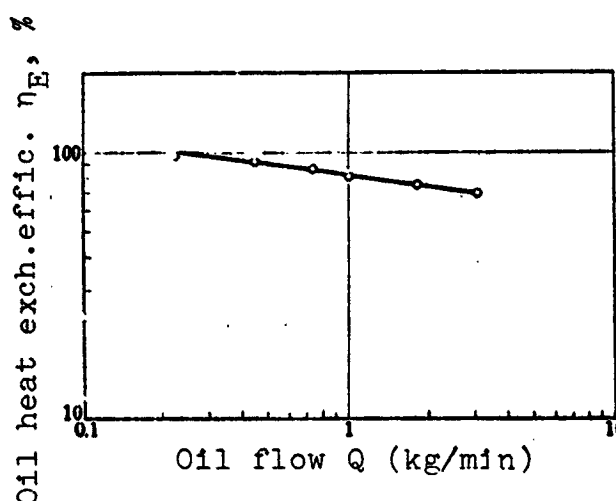


Figure 48. Heat exchange efficiency of oil and oil flow

4.8. Bearing Friction

Figure 49 shows the friction torque as a function of speed for each oil flow rate from the data in Table 3. The friction torque increases with increasing speed, but decreases with decreasing oil flow. Figure 49 is for the case of a 50 kg thrust load. If the load

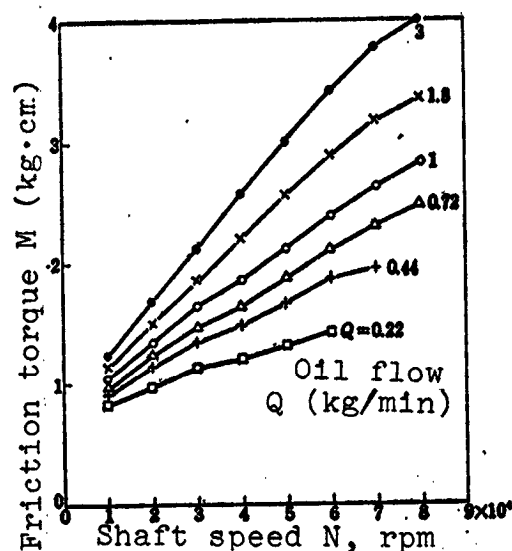


Figure 49. Friction torque and shaft speed

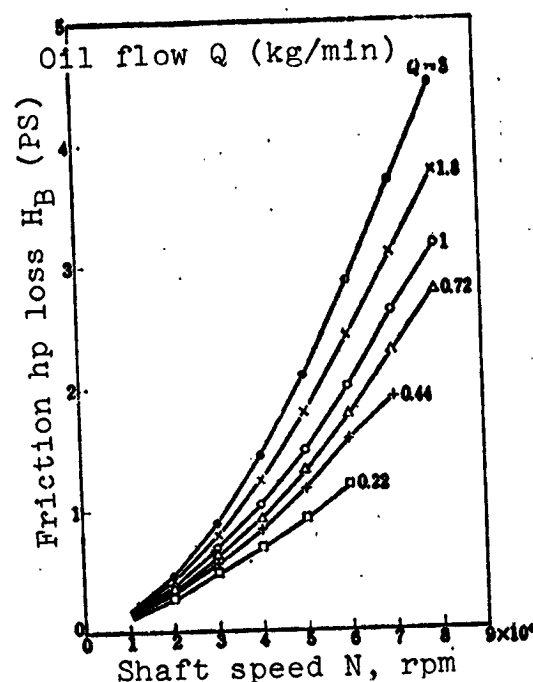


Figure 50. Friction horsepower loss and shaft speed

is increased, the friction torque will increase also, but the behavior as a function of oil flow and speed are identical with Figure 49. Figure 50 shows the friction horsepower loss obtained from the friction torque in Figure 49 as a function of speed for each oil flow rate. In order to reduce the bearing temperature rise at high speed, a large quantity of oil must be supplied, but the friction horsepower loss correspondingly increases, reaching 4.5 PS at 80,000 rpm speed and 3 kg/min oil flow. Compared to the horsepower absorption by oil in Figure 30, they are of about the same magnitude, indicating that most of frictional heat is carried away by oil, although there are some differences depending on the magnitude of oil flow.

4.9. Friction Characteristics of the High Speed Roller Bearing

As most of the bearing frictional heat is removed by oil in jet lubrication with a large amount of oil flow, the bearing temperature is roughly determined from the relationship between them. The friction force or the friction-generated heat of the high speed roller bearing will be the main problem here.

In the relatively low speed experiment by Hirano [7], the frictional force F and the friction generated heat H with large oil flow jet lubrication are approximated by

$$F = C_1 Z_B N \quad (15)$$

$$H = C_2 Z_B N^3 \quad (16)$$

where Z_B is oil viscosity at the bearing temperature, N is the shaft speed, and C_1 and C_2 are constants. The above results also hold in the low speed experiment by Soda and others [8].

Based on the above results, let us discuss friction torque in the case of high dn values in Figure 49. In the group of friction torque curves in Figure 49, at the identical speed, the friction torque is greater for greater oil flow. This can be thought of as the effect of viscosity change due to oil flow change, rather than the effect of oil flow itself. As the bearing temperature is roughly inversely proportional to $(\text{oil flow})^{1/2}$ from Equation (2), at the identical speed, the bearing temperature becomes lower as oil flow increases (fig. 40); in other words, viscosity Z_B becomes greater. Thus, the behavior of the friction torque curves with respect to oil flow and speed confirm Equation (15). In order to verify this, friction torque in Figure 49 is rearranged using the product $Z_B N$ — where Z_B is viscosity at the bearing temperature and N is the shaft speed — as a parameter, and the result is shown in Figure 51. With increasing speed, $Z_B N$ increases, but above a certain speed, $Z_B N$ decreases with an increasing N . This critical $Z_B N$ value, the point at which $Z_B N$ starts to decrease as N increases, shifts toward greater $Z_B N$ as oil flow rate increases. Since the bearing temperature rise increases in proportion to $N^{1.44-1.7}$, shown in Equation (1), the percentage decrease in viscosity due to the temperature rise becomes greater than the percentage increase in N at high speed, and, on the whole, $Z_B N$ decreases as N increases. As the bearing temperature rise decreases with an increasing oil flow, the critical $Z_B N$ value shifts

/30

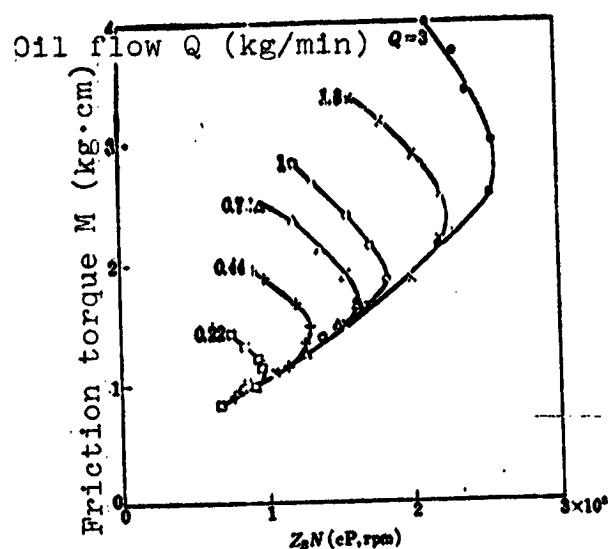


Figure 51. Friction torque and $Z_B N$

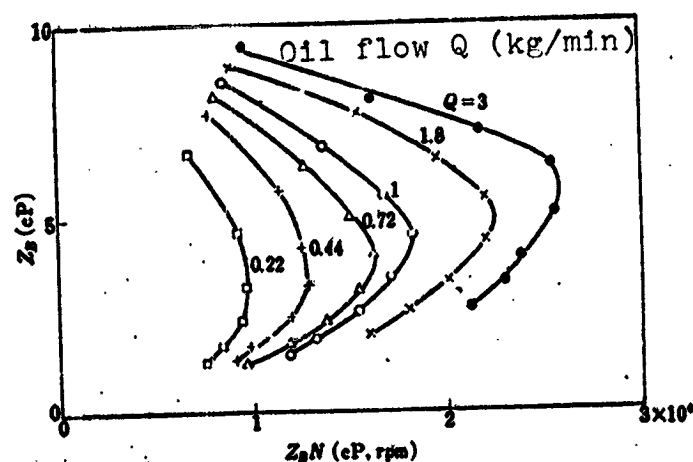


Figure 52. Viscosity at the bearing temperature and $Z_B N$

correspondingly to the greater value. In regard to the friction torque corresponding to this change in $Z_B N$, in the region in which $Z_B N$ increases with an increasing N , friction torque also increases with N and up to the critical $Z_B N$ value. It lies on a single straight line regardless of oil flow. On the other hand, in the region in which $Z_B N$ decreases with an increasing N , friction torque increases despite decreasing $Z_B N$. Up to the critical $Z_B N$ value, friction torque can be roughly expressed by $Z_B N$, regardless of oil flow. However, at high speed with an excessive increase in the temperature rise and a decrease in viscosity, friction torque cannot be only expressed by $Z_B N$. This critical value is also affected by the magnitude of the oil flow. Figure 52 shows the viscosity at the bearing temperature Z_B for each point in Figure 51 as a function of $Z_B N$. Irrespective of oil flow, the critical point of viscosity at which friction torque starts to deviate from the $Z_B N$ straight line is always in the neighborhood of 5 cP. From this, it can be said that, when the viscosity at the bearing temperature is above 5 cP, the bearing friction is primarily governed by the viscous friction,

whereas when the viscosity is below 5 cP, the boundary friction greatly enters into the picture, causing a deviation and increase of friction torque. Hirano [6] estimated the safe lower limits of Z_B as 10 cP by studying the oil film formation in the measurement of electrical resistance in various parts of the roller bearing. Absolute values of Z_B may be slightly different due to the effects of bearing precision and type, but qualitatively they are in agreement.

The above conclusions based on the friction experiments seem to be reasonable at first glance, but when their content is studied in more detail, many unconvincing points appear. First of all, the lower limit of Z_B as 5 cP is too large, considering an introduction of the boundary friction. For example, most of the ball bearings for the main bearing of jet engines are used at much lower viscosity condition. If the boundary friction is to start below 5 cP, then the sliding contact portions of the cage should rapidly wear out and become unusable in a very short time. But in reality, a jet engine operates safely. The second problem is in regard to the range within which Equation (15) — that is, the proportionality of frictional force to viscosity and speed — holds. Even if Equation (15) can be applied to an experiment in which the dn value is 10×10^4 , there is a question as whether it holds when the dn value is up as high as 200×10^4 or greater. Yamada and others [9] measured the friction torque of cylindrical roller bearing #215 for dn values of up to 120×10^4 , and found the friction torque to be a function of Z_B and N with a certain exponent. Although the bearing friction is a basic factor which determines the bearing temperature rise and other factors, experiments which measure friction are very rare, and, in particular, there is no experiment which measured it for dn values of up to 250×10^4 . Until this friction characteristic is confirmed by experiments, it is dangerous to reach a conclusion. Consequently, the characteristics of friction torque will be discussed in more detail in the next section. /31

4.10. Various Factors Affecting Friction Torque

The friction torque shown previously is measured by keeping oil flow constant, but varying the shaft speed. In order to clarify the friction torque characteristics, the manner in which viscosity at the bearing temperature affects the friction torque must be investigated. For this purpose, inlet oil temperature is varied from 30° C to 120° C while maintaining constant speed, and the relation between the viscosity at the bearing outer race temperature Z_B and the friction torque for each oil flow are examined. The results are shown in Figures 53, 54, 56, and 57. For the relation between the friction torque M and Z_B , an exponent of Z_B increases as speed decreases. On the average, in the relatively high speed region, it can be expressed by

$$M \propto Z_B^{0.4}$$

(17)

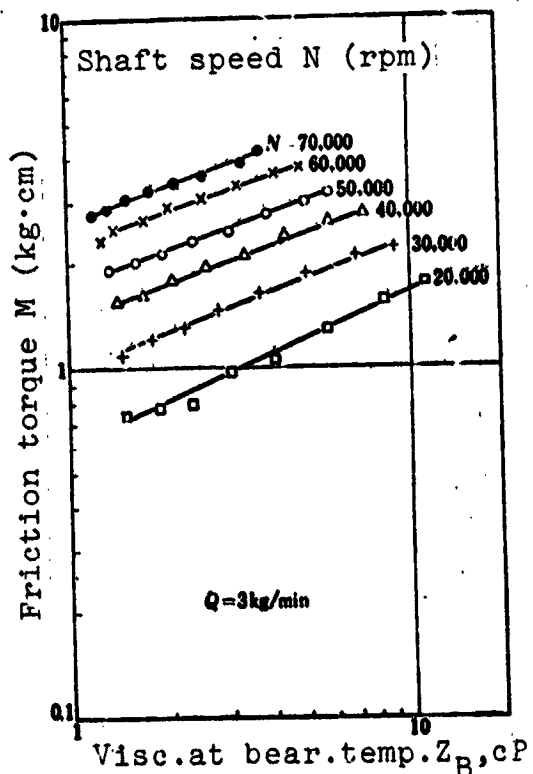


Figure 53. Friction torque and viscosity at the bearing temperature

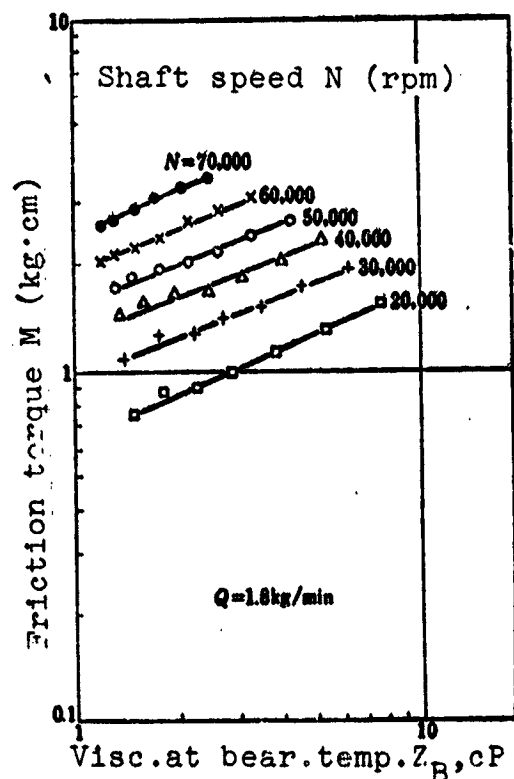


Figure 54. Friction torque and viscosity at the bearing temperature

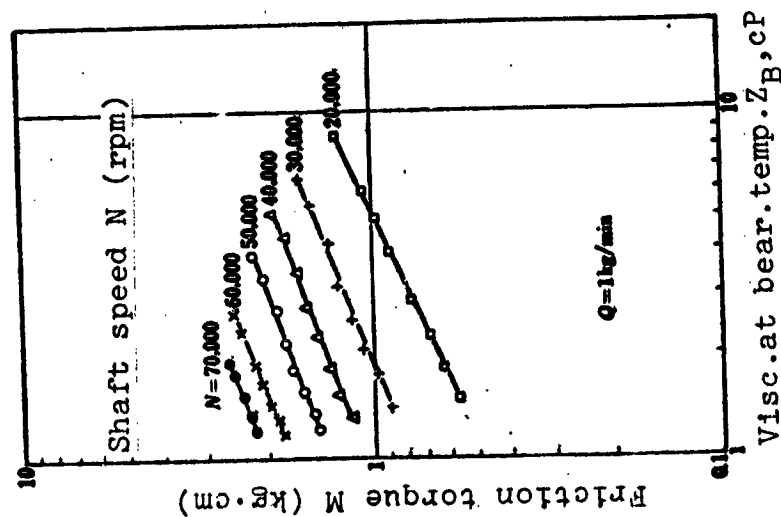


Figure 55. Friction torque and viscosity at the bearing temperature

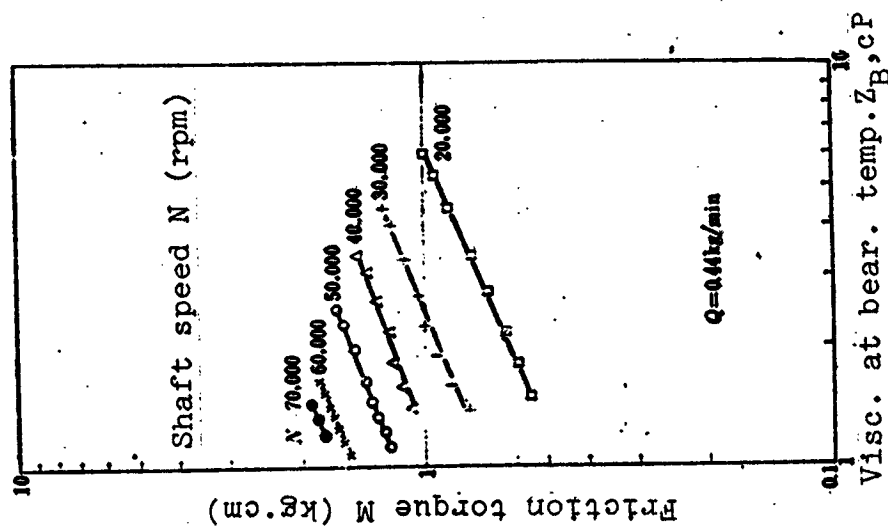


Figure 56. Friction torque and viscosity at the bearing temperature

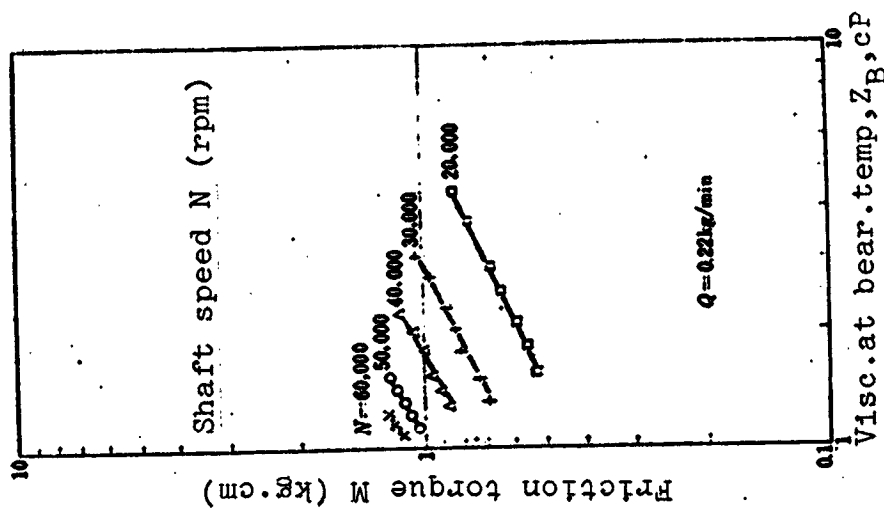


Figure 57. Friction torque and viscosity at the bearing temperature

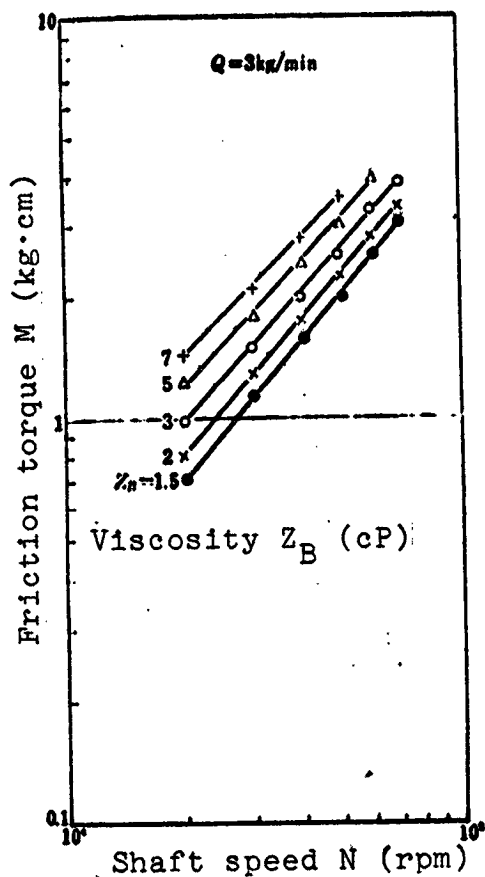


Figure 58. Friction torque and shaft speed

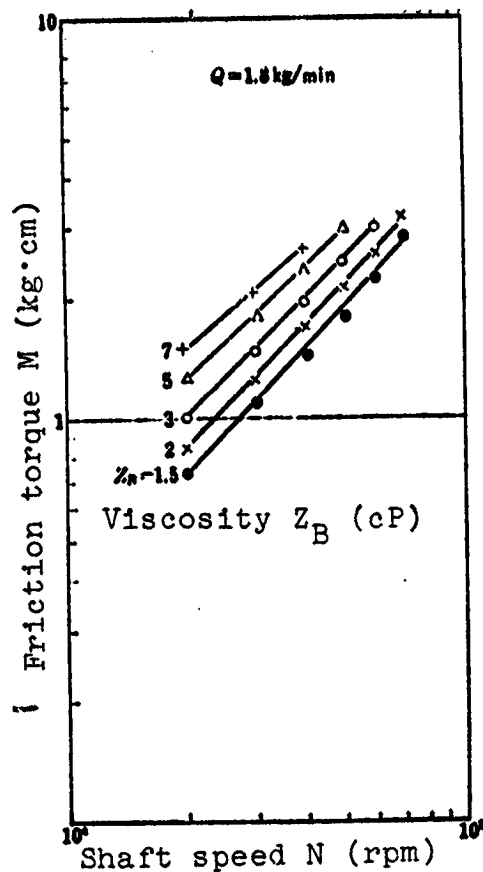


Figure 59. Friction torque and shaft speed

From the above series of curves for M and Z_B , the relation between M and N can be obtained for a fixed Z_B . This is shown in Figures 58, 59, 60, 61, and 62. The average when Z_B is small — that is, when $T_B - T_I$ is large — can be expressed as

$$M \propto N^{1.1}$$

(18)

Figure 63 shows the effect of oil flow on the friction torque when N and Z_B are fixed. As the experiment this time is conducted with each factor separated, there is a difference in content compared to the effect of oil flow accompanying a change in the bearing temperature which appeared in Figure 49. The effect of oil flow can be

/34

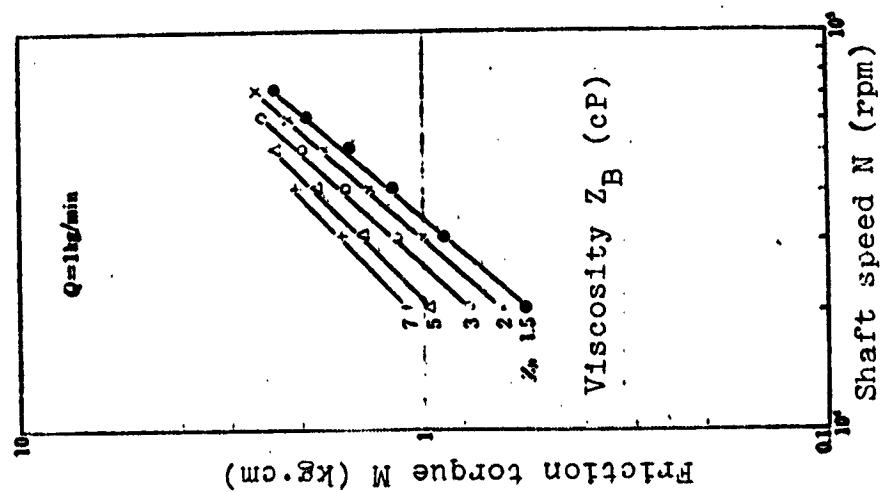


Figure 60. Friction torque and shaft speed

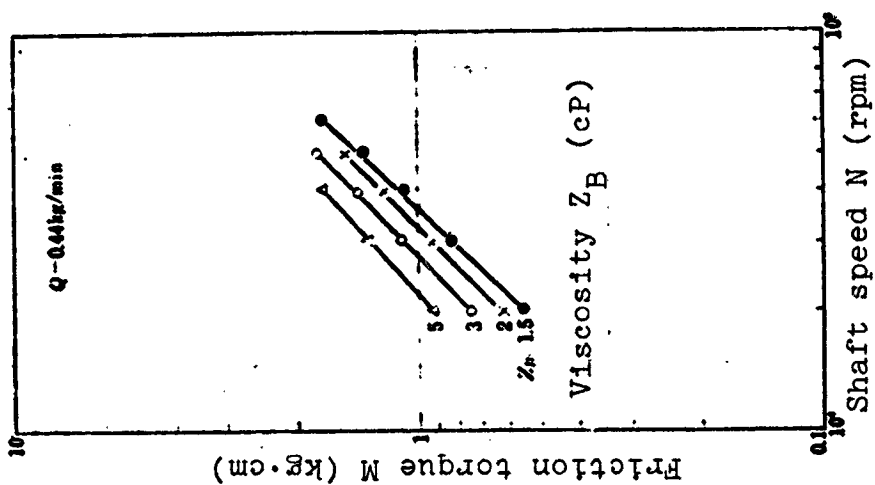


Figure 61. Friction torque and shaft speed

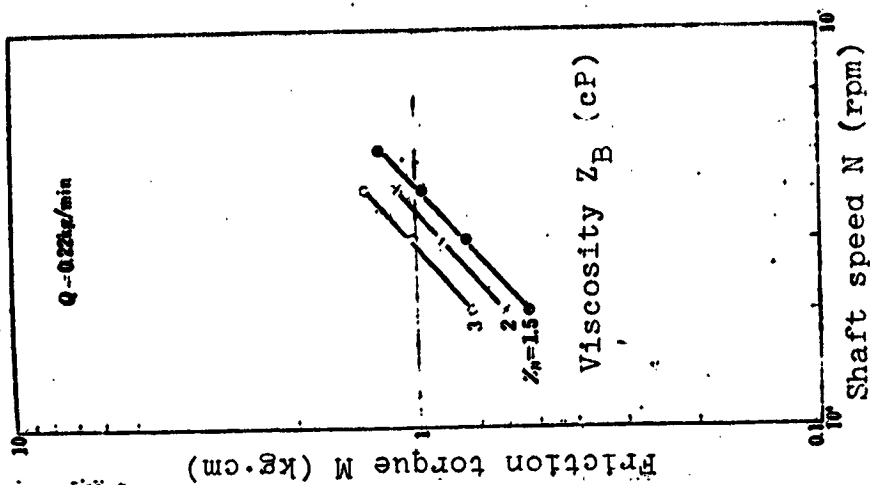


Figure 62. Friction torque and shaft speed

considered to be genuinely based on the churning resistance of oil inside the bearing. From Figure 63, the following approximation holds:

$$M \propto Q^{0.2} \quad (19)$$

Summarizing, unlike Equation (15), the friction torque at high dn values can be approximated by the following formula containing Q :

$$M \propto Z_B^{0.4} N^{1.2} Q^{0.2} \quad (20)$$

If the friction curves in Figure 49 are arranged according to Equation (20), they should fall on a single line. Figure 64 is the result of obtaining the viscosity at the bearing temperature Z_B for each point in

Figure 49, and arranging, using $Z_B^{0.4} N^{1.2} Q^{0.2}$ in Equation (20). As shown in Figure 51, the friction torque M branches off depending on oil flow when correlated with $Z_B N$, but when arranged with $Z_B^{0.4} N^{1.2} Q^{0.2}$, they fall on a single line. At 10,000 rpm, a slight deviation from this straight line occurred, but that is expected, as Equation (20) is assumed to hold in a relatively high speed region. Under the friction conditions of 80,000 rpm maximum speed, 240×10^4 maximum dn value, 1.5 cP minimum viscosity at the bearing temperature, and 0.22 - 3 kg/min oil flow, viscous friction primarily controls the bearing friction, and the friction torque up to the high dn value of 240×10^4 can be generally expressed by Equation (20). The fact that it is applicable up to the minimum viscosity of 1.5 cP requires a new

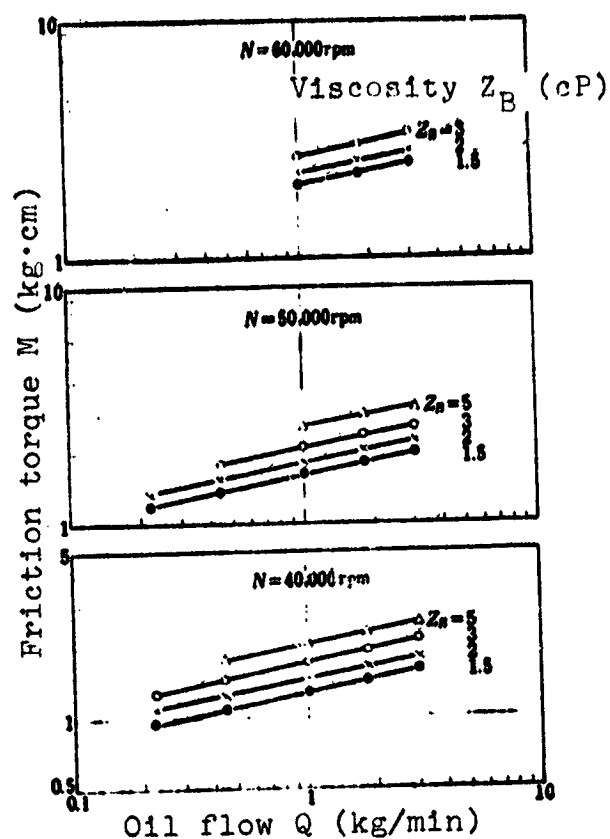


Figure 63. Friction torque and oil flow

interpretation of the physical meaning of the critical viscosity (10 cP) reported by Hirano in the previous section. This can be understood by the following explanation. The critical viscosity is not just determined by a single factor, but rather it is affected by the friction conditions such as load and speed, just as for the sliding bearing. In fact, the critical viscosity of 10 cP by Hirano is estimated from the low speed experiment, and it cannot be applied as is to the high speed condition. It became clear from this experiment that at high speeds a quite safe operation can be performed even in the neighborhood of the low viscosity of 1.5 cP.

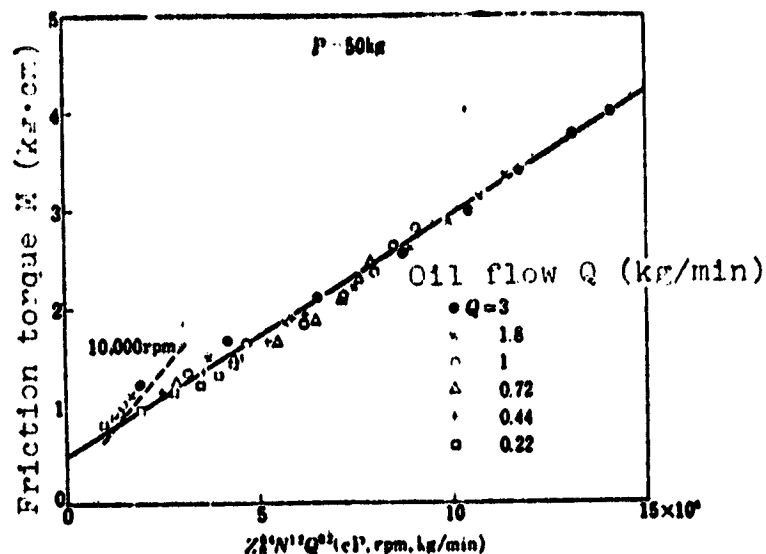


Figure 64. Friction torque, viscosity, shaft speed, and oil flow

Figures 65, 66, 67, 68 show the similarly arranged results for friction torque under a thrust load other than 50 kg. Just as for a 50 kg load, Equation (20) holds for other loads also. The case for 10,000 rpm is omitted because of the deviations. These results are summarized in Figure 69. It can be seen that the friction torque M consists of a velocity term M_v which increases with an increasing Z_B , N , and Q , and a non-velocity term which increases with an increasing bearing load. As is clear from Figure 69, at high dn values, the velocity term makes up most of the friction torque and the percentage contribution of the non-velocity term is extremely small. A percentage increase in the non-velocity term due to a load increase is also small. The fact that the exponent of P 0.13 - 0.17 was extremely small compared to the exponent of N 1.44 - 1.7 in the experimental equation for the bearing temperature rise [Equation (5)] is based on the above friction characteristics. Although the velocity term of

friction torque M_v slightly changes with load in Figure 69, it can be assumed to be roughly constant. M_v (kg · cm) can then be expressed on the average by

$$M_v = 2.5 \times 10^{-3} Z_p^{0.4} N^{0.4} Q^{0.4} \quad (21)$$

where Z_p is in cP, N in rpm, and Q in kg/min.

On the other hand, the non-velocity term of friction torque, M_p (kg · cm), varies as a function of the thrust load P as shown in Figure 70, and can be expressed by

$$M_p = 7 \times 10^{-3} P^{0.4} \quad (22)$$

where P is in kg.

The friction torque M (kg · cm) then becomes

$$M = M_p + M_v = 7 \times 10^{-3} P^{0.4} + 2.5 \times 10^{-3} Z_p^{0.4} N^{0.4} Q^{0.4} \quad (23)$$

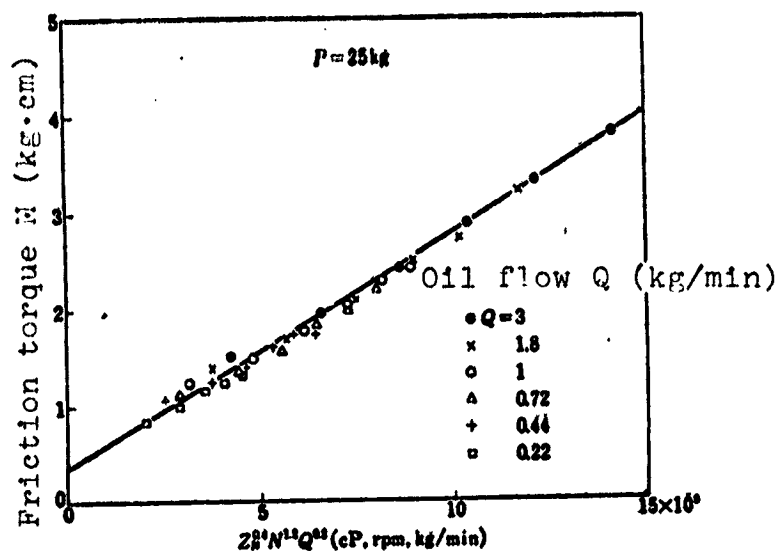


Figure 65. Friction torque, viscosity, shaft speed and oil flow

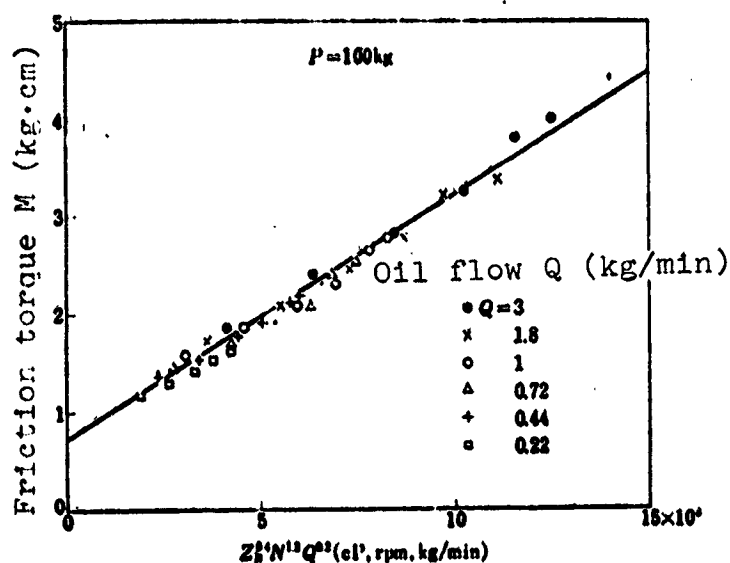


Figure 66. Friction torque, viscosity, shaft speed, and oil flow

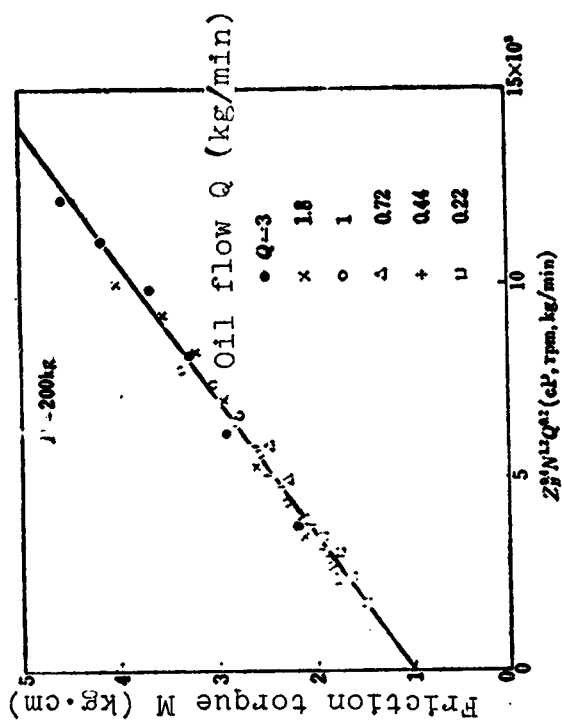


Figure 68. Friction torque, viscosity, shaft speed and oil flow

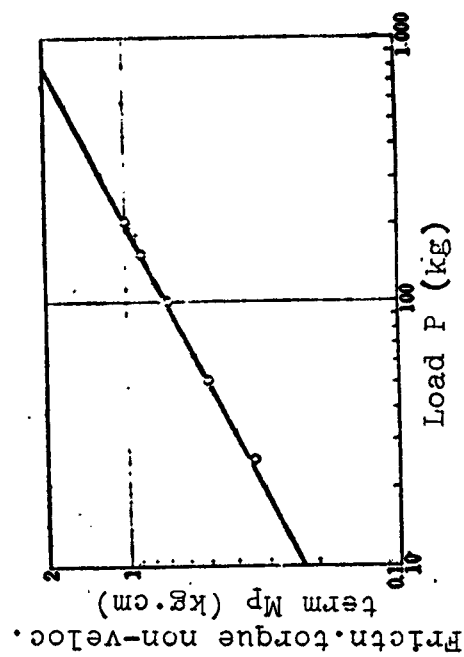


Figure 70. Non-velocity term of friction torque and load

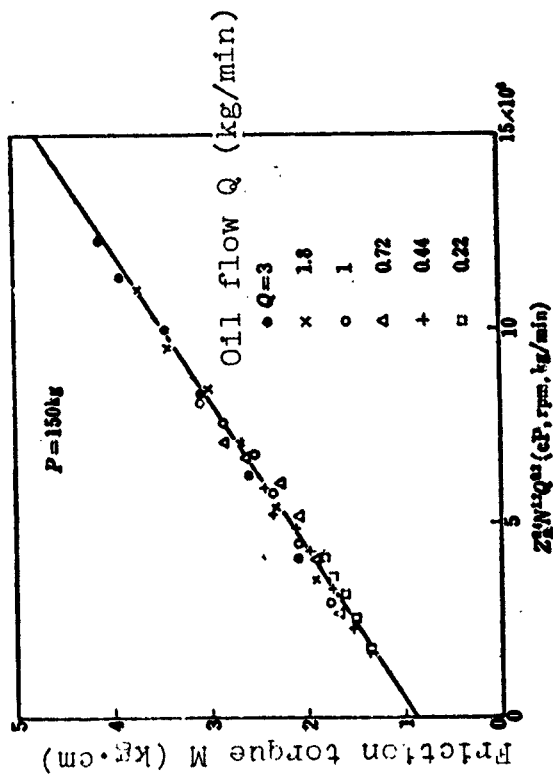


Figure 67. Friction torque, viscosity, shaft speed and oil flow

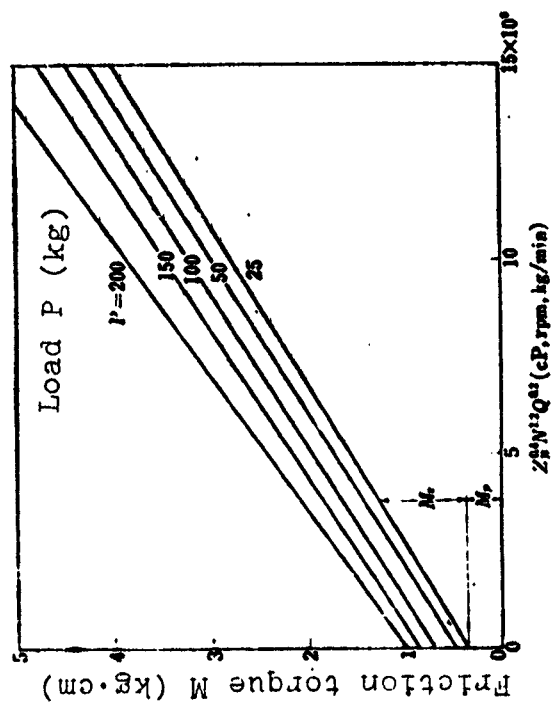


Figure 69. Friction torque, viscosity, shaft speed and oil flow

The bearing friction horsepower loss H_B (PS) is calculated from Equation (23) as follows:

$$H_B = 9.8 \times 10^{-7} P^{0.5} N + 3.5 \times 10^{-11} Z_B^{0.4} N^{0.3} Q^{0.3} \quad (24)$$

where P is in kg, Z_B in cP, N in rpm, and Q in kg/min, just like Equation (23) for the friction torque.

4.11. Equation for Estimating the Bearing Temperature Rise

In the previous section, an experimental equation for the friction power loss was determined. Based on this friction power loss, the bearing temperature may be stipulated. As mentioned before, most of frictional heat is carried away by the oil in large-oil-flow jet lubrication. Therefore, by substituting Equation (24) in Equation (11) and using Equation (13), the bearing temperature rise can be established as

$$\frac{5.691}{60} \eta_E C_p Q (T_B - T_I) = 9.8 \times 10^{-7} P^{0.5} N + 3.5 \times 10^{-11} Z_B^{0.4} N^{0.3} Q^{0.3} \quad (25)$$

As the heat exchange efficiency of lubricating oil η_E varies with oil flow Q and its relation is given by Equation (14), the bearing temperature rise can be shown by the following for the specific heat of oil C_p of 0.5 kcal/kg \cdot $^{\circ}\text{C}$:

$$(T_B - T_I) = 2.5 \times 10^{-6} P^{0.5} N Q^{-0.66} + 9 \times 10^{-10} Z_B^{0.4} N^{0.3} Q^{-0.66} \quad (26)$$

Here, if

$$\frac{Z_B}{Z_I} \propto (T_B - T_I)^{-0.66} \quad (27)$$

holds, then $T_B - T_I$ can be determined. Z_I is oil viscosity at the inlet oil temperature.

Figure 71 shows the relation between $T_B - T_I$ and Z_B/Z_I calculated from the viscosity-temperature curve in Figure 4 when the inlet oil temperature T_I is 30°C . It is seen that from Figure 71, Equation (27) holds corresponding to the range of $T_B - T_I$. This relation holds in about the same way when the inlet oil temperature is varied. From Figure 71, Equation (27), corresponding to the temperature range of $T_B - T_I$ can be expressed by the following:

- (1) when $T_B - T_I$ is $7 - 20^\circ \text{C}$,

$$Z_B = 1.6 Z_I (T_B - T_I)^{0.33} \quad (28)$$

- (2) when $T_B - T_I$ is $15 - 40^\circ \text{C}$,

$$Z_B = 3.5 Z_I (T_B - T_I)^{0.3} \quad (29)$$

- (3) when $T_B - T_I$ is $35 - 120^\circ \text{C}$,

$$Z_B = 14 Z_I (T_B - T_I)^{-1} \quad (30)$$

where Z_B and Z_I are in cP, and T_B and T_I are in $^\circ \text{C}$.

By substituting the above equations into Equation (26), the bearing temperature rise can be obtained. From the range of the bearing temperature rise shown in Figure 24, Z_B in Equation (29) or Equation (30) is to be used depending on the magnitude of $T_B - T_I$. The following equations for the bearing temperature rise ($^\circ \text{C}$) are

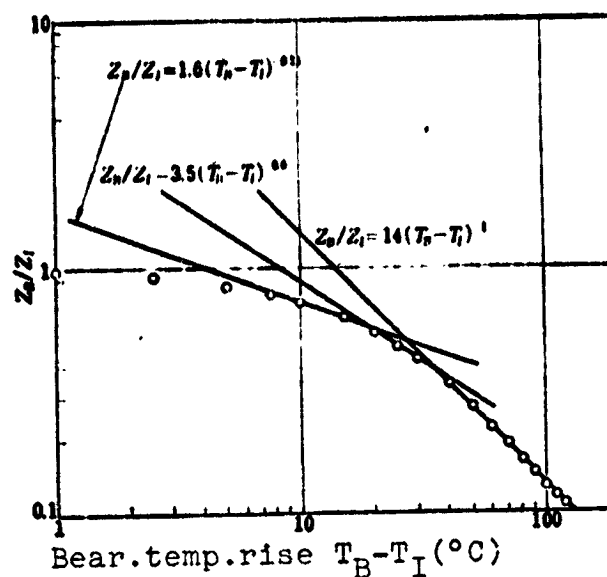


Figure 71. Bearing temperature rise and Z_B/Z_I

derived by substituting Equation (29) or Equation (30) into Equation (26):

/40

(1) when $T_B - T_I$ is small (15 - 40° C),

$$T_B - T_I = 2.3 \times 10^{-4} P^{0.41} N^{0.51} Q^{-0.79} (T_B - T_I)^{0.10} + 7.6 \times 10^{-5} Z_I^{0.33} N^{1.78} Q^{-0.33} \quad (31)$$

(2) when $T_B - T_I$ is large (35 - 120° C),

$$T_B - T_I = 5.2 \times 10^{-4} P^{0.38} N^{0.73} Q^{-0.51} (T_B - T_I)^{0.09} + 7.4 \times 10^{-7} Z_I^{0.33} N^{1.58} Q^{-0.46} \quad (32)$$

Consequently, the bearing temperature rise can be obtained by solving Equation (31) or Equation (32) depending on the magnitude of $T_B - T_I$. The first term in Equation (31) or (32) is based on the non-velocity term, which varies with load, or friction torque, while the second term is based on the velocity term. As the non-velocity term is extremely small, compared to the velocity term at high speed, the first term in Equations (31) and (32) may be omitted, and the bearing temperature rise (°C) then becomes as follows:

(1) when $T_B - T_I$ is small (15 - 40° C),

$$T_B - T_I = 7.6 \times 10^{-5} Z_I^{0.33} N^{1.78} Q^{-0.33} \quad (33)$$

(2) when $T_B - T_I$ is large (35 - 120° C),

$$T_B - T_I = 7.4 \times 10^{-7} Z_I^{0.33} N^{1.58} Q^{-0.46} \quad (34)$$

Depending on the magnitude of $T_B - T_I$, the exponents of Z_I , N , and Q vary from 0.29 to 0.32, 1.58 to 1.78, and -0.46 to -0.53, respectively. There is a good correspondence to the experimental equation for the bearing temperature rise [Equation (5)] in which the exponents of Z_I , N , and Q vary from 0.25 to 0.5, 1.44 to 1.7, and -0.41 to -0.58, respectively, depending on the magnitude of $T_B - T_I$. As the exponents in Equations (28), (29), and (30) decrease as the oil viscosity exponent increases, the exponent of each factor above increases as the viscosity exponent of oil used increases.

The relationship between the bearing temperature rise and Z_I , N , and Q is thus explained based on the equation for the friction power loss. The experimental equation for the bearing temperature rise (5) contains load P , but Equations (33) and (34) do not contain P . This is because (33) and (34) have omitted the first term in Equations (31) and (32) based on the non-velocity term of friction torque which varies with the load. If the load is included, Equation (31) or (32) must be directly solved. In this case then, the bearing temperature rise cannot be expressed by a simple form, such as the experimental equation for the bearing temperature rise (5). However, it can be approximated to the form of Equation (5) for the bearing temperature rise as follows. As friction power loss can be expressed by Equation (24), if it is arranged with $Z_B^{0.4} N^{2.2} Q^{0.2}$, it should fall on a single curve for each load. Figures 72, 73, 74, 75, and 76 are the results of arranging friction power loss for each load with $Z_B^{0.4} N^{2.2} Q^{0.2}$, and they indicate that Equation (24) holds. Figure 77 is a summary of Figures 72 - 76. An increase in a straight line slope with an increasing load is due to the first term of Equation (24). The friction power loss as a function of load for $Z_B^{0.4} N^{2.2} Q^{0.2}$ of 3×10^{10} , 5×10^{10} , 7×10^{10} , and 9×10^{10} is shown in Figure 78, and /44 the following approximation results:

$$H_B \propto P^{0.17} \quad (35)$$

Thus, the friction power loss H_B (PS) can also be approximated by the following equation, instead of Equation (24):

$$\begin{aligned} H_B &= 3.8 \times 10^{-11} \left(\frac{P}{25} \right)^{0.17} Z_B^{0.4} N^{2.2} Q^{0.2} \\ &= 2.2 \times 10^{-11} P^{0.17} Z_B^{0.4} N^{2.2} Q^{0.2} \end{aligned} \quad (36)$$

where P is in kg, Z_B in cP, N in rpm, and Q in kg/min, just as in Equation (24). Using Equation (36) instead of (24), and using the same method used in obtaining (31) or (32), the bearing temperature rise can be obtained as follows:

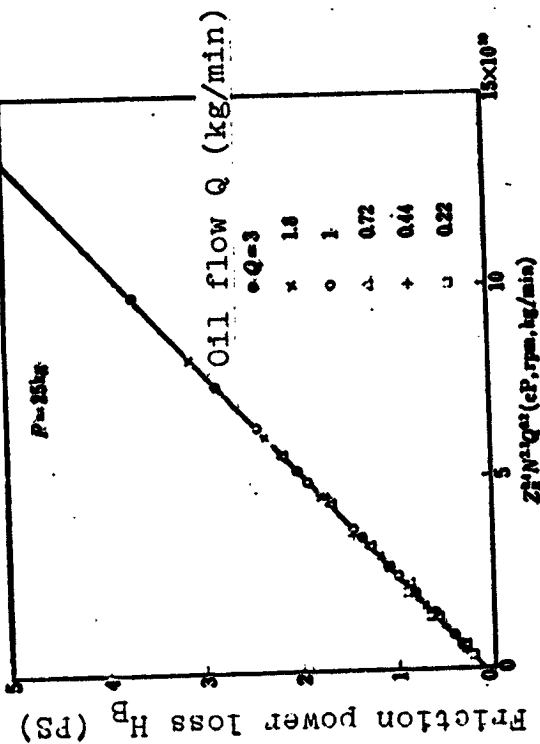


Figure 72. Friction power loss, viscosity, shaft speed, and oil flow

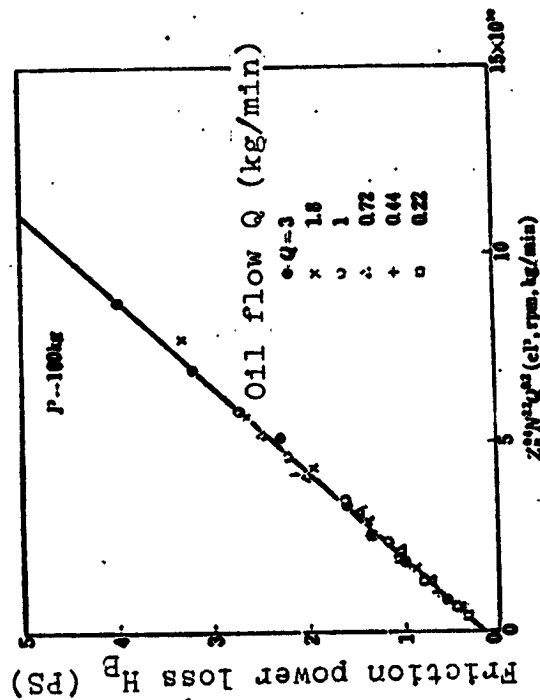


Figure 74. Friction power loss, viscosity, shaft speed, and oil flow

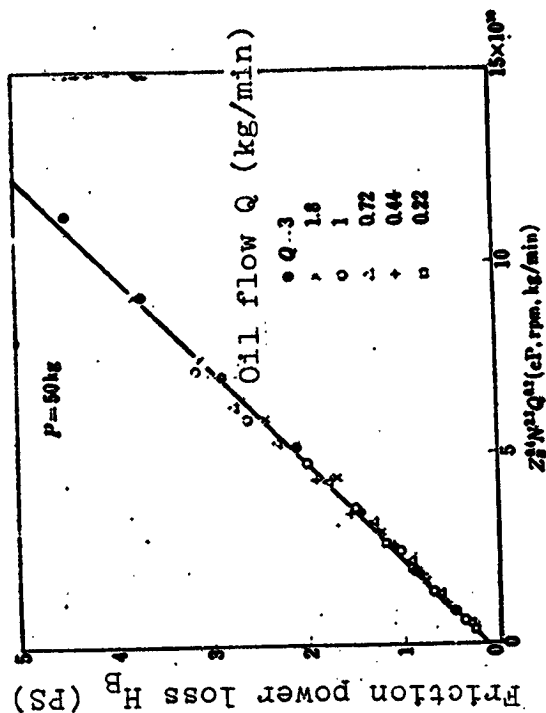


Figure 73. Friction power loss, viscosity, shaft speed, and oil flow

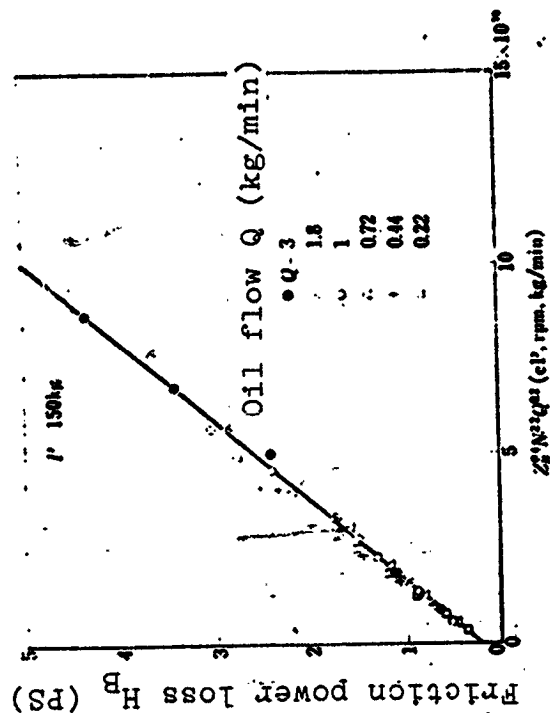


Figure 75. Friction power loss, viscosity, shaft speed, and oil flow

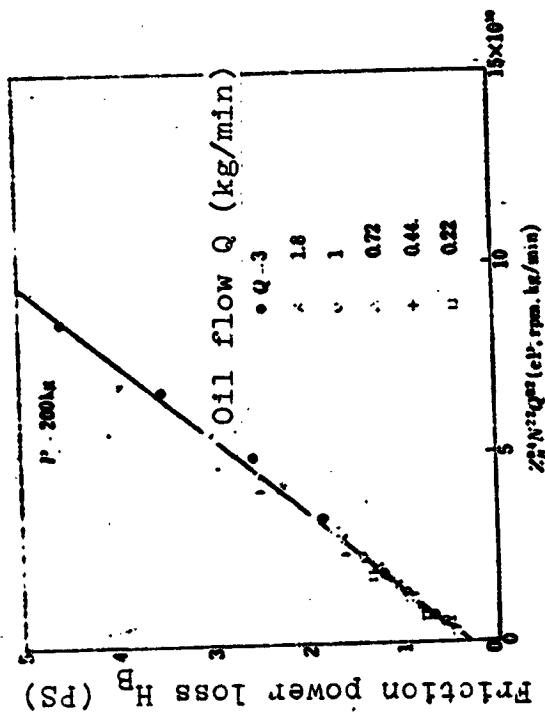


Figure 76. Friction power loss, viscosity, shaft speed, and oil flow

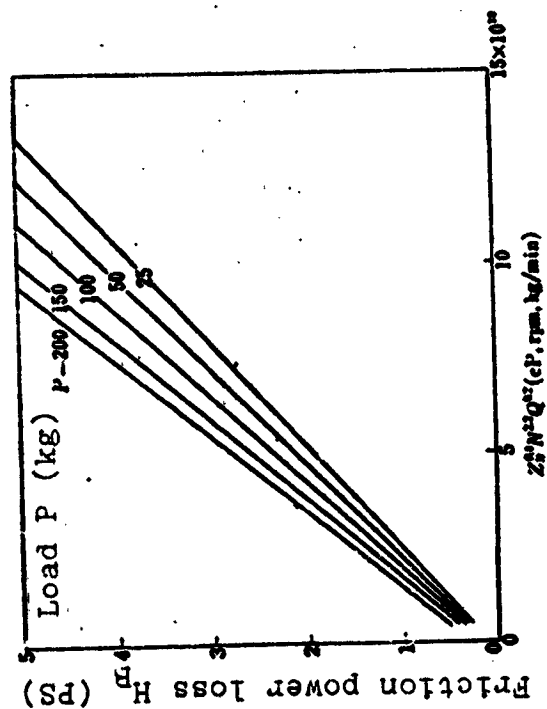


Figure 77. Friction power loss, viscosity, shaft speed, and oil flow

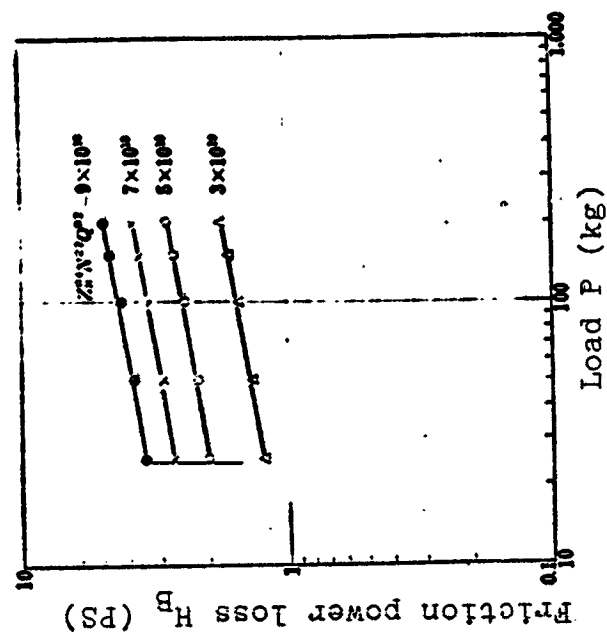


Figure 78. Friction power loss and load under various Z_B

(1) when $T_B - T_I$ is small ($15 - 40^\circ \text{C}$),

$$T_B - T_I = 5.2 \times 10^{-3} Z_I^{0.29} P^{0.12} N^{1.58} Q^{-0.46} \quad (37)$$

(2) when $T_B - T_I$ is large ($35 - 120^\circ \text{C}$),

$$T_B - T_I = 5.2 \times 10^{-3} Z_I^{0.29} P^{0.12} N^{1.58} Q^{-0.46} \quad (38)$$

The exponents of Z_I , N , and Q in Equations (37) and (38) are the same as in Equations (33) and (34), of course, but the exponent of P varies from 0.1 to 0.14, depending on the magnitude of $T_B - T_I$. This corresponds fairly well to the experimental equation for the bearing temperature rise (5), in which the exponent of P varies from 0.13 to 0.17, depending on the magnitude of $T_B - T_I$.

Let us now compare the bearing temperature rise, determined in Equation (37) or (38) from friction power loss, with the observed data. As this experiment has as its subject the case of high dn value, or large $T_B - T_I$, the comparison will be between Equation (38) and the observed data. Figure 79 is a result of using $Z_I^{0.29} P^{0.12} N^{1.58} Q^{-0.46}$ in Equation (38), which holds when $T_B - T_I$ is large, the bearing outer race temperature rise shown in Figure 24. Though there are deviations at 10,000 rpm, 20,000 rpm, and 30,000 rpm, Equation (38) holds in the high speed region above 40,000 rpm. In the low speed region below 30,000 rpm, Equation (37) is expected to hold. The bearing outer race temperature rise above 40,000 rpm will then be governed by Equation (38). Figure 80 is a

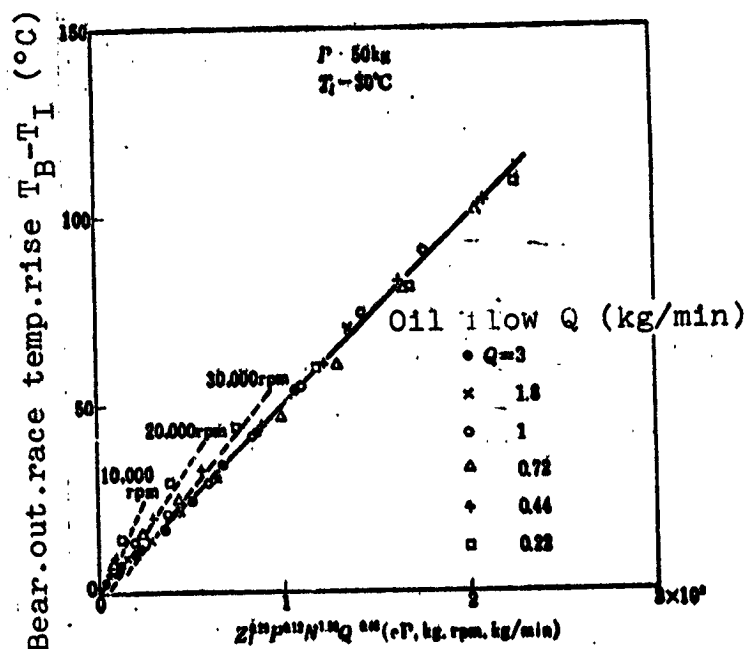


Figure 79. Bearing temperature rise, viscosity, load, shaft speed, and oil flow

result of using $Z_I^{0.29} P^{0.12} N^{1.58} Q^{-0.46}$ in Equation (38) to plot the observed data on the bearing outer race temperature rise $T_B - T_I$ under the following variable conditions: speed of 40,000 rpm, oil flow of 0.22 - 3 kg/min, thrust load of 25 - 200 kg, and inlet oil temperature of 30 - 120° C. As is clear from Figure 80, the estimating equation and the observed data for the bearing temperature rise under various conditions at high speed agree extremely well.

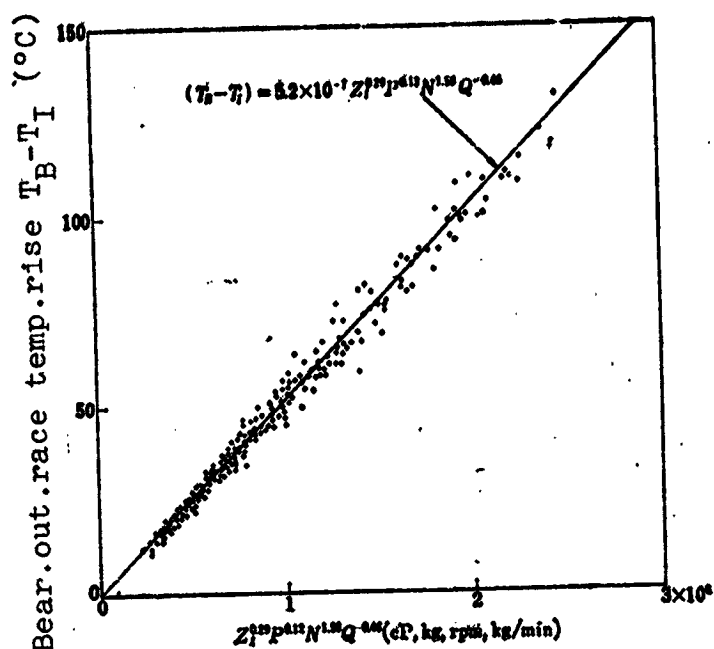


Figure 80. Bearing temperature rise, viscosity, load, shaft speed, and oil flow

The equation for the bearing temperature rise is thus estimated inversely from the friction torque, and it agreed with the observed data very well. It is important that the high speed roller bearing friction under jet lubrication be expressed by Equation (20), rather than being simply proportional to $Z_B N$, and that a certain viscous friction law holds within the authors' experimental range despite a severe high-speed low-viscosity condition. The constants as well as the exponent of each factor in the above equations are expected to vary depending on the bearing structure, such as the cage guide type, and the bearing dimensions. We will touch on this point later on.

/46

4.12. Allowable Limiting dn Value

It is clear that, except for the case of extremely small oil flow, the bearing friction up to the dn value of 240×10^4 is, on the whole, composed of viscous friction. Thus, the region up to this dn value belongs within the safe limit. If the speed is increased

further, a deviation from the relationship shown in Figure 80 would appear, and the limiting speed would be reached. As the bearing temperature rise increases in proportion to (speed)^{1.44-1.7} as indicated by Equation (5), considerable overheating of the bearing takes place at high speed. As a result, there is a limit based on the mechanical strength of the bearing material and the thermostability of lubricating oil at high temperatures. In addition, even if the bearing temperature is within the safe range, the limit should appear from the lubrication difficulty in the sliding friction portion inside the bearing, particularly in the cage, roller body, and the race riding surface of the inner and outer races. This limiting speed varies substantially depending on the method of lubrication. The problem is that, even if a positive lubrication is used, oil is not well accepted due to the churning of the surrounding air and oil at high speeds.

A result of the experiment conducted to clarify the allowable limiting speed under jet lubrication is shown in Figure 81. Although there are slight variations, the friction torque rapidly increases, accompanied by violent fluctuations, and results in failure in the neighborhood of 70,000 rpm with oil flow of 0.22 kg/min, 80,000 rpm with 0.44 kg/min, 90,000 rpm with 0.72 kg/min, and 95,000 rpm with more than 1 kg/min. The corresponding dn values are 210×10^4 , 240×10^4 , 270×10^4 , and 285×10^4 , respectively, as shown in Figure 82. When the speed was increased above 80,000 rpm, a phenomenon of temporary friction increase appeared, followed by its decrease and stabilization. This can be considered as the sliding friction

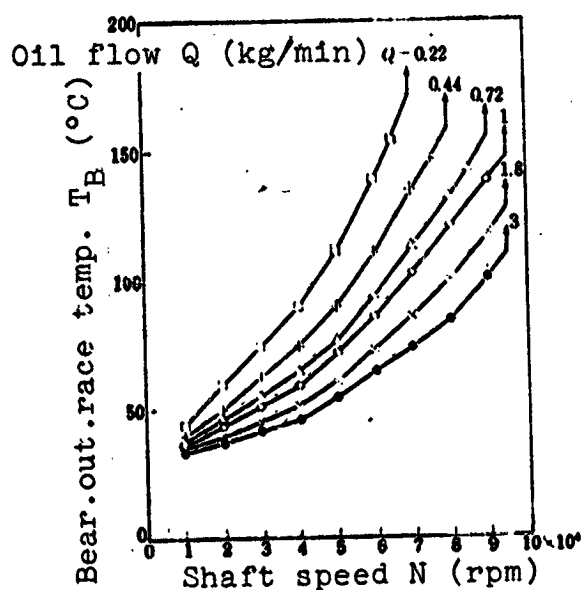


Figure 81. Bearing temperature and shaft speed (limiting speed)

portion of the cage becoming used to the wear by having local metallic contact and wear, just as for the slider bearing. Hence, some risk exists above 80,000 rpm, even if the speed is below the limiting value. Even when the oil flow is quite large, the limiting dn

value appears around 280×10^4 ; the peripheral speed at this time is about 140 m/s. Currently, a peripheral speed of up to 157 m/s with the slider bearing has been reported [10]. As a kind of viscous pump, the slider bearing

feeds the oil flow at least proportional to speed into the bearing. No such automatic pump action exists for the roller bearing. It also begins to reject a forced-feeding of oil from outside by churning the air and causing wind pressure at high speeds. In addition, the rotation must occur with attachments. This experiment thus exhibited again the significant disadvantage of the roller bearing compared to the slider bearing at high speed.

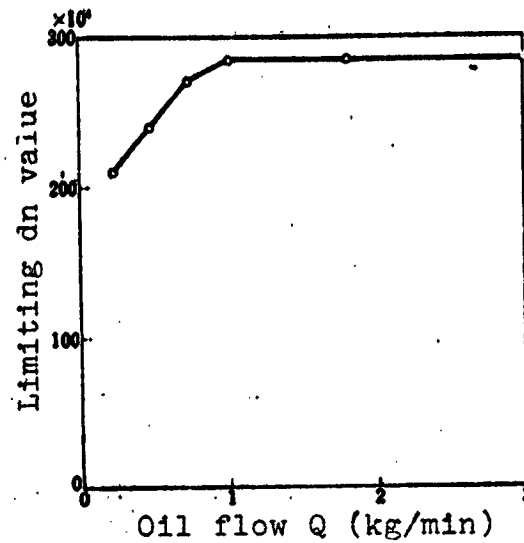


Figure 82. Limiting dn value and oil flow

The wear and the failure of the bearing occur on the sliding friction portion of the cage, rather than the track surface or the surface of the roller body. Figure 83 is an exterior view of the cage and the inner and outer races of the bearing which failed at the speed of 90,000 rpm and oil flow of 0.72 kg/min. Although the race riding surface at the nozzle side and the pocket hole of the cage are also slightly worn, the race riding surface at the opposite side of the nozzle is particularly worn and the race riding surface of the outer race facing it also has a burn. Wiping the cage material indicates a quite high temperature. This indicates that, because of oil having difficulty entering inside the bearing, the sliding friction portion of the cage enters into the boundary lubrication conditions, and rapid wear and the failure of the friction

portion occur. This is restraining the limiting speeds today. The limiting speed can be further raised by further improvements in the precision of the bearing and the cage, the development of a lubrication method and cage structure whereby sufficient oil can enter the bearing even at high speeds, and the development of material which can withstand boundary lubrication. This point will be discussed later on.



Figure 83. Exterior view of the failed bearing

Finally, we would like to add a couple of factors we experienced in regard to the speed limit. The limiting speed of the roller bearing is affected not only by the lubrication method and the bearing, but also by the condition of the bearing environs. For example, a slight decrease in the precision of the bearing leads to vibrations at high speeds, and the limiting speed may be suppressed by vibrations. Also, when the bearing mounting precision was bad, there was conspicuous wear of the cage at a speed much lower than the limiting speed, shown in Figure 81. Therefore, the limiting speed of the high speed roller bearing must be determined not just by the bearing, but rather by the overall bearing system.

4.13. Conclusions for Chapter 4

The following conclusions are obtained from experiments with jet lubrication under various conditions to investigate the performance characteristics up to the high dn value of 240×10^4 and the limiting dn value for the case of the deep-groove ball bearing #6206 equipped with an outer-race-riding cage:

- (1) The temperature rise from the inlet oil temperature T_I to the bearing outer race temperature T_B in the region of a dn value of

up to 240×10^4 can be approximated from the experiment as

$$(T_B - T_I) \propto Z_I^{0.2-0.3} P^{0.2-0.3} N^{0.2-0.3} Q^{-0.2-0.3}$$

where Z_I is oil viscosity at an inlet oil temperature, P is thrust load, N is the shaft speed, and Q is oil flow. The smaller exponent of each factor corresponds to the larger value of $T_B - T_I$.

(2) The horsepower absorption by lubricating oil H_0 can be approximated from the experiment as

$$H_0 \propto Z_I^{0.2-0.3} P^{0.2-0.3} N^{0.2-0.3} Q^{0.2-0.3}$$

The smaller exponents of Z_I , P , and N , and the larger exponent of Q correspond to the larger value of $T_B - T_I$.

Compared to the experimental equation for the bearing temperature rise, the exponents of Z_I , P , and N are similar, but the sign of the exponent of Q is reversed. The fact that the smaller exponent of Q in the bearing temperature rise and the larger exponent of Q in the horsepower absorption by oil correspond to the larger value of $T_B - T_I$ indicates that, under jet lubrication, most of the friction-generated heat is carried away by the oil and the oil acts as a coolant.

(3) The heat exchange efficiency of lubricating oil η_E (%) as a function of oil flow Q (kg/min) can be approximated by

$$\eta_E = 82 Q^{-0.2}$$

748

η_E decreases with an increasing oil flow, because when oil flow is large, the percentage of oil flow actually coming in contact with the bearing surface and performing effective heat exchange decreases.

In the heat exchange efficiency of oil, the heat exchange efficiency of the transmitted oil increases with increasing speed, reaching over 100% in every case at high dn values. On the other hand, the heat exchange efficiency of the deflected oil decreases with

Increasing speed, decreasing to about 50% when the oil flow is large. Hence, in order to make cooling by oil effective in high speed roller bearings, oil flow should be increased, but at the same time, the penetration ratio and, thus, η_E should also be increased.

(4) The bearing friction up to the dn value of 240×10^4 consists of viscous friction, on the whole. Contrary to what has been said heretofore, it is not simply proportional to the product $Z_B N$ of viscosity at the bearing temperature Z_B and speed N . The friction torque M (kg · cm) and the friction power loss H_B (PS) can be approximated by

$$M = 7 \times 10^{-3} P^{0.8} + 2.5 \times 10^{-6} Z_B^{0.4} N^{1.2} Q^{0.3}$$

$$H_B = 9.8 \times 10^{-7} P^{0.8} N + 3.5 \times 10^{-11} Z_B^{0.4} N^{1.2} Q^{0.3}$$

where P is thrust load in kg, Z_B is oil viscosity at the bearing outer race temperature in cP, N is speed in rpm, and Q is oil flow in kg/min.

The above equation holds within the range of the maximum speed of 80,000 rpm, the maximum dn value of 240×10^4 , the minimum viscosity at the bearing temperature of 1.5 cP, the oil flow of 0.22 - 3 kg/min, and the thrust load of 25 - 200 kg. It is important that a certain viscous friction law holds even under such severe high-speed low-viscosity conditions.

(5) Assuming all friction heat is removed by oil, the temperature rise from the inlet oil temperature T_I to the bearing outer race temperature T_B can be obtained from the experimental equation for the friction power loss as follows:

$$(T_B - T_I) \propto Z_I^{0.8-0.85} P^{0.8-0.85} N^{1.2-1.25} Q^{0.3-0.35}$$

The smaller exponent of each factor corresponds to the larger value of $T_B - T_I$. The bearing temperature equation thus derived from the friction power loss agrees well with the experimental equation.

When $T_B - T_I$ is large — that is, in the high dn region — an estimating equation for the bearing temperature rise ($^{\circ}\text{C}$) can be expressed by

$$(T_B - T_I) = 5.2 \times 10^{-1} Z_I^{0.39} P^{0.13} N^{1.44} Q^{-0.46}$$

where Z_I is in cP, P in kg, N in rpm, and Q in kg/min. The estimating equation for the bearing temperature rise thus derived from the friction power loss agrees very well with the observed data, indicating an appropriateness of the friction torque equation.

(6) A viscous friction occupies a major portion of the friction up to the dn value of 240×10^4 . If the speed is increased further, the bearing wear and failure occur and the limiting dn value exists. This limiting dn value varies depending on oil flow, and appears at 210×10^4 for oil flow of 0.22 kg/min, 240×10^4 for 0.44 kg/min, 270×10^4 for 0.72 kg/min, and at 285×10^4 for 1 - 3 kg/min.. The wear and the failure always occur on the race riding surface of the outer race and the race riding surface of the cage on the opposite side of the nozzle, indicating that the cage lubrication influences the limiting dn value of the high speed roller bearing.

CHAPTER 5. EFFECT OF CAGE GUIDE TYPE WITH DEEP-GROOVE BALL BEARING (#6206)

5.1. Introduction

In the previous chapter, it was shown that the bearing wear and the failure at high dn value occurred on the sliding friction portion of the cage, and that the cage lubrication was the factor which influenced the limiting speed of the roller bearing. Consequently, the cage guide type is expected to greatly affect the limiting speed.

In the previous chapter, the results for an outer-race-riding cage were given, but in this chapter, how oil flow and other factors

affect the limiting speed, the bearing temperature rise, and the friction torque for the same bearing but equipped with an inner-race-riding cage is investigated, and the results are compared with those for an outer-race-riding cage. As a result, it became clear that the cage guide type had a decisive effect on the limiting speed at high dn value. How the lubrication of the high speed roller bearing should be performed was also elucidated.

5.2. Experimental Conditions

Although already mentioned in Chapters 2 and 3, the conditions used in this experiment are summarized. A single nozzle is placed on the thrust loaded side of the inner race. The distance between the leading edge of the nozzle and the face of the inner race is set at 8 mm, and the jet velocity is fixed at roughly 20 m/s, irrespective of oil flow. In the previous chapter, the nozzle was always directed perpendicularly to the center of the clearance space between the cage and the inner race. Unless otherwise specified, this method is used again in this experiment. An experiment is also performed by placing the nozzle perpendicularly to the center of the clearance between the cage and the outer race.

Unless explicitly specified, both the thrust load and the inlet oil temperature are kept constant at 50 kg and 30° C, respectively.

5.3. Test Bearing

The same test bearing used in the previous chapter — #6206 SP-class ball bearing — is again used. The only difference is that it is now equipped with an inner-race-riding cage. The cage configuration is shown in Figure 84. Just like for an outer-race-riding cage, a groove is set up on the inside perimeter of the cage to make it easier for oil to enter the bearing. The guide clearance of the cage is $0.25 \begin{pmatrix} +0.1 \\ -0.07 \end{pmatrix}$ mm, and the bearing dimensions, precision, radial clearance, and bearing fits are the same as in the previous chapter.

/49

5.4. Experimental Results

The limiting speed, bearing outer race temperature, outlet oil temperature at the nozzle side as well as the bearing transmitted side, friction torque, and penetration ratio as a function of shaft speed for each oil flow under the constant thrust load of 50 kg and the inlet oil temperature of 30° C are shown in Table 6.

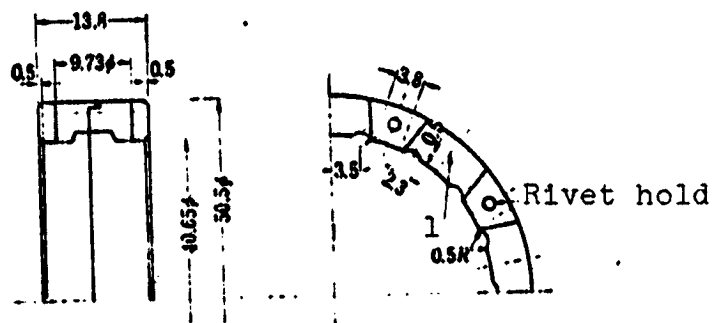


Figure 84. Cage confirmation:
1 — pocket hole for each of 9 equivalent slots on the circumference

The experimental results above, together with the results when the thrust load and the inlet oil temperature are changed, are discussed, and the effect of the cage guide type on the performance of the high speed roller bearing is investigated next.

TABLE 6. BEARING TEMPERATURE, OUTLET OIL TEMPERATURE, FRICTION TORQUE, PENETRATION RATIO AND SHAFT SPEED
(30° C inlet oil temperature and 50 kg thrust load)

Oil flow $Q = 3$ kg/min (room temperature 17 °C)

Shaft speed, rpm	Bearing outer race temp., °C	Outlet oil temp. (nozzle side), °C	Outlet oil temp. (transm. side), °C	Friction torque, kg·cm	Penetration ratio, %
10,000	32.5	31.5	32.5	1.02	32.7
15,000	34.5	32.5	34.5	1.18	27.0
20,000	37	33.5	37	1.32	22.4
25,000	40	34.5	40	1.41	21.2
30,000	43	36	43	1.50	18.5
35,000	46.5	38	47.5	1.57	15.2
40,000	50.5	40	52	1.63	14.1
45,000	54.5	42	56	1.69	13.7

50,000~55,000 Failure

(Table continued on following page)

TABLE 6 (continued)

 $Q = 1.8 \text{ kg/min}$ (room temperature 18°C)

Shaft speed, rpm	Bearing outer race temp., $^\circ\text{C}$	Outlet oil temp. (nozzle side), $^\circ\text{C}$	Outlet oil temp. (transm. side), $^\circ\text{C}$	Friction torque, kg·cm	Penetration ratio, %
10,000	33.5	33.5	33.5	0.94	34.8
15,000	36.5	34.5	36.5	1.09	32.8
20,000	39.5	35	39.5	1.21	25.9
25,000	43	37	43	1.31	25.3
30,000	46.5	39.5	46.5	1.37	20.7
35,000	50	41.5	51	1.45	17.9
40,000	54.5	44	56	1.49	16.5
45,000	59	46.5	61	1.55	16.5
50,000~55,000	Failure				

 $Q = 1 \text{ kg/min}$ (room temperature 20°C)

Shaft speed, rpm	Bearing outer race temp., $^\circ\text{C}$	Outlet oil temp. (nozzle side), $^\circ\text{C}$	Outlet oil temp. (transm. side), $^\circ\text{C}$	Friction torque, kg·cm	Penetration ratio, %
10,000	34.5	33	35	0.88	44.2
15,000	38.5	34.5	38.5	1.03	39.7
20,000	42.5	37.5	43	1.13	25.3
25,000	47	40.5	47	1.19	25.4
30,000	51.5	44	51.5	1.23	20.5
35,000	57	47.5	58	1.26	17.2
40,000	62.5	50	63.5	1.32	17.1
45,000	67.5	52.5	68.5	1.34	18.5
50,000~55,000	Failure				

 $Q = 0.72 \text{ kg/min}$ (room temperature 21°C)

Shaft speed, rpm	Bearing outer race temp., $^\circ\text{C}$	Outlet oil temp. (nozzle side), $^\circ\text{C}$	Outlet oil temp. (transm. side), $^\circ\text{C}$	Friction torque, kg·cm	Penetration ratio, %
10,000	36	34.5	36	0.84	52.8
15,000	40.5	37	40.5	0.97	47.8
20,000	45	41	45	1.07	30.8
25,000	49.5	44.5	49.5	1.11	30.6
30,000	54.5	48	55	1.18	24.2

(Table concluded on following page)

TABLE 6 (concluded)

Q = 0.72 kg/min (room temperature 21°C) (cont.)

Shaft speed, rpm	Bearing outer race temp., °C	Outlet oil temp. (nozzle side), °C	Outlet oil temp. (transm. side), °C	Friction torque, kg·cm	Penetration ratio, %
35,000	60.5	51.5	60.5	1.22	20.8
40,000	66	55	67	1.24	21.5
45,000	71.5	58	73	1.25	25.0
50,000~55,000	Failure				

Q = 0.44 kg/min (room temperature 17° C)

Shaft speed, rpm	Bearing outer race temp., °C	Outlet oil temp. (nozzle side), °C	Outlet oil temp. (transm. side), °C	Friction torque, kg·cm	Penetration ratio, %
10,000	37	35	37	0.80	52.8
15,000	42	39	42.5	0.92	50.0
20,000	48	45	48.5	1.00	29.2
25,000	54	49	54	1.05	29.2
30,000	61.5	54	61	1.09	23.0
35,000	67	58.5	67	1.12	20.4
40,000	73	62	74	1.13	22.5
45,000	80	67	82	1.14	26.8
50,000~55,000	Failure				

Q = 0.22 kg/min (room temperature 20° C)

Shaft speed, rpm	Bearing outer race temp., °C	Outlet oil temp. (nozzle side), °C	Outlet oil temp. (transm. side), °C	Friction torque, kg·cm	Penetration ratio, %
10,000	43	37.5	40.5	0.74	50.8
15,000	47.5	43.5	48	0.79	42.3
20,000	56	52	56.5	0.86	18.5
25,000	62.5	58	64.5	0.88	23.4
30,000	73	65	73	0.90	17.5
35,000	81	71	82	0.91	18.0
40,000	89.5	76	92	0.92	27.2
50,000	98	82	101	0.93	32.5
50,000~55,000	Failure				

5.5 Allowable Limiting dn Value

As mentioned in the previous chapter, for #6206 equipped with an outer-race-riding cage, the bearing failure occurred at 70,000 rpm with oil flow of 0.22 kg/min, 80,000 rpm with 0.44 kg/min, 90,000 rpm with 0.72 kg/min, and at 95,000 rpm with 1 - 3 kg/min. The respective dn values were 210×10^4 , 240×10^4 , 270×10^4 and 285×10^4 . On the other hand, when an inner-race-riding cage is used, the friction force which has been smooth up to then shows a sudden violent fluctuation at 50,000 to 55,000 rpm and rapidly increases, regardless of oil flow. The dn value decreases to $150 - 165 \times 10^4$, approximately half of an outer-race-riding cage.

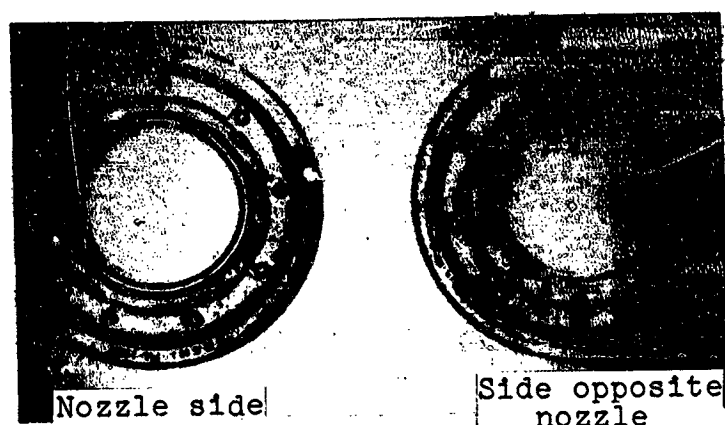


Figure 85: Exterior view of the failed bearing

As is clear from the above results, the cage guide type has a tremendous influence on the limiting speed of the ball bearing. Let us now consider how such a difference in the cage guide type is affecting the limiting speed. Figures 86, 87, 88, 89, 90, and 91 show the temperature rise $T_B - T_I$ from the inlet oil temperature T_I (30°C) to the bearing outer race temperature T_B and the penetration ratio as a function of shaft speed for various oil flows obtained from the results in Table 6. For comparison purposes, the results for an outer-race-riding cage from the previous chapter are also shown. The nozzle position is at the center of the clearance space between the cage and the inner race for both an outer-race-riding cage and an inner-race-riding cage. For an inner-race-riding cage, the results when the nozzle is placed at the center of the clearance between the cage and the outer race are also shown, so that the effect of the penetration ratio can be studied.

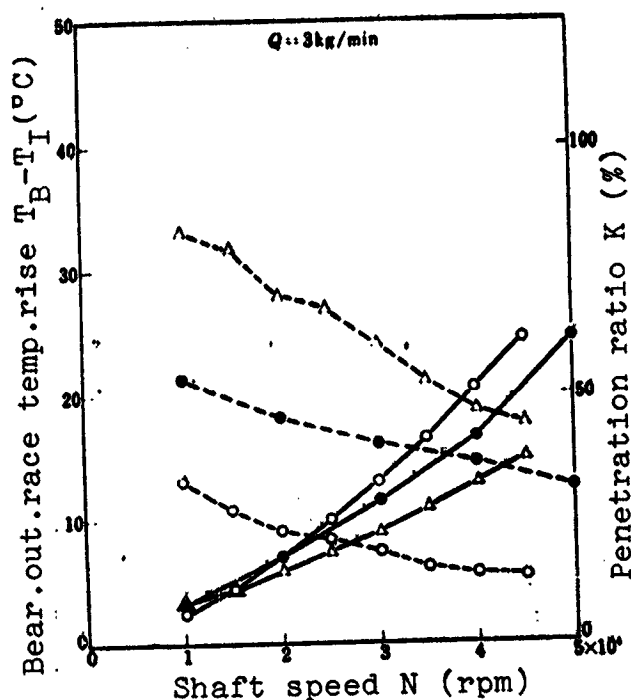


Figure 86. Bearing temperature rise, penetration ratio, and shaft speed:

● — outer-race-riding cage (nozzle between cage and inner race); ▲ — inner-race-riding cage (nozzle between cage and inner race); ○ — inner-race-riding cage (nozzle between cage and outer race); — — — bearing temperature rise; - - - - penetration ratio

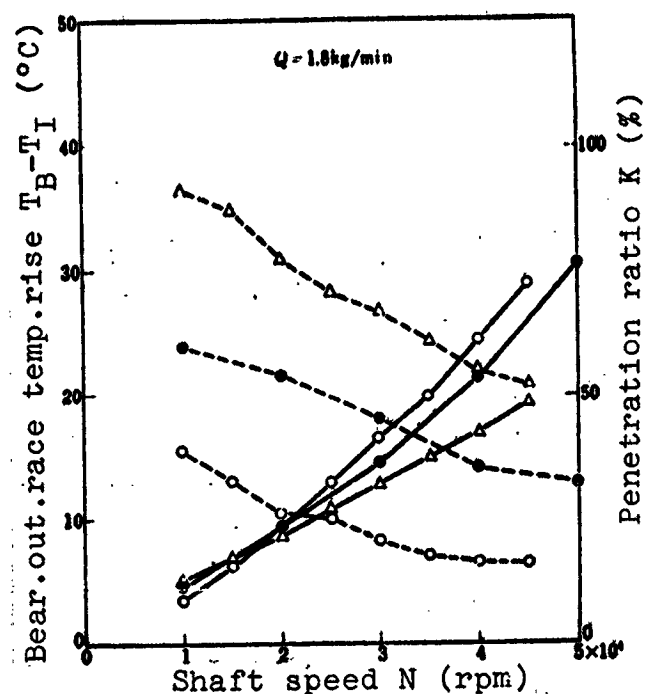


Figure 87. Bearing temperature rise, penetration ratio, and shaft speed:

● — outer-race-riding cage (nozzle between the cage and inner race); ▲ — inner-race-riding cage (nozzle between cage and inner race); ○ — inner-race-riding cage (nozzle between cage and outer race) — — — bearing temperature rise; - - - - penetration ratio

In Figures 86 - 91, when the nozzle is placed at the center of the clearance between the cage and the inner race, the penetration ratio of an inner-race-riding cage is reduced to about half of an outer-race-riding cage for each oil flow. This is because the diametral clearance between the cage and the inner race of an outer-race-riding cage is 1.5 mm, but the guide clearance of an inner-race-riding cage is 0.25 mm; hence, oil has difficulty entering the bearing due to the very small clearance of the latter. As mentioned in the previous chapter, an effective method of cooling the high speed roller bearing with the same oil flow rate is to effectively feed

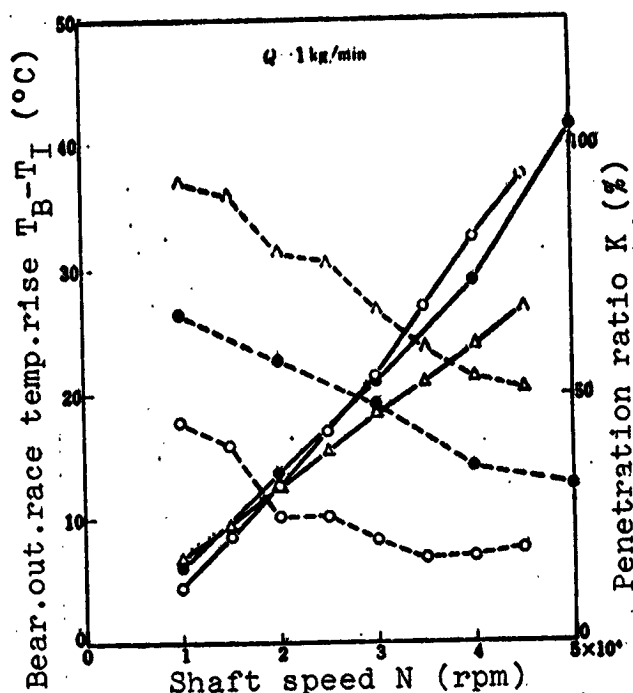


Figure 88. Bearing temperature rise, penetration ratio, and shaft speed:

— — bearing temperature rise; - - - — penetration ratio

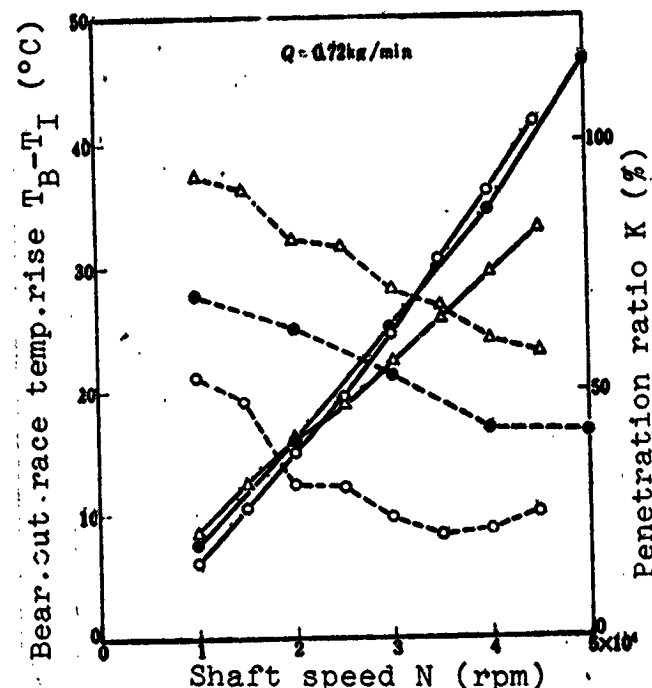


Figure 89. Bearing temperature rise, penetration ratio, and shaft speed:

— — bearing temperature rise; - - - — penetration ratio

oil inside the bearing and increase the penetration ratio. On this point, an inner-race-riding cage is disadvantageous, compared to an outer-race-riding cage at high speed.

It may be thought that the difference in penetration ratio was dominant in the limiting dn value. However, if it were due only to the magnitude of the penetration ratio, the penetration ratio could be substantially increased by placing the nozzle at the center of the clearance space between the cage and the outer race for an inner-race-riding cage as well, since the diametral clearance there is 2.8 mm. The question is whether the limiting dn value of an inner-race-riding cage would increase to the level of an outer-race-riding cage if this was done. The penetration ratio and the bearing outer race temperature rise for this case are shown in Figures 86 - 91

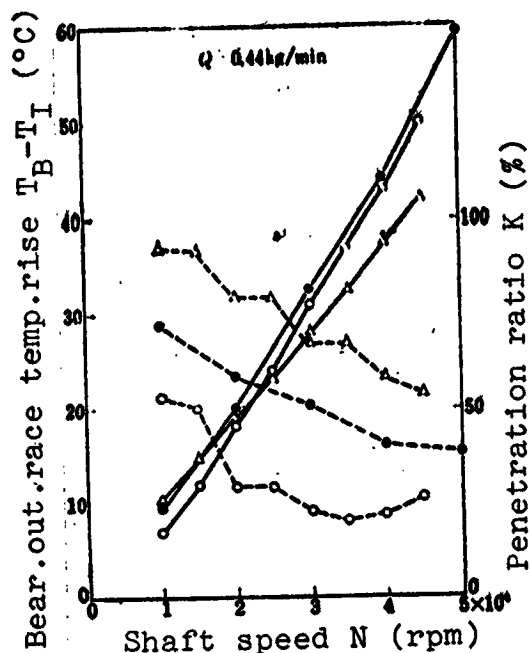


Figure 90. Bearing temperature rise, penetration ratio, and shaft speed:

— — — bearing temperature rise; - - - - - penetration ratio

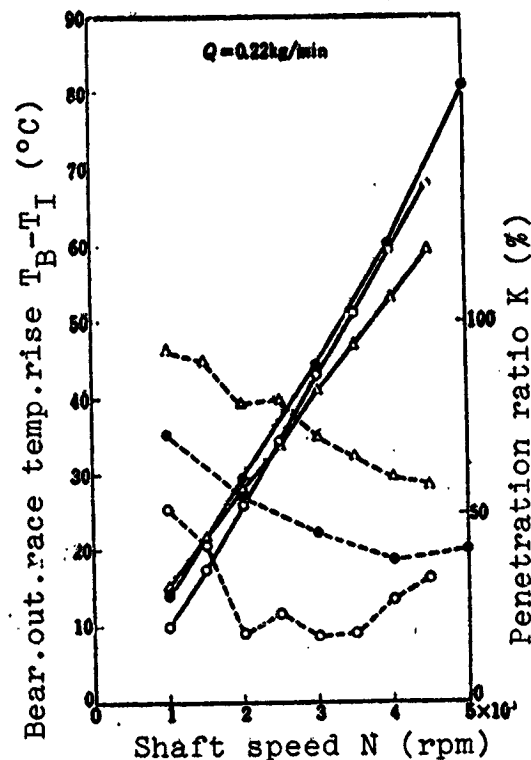


Figure 91. Bearing temperature rise, penetration ratio, and shaft speed:

— — — bearing temperature rise; - - - - - penetration ratio

also. Regardless of oil flow, the penetration ratio substantially increased and the bearing outer race temperature rise became a minimum compared to an outer-race-riding cage when the nozzle was placed between the cage and the outer race. However, the friction torque, when the nozzle is placed between the cage and the inner race, is smooth up to 45,000 rpm; but when the nozzle is placed between the cage and the outer race, it is smooth up to 35,000 rpm. When the speed is increased further, a large friction torque and fluctuations occur, followed by stabilization. This indicates that the sliding contact area of the cage becomes used to the failure locally. Hence, when the nozzle is placed between the cage and the outer race, the penetration ratio is large, and the bearing outer race temperature rise

is small, but failure tends to occur more often than when the nozzle is placed between the cage and the inner race.

/55

It is clear from the above results that no direct relationship exists between the magnitude of the penetration ratio or the bearing temperature rise and the limiting speed. That is, when the nozzle is directed to the center between the cage and the outer race for an inner-race-riding cage, the penetration ratio is maximum, but the most failures tend to occur. Hence, this is inferior in performance compared to the case in which the nozzle is directed between the cage and the inner race for an inner-race-riding cage, and the penetration is minimum. As mentioned in the previous chapter, the large penetration ratio means a large oil flow passing through the bearing and an effective heat exchange; therefore, it is extremely beneficial for the cooling of the bearing. As shown in Figures 86 - 91, in which the bearing outer race temperature rise decreases as the penetration ratio increases, the penetration ratio is a factor which affects the average temperature of the bearing. Since the race riding surface of the cage at the opposite side of the nozzle is the one which fails at high speeds, as mentioned before, the temperature here and the bearing outer race temperature may not necessarily be related. The limiting speed is influenced by whether oil is effectively supplied to the race riding surface of the cage susceptible to failure, rather than just the magnitude of the penetration ratio or the bearing outer race temperature rise. Let us now discuss this further from such a viewpoint.

Figure 92 shows the model of oil flow inside the bearing of both an outer-race-riding cage, and an inner-race-riding cage. In Figure 92(a), which shows the case of an outer-race-riding cage, oil can easily enter inside the bearing because the clearance (diametral clearance of 1.5 mm) between the cage and the inner race is large. A portion of the oil will be transmitted through the bearing but a substantial portion of oil flows to the outer race side by centrifugal force accompanying the rotation of the inner race and roller body, passing through the race riding surface of the cage

susceptible to wear and failure, and then discharged. This benefits the lubrication problem. In addition, the fact that the part susceptible to failure is located on the oil outlet side is very advantageous, because an abrasive dust generated is immediately discharged out of the bearing

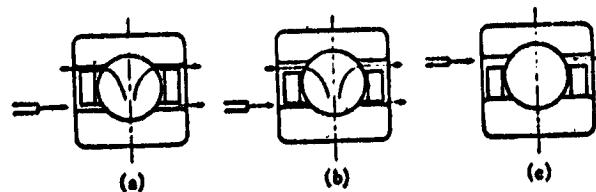


Figure 92. Oil passage inside the bearing for both an outer-race-riding cage and an inner-race-riding cage

rather than entering the bearing. On the other hand, in Figure 92(b), which shows the case of an inner-race-riding cage, oil has difficulty entering inside the bearing because of the small clearance (a guide clearance of 0.25 mm) between the cage and the inner race. Most of the oil which enters inside the bearing flows to the outer race side by centrifugal force, and not the race surface of the cage at the opposite side of the nozzle which requires the most lubrication. Furthermore, because the race surface of the cage on the nozzle side is located at the oil inlet side, an abrasive dust generated when this surface is abraded at high speed is sent, unlike the case of an outer-race-riding cage, into the bearing, inviting bearing failure. In fact, with an outer-race-riding cage, when the speed is increased in the region of high dn value above 240×10^4 , friction temporarily increases, rapidly followed by a decrease and stabilization. This is considered to be due to the sliding friction portion of the cage getting used to the wear, just as in the case of the slider bearing. On the contrary, with an inner-race-riding cage, there frequently was a rapid failure during this process, probably because any generated abrasive dust gets inside the bearing together with the oil. In Figure 92(c), which shows the case of an inner-race-riding cage with the nozzle placed between the cage and the outer race, the penetration increases due to the large clearance (diametral clearance of 2.8 mm), but it is inferior than the case of Figure 93(b) in that, because of centrifugal force, oil has difficulty reaching the race surface of the cage at the opposite side of the nozzle which needs the lubrication most.

The race surface of an inner-race-riding cage tends to favor boundary lubrication condition compared to an outer-race-riding cage, and creates rapid wear followed by the failure at a low dn value. Thus at high speed, an outer-race-riding cage is more advantageous than an inner-race-riding cage, but in practical applications there are many other factors to be considered. For example, even with an inner-race-riding cage, it is possible to raise the limiting dn value by using a cage structure such that sufficient oil can enter inside the bearing at high speed. In this regard, one example is given here, although the details will not be given until the next opportunity arises. The race surface of an inner-race-riding cage used in this experiment has a configuration shown in Figure 93(a), and has an oil groove to make it easier to enter inside the bearing; but because of the shallow depth of the groove (0.5 mm), it is not very effective. In Figure 93(b), the width of the rivet part is made small so that oil can easily enter the race surface of the cage, while in Figure 93(c), an oil groove is also used. Comparing these three, the limiting dn values with oil flow of 3 kg/min are $150 - 165 \times 10^4$ in (a), 180×10^4 in (b), and 240×10^4 in (c), indicating that the limiting dn value can be substantially raised by taking the cage configuration into consideration.

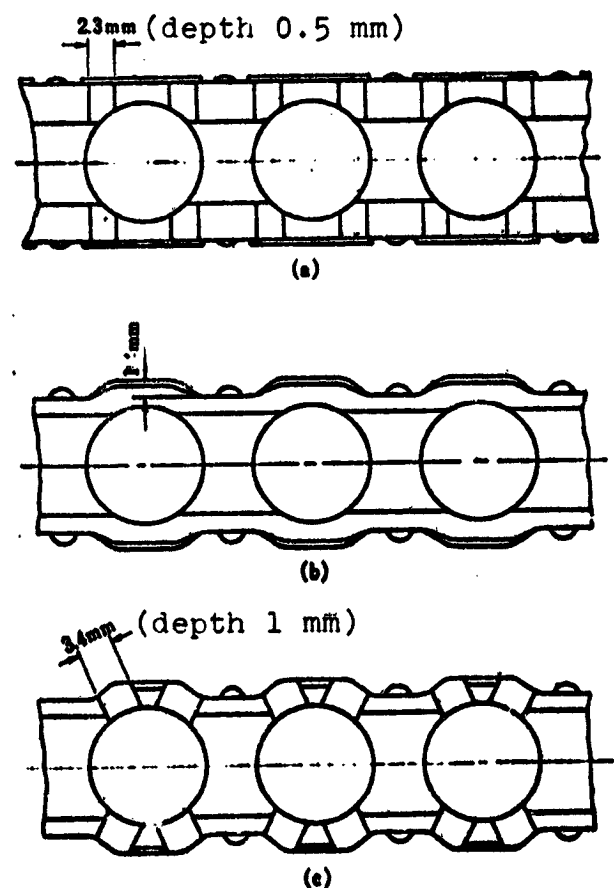


Figure 93. Configuration of the race riding surface of an inner-race-riding cage

In summary, it is possible to raise the limiting speed of an inner-race-riding cage by considering the cage configuration which let in oil easily, but compared to an outer-race-riding cage, its performance is inferior in that it tends to lead to failure in general.

5.6. Bearing Temperature Rise

Figure 94 shows the temperature rise $T_B - T_I$ from the inlet oil temperature T_I (30°C) to the bearing outer race temperature T_B , as a function of speed obtained from the results in Table 6. This bearing outer race temperature rise $T_B - T_I$ as a function of speed N and oil flow Q can be expressed from Figures 95 and 96, respectively, by

$$\left. \begin{aligned} (T_B - T_I) &\propto N^{1.2-1.35} \\ (T_B - T_I) &\propto Q^{-0.25-0.35} \end{aligned} \right\} \quad (39)$$

The smaller exponents of N and Q correspond to the larger values of $T_B - T_I$.

Equation (39) is for the case in which the nozzle is placed at the center between the cage and inner race. When the nozzle is placed at the center between the cage and the outer race, the following relation can be obtained:

$$\left. \begin{aligned} (T_B - T_I) &\propto N^{0.8-1.1} \\ (T_B - T_I) &\propto Q^{-0.25-0.35} \end{aligned} \right\} \quad (40)$$

The smaller exponents of N and Q correspond to the larger value of $T_B - T_I$, as in Equation (39). Comparing Equation (39) and (40), the exponent of N when the nozzle is placed between the cage and the

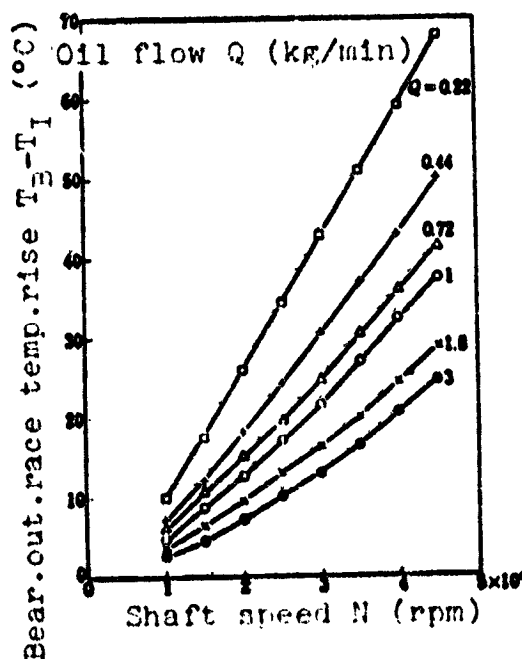


Figure 94. Bearing temperature rise and shaft speed

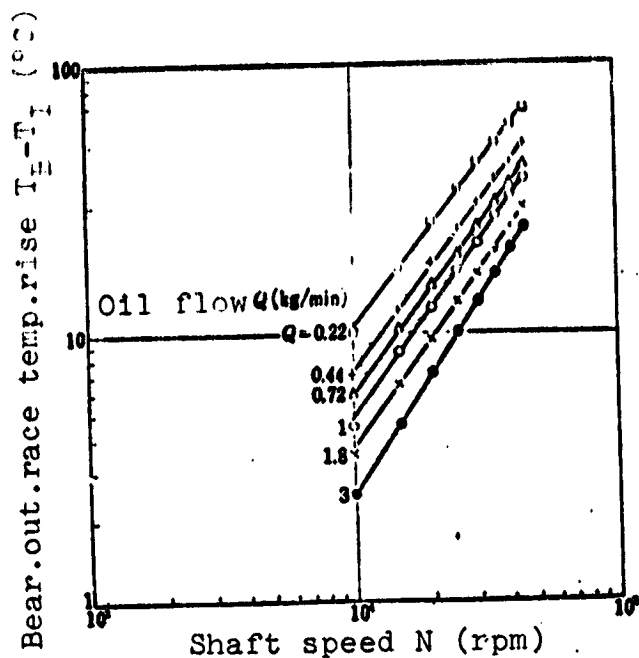


Figure 95. Bearing temperature rise and shaft speed

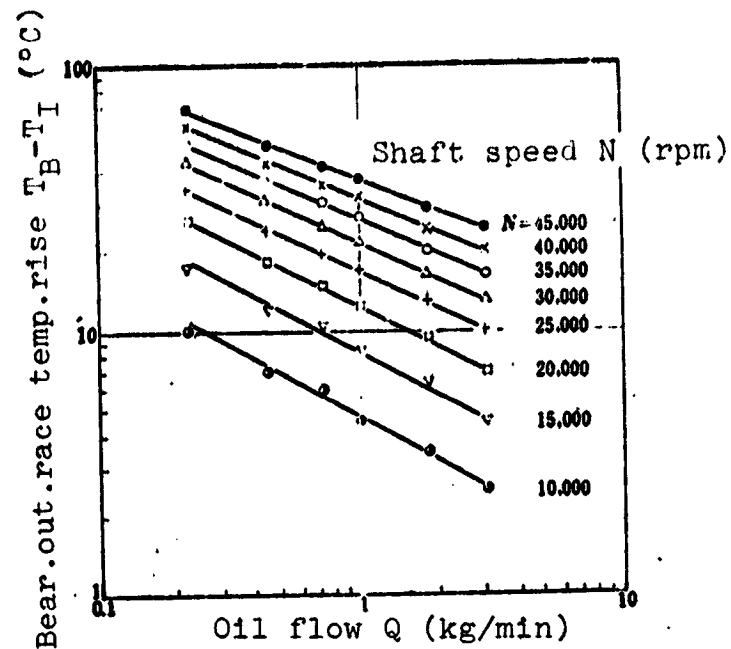


Figure 96. Bearing temperature rise and oil flow

outer race is smaller than that when the nozzle is placed between the cage and the inner race, but the exponent of Q is larger. This is because the penetration ratio of the former is greater than the latter, and the cooling effect is greater. However, even though the cooling effect is large, it is still worse compared to the failure, as mentioned previously. Consequently, the failure limit cannot be discussed considering the magnitude of exponents N and Q alone.

The result in Equation (39) is for the case of the constant thrust load of 50 kg in Table 6. A sample of the temperature rise $T_B - T_I$ from the inlet oil temperature T_I (30°C) to the bearing outer race temperature T_B as a function of thrust load P is shown in Figure 97. Their relationship can be approximated by

$$(T_B - T_I) \propto P^{0.12-0.1} \quad (41)$$

As the speed and $T_B - T_I$ increase, the exponent of P decreases.

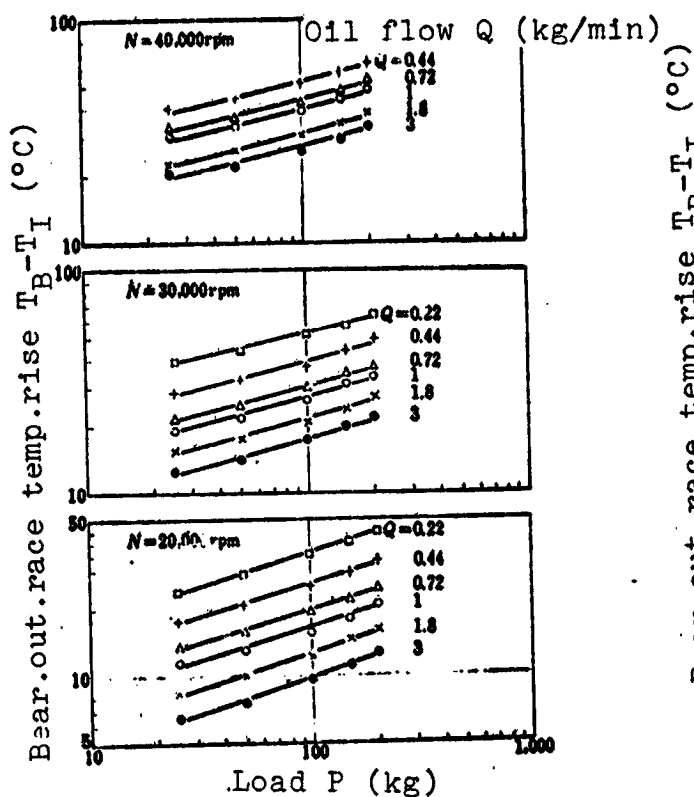


Figure 97. Bearing temperature rise and load

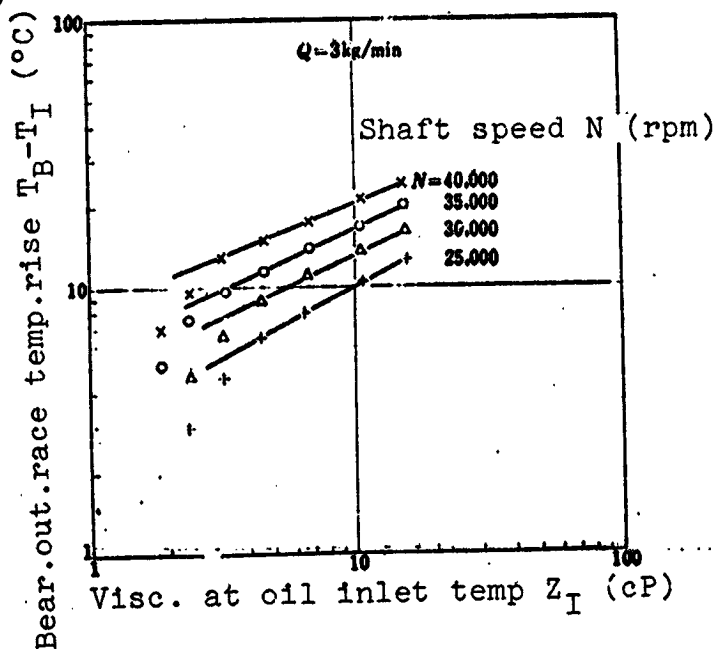


Figure 98. Bearing temperature rise and viscosity at inlet oil temperature

The above results are all for the case of constant inlet oil temperature at 30° C. A sample of the bearing outer race temperature rise from the inlet oil temperature, as a function of viscosity at inlet oil temperature Z_I when the inlet oil temperature is varied from 20° C to 120° C, is shown in Figure 98. There is a deviation at an inlet oil temperature of above 90° C. This is thought to be due to the error caused by the low speed and the small temperature rise, as mentioned in the previous chapter. Within the range of an inlet oil temperature of 20 - 75° C, the relation between the bearing outer race temperature rise $T_B - T_I$ and Z_I can be approximated by

$$(T_B - T_I) \propto Z_I^{0.4-0.5} \quad (42)$$

A smaller exponent corresponds to the larger value of $T_B - T_I$.

Summing up, the bearing outer race temperature rise can be approximated by

$$(T_B - T_I) \propto Z_I^{0.4-0.5} P^{0.25-0.3} N^{1.5-1.85} Q^{-0.25-0.35} \quad (43)$$

The smaller exponent of each factor corresponds to the larger value of $T_B - T_I$.

The experimental equation (5) for the bearing outer race temperature rise for an outer-race-riding cage in the previous chapter is applicable in the high speed region. As the maximum speed with an inner-race-riding cage is 45,000 rpm, the temperature rise of an outer-race-riding cage within roughly the same range can be expressed from the data in the previous chapter by:

$$(T_B - T_I) \propto Z_I^{0.35-0.45} P^{0.17-0.3} N^{1.05-1.35} Q^{-0.47-0.55} \quad (44)$$

Comparing Equations (43) and (44), the exponents of Z_I and P are nearly equal, but the exponent of N is larger and the exponent of Q is smaller for an inner-race-riding cage than for an outer-race-riding cage. This is because the penetration ratio of an inner-race-riding cage is small and cooling by oil is ineffective, compared to an outer-race-riding cage. For example, even with an inner-race-riding cage, if the nozzle is placed between the cage and the outer race to increase the penetration ratio as indicated in Equation (40), then the exponent of N becomes smaller and the exponent of Q becomes larger for an inner-race-riding cage compared to an outer-race-riding cage. The details on these experiments will be discussed later.

5.7. Amount of Heat Absorption by Lubricating Oil

Table 7 shows the horsepower absorptions by the deflected oil and the transmitted oil, as well as the total horsepower absorption by oil obtained from Table 6. Figure 99 shows the total horsepower absorption by oil H_0 as a function of speed from the results in Table 7. From Figures 100 and 101, the total horsepower absorption

TABLE 7. HORSEPOWER ABSORPTION BY OIL AND SHAFT SPEED
(30° C inlet oil temperature and 50 kg thrust load)

Oil flow $Q = 3 \text{ kg/min}$

Shaft speed, rpm	Horsepower absorption by oil (nozzle side), PS	Horsepower absorption by oil (transm. side), PS	Total horsepower absorption by oil, PS
15,000	0.27	0.18	0.45
20,000	0.38	0.23	0.61
25,000	0.51	0.30	0.81
30,000	0.70	0.35	1.05
35,000	0.97	0.38	1.35
40,000	1.17	0.44	1.61
45,000	1.49	0.49	1.98

$Q = 1.8 \text{ kg/min}$

Shaft speed, rpm	Horsepower absorption by oil (nozzle side), PS	Horsepower absorption by oil (transm. side), PS	Total horsepower absorption by oil, PS
15,000	0.20	0.18	0.38
20,000	0.33	0.22	0.54
25,000	0.46	0.28	0.74
30,000	0.67	0.30	0.97
35,000	0.82	0.33	1.15
40,000	1.03	0.37	1.40
45,000	1.20	0.44	1.64

$Q = 1 \text{ kg/min}$

Shaft speed, rpm	Horsepower absorption by oil (nozzle side), PS	Horsepower absorption by oil (transm. side), PS	Total horsepower absorption by oil, PS
15,000	0.13	0.17	0.30
20,000	0.27	0.17	0.44
25,000	0.38	0.21	0.59
30,000	0.54	0.21	0.75
35,000	0.70	0.23	0.93
40,000	0.81	0.28	1.09
45,000	0.90	0.35	1.25

(Table concluded on following page)

TABLE 7 (concluded)

 $Q = 0.72 \text{ kg/min}$

Shaft speed, rpm	Horsepower absorption by oil (nozzle side), PS	Horsepower absorption by oil (transm. side), PS	Total horsepower absorption by oil, PS
15,000	0.12	0.17	0.29
20,000	0.26	0.16	0.42
25,000	0.34	0.20	0.54
30,000	0.47	0.21	0.68
35,000	0.58	0.22	0.80
40,000	0.67	0.27	0.94
45,000	0.73	0.37	1.10

 $Q = 0.44 \text{ kg/min}$

Shaft speed, rpm	Horsepower absorption by oil (nozzle side), PS	Horsepower absorption by oil (transm. side), PS	Total horsepower absorption by oil, PS
15,000	0.10	0.13	0.23
20,000	0.22	0.11	0.33
25,000	0.28	0.16	0.44
30,000	0.39	0.15	0.54
35,000	0.48	0.16	0.64
40,000	0.52	0.21	0.73
45,000	0.57	0.29	0.86

 $Q = 0.22 \text{ kg/min}$

Shaft speed, rpm	Horsepower absorption by oil (nozzle side), PS	Horsepower absorption by oil (transm. side), PS	Total horsepower absorption by oil, PS
15,000	0.08	0.08	0.16
20,000	0.19	0.05	0.24
25,000	0.23	0.09	0.32
30,000	0.31	0.08	0.39
35,000	0.36	0.10	0.46
40,000	0.37	0.19	0.56
45,000	0.40	0.26	0.66

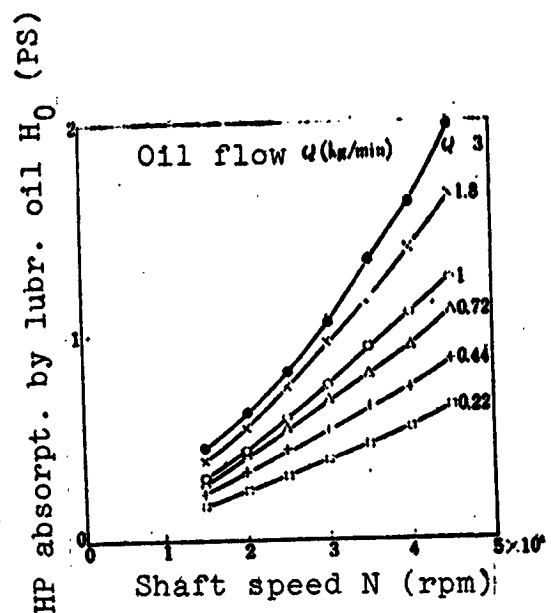


Figure 99. Horsepower absorption by oil and shaft speed

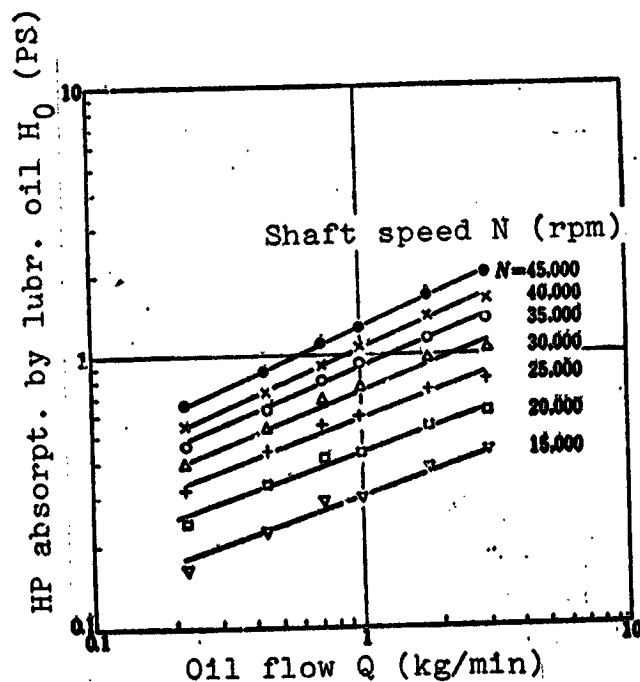


Figure 101. Horsepower absorption by oil and shaft speed

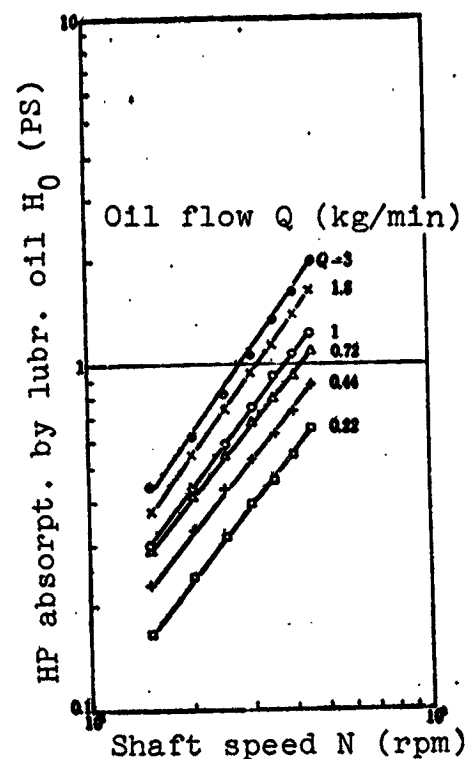


Figure 100. Horsepower absorption by oil and shaft speed

by oil H_0 as a function of speed and oil flow Q can be expressed, respectively, by

$$\left. \begin{aligned} H_0 &\propto N^{1.3-1.4} \\ H_0 &\propto Q^{2.4-2.8} \end{aligned} \right\} \quad (45)$$

The smaller exponent of N and the larger exponent of Q correspond to the larger value of $T_B - T_I$.

The above results are for the case of the constant thrust load of 50 kg and an inlet oil temperature of 30° C. The total horsepower absorption by oil H_0 as a function of thrust load P when the thrust load is varied from 25 kg to 200 kg is shown in Figure 102. Figure

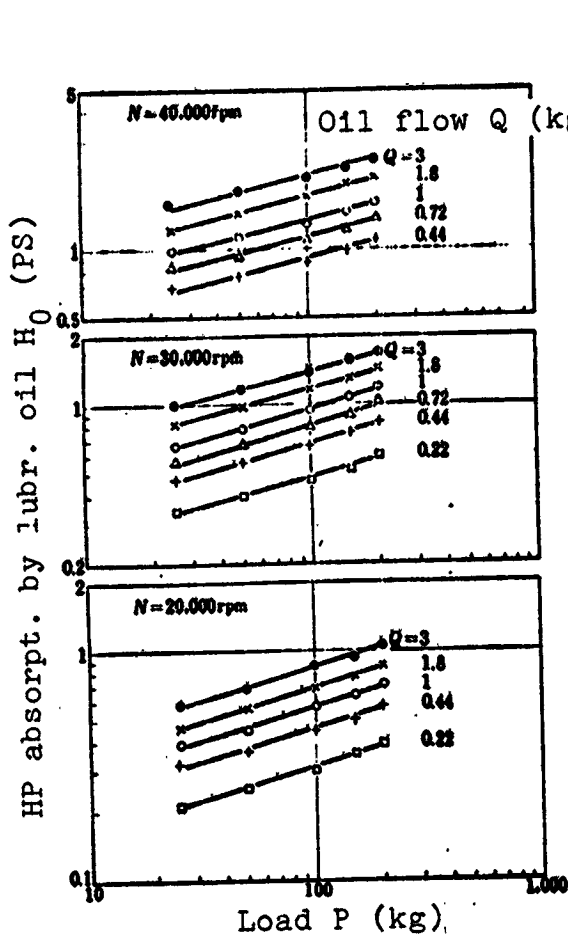


Figure 102. Horsepower absorption by oil and load

from 20° to 120° C. From Figures 102 and 103, the following approximations can be made:

$$\left. \begin{aligned} H_0 &\propto P^{0.25-0.3} \\ H_0 &\propto Z_I^{0.25-0.45} \end{aligned} \right\} \quad (46)$$

The exponents of P and Z_I become smaller as the speed and $T_B - T_I$ increase.

Summarizing above, the total horsepower absorption by oil H_0 can be approximated by

$$H_0 \propto Z_I^{0.25-0.45} P^{0.25-0.3} N^{1.5-1.4} Q^{0.44-0.34} \quad (47)$$

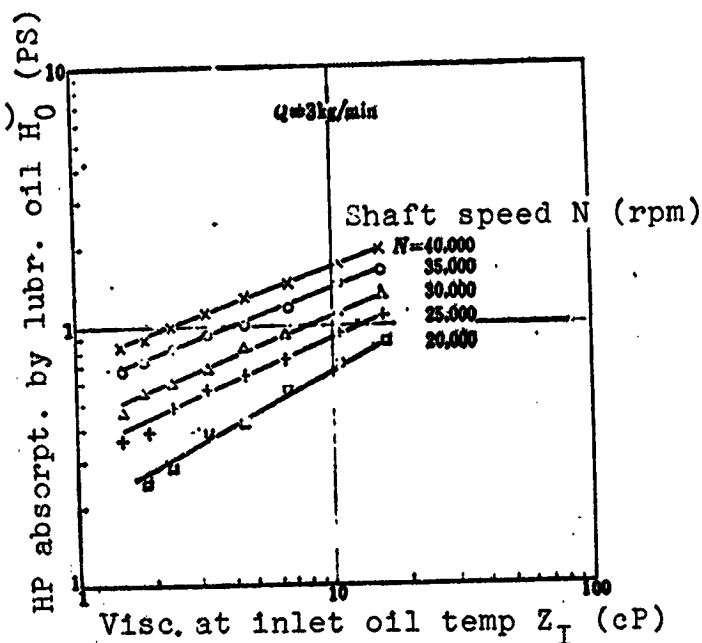


Figure 103. Horsepower absorption by oil and viscosity at inlet oil temperature

103 shows a sample of the total horsepower absorption by oil H_0 as a function of thrust load P when the thrust load is varied

The smaller exponents of Z_I , P , and N , and the larger exponent of Q correspond to the larger value of $T_B - T_I$. It agrees well with Equation (45) for the bearing outer race temperature rise, and almost all of the generated friction heat is carried away by oil, just as in the previous chapter.

Let us next discuss how the cooling effect by oil differs, depending on the cage guide type. Figures 104, 105, and 106 show the total horsepower absorption by oil H_0 , horsepower absorption by the deflected oil H_R , and horsepower

/63

absorption by the transmitted oil H_P from Tables 4 and 7 for both an outer-race-riding cage and an inner-race-riding cage. There is no big difference in the horsepower absorption by the deflected oil regardless of an inner-race-riding cage or an outer-race-riding cage, but the horsepower absorption by the transmitted oil is smaller for an inner-race-riding cage than for an outer race-riding, and this appears as a difference in the total horsepower absorption of an outer race-riding cage and an inner-race-riding cage. The higher bearing outer race temperature rise of an inner-race-riding cage relative to an outer-race-riding cage is caused by this difference in the total horsepower absorption. This is because the penetration ratio of an inner-race-riding cage is small compared to

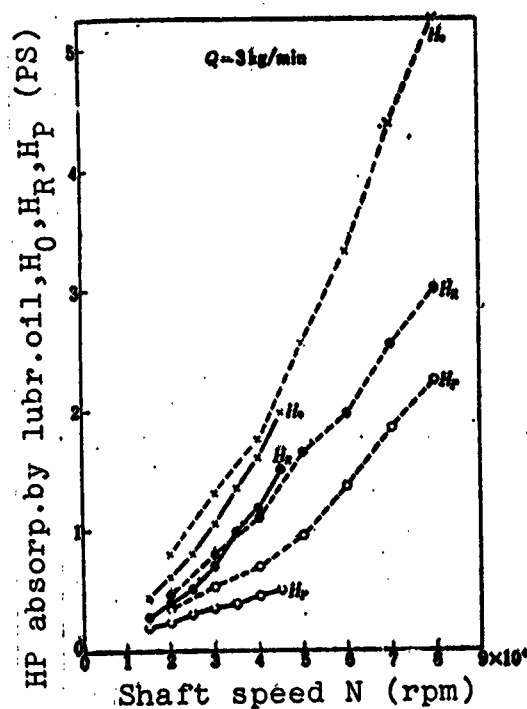


Figure 104. Horsepower absorption by oil and shaft speed:

— — — inner-race-riding cage; - - - - - outer race riding cage; x — total horsepower absorption by oil; • — horsepower absorption by deflected oil; o — horsepower absorption by transmitted oil

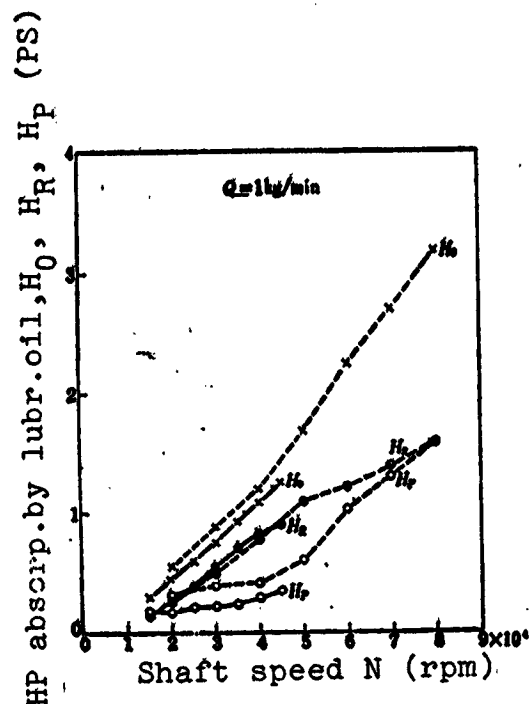


Figure 105. Horsepower absorption by oil and shaft speed:

— inner-race-riding cage;
 - - - outer-race-riding cage

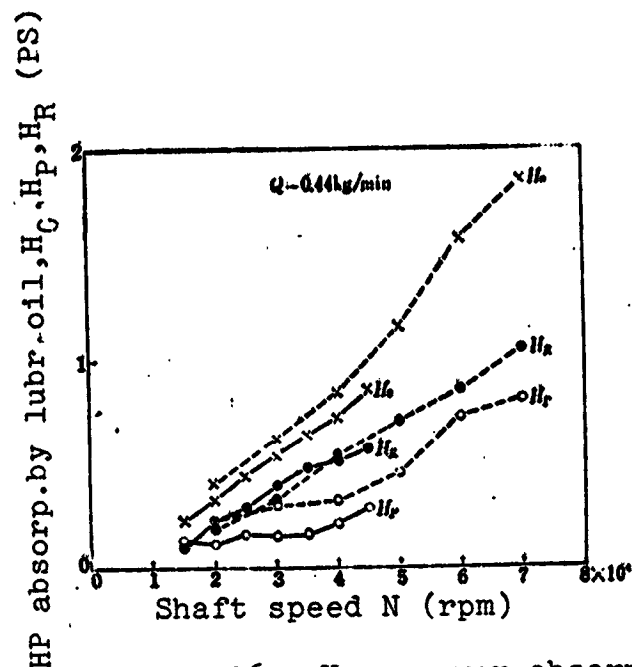


Figure 106. Horsepower absorption by oil and shaft speed:

— inner-race-riding cage;
 - - - outer-race-riding cage

an outer-race-riding cage, as mentioned before, and it again indicates the disadvantage of an inner-race-riding cage.

5.8. Heat Exchange Efficiency of Lubricating Oil

/64

Table 8 shows the heat exchange efficiency of the deflected oil η_R , the heat exchange efficiency of the transmitted oil η_P , and the overall heat exchange efficiency η_E as a function of shaft speed for the various quantities of oil flow, obtained from the data in Table 6, using the same method as described in the previous chapter. Figures 107, 108, and 109 show these results together with the results for an outer-race-riding cage from the previous chapter. η_P of an inner-race-riding cage is greater than that of an outer-race-riding cage, exhibiting 100% or more even at the low speed, because the amount of the transmitted oil is small, and, consequently, sufficient heat exchange is performed. However, η_R is substantially reduced compared to the case with an outer-race-riding cage. This is because,

TABLE 8. HEAT EXCHANGE EFFICIENCIES OF OIL η_R ,
 η_P , AND η_E , AND SHAFT SPEED FOR VARIOUS OIL FLOW
RATES

(30° C inlet oil temperature and 50 kg thrust
load)

Shaft speed rpm	η_R %					
	Amount of supplied oil kg·min					
	3	1.8	1	0.72	0.44	0.22
15,000	55.6	53.8	52.9	66.7	75	77.1
20,000	50	52.6	50	73.4	83.4	84.6
25,000	45	53.9	61.8	74.4	79.2	81.2
30,000	46.1	57.6	65.1	73.5	78.7	81.4
35,000	48.5	57.5	64.8	70.5	77	80.4
40,000	48.8	57.1	61.6	69.5	74.4	77.3
45,000	49	56.9	60	67.5	74	76.5

Shaft speed rpm	η_P %					
	Amount of supplied oil kg·min					
	3	1.8	1	0.72	0.44	0.22
15,000	100	100	100	100	104	102.8
20,000	100	100	104	100	102.9	102
25,000	100	100	100	100	100	100
30,000	100	100	100	102	101.6	100
35,000	106	106	103.6	100	100	102
40,000	107	106.2	103	102.8	102.5	104.2
45,000	106.2	107	102.2	103.6	104	104.4

Shaft speed rpm	η_E %					
	Amount of supplied oil kg·min					
	3	1.8	1	0.72	0.44	0.22
15,000	67.9	69	71.6	82.6	89.5	87.8
20,000	61.2	65	71.1	81.6	89.1	87.8
25,000	56.7	65.6	71.5	82.2	85.3	85.6
30,000	57.1	66.4	72.3	80.4	84	84.7
35,000	57.2	66	71.5	76.6	81.4	84.3
40,000	57	65.2	68.7	76.7	80.7	84.6
45,000	56.8	65.2	67.9	76.5	82	85.6

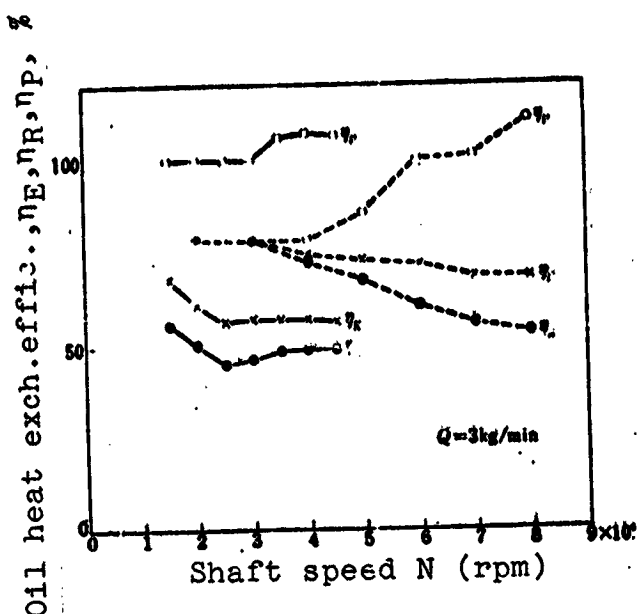


Figure 107. Heat exchange efficiency of oil and shaft speed:

— — — inner-race-riding cage;
- - - - - outer-race-riding cage

with an inner-race-riding cage, oil has more difficulty getting inside the bearing and most of the oil flows backward without heat exchange. Thus, looking at the oil which passes through the bearing, η_P of an inner-race-riding cage is greater than that of an outer-race-riding cage. However, because of the small penetration ratio, the overall heat exchange efficiency η_E of oil increases only slightly above η_R , resulting in a markedly smaller value than for an outer-race-riding cage.

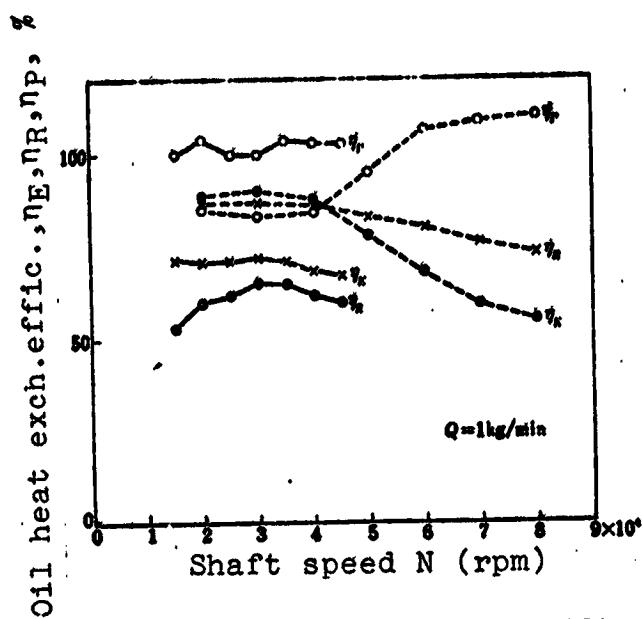


Figure 108. Heat exchange efficiency of oil and shaft speed:

— — — inner-race-riding cage;
- - - - - outer-race-riding cage

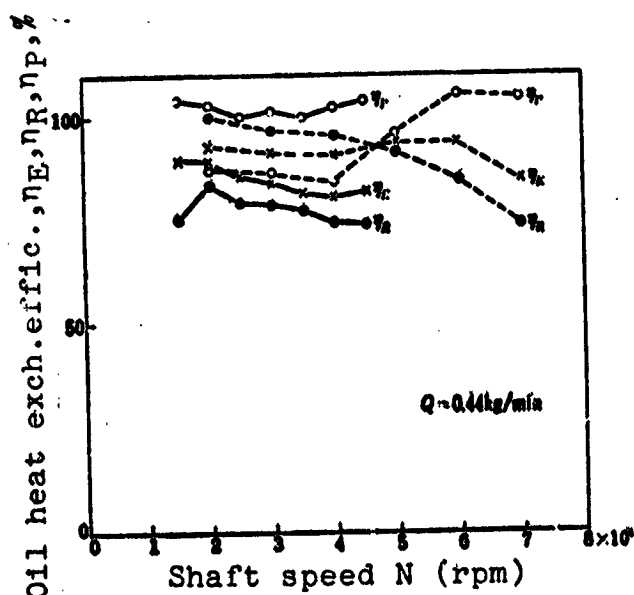


Figure 109. Heat exchange efficiency of oil and shaft speed:

— — — inner-race-riding cage;
- - - - - outer-race-riding cage

Figure 110 shows the relationship between oil flow Q and the average value of η_E in the high speed region. For comparison purposes, the results when the nozzle is placed between the cage and the outer race for an inner-race-riding cage, and the results on an outer-race-riding cage from the previous chapter, are also shown. From Figure 110, the relation between η_E (%) and oil flow Q (kg/min) can be expressed as follows:

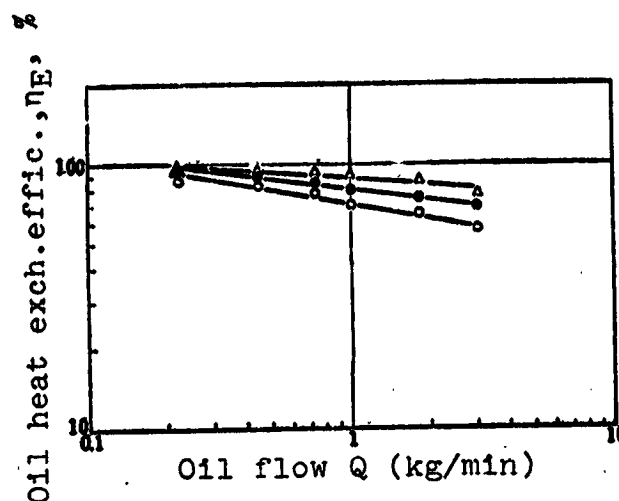


Figure 110. Heat exchange efficiency of oil and oil flow:

- — outer-race-riding cage (nozzle between cage and inner race);
- — inner-race-riding cage (nozzle between cage and inner race);
- △ — inner race-riding cage (nozzle between cage and outer race)

inner-race-riding cage (nozzle between the cage and inner race):

$$\eta_E = 70Q^{-0.11} \quad (48)$$

outer-race-riding cage (nozzle between the cage and inner race):

$$\eta_E = 80Q^{-0.11} \quad (49)$$

inner-race-riding cage (nozzle between the cage and outer race):

$$\eta_E = 90Q^{-0.07} \quad (50)$$

In Figures 86 - 91, the greater the penetration ratio, the larger η_E becomes, and the bearing temperature rise is correspondingly reduced. However, as mentioned before, when the nozzle is placed between the cage and the outer race for an inner-race-riding cage, η_E has the largest value, and the bearing temperature rise is minimum, but it is most susceptible to failure. Consequently, it is necessary to observe that the heat exchange efficiency of oil does affect the bearing temperature rise, but does not necessarily affect the failure limit of the bearing. From the standpoint of the failure

prevention, it is better to place the nozzle in the center between the cage and the inner race for both an inner-race-riding cage and an outer-race-riding cage. The, compared to an outer-race-riding cage, an inner-race-riding cage has the lower limiting dn value and smaller heat exchange efficiency of oil as seen from Equation (48) and (49), and is quite disadvantageous in the cooling of the bearing /67 also. Summing up the above points, an outer-race-riding cage is considerably more advantageous than an inner-race-riding cage for high-speed operations.

5.9. Bearing Friction

Figure 111 shows the relationship between the friction torque and the shaft speed for each oil flow rate, from the experimental data in Table 6. Figure 112 shows the relationship between the friction power loss obtained from the friction torque and the shaft speed again for each oil flow. Figures 113 and 114 show the comparison of these friction torque and friction power losses with the corresponding results for an outer-race-riding cage in the previous chapter. Compared to an outer-race-riding cage, the friction torque of an inner-race riding cage is small, and the difference becomes conspicuous at

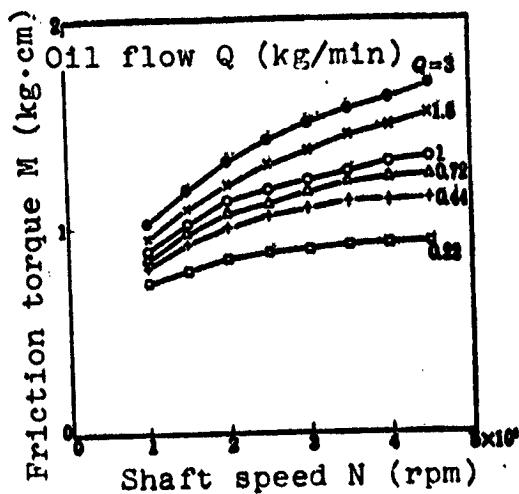


Figure 111. Friction torque and shaft speed

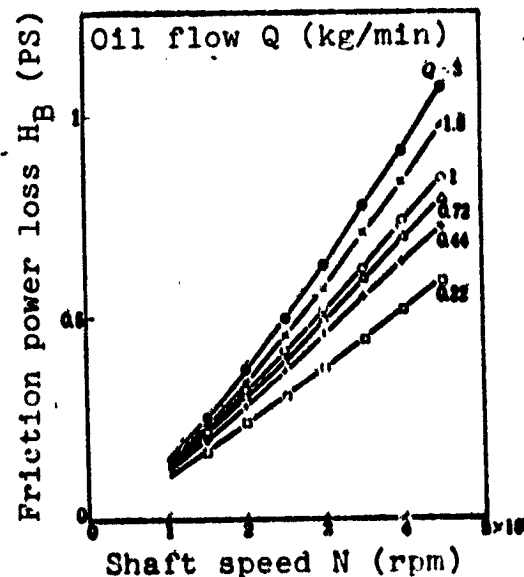


Figure 112. Friction power loss and shaft speed

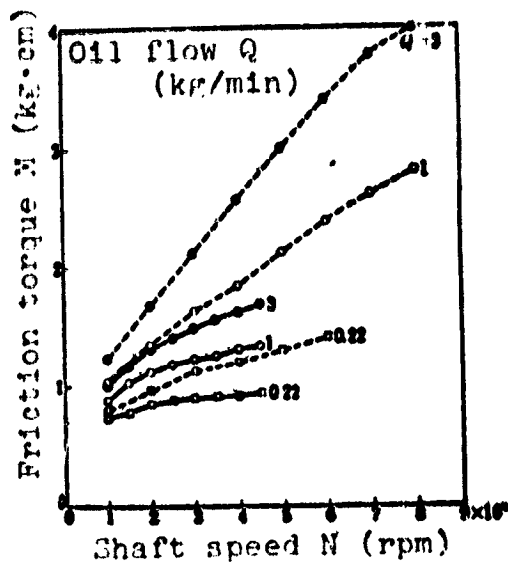


Figure 113. Friction torque and shaft speed

— — — inner-race-riding cage;
- - - - - outer-race-riding cage

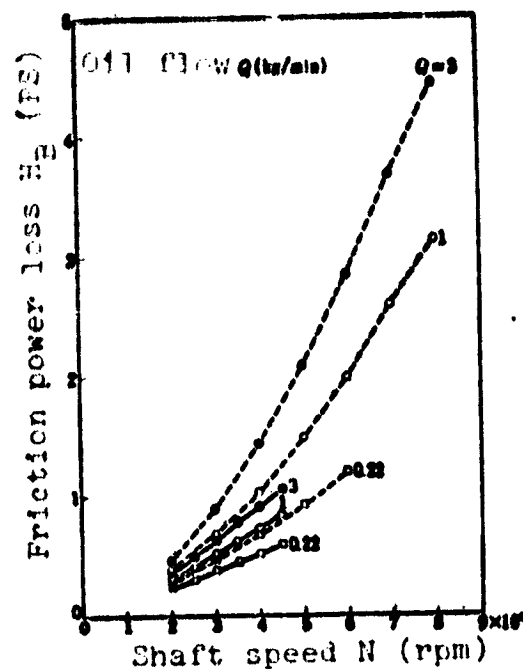


Figure 114. Friction power loss and shaft speed:

— — — inner-race-riding cage;
- - - - - outer-race-riding cage

high speed. Such a difference in the friction characteristics is due to the difference in the cage guide type. We will discuss this point later on.

A sample of the results examining the relationships among the friction torque, the viscosity at the bearing outer race temperature Z_B , the shaft speed N , and oil flow Q by varying an inlet oil temperature from 20°C to 120°C , as for an outer-race-riding cage in the previous chapter, is shown in Figures 115, 116, and 117. From these, the friction torque in the high speed region can be approximated by

$$M = Z_B^{0.5} N^{0.8} Q^{0.15} \quad (51)$$

Figure 118 is a result of obtaining the viscosity at the bearing temperature Z_B for each point in Figure 111, and arranging with

$Z_B^{0.5} N^{0.8} Q^{0.15}$ in Equation (51). In addition, the similar results

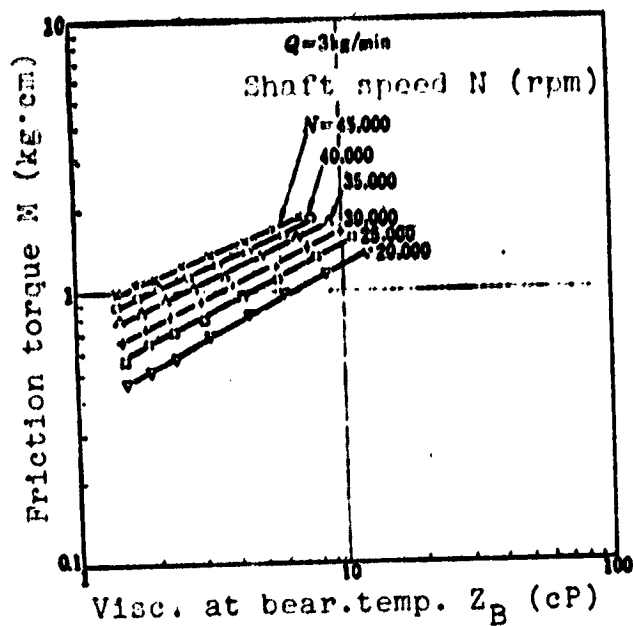


Figure 115. Friction torque and viscosity at the bearing temperature

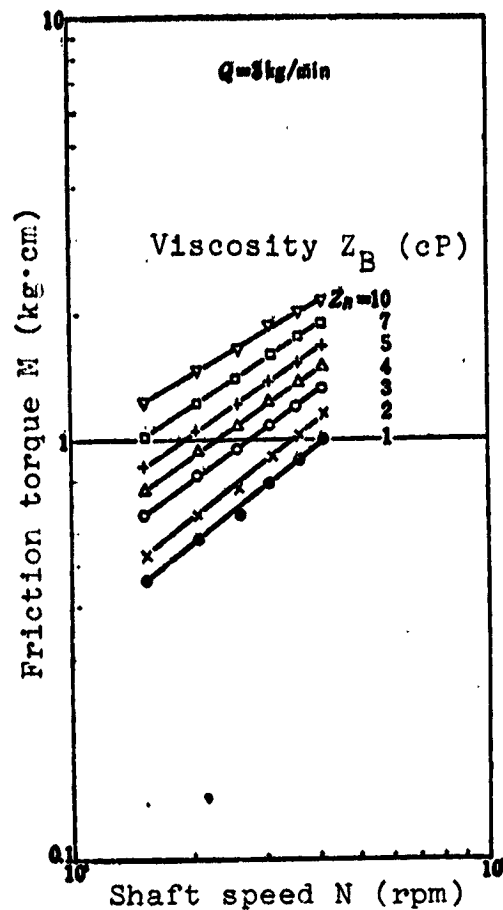


Figure 116. Friction torque and oil flow

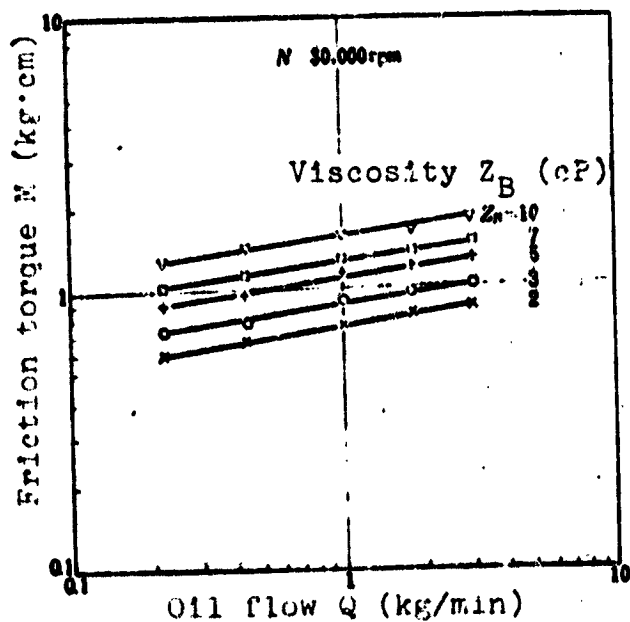


Figure 117. Friction torque and oil flow

for the thrust load of 25, 100, 150, and 200 kg are also shown. From this, it is clear that the friction torque can be approximately expressed by Equation (51). From Figure 118, the average velocity term M_v (kg · cm) of the friction torque can be expressed as

$$M_v = 10^{-4} Z_B^{0.5} N^{0.5} Q^{0.5} \quad (52)$$

where Z_B is in cP, N is in rpm, and Q in kg/min.

The non-velocity term M_p (kg · cm) of the friction torque can be expressed from Figure 119 as:

$$M_p = 2.3 \times 10^{-3} P^{0.7} \quad (53)$$

where P is in kg.

Consequently, the friction torque becomes:

$$M = 2.3 \times 10^{-3} P^{0.7} + 10^{-4} Z_B^{0.8} N^{1.2} Q^{0.3} \quad (54)$$

The friction power loss H_B (PS) of the bearing can be computed to be the following from Equation (54):

$$H_B = 3.2 \times 10^{-7} P^{0.7} N + 1.4 \times 10^{-8} Z_B^{0.8} N^{1.2} Q^{0.3} \quad (55)$$

where P is in kg, Z_B in cP, N in rpm, and Q in kg/min, just as in Equation (54) for the friction torque.

The friction torque of an outer-race-riding cage in the previous chapter was expressed as

$$M = 7 \times 10^{-3} P^{0.8} + 2.5 \times 10^{-4} Z_B^{0.8} N^{1.2} Q^{0.3} \quad (56)$$

Comparing Equations (54) and (56), the exponents of P and Z_B are greater for an inner-race-riding cage than for an outer-race-riding cage. This is considered to be caused by the fact that the maximum speed of an inner-race-riding cage is 45,000 rpm, whereas that for an outer-race-riding cage is 80,000 rpm, and that, as mentioned in the previous chapter, normally the lower the speed and the smaller the $T_B - T_I$, the greater becomes the exponent. An exponent

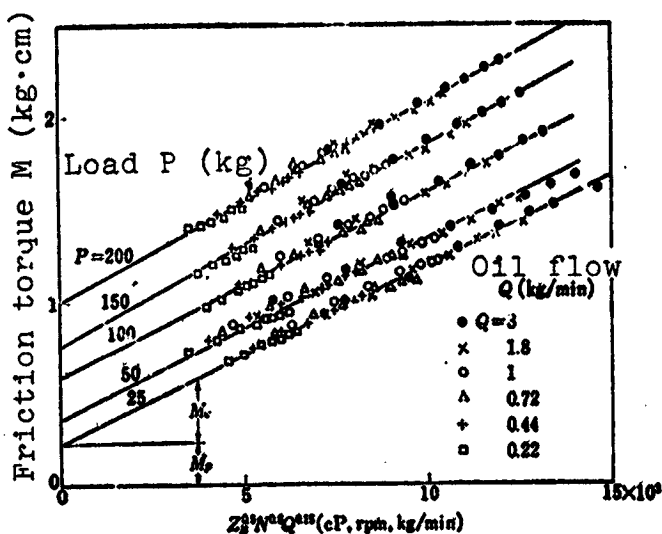


Figure 118. Friction torque, viscosity, shaft speed, and oil flow under various loads

of N for an inner-race-riding cage is 0.8, whereas for an outer-race-riding cage it is 1.2. Because we are measuring the friction torque of the outer race in this experiment, the larger exponent of an outer-race-riding cage is thought to be due to the sliding friction of the race riding surface of the cage and the outer race. The exponent Q is also smaller for

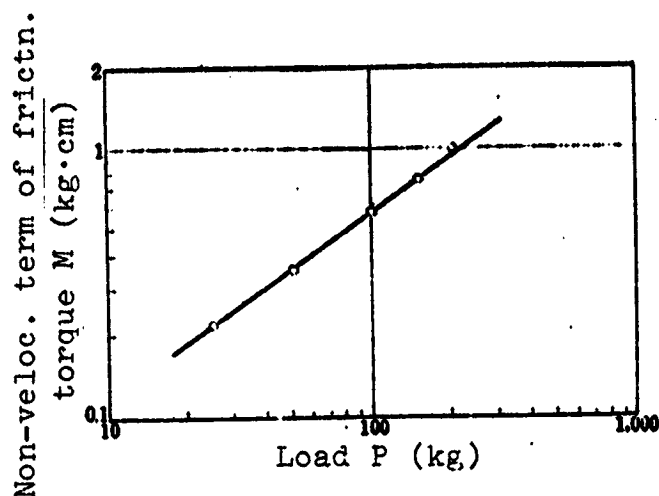


Figure 119. Non-velocity term of torque and load

an inner-race-riding cage than for an outer-race-riding cage. This can be explained by the fact that the penetration ratio of an inner-race-riding cage at high speed is extremely small compared to an outer-race-riding cage. That is, as the effects of Q in Equations (54) and (56) are caused by the churning resistance of oil inside the bearing, it seems natural that an inner-race-riding cage, for which it is more difficult for oil to enter inside the bearing, has a smaller exponent of Q than an outer-race-riding cage. Figure 120 shows the relation between the friction torque and the viscosity at the bearing temperature Z_B for both an outer-race-riding cage and an inner-race-riding cage, computed from Equation (54) for the thrust load of 50 kg, speed of 40,000 rpm, and oil flow of 3 kg/min. It is clear from Figure 120 that the friction torque of an outer-race-riding cage is approximately 50% greater than that of an inner-race-riding cage under identical friction conditions. As the friction torque of the outer race is measured in this experiment, the difference between the friction torques of an outer-race-riding cage and an inner-race-riding cage is considered to be equivalent to the sliding friction of the race riding surface of the cage and the outer race. The sliding friction of the cage constitutes a substantial part of the friction torque. At high speed, this difference becomes even greater.

5.10. Equation for Estimating Bearing Temperature Rise

Using the same method as in the previous chapter, the bearing temperature rise is obtained from the friction power loss in Equation (55) as follows, assuming all of friction heat is carried away by oil:

$$(T_B - T_I) = 9.6 \times 10^{-6} P^{0.7} N Q^{-0.76} + 4.2 \times 10^{-6} Z_B^{0.5} N^{1.5} Q^{-0.63} \quad (57)$$

Equation (28) or (29) is to be used as the relation between Z_B/Z_I and $T_B - T_I$ depending on the magnitude of $T_B - T_I$, because the maximum value of the bearing outer race temperature rise for an inner-race-riding cage is low compared to an outer-race-riding cage. From these, the following equations for the bearing temperature rise are derived:

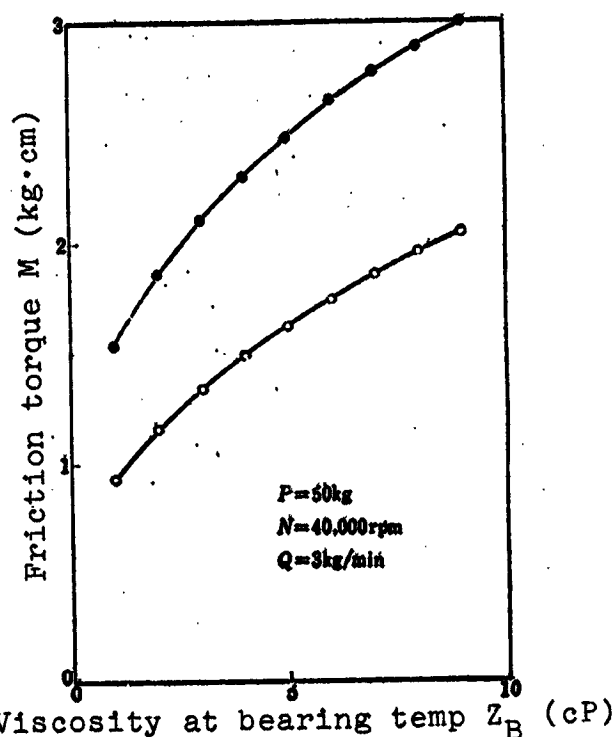
- (1) when $T_B - T_I$ is small
(7 - 20° C)

$$T_B - T_I = 5.4 \times 10^{-6} P^{0.6} N^{0.8} Q^{-0.63} (T_B - T_I)^{0.15} + 6.5 \times 10^{-6} Z_I^{0.43} N^{1.33} Q^{-0.64} \quad (58)$$

- (2) when $T_B - T_I$ is large (15 - 40° C),

$$T_B - T_I = 1.4 \times 10^{-6} P^{0.6} N^{0.77} Q^{-0.6} (T_B - T_I)^{0.15} + 3.4 \times 10^{-6} Z_I^{0.38} N^{1.33} Q^{-0.63} \quad (59)$$

Omitting the first term, which is based on the non-velocity term of the friction torque, in Equations (58) and (59), we get



$$T_B - T_I \propto Z_B^{0.48-0.45} N^{1.22-1.22} Q^{0.48-0.44} \quad (60)$$

The smaller value of exponent of each factor corresponds to the larger value of $T_B - T_I$. The exponent of each factor is approximately equivalent to those in the experimental equation (43) for the bearing outer race temperature rise.

As in the previous chapter, an approximate equation for the bearing outer race temperature rise, including the non-velocity term of the friction torque, can be formed as follows. Since, from Equation (55), the friction horsepower loss is proportional to $Z_B^{0.5} N^{1.8} Q^{0.15}$, the friction horsepower loss in Figure 112 may be formulated with $Z_B^{0.5} N^{1.8} Q^{0.15}$, resulting in Figure 121, and establishing Equation (55). A similar arrangement for other loads is performed, and the result summarized in Figure 122. The relation between the friction horsepower loss and load for $Z_B^{0.5} N^{1.8} Q^{0.15}$ equal to 1×10^8 , 2×10^8 , 3×10^8 , 4×10^8 , 5×10^8 in Figure 122, is obtained and

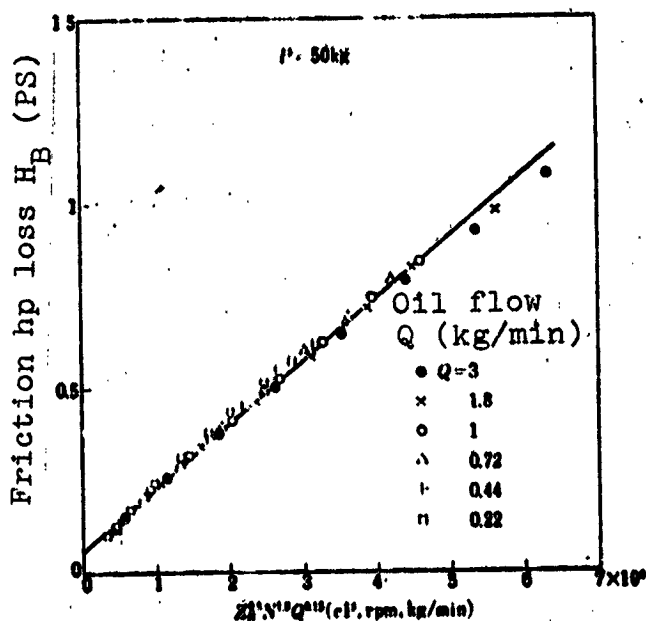


Figure 121. Friction horsepower loss, viscosity, shaft speed, and oil flow

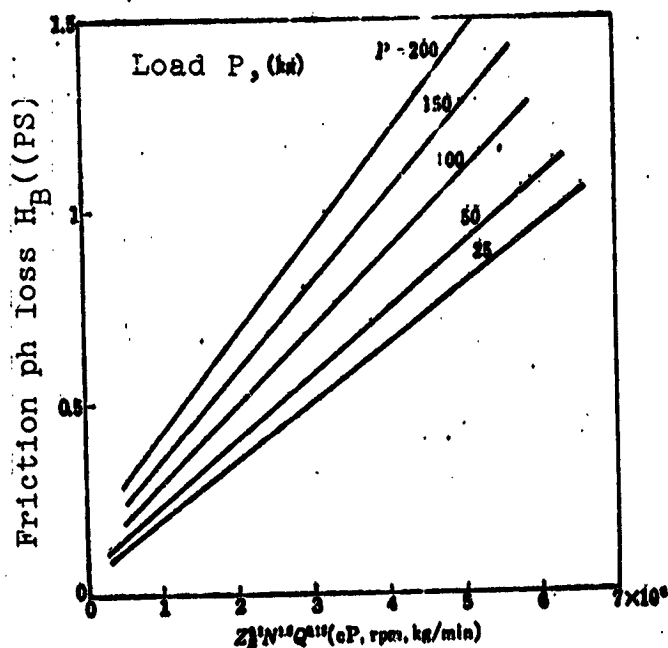


Figure 122. Friction horsepower loss, viscosity, shaft speed, and oil flow

shown in Figure 123. From this, the following approximation holds:

$$H_B \propto P^{0.5} \quad (61)$$

Therefore, the friction horsepower loss H_B (PS) can be approximated by the following equation instead of Equation (55)

$$H_B = 5.6 \times 10^{-10} Z_B^{0.5} P^{0.5} N^{1.8} Q^{0.2} \quad (62)$$

As before, P is in kg, Z_B

in cP, N in rpm, and Q in kg/min. Using Equation (62) to obtain the bearing temperature rise as before,

(1) when $T_B - T_I$ is small ($7 - 20^\circ \text{C}$),

$$T_B - T_I = 3.0 \times 10^{-4} Z_I^{0.4} P^{0.25} N^{1.39} Q^{-0.48} \quad (63)$$

(2) when $T_B - T_I$ is large ($15^\circ - 40^\circ \text{C}$)

$$T_B - T_I = 1.8 \times 10^{-4} Z_I^{0.4} P^{0.25} N^{1.39} Q^{-0.48} \quad (64)$$

The exponents of Z_I , N and Q in Equations (63) and (64) are naturally the same as in Equation (60), but an exponent of P varies from 0.25 to 0.28 depending on the magnitude of $T_B - T_I$, and roughly corresponds to the change in an exponent of P in Equation (43).

Figure 124 is a result of correlating $Z_I^{0.38} P^{0.25} N^{1.39} Q^{-0.48}$ in Equation (64) for the case of large $T_B - T_I$ with the bearing outer race temperature rise in Figure (94). Equation (64) holds within the range of 10,000 - 45,000 rpm speed and 0.22 - 3 kg/min oil flow.

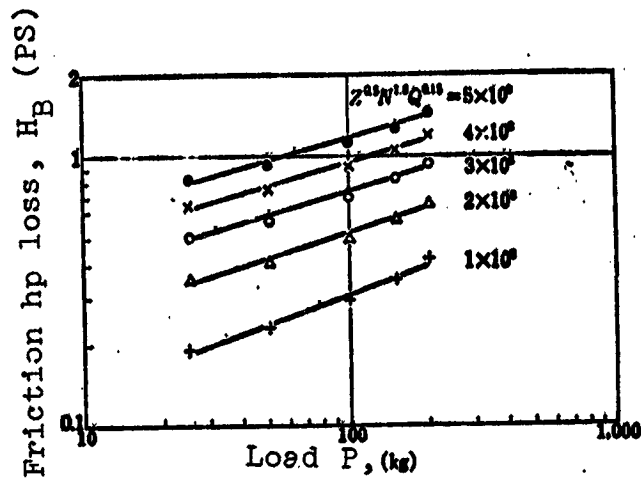


Figure 123. Friction horsepower loss and load for various values of $Z_B^{0.5} N^{1.8} Q^{0.2}$

In this case, an entire range can be approximated by Equation (64). Figure 125 is a result of correlating $Z_I^{0.38} P^{0.25} N^{1.39} Q^{-0.48}$ in Equation (64) and the bearing temperature rise under the various conditions: i.e., the bearing outer race temperature rise $T_B - T_I$ with a speed of 10,000 - 45,000 rpm, oil flow of 0.22 - 3 kg/min, thrust load of 25 - 200 kg, and inlet oil temperature of 25 - 75° C. As is clear from Figure 125, the observed values of the bearing outer race temperature rise under the various conditions roughly correspond to Equation (64), calculated from the friction horsepower loss.

Thus it was possible to formularize the relationship between the friction torque and the bearing temperature rise and each factor for an inner-race-riding cage. Despite the fact that the friction torque of an inner-race-riding cage is drastically smaller than that of an outer-race-riding cage, the bearing outer race temperature rise is higher for an inner-race-riding cage. As indicated in Equations (43) and (44), the large exponent of N and the small exponent of Q for an inner-race-riding cage are due to the small penetration ratio and the small heat exchange efficiency η_E of oil.

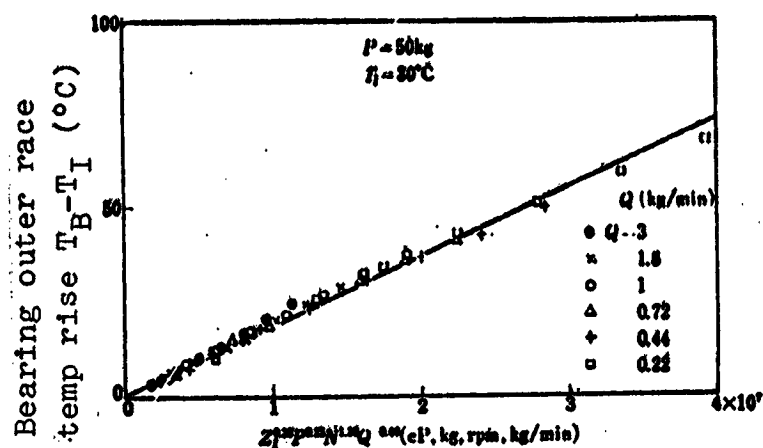


Figure 124. Bearing temperature rise, viscosity, load, shaft speed, and oil flow

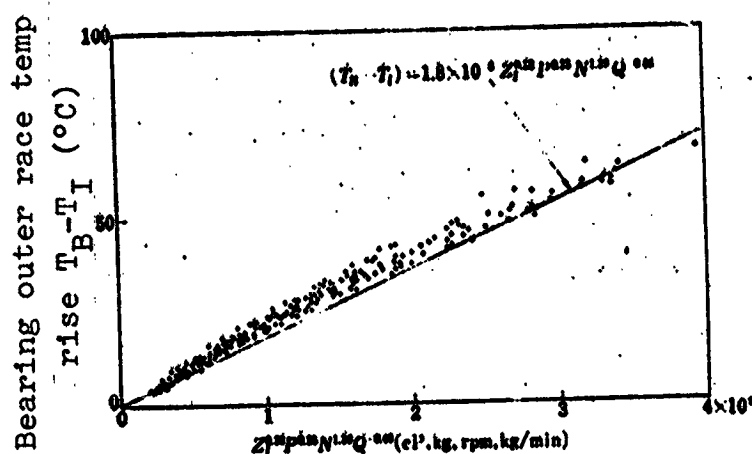


Figure 125. Bearing temperature rise, viscosity, load, shaft speed, and oil flow

5.11. Conclusions to Chapter 5

The limiting speed of an inner-race-riding cage type deep-groove ball bearing #6206, as well as the effects of shaft speed, oil flow, and other factors on the bearing temperature rise and the friction torque were studied and compared with the findings for an outer-race-riding cage given in the previous chapter.

(1) As mentioned in the previous chapter, the limiting dn value for an outer-race-riding cage is 210×10^4 at 0.22 kg/min oil flow, 240×10^4 at 0.44 kg/min, 270×10^4 at 0.72 kg/min, and 285×10^4 at 1 - 3 kg/min. The limiting dn value for an inner-race-riding cage, on the other hand, is $150 - 165 \times 10^4$, regardless of oil flow, and is substantially lower than for an outer-race-riding cage. In both cases, failure occurs on the race riding surface of the cage at the side opposite the nozzle. The difference in the limiting dn value is due to the difficulty of oil reaching inside of the bearing, especially the race riding surface of the cage on the side opposite the nozzle, for an inner-race-riding cage. Consequently, for high speed operations, an outer-race-riding-cage is more appropriate than an inner-race-riding cage.

(2) The heat exchange efficiency of lubricating oil η_E (%) can be expressed as a function of oil flow Q (kg/min) as follows, when the nozzle is directed at the center of the clearance between the cage and the inner race:

$$\begin{aligned} \text{(outer-race-riding cage)} \quad \eta_E &= 82Q^{-0.16} \\ \text{(inner-race-riding cage)} \quad \eta_E &= 70Q^{-0.22} \end{aligned}$$

74

Compared to an outer-race-riding cage, the heat exchange efficiency of oil for an inner-race-riding cage is low, especially when the oil flow rate is large. Corresponding to this, the bearing outer race temperature rise of an inner-race-riding cage is larger than for an outer-race-riding cage. This is because it is harder for oil to

enter inside the bearing for an inner-race-riding cage than for an outer-race-riding cage; that is, the penetration ratio is small. For high speed operation, therefore, an inner-race-riding cage is quite disadvantageous.

However, even with an inner-race-riding cage, if the nozzle is placed between the cage and the outer race, the penetration ratio increases substantially. The heat exchange efficiency of oil in this case becomes

$$\eta_B = 90 Q^{-0.07}$$

which is greater than for an outer-race-riding cage, and the bearing temperature rise also reaches a minimum. But the limiting dn value is the lowest. Consequently, the magnitude of the penetration ratio and the heat exchange efficiency of oil affect the bearing temperature rise, but are not related to the bearing failure. At high speed, it becomes important to have a large penetration ratio and, at the same time, effectively supply oil to the race riding surface of the cage at the opposite side of the nozzle, which is most vulnerable to failure. From this viewpoint also, an outer-race-riding cage is more suitable for high speed operation.

(3) The bearing temperature rise of the bearing outer race temperature T_B , from the oil inlet temperature T_I in the region up to 135×10^4 dn value, can be approximated by

$$(T_B - T_I) \propto Z_I^{0.4-0.5} P^{0.2-0.3} N^{1.2-1.4} Q^{0.2-0.3}$$

where Z_I is the oil viscosity at inlet oil temperature, P is thrust load, N is the speed, and Q is the oil flow rate. The smaller value of each exponent corresponds to the larger value of $T_B - T_I$.

(4) The horsepower absorption by lubricating oil H_0 can be approximated by

$$H_0 \propto Z_I^{0.2-0.3} P^{0.2-0.3} N^{1.2-1.4} Q^{0.4-0.5}$$

The smaller values of exponents of Z_I , P , and N , and the larger value of exponent of Q , correspond to the larger value of $T_B - T_I$. There exists a good correspondence with the equation for the bearing outer race temperature rise, indicating the fact that the oil acts like a coolant, as mentioned in the previous chapter.

(5) The limiting dn value for an inner-race-riding cage is $150 - 165 \times 10^4$, regardless of oil flow. Just as for an outer-race-riding cage, the bearing friction up to the dn value of 135×10^4 is mainly a viscous friction. The friction torque M (kg · cm) and the friction horsepower loss H_B (PS) can be approximately expressed as follows:

$$M = 2.3 \times 10^{-3} P^{0.7} + 10^{-4} Z_B^{0.5} N^{0.5} Q^{0.8}$$

$$H_B = 3.2 \times 10^{-7} P^{0.7} N + 1.4 \times 10^{-6} Z_B^{0.5} N^{0.5} Q^{0.8}$$

where Z_B is oil viscosity at the bearing temperature and is in cP, P is in kg, N in rpm, and Q in kg/min.

Compared to an outer-race-riding cage, the exponent of N for an inner-race-riding cage is small. This is because, for an inner-race-riding cage, the sliding friction of the race riding surface of the cage does not involve the friction torque of the outer race. The friction torque of an inner-race-riding cage is small compared to an outer-race-riding cage, but because of the small penetration ratio, the bearing outer race temperature rise is greater than for an outer-race-riding cage.

(6) If all the friction heat is assumed to be carried away by oil, the bearing outer race temperature rise ($^{\circ}\text{C}$) in the high speed region becomes the following, from the experimental equation for the friction horsepower loss:

$$T_B - T_I = 1.8 \times 10^{-6} Z_B^{0.5} P^{0.7} N^{0.5} Q^{-0.8}$$

where Z_I is in cP, P in kg, N in rpm, and Q in kg/min. The equation for estimating the bearing temperature rise derived from the friction horsepower loss agrees very well with the observed data.

CHAPTER 6. ANGULAR CONTACT BALL BEARING (#17206)

6.1. Introduction

In Chapters 4 and 5, the limiting dn value as well as the various characteristics of the deep-groove ball bearings (#6206) were discussed. In this chapter, the limiting dn value and the high speed performance of the angular contact ball bearing (#17206) will be discussed. This type of bearing is being widely used in high speed spindles of machine tools and an elucidation of its limiting dn value and the bearing performance is quite desirable from the practical viewpoint.

In Chapter 5, it was indicated that the type of cage guide type had a decisive effect on the limiting dn value of the deep-groove ball bearing (#6206). That is, when an outer-race-riding cage was used, the limiting dn values were 210×10^4 at an oil flow rate of 0.22 kg/min, 240×10^4 at 0.44 kg/min, 270×10^4 at 0.72 kg/min, and 284×10^4 at 1 - 3 kg/min, whereas when an inner-race-riding cage was used, it was substantially reduced to $150 - 165 \times 10^4$, regardless of oil flow. This is because, for an inner-race-riding cage, it is more difficult for oil to get inside the bearing compared to an outer-race-riding cage. Further, even oil which reaches the inside of the bearing has difficulty getting to the race riding surface of the cage at the opposite side of the nozzle, which is most vulnerable to failure. In addition, for an inner-race-riding cage, when the race riding surface of the cage at the nozzle side is abraded, the abrasive dust, together with the oil is drawn into the bearing, causing early failure. As a result, compared to an outer-race-riding cage, an inner-race-riding cage is quite disadvantageous at

high speeds, and special measures become necessary in order to raise the limiting dn value of an inner-race-riding cage. In Chapter 5, it was stated that the limiting dn value could be raised by using a particular cage configuration, such that oil can easily enter the bearing at high speed even for an inner-race-riding cage. It is naturally expected that the limiting dn value would also be changed by the material used for the cage. Bearing #17206 is equipped with an inner-race-riding cage, and its cage material is phenolic resin, as opposed to high-strength yellow brass for #6206. Thus, the influence of the cage material on the limiting dn value can also be studied. /75

6.2. Experimental Conditions

Although already mentioned in Chapters 2 and 3, the conditions used in this experiment are summarized here. The nozzle is directed to the center of the clearance between the cage and the inner race. A distance between the leading edge of the nozzle and the face of the inner race is 8 mm. The jet velocity is constant at roughly 20 m/s irrespective of oil flow. Unless specified explicitly, the number of nozzles is one, and the nozzle is placed at the unloaded side of the inner race. Besides this, an experiment was conducted by placing the nozzle on the thrust loaded side of the inner race, and also using two nozzles facing each other; these will be mentioned as they arise later.

Also, unless specified explicitly, the thrust load is constant at 50 kg, and oil inlet temperature is also constant at 30° C.

6.3. Test Bearing

The test bearing is an SP-class #17206 angular contact ball bearing. The cage is made of phenolic resin, and the cage guide type is an inner-race-riding cage. The test bearing is commercially available and no special measures are necessary, such as an oil groove to improve the feeding and discharging of oil found in #6206. The dimensions of the test bearing are shown in Table 9.

TABLE 9. TEST BEARING #17206 (SP)

Diameter of steel balls, mm	9.525 (3/8")
Number of steel balls	11
Percentage of groove radius to steel ball	
Outer race, %	51.0 - 52.0
Inner race, %	50.5 - 51.0
Contact angle, deg.	15
Cage guide type	Inner-race-riding cage
Cage material	Phenolic resin
Guide clearance, mm	0.4 + 0.1 - 0.02
Pocket clearance, mm	0.155 ± 0.05

6.4. Experimental Results

The limiting speed, the bearing outer race temperature, the outlet oil temperature at the nozzle side as well as the bearing transmitted side, the friction torque, the penetration ratio, and the shaft speed for various oil flows under the constant thrust load of 50 kg, and the constant inlet oil temperature of 30° C are shown in Table 10.

The above experimental results, as well as the results obtained by changing the thrust load and inlet oil temperature are discussed below.

6.5. Allowable Limiting dn Value

Figure 126 shows the relationship between the bearing outer race temperature and shaft speed from the results of Table 10. In the neighborhood of 65,000 rpm for oil flow of 0.22 kg/min or 0.44 kg/min, 70,000 rpm for 0.72 kg/min, and 75,000 rpm for 1 - 3 kg/min, the frictional force which has been smooth up to then suddenly increases

TABLE 10. BEARING TEMPERATURE, OUTLET OIL TEMPERATURE, FRICTION TORQUE, PENETRATION RATIO, AND SHAFT SPEED (30° C inlet oil temperature and 50 kg thrust load)

Oil flow $Q = 3$ kg/min (room temperature 24° C)

Shaft speed, rpm	Bearing outer race temp., °C	Outlet oil temp. (nozzle side), °C	Outlet oil temp. (transm. side), °C	Friction torque kg·cm	Penetration ratio, %
10,000	33	31	33	1.15	46.9
20,000	37	31.5	37	1.32	41.1
30,000	41.5	32.5	41.5	1.64	35.0
40,000	47	34.5	46.5	1.75	30.6
50,000	52.5	36.5	52.5	1.85	27.0
60,000	58.5	40	58.5	1.95	24.4
70,000	65.5	43.5	66	2.03	23.3
75,000	failure				

$Q = 1.8$ kg/min (room temperature 26° C)

Shaft speed, rpm	Bearing outer race temp., °C	Outlet oil temp. (nozzle side), °C	Outlet oil temp. (transm. side), °C	Friction torque kg·cm	Penetration ratio, %
10,000	34	31.5	34	1.07	50.4
20,000	39.5	33	39	1.33	48.4
30,000	44.5	35	43.5	1.51	43.4
40,000	50	37.5	49.5	1.63	38.4
50,000	53.5	41	57	1.69	34.2
60,000	64.5	45.5	65	1.77	31.2
70,000	72	50	73.5	1.82	23.4
75,000	failure				

$Q = 1$ kg/min (room temperature 27° C)

Shaft speed, rpm	Bearing outer race temp., °C	Outlet oil temp. (nozzle side), °C	Outlet oil temp. (transm. side), °C	Friction torque kg·cm	Penetration ratio, %
10,000	35.5	32.5	35.5	1.02	53.8
20,000	42.5	35	42.5	1.24	53.3
30,000	49.5	38	49	1.37	50.8
40,000	57	41.3	56.5	1.47	45.7
50,000	64	46	66	1.53	40.0
60,000	76	52.5	76	1.58	34.1
70,000	87.5	59	89.5	1.64	30.8
75,000	failure				

(Table continued on following page)

TABLE 10 (continued)

 $Q = 0.72 \text{ kg/min}$ (room temperature 30°C)

Shaft speed, rpm	Bearing outer race temp., $^\circ\text{C}$	Outlet oil temp. (nozzle side), $^\circ\text{C}$	Outlet oil temp. (transm. side), $^\circ\text{C}$	Friction torque, kg·cm	Penetration ratio, %
10,000	37.5	34	37	0.97	57.2
20,000	44.5	36.5	44.5	1.18	58.0
30,000	53	40	54	1.28	56.2
40,000	61.5	45.5	62	1.36	51.7
50,000	70.5	51.5	72	1.41	46.1
60,000	83	60	84	1.44	38.5
70,000	failure				

 $Q = 44 \text{ kg/min}$ (room temperature 28°C)

Shaft speed, rpm	Bearing outer race temp., $^\circ\text{C}$	Outlet oil temp. (nozzle side), $^\circ\text{C}$	Outlet oil temp. (transm. side), $^\circ\text{C}$	Friction torque, kg·cm	Penetration ratio, %
10,000	39.5	36.5	39	0.92	59.7
20,000	48.5	40.5	49	1.08	64.8
30,000	59	46.5	60	1.16	64.5
40,000	69	52.5	70.5	1.23	60.3
50,000	80.5	60.5	83.5	1.27	52.8
60,000	95	73	99.5	1.33	43.5
65,000	failure				

 $Q = 0.22 \text{ kg/min}$ (room temperature 25°C)

Shaft speed, rpm	Bearing outer race temp., $^\circ\text{C}$	Outlet oil temp. (nozzle side), $^\circ\text{C}$	Outlet oil temp. (transm. side), $^\circ\text{C}$	Friction torque, kg·cm	Penetration ratio, %
10,000	42.5	39	42	0.86	54.8
20,000	56	46.5	56	0.96	67.0
30,000	68.5	55	69.5	1.04	68.6
40,000	81	66	82.5	1.10	67.8
50,000	94	77	99.5	1.15	59.8
60,000	106	92.5	120.5	1.18	50.6
65,000	failure				

very rapidly and causes a bearing failure within a very short time. Although the bearing outer race temperature at this time is low at 70 - 100° C, the failure occurs on the race riding surface of the cage at the opposite side of the nozzle, as shown in Figure 127. Phenolic resin has carbonized, and at the inner race facing it is also discolored, indicating quite a high temperature. Figure 128 shows the relation between the limiting dn value and oil flow. For comparison purposes, the limiting dn values of the two deep-groove ball bearings (#6206) equipped with an outer-race-riding cage and an inner race-riding-cage, respectively, in Chapters 4 and 5, are also shown together. The limiting dn value of #6206 with an inner-race-riding cage was $150 - 165 \times 10^4$, regardless of oil flow, but for #17206, the limiting dn value increased substantially, despite the fact that the same inner-race-riding cage was used, approaching the limiting dn value of #6206 with an outer-race-riding cage.

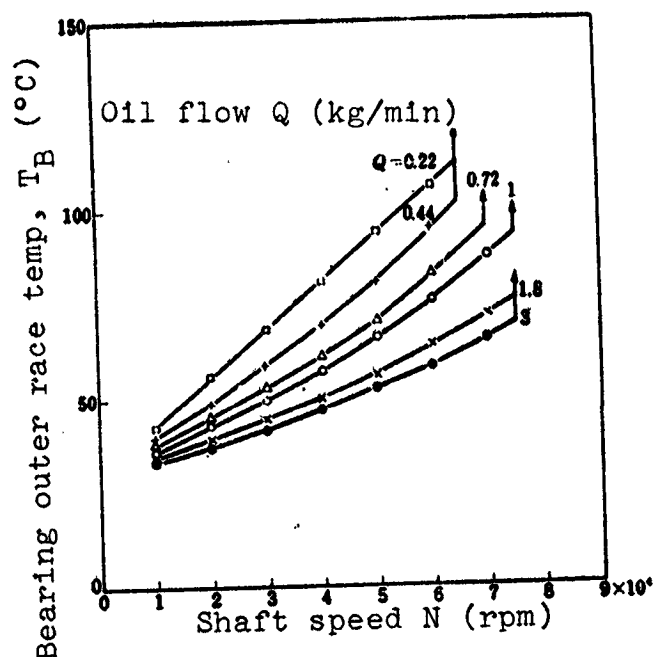


Figure 126. Bearing outer race temperature and shaft speed

Although #6206 and #17206 have different internal bearing dimensions, and thus exhibit different behaviors at high speed, the failure at high speed occurs in both cases at the sliding friction portion of the race surface of the cage at the opposite

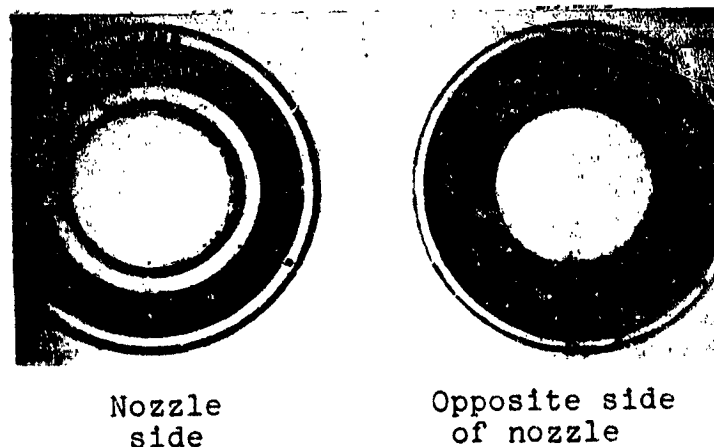


Figure 127. Exterior view of the failed bearing

side of the nozzle. Thus, the large difference in the limiting dn value could be explained by the difference in the cage material. Because the cage of #6206 is made of a high-strength yellow brass, the failure tends to occur at high speed for the oil-less condition. When equipped with an inner-race-riding cage, an abrasive dust, created on the race surface of the cage, is drawn inside the bearing by the oil jet flow, prompting the bearing failure. On the other hand, because the cage of #17206 is made of phenolic resin, compared to high-strength yellow brass, it is more resistant to failure, even for the boundary lubrication condition. The wear resistance is also large. This difference is considered to have caused the big difference in the limiting dn value even for the same inner-race-riding cages. Although a phenolic resin is superior in wear resistance, it is inferior in heat resistance, and thus the limiting dn value is suppressed by the carbonization of phenolic resin, as shown in Figure 127. By using the material which possesses better wear resistance and heat resistance, the limiting dn value can be further increased.

Let us analyze the above results in more detail. Figures 129, 130, 131, 132, 133, and 134 show the bearing outer race temperature rise $T_B - T_I$ due to the inlet oil temperature T_I (30°C) to the bearing outer race temperature T_B and the penetration ratio as a function of shaft speed. As mentioned in Chapter 3, for #17206, there is a large difference in the penetration ratio depending on which side of the inner race the nozzle is placed; therefore, the results when the nozzle is placed on the thrust loaded side of the inner race are also shown. Further, for comparison purposes, the results for #6206 equipped with an inner-race-riding cage in Chapter 5 are also shown. With #17206, when the nozzle was placed on the unloaded side of the inner race, the penetration ratio was highest, matching #6206 with an outer-race-riding cage in Chapter 4. #6206 with an inner-race-riding cage follows next, and #17206 with the nozzle placed at the thrust loaded side of the inner race was the lowest, with a reduction to only a few percent at high speed. The bearing outer race temperature rise also corresponds to the magnitude of the penetration

/80

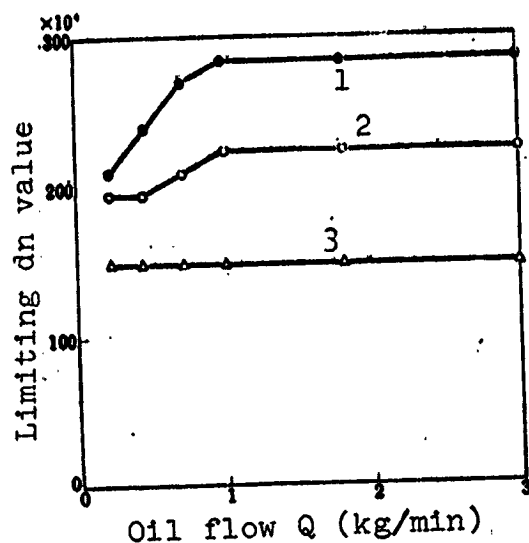


Figure 128. Limiting dn value and oil flow

1 — #6206 (outer-race-riding cage); 2 — #17206 (inner-race riding cage); 3 — #6206 (inner-race-riding cage)

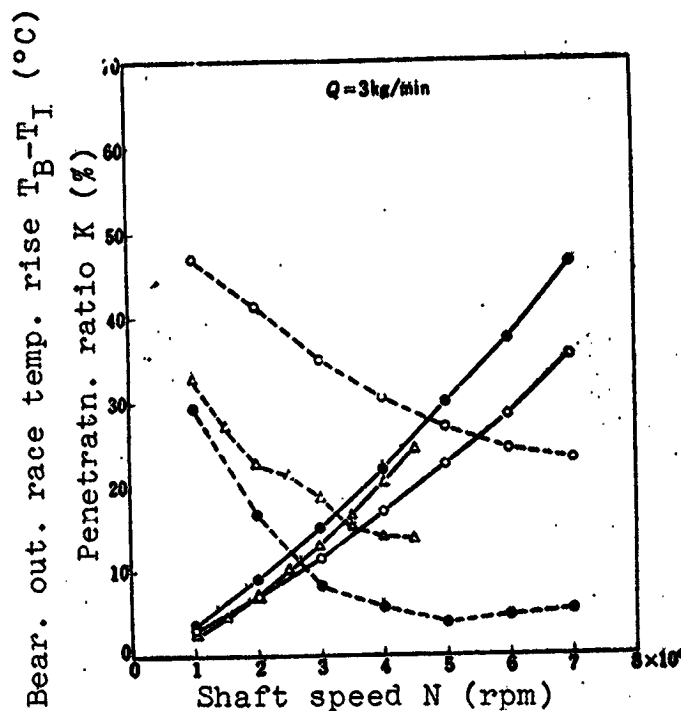


Figure 129. Bearing temperature rise, penetration ratio, and shaft speed:

o — #17206 (nozzle at unloaded side of inner race); • — #17206 (nozzle at thrust loaded side of inner race); Δ — #6206 (nozzle at thrust loaded side of inner race); — — — bearing temperature rise; - - - - - penetration ratio

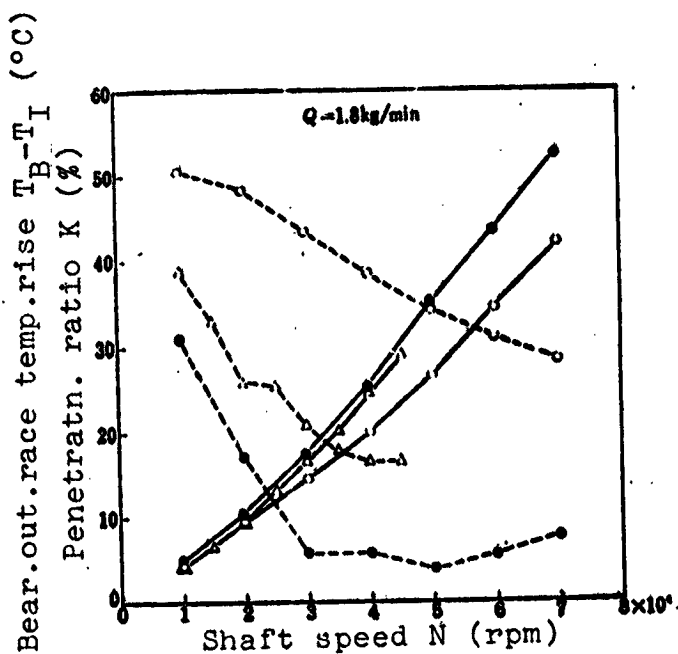


Figure 130: Bearing temperature rise, penetration ratio, and shaft speed.

— — — bearing temperature rise; - - - - - penetration ratio

ratio; the greater the penetration ratio, the lower becomes the bearing outer race temperature rise. An increase in the penetration ratio can be thought of as one of the reasons for a substantial increase in the limiting dn value when the nozzle is placed at the unloaded side of the inner race of #17206, compared to #6206 with an

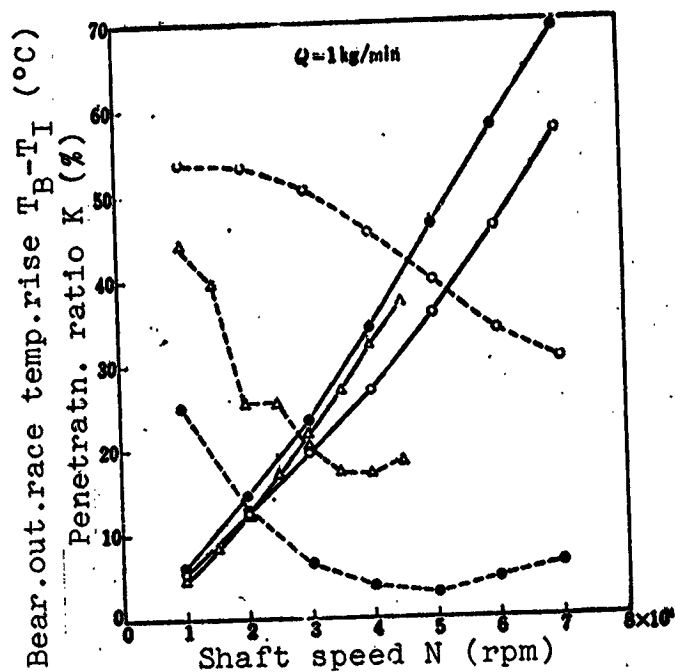


Figure 131. Bearing temperature rise, penetration ratio, and shaft speed:

— — bearing temperature rise; - - - - penetration ratio

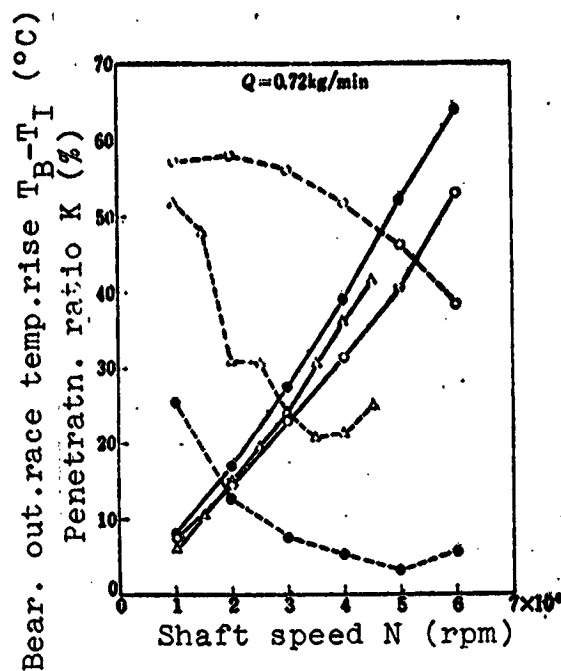


Figure 132. Bearing temperature rise, penetration ratio, and shaft speed:

— — bearing temperature rise; - - - - penetration ratio

inner-race-riding cage. Although with #17206 the penetration ratio is small when the nozzle is placed at the thrust loaded side of the inner race, compared to when it is placed at the unloaded side of the inner race, the bearing failure takes place in both cases at 75,000 rpm, as shown in Figure 135. This indicates that, as shown in Figure 15, in both cases, most of the oil flows through the empty space between the cage and the shoulder drop of the outer race. Even though there is a wide difference in the penetration ratio, there is not much difference in oil flow passing through the race surface of the cage at the opposite side of the nozzle, which is most susceptible to failure. Thus, with an inner-race-riding cage, even if there is a wide difference in the penetration ratio, the difficulty of oil reaching the race surface of the cage, which is susceptible to failure, is the same. Consequently, the difference in the limiting dn values of #6206 and #17206, both of which are

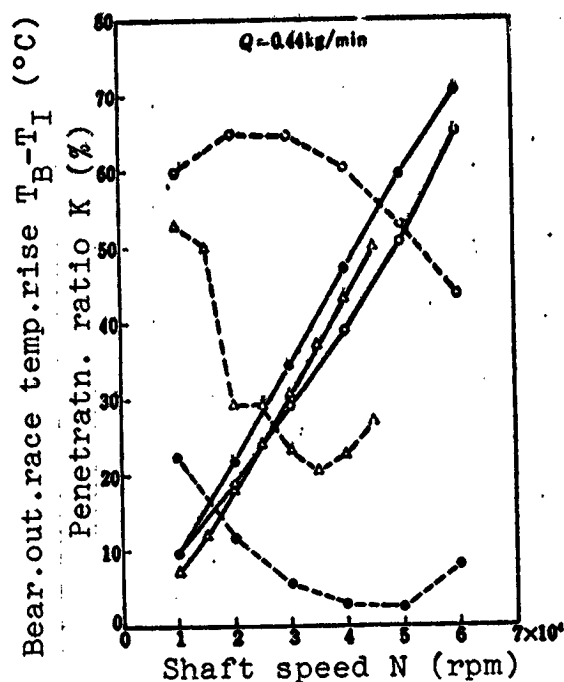


Figure 133. Bearing temperature rise, penetration ratio, and shaft speed:

— — bearing temperature rise; - - - - - penetration ratio

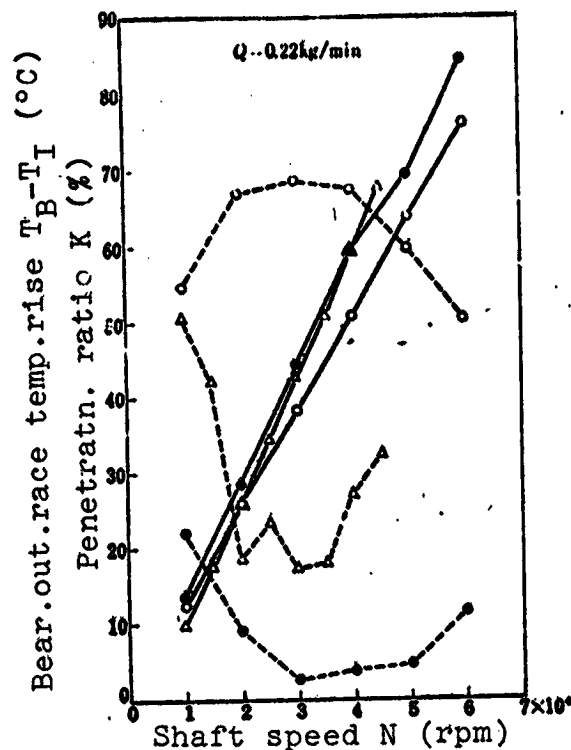


Figure 134. Bearing temperature rise, penetration ratio, and shaft speed:

— — bearing temperature rise; - - - - - penetration ratio

equipped with an inner-race-riding cage, must be mainly due to the difference in the cage material. /81

As is clear from the above results, the factor which governs the limiting speed of the high speed roller bearing is the lubrication of the cage. In order to reduce the average temperature of the bearing, increasing the penetration ratio by feeding a large amount of oil into the bearing is effective. On the other hand, it is more important to consider how to effectively supply oil to the area of the cage most susceptible to failure, particularly the race surface of the cage at the opposite side of the nozzle, rather than just consider the average temperature of the bearing or the magnitude of the penetration ratio. From this point, it seems effective, especially with an inner-race-riding cage, to use two nozzles facing

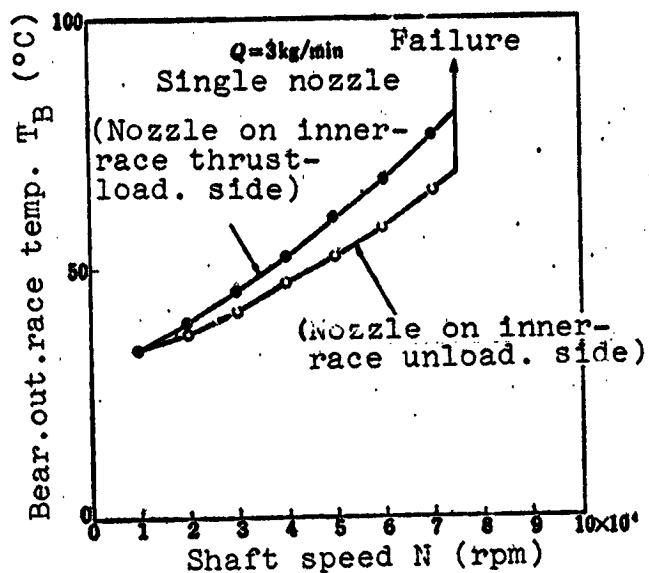


Figure 135. Limiting shaft speed and nozzle position

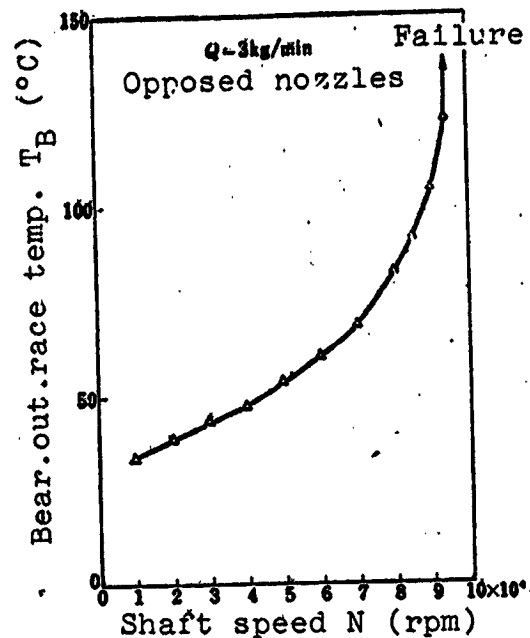


Figure 136. Limiting shaft speed and opposed nozzles

each other 180° apart with the same total oil flow. Figure 136 shows the relation between the bearing outer race temperature rise and shaft speed when the two facing nozzles, with 1.5 kg/min each for a total oil flow of 3 kg/min, are used. Whereas for a single nozzle, the failure occurred at 75,000 rpm, as shown in Figure 135, for two opposed nozzles the limiting speed greatly increased to 95,000 rpm, even though the total oil flow was identical. However, as the speed is increased above 80,000 rpm, the friction temporarily increases, and then decreases and becomes stable, indicating some risk above the 80,000 rpm speed.

6.6. Bearing Temperature Rise

Figure 137 shows the relationship between the rise in temperature $T_B - T_I$ from the inlet oil temperature T_I (30°C) to the bearing outer race temperature T_B and shaft speed, from the results in Table 10. The relations among the bearing outer race temperature rise $T_B - T_I$, shaft speed N , and oil flow Q are shown in Figures 138, 139.

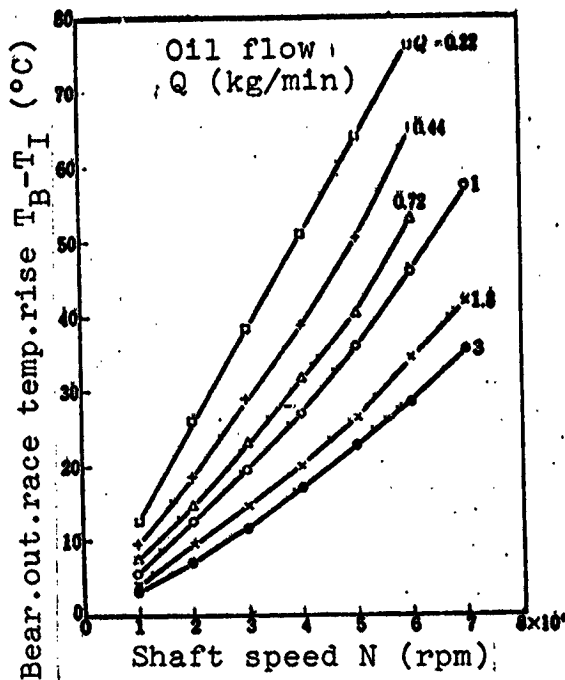


Figure 137. Bearing temperature rise and shaft speed

In Figure 138, the relation between $T_B - T_I$ and N changes at 40,000 rpm, just as for #6206 equipped with an outer-race-riding cage in Chapter 4. In the high speed region above 40,000 rpm, it can be expressed as

$$(T_B - T_I) \propto N^{0.4-0.5} \quad (65)$$

From Figure 139, the relation between $T_B - T_I$ and Q can be expressed as

$$(T_B - T_I) \propto Q^{-0.41-0.57} \quad (66)$$

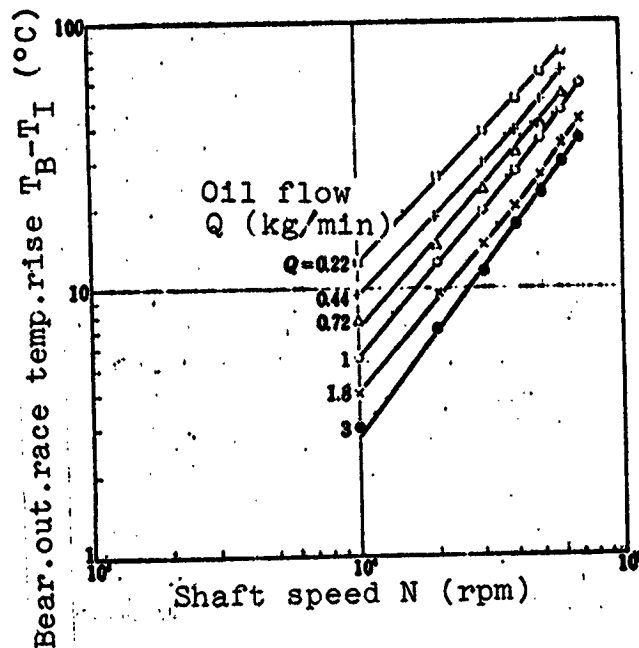


Figure 138. Bearing temperature rise and shaft speed

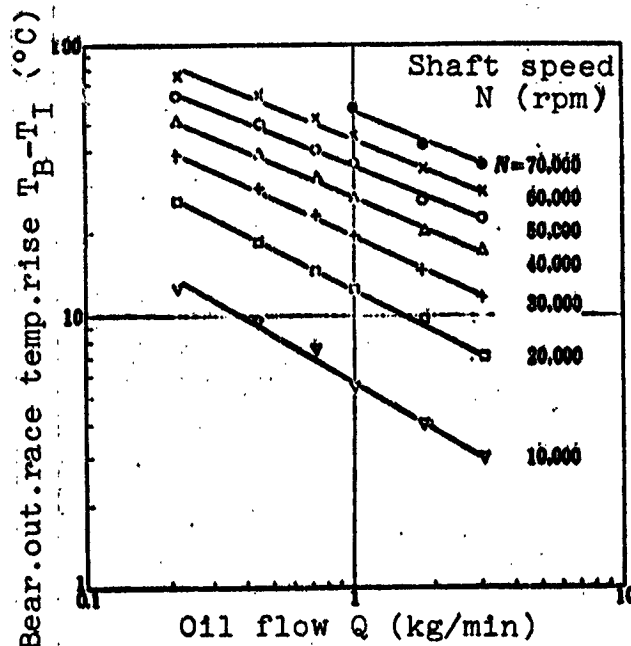


Figure 139. Bearing temperature rise and oil flow

The smaller values of the exponents of N and Q correspond to the larger value of $T_B - T_I$.

Equations (65) and (66) represent the case in which the nozzle is placed on the unloaded side of the inner race. When the nozzle is placed on the thrust loaded side of the inner race, the following holds simultaneously:

$$\left. \begin{aligned} (T_B - T_I) &\propto N^{1.0-1.25} \\ (T_B - T_I) &\propto Q^{-0.25-0.35} \end{aligned} \right\} \quad (67)$$

Again, the smaller values of exponents of N and Q correspond to the larger value of $T_B - T_I$.

The above results are for the constant thrust load of 50 kg and the constant inlet oil temperature of 30° C. The relation between the bearing outer race temperature $T_B - T_I$ versus the load P and the oil viscosity at an inlet oil temperature Z_I , when the thrust load is varied from 25 kg to 200 kg, and inlet oil temperature is varied from 30° C to 90° C, can be approximated by the following. The details are omitted:

$$\left. \begin{aligned} (T_B - T_I) &\propto P^{0.15-0.25} \\ (T_B - T_I) &\propto Z_I^{0.5-0.8} \end{aligned} \right\} \quad (68)$$

The smaller values of exponents of P and Z_I correspond to the larger value of $T_B - T_I$.

Summarizing the above, the bearing outer race temperature rise in the high speed region can be expressed as:

$$(T_B - T_I) \propto Z_I^{0.3-0.5} P^{0.15-0.25} N^{1.0-1.25} Q^{-0.25-0.35} \quad (69)$$

The smaller values of exponents of each factor correspond to the larger value of $T_B - T_I$. Compared to Equation (5) for the bearing outer race temperature rise of #6206 equipped with an outer-race-riding cage in Chapter 4, the exponents of Z_I , P, and Q are nearly the same but the exponent of N is quite small for #17206. As mentioned in Chapter 5, the exponent of N of #6206 is larger for an

inner-race-riding cage than for an outer-race-riding cage, because of the smaller penetration ratio of an inner-race-riding cage. As the penetration ratio of #17206 is roughly the same as that of #6206 (outer-race-riding cage), the exponent of N for the bearing temperature rise becomes small because of the small exponent of N for friction torque of an inner-race-riding cage, compared to an outer-race-riding cage under such conditions. This point will be discussed again in the section on friction torque. Although the penetration ratio becomes very small and the bearing outer race temperature rise becomes large when the nozzle is placed on the thrust loaded side of the inner race, the relation of the temperature rise to shaft speed and oil flow are nearly the same as when the nozzle is placed on the thrust loaded side of the outer race, as shown in Equation (67). This is probably because most of the oil flows through the empty space around the shoulder drop of the outer race, as shown in Figure 15, thereby not affecting the characteristics of the bearing outer race temperature much, even if there is a large difference in the penetration ratio.

6.7. Amount of Heat Absorption by Lubricating Oil

From Table 10, the horsepower absorption by the deflected oil and the transmitted oil, as well as the total horsepower absorption by oil, are calculated and shown in Table 11. Figure 140 shows the relation between the total horsepower absorption by oil H_0 and shaft speed from the results in Table 11. The relationship of the total horsepower absorption by oil H_0 , with shaft speed N and oil flow Q, are shown in Figures 141 and 142. In Figure 141, the relation between H_0 and H changes at 40,000 rpm, just like for the bearing outer race temperature rise, and H_0 in the high speed region above 40,000 rpm can be expressed as:

$$\left. \begin{aligned} H_0 &\propto N^{1.17} \\ H_0 &\propto Q^{0.88} \end{aligned} \right\} \quad (70)$$

The smaller exponent of N and the larger exponent of Q correspond to the larger value of $T_B - T_I$.

/84

TABLE 11. HORSEPOWER ABSORPTION BY OIL VERSUS SHAFT
SPEED
(30° C inlet oil temperature and 50 kg thrust load)

Oil flow Q = 3 kg/min

Shaft speed, rpm	Horsepower absorption by oil (nozzle side), PS	Horsepower absorption by oil (transm. side), PS	Total hp absorption by oil, PS
20,000	0.13	0.42	0.55
30,000	0.24	0.60	0.84
40,000	0.45	0.73	1.18
50,000	0.68	0.87	1.55
60,000	1.07	0.99	2.06
70,000	1.49	1.20	2.69

Q = 1.8 kg/min

Shaft speed, rpm	Horsepower absorption by oil (nozzle side), PS	Horsepower absorption by oil (transm. side), PS	Total hp absorption by oil, PS
20,000	0.13	0.38	0.51
30,000	0.25	0.51	0.76
40,000	0.40	0.64	1.04
50,000	0.63	0.81	1.44
60,000	0.93	0.95	1.88
70,000	1.24	1.08	2.32

Q = 1 kg/min

Shaft speed, rpm	Horsepower absorption by oil (nozzle side), PS	Horsepower absorption by oil (transm. side), PS	Total hp absorption by oil, PS
20,000	0.11	0.32	0.43
30,000	0.19	0.47	0.66
40,000	0.30	0.57	0.87
50,000	0.48	0.69	1.15
60,000	0.72	0.75	1.47
70,000	0.98	0.88	1.86

(Table continued on following page)

TABLE 11 (continued)

 $Q = 0.72 \text{ kg/min}$

Shaft speed, rpm	Horsepower absorption by oil (nozzle side) PS	Horsepower absorption by oil (transm. side), PS	Total hp absorption by oil, PS
20,000	0.09	0.29	0.38
30,000	0.15	0.46	0.61
40,000	0.26	0.57	0.83
50,000	0.40	0.67	1.07
60,000	0.63	0.71	1.34

 $Q = 0.44 \text{ kg/min}$

Shaft speed, rpm	Horsepower absorption by oil (nozzle side) PS	Horsepower absorption by oil (transm. side), PS	Total hp absorption by oil, PS
20,000	0.08	0.26	0.34
30,000	0.12	0.40	0.52
40,000	0.19	0.51	0.70
50,000	0.31	0.60	0.91
60,000	0.51	0.63	1.14

 $Q = 0.22 \text{ kg/min}$

Shaft speed, rpm	Horsepower absorption by oil (nozzle side) PS	Horsepower absorption by oil (transm. side), PS	Total hp absorption by oil, PS
20,000	0.06	0.19	0.25
30,000	0.08	0.25	0.33
40,000	0.12	0.38	0.50
50,000	0.20	0.45	0.65
60,000	0.33	0.49	0.82

The above results are for the constant thrust load of 50 kg and the constant inlet oil temperature of 30° C. When the thrust load is varied from 25 kg to 200 kg and inlet oil temperature is varied from 30° C to 90° C, the relation of the total horsepower absorption by oil H_0 with the thrust load P and the oil viscosity at the inlet

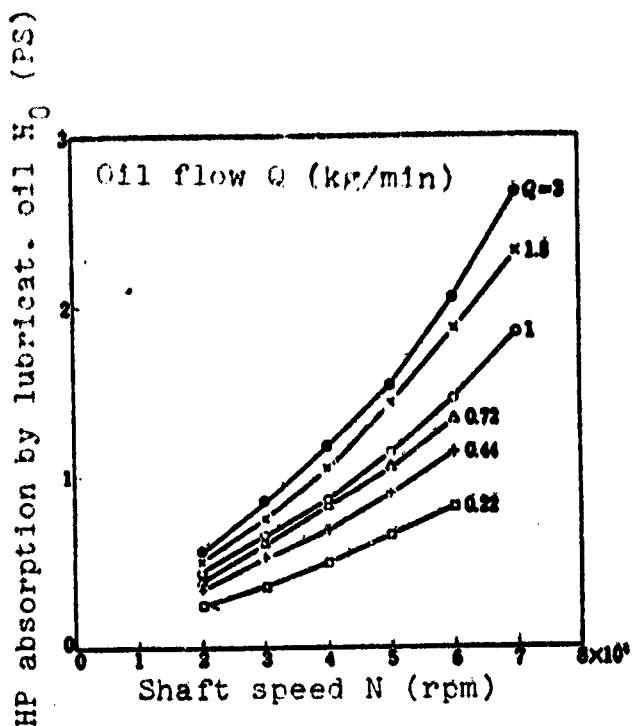


Figure 140. Horsepower absorption by oil versus shaft speed

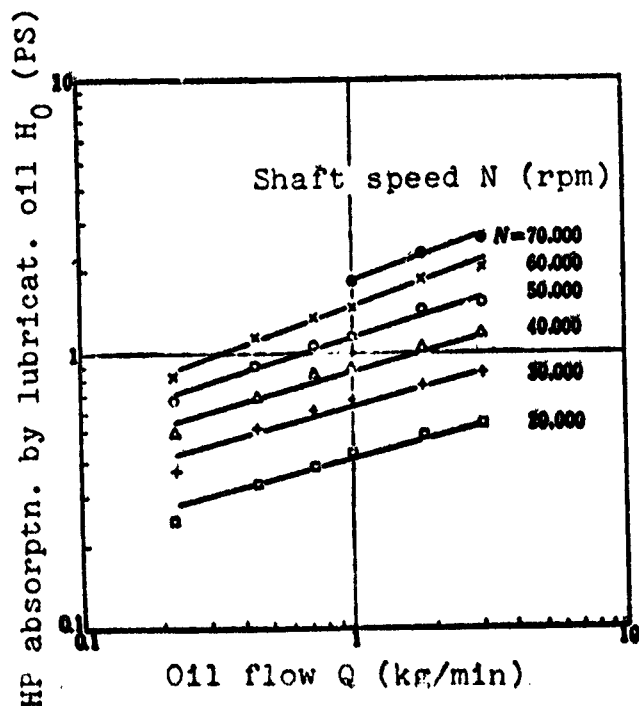


Figure 142. Horsepower absorption by oil versus oil flow

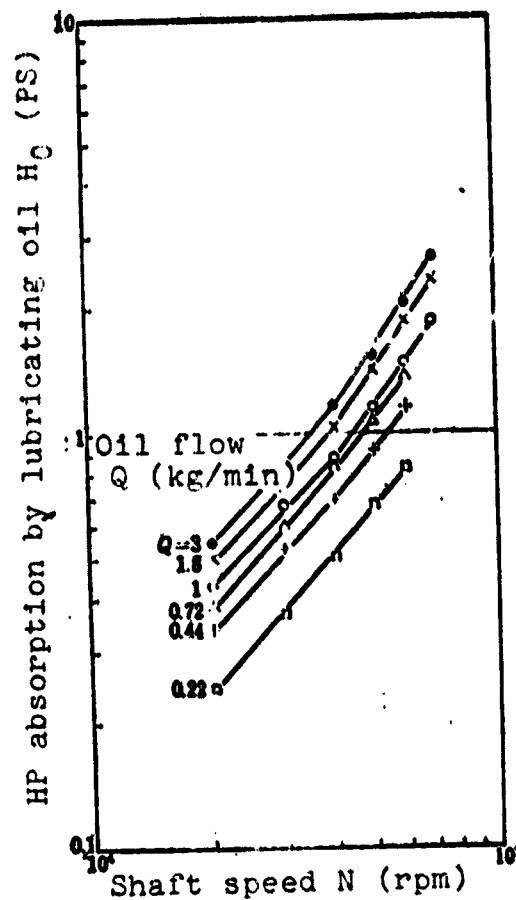


Figure 141. Horsepower absorption by oil versus shaft speed

oil temperature Z_I can be expressed by

$$\left. \begin{aligned} H_0 &\propto P^{0.8-0.9} \\ H_0 &\propto Z_I^{0.8-0.9} \end{aligned} \right\} \quad (71)$$

The smaller exponents of P and Z_I correspond to the larger value of $T_B - T_I$.

Summarizing the above, the total horsepower absorption by oil H_0 in the high speed region can be expressed as:

Just as for #6206, there is a good correspondence to the equation /87
for the bearing outer race temperature rise.

In the previous chapter, the influence of the cage guide type on the horsepower absorption by oil was discussed. There, the horsepower absorptions by the deflected oil were just about the same because of the smaller penetration ratio of an inner-race-riding cage compared to an outer-race-riding cage, but the horsepower absorption by the transmitted oil for an inner-race-riding cage was considerably lower. As the penetration ratio of #17206 is only slightly smaller than that of #6206 (outer-race-riding cage), a comparison of the horsepower absorption by oil for these cases becomes as shown in Figures 143, 144, and 145. Although the absolute values cannot be compared due to the different frictional characteristics of the two, the trend shows that the horsepower absorptions by the transmitted oil are nearly equal because the penetration ratios are equal. At a high speed above 60,000 rpm, the horsepower absorption of #6206 becomes considerably greater than that of #17206. As is clear from the comparison of Tables 3 and 10, this is because the bearing outer race temperature rise of #6206 (outer-race-riding cage) at high speed /88 is greater than for #17206. This difference in the temperature rise is thought to be due to the difference in the bearing type. On the other hand, the horsepower absorption by the deflected oil is very much smaller for #17206 compared to #6206. This can be due to the fact that with an inner-race-riding cage, most of the deflected oil flows backward at the contact area with the bearing and there is not sufficient heat exchange. With an outer-race-riding cage, oil enters inside the bearing, carries out heat exchange, and is also discharged to the nozzle side. This difference in the horsepower absorption by the deflected oil appears as the difference in the total horsepower absorption. Consequently, even if the penetration ratios are nearly the same, an inner-race-riding cage is disadvantageous relative to an outer-race-riding cage for cooling of the bearing.

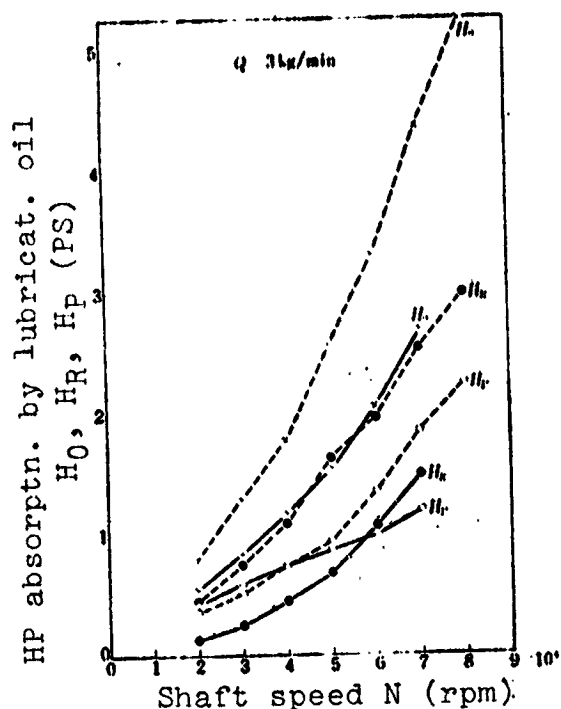


Figure 143. Horsepower absorption by oil versus shaft speed:

— — #17206; - - - - #6206 (outer-race-riding cage); x — total horsepower absorption by oil; • — horsepower absorption by the deflected oil; o — horsepower absorption by the transmitted oil

As has been previously mentioned, with #17206, where the nozzle is placed in the inner race, the thrust load direction affects the penetration ratio greatly. The effects of the nozzle position on the horsepower absorption by oil are shown in Figures 146, 147, and 148.

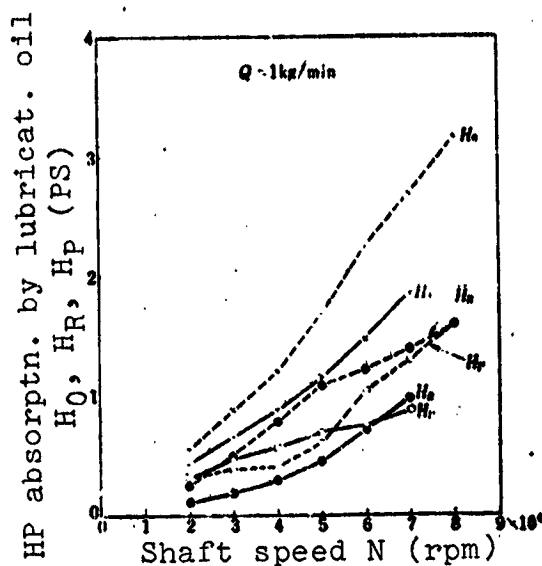


Figure 144. Horsepower absorption by oil versus shaft speed

— — #17206; - - - - #6206 (outer-race-riding cage)

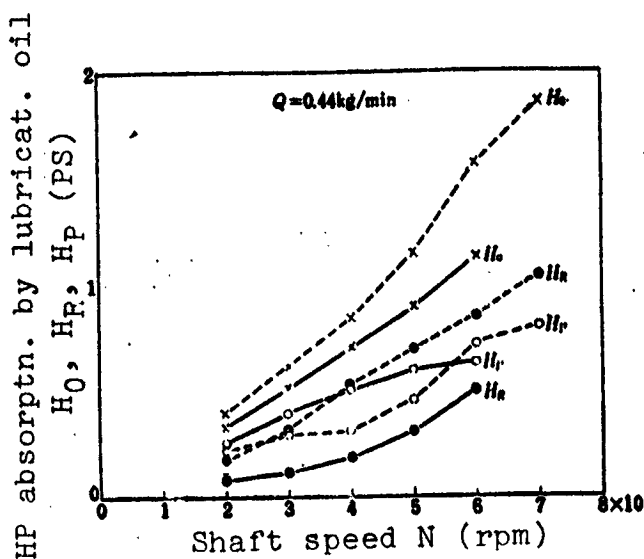


Figure 145. Horsepower absorption by oil versus shaft speed:

— — #17206; - - - - #6206 (outer-race-riding cage)

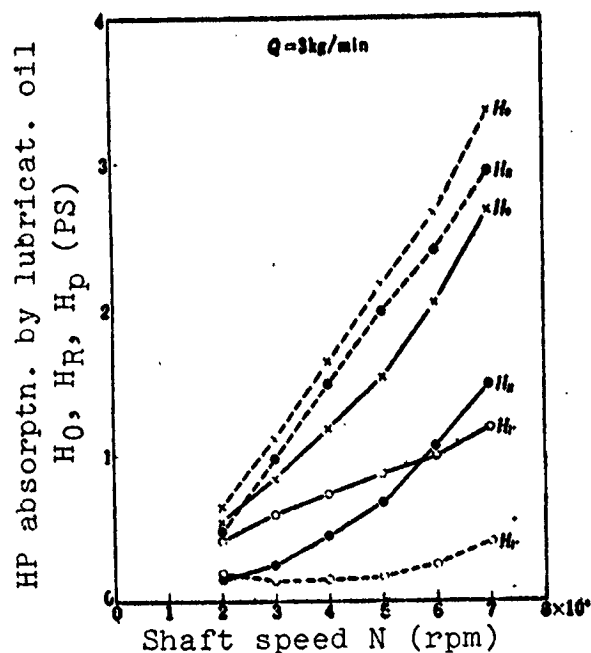


Figure 146. Horsepower absorption by oil versus shaft speed:

— — — #17206 (nozzle at unloaded side of the inner race); — — — — #17206 (nozzle at thrust side of inner race); x — total horsepower absorption by oil; ● — horsepower absorption by deflected oil; o — horsepower absorption by transmitted oil

by the deflected oil, because of a conspicuously small penetration ratio. The total horsepower absorption by oil is greater when the nozzle is placed at the thrust loaded side of the inner race than at the unloaded side of the inner race, especially as oil flow increases. This is due to the fact that when the nozzle is placed at the thrust loaded side of the inner race, the bearing temperature rise becomes larger and the horsepower absorption by oil increases correspondingly. Consequently, from the standpoint of heat load on the lubricating oil, it is advantageous to place the nozzle at the unloaded side of the inner race.

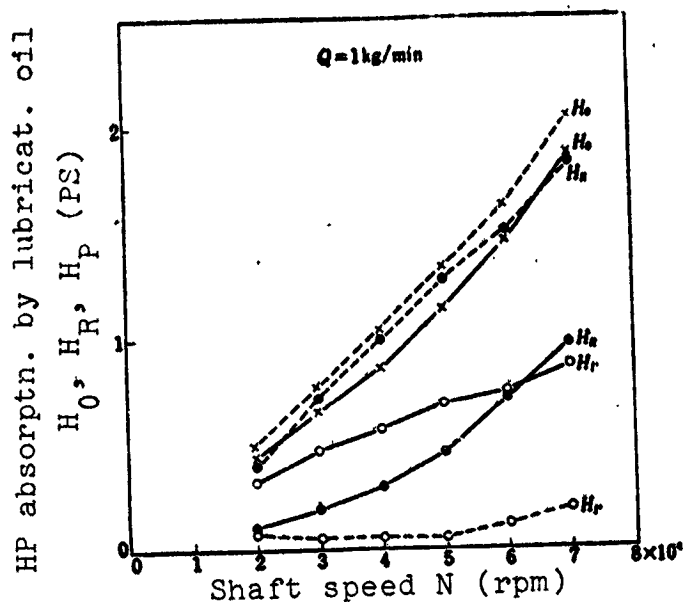


Figure 147. Horsepower absorption by oil versus shaft speed:

— — — #17206 (nozzle at unloaded side of inner race); — — — — #17206 (nozzle at thrust loaded side of inner race)

It is seen that when the nozzle is placed at the inner race thrust loaded side, most of the total horsepower absorption by oil consists of the horsepower absorption

6.8. Heat Exchange Efficiency of Lubricating Oil

Table 12 shows the relation between shaft speed and the heat exchange efficiency of the deflected oil η_R , heat exchange efficiency of the transmitted oil η_P , and overall heat exchange efficiency η_E for various quantities of oil flow, calculated from Table 10. A comparison with the results for #6206 (outer-race-riding cage) is made in Figures 149, 150, and 151. The penetration ratios of #6206 (outer-race-riding cage) and #17206 are just about the same. The heat exchange efficiency of the transmitted oil η_P is greater for #17206, but the heat exchange efficiency of the deflected oil is significantly smaller for #17206 compared to #6206. Therefore, the total heat exchange efficiency is also much lower than #6206. The reason for this has been mentioned already. It indicates that even if the penetration ratios are about the same, an inner-race-riding cage is significantly more disadvantageous, compared to an outer-race-riding cage in terms of the heat exchange efficiency.

For comparison purposes, the heat exchange efficiencies, when the nozzle is placed at the thrust loaded side of the inner race, are shown in Figures 152, 153, and 154. Even when there is a large difference in penetration ratios, the overall heat exchange efficiencies are of nearly the same magnitude.

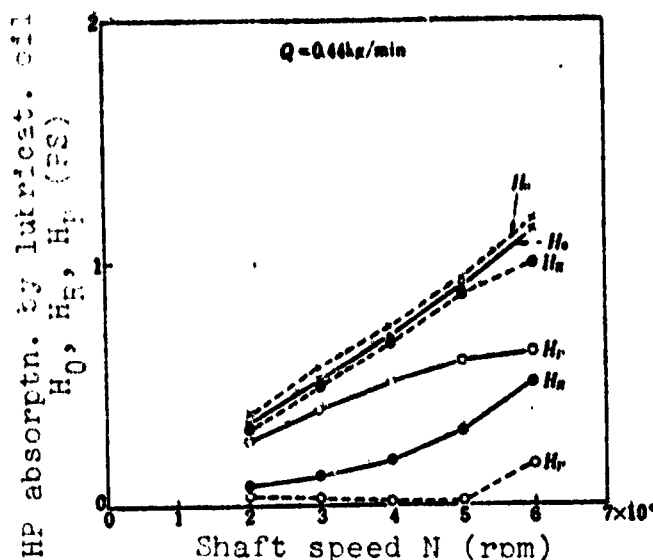


Figure 148. Horsepower absorption by oil versus shaft speed:
 — — — #17206 (nozzle at unloaded side of inner race);
 - - - - #17206 (nozzle at thrust loaded side of inner race)

TABLE 12. HEAT EXCHANGE EFFICIENCIES OF OIL η_R , η_P , η_E AND
SHAFT SPEED FOR VARIOUS LEVELS OF OIL FLOW
(30° C inlet oil temperature and 50 kg thrust load)

Shaft speed rpm	η_R %					
	Quantity of supplied oil kg/min					
	3	1.8	1	0.72	0.44	0.22
20,000	16.2	36.9	40.0	44.8	56.8	63.5
30,000	21.7	37.9	41.0	43.5	56.9	65.0
40,000	26.5	37.5	41.9	49.2	57.7	70.6
50,000	28.9	41.5	44.5	53.1	60.4	73.5
60,000	35.1	45.0	48.9	56.6	65.2	82.2
70,000	38.1	47.7	50.4			

Shaft speed rpm	η_P %					
	Quantity of supplied oil kg/min					
	3	1.8	1	0.72	0.44	0.22
20,000	100	100	100	100	102.6	100
30,000	100	100	97.5	104.4	103.5	112.5
40,000	97.1	97.5	98.1	101.6	103.7	112.9
50,000	100	101.8	100	103.6	106	101.5
60,000	100	101.4	100	101.9	107	119
70,000	101.5	103.5	103.5			

Shaft speed rpm	η_E %					
	Quantity of supplied oil kg/min					
	3	1.8	1	0.72	0.44	0.22
20,000	50.6	67.4	72.0	76.8	86.5	88.0
30,000	49.1	64.9	69.7	77.7	87.0	90.7
40,000	48.1	60.5	67.6	76.3	85.4	92.5
50,000	48.1	62.1	66.7	76.4	84.5	94.4
60,000	50.9	62.6	66.3	74.0	84.0	100.8
70,000	52.9	63.5	66.8			

The relation between oil flow Q and the average value of η_E in the high speed region for various quantities of oil flow is shown in Figure 155. From Figure 155, the relation between η_E (%) and oil flow Q (kg/min) can be expressed as follows:

when the nozzle is at the unloaded side of the inner race

$$\eta_E = 68Q^{-0.25}$$

(73)

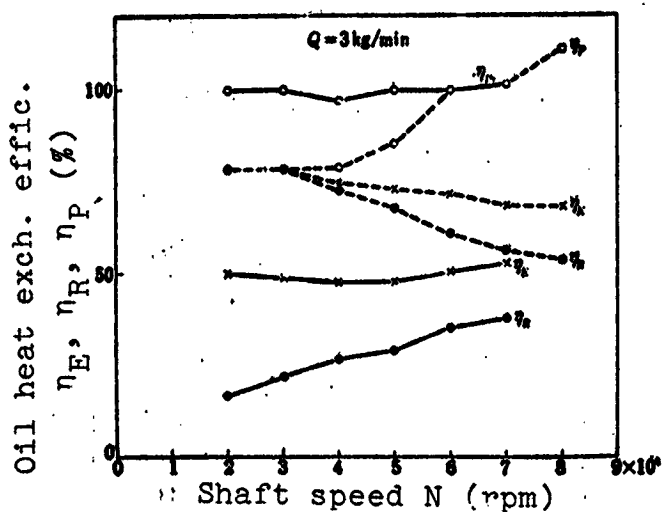


Figure 149. Heat exchange efficiency of oil versus shaft speed:

— — #17206; - - - - #6206
(outer race-riding cage)

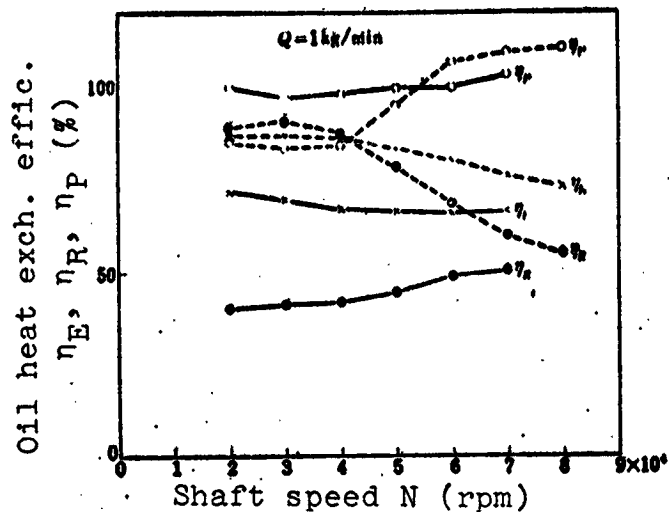


Figure 150. Heat exchange efficiency of oil versus shaft speed:

— — #17206; - - - - #6206
(outer-race-riding cage)

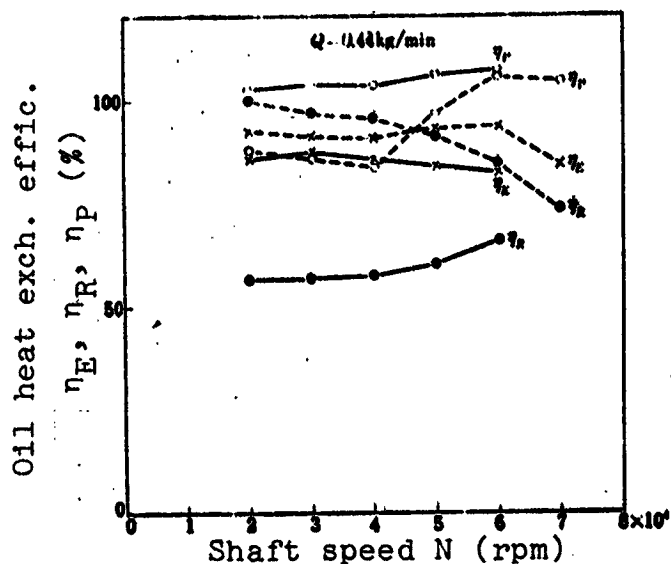


Figure 151. Heat exchange efficiency of oil versus shaft speed:

— — #17206; - - - - #6206
(outer-race-riding cage)

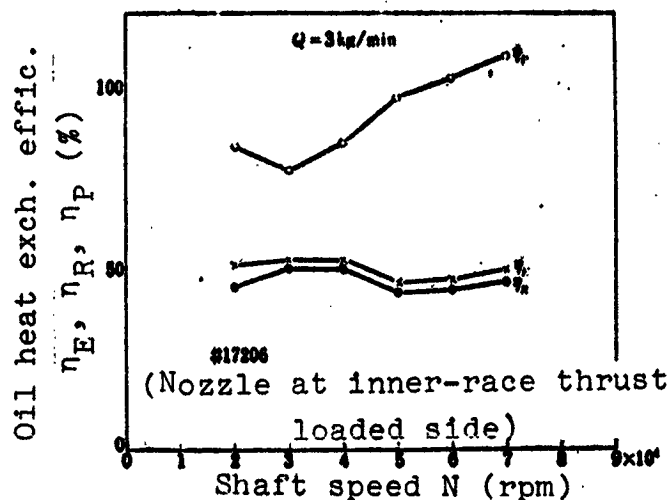


Figure 152. Heat exchange efficiency of oil versus shaft speed

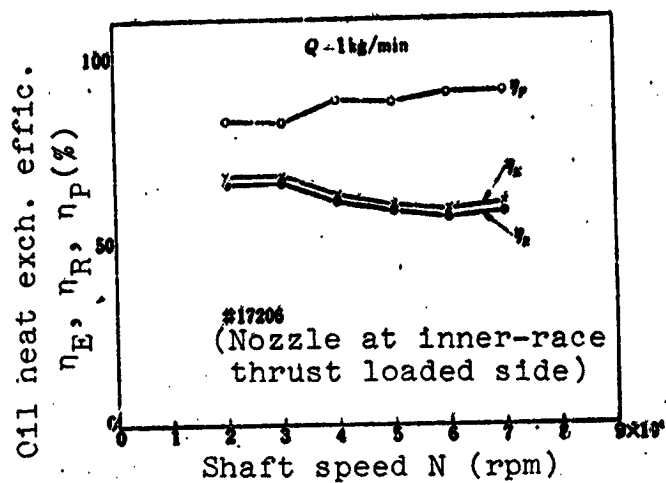


Figure 153. Heat exchange efficiency of oil versus shaft speed

when the nozzle is at the thrust loaded side of the inner race:

$$\eta_E = 62 Q^{-0.22} \quad (74)$$

Depending on the position of the nozzle relative to the thrust load direction of the inner race, a wide difference in penetration ratios was observed, but the difference in the heat exchange efficiencies was not that wide. However, placing the nozzle at the unloaded side of the inner race rather than the thrust loaded side of the inner race is

slightly advantageous in terms of the heat exchange efficiency. The heat exchange efficiency of #6206, which is equipped with the same inner-race-riding cage, was $\eta_E = 70 Q^{-0.22}$, as indicated in Chapter 5. Compared to this, the heat exchange efficiency of #17206 is slightly smaller, but is of the same magnitude. For inner-race-riding

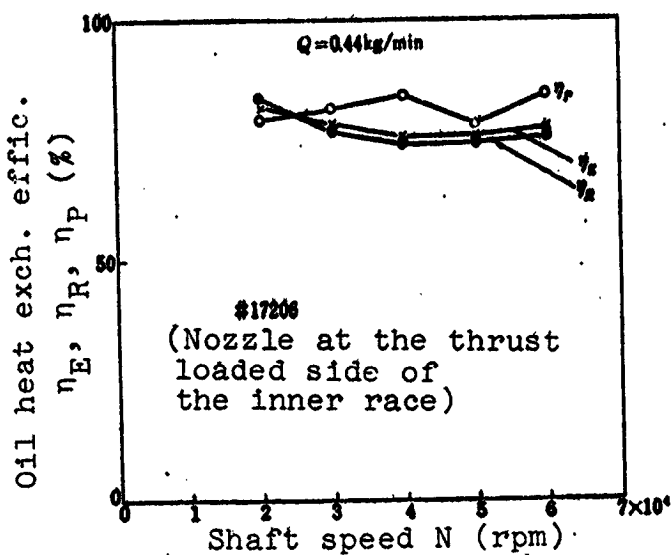


Figure 154. Heat exchange efficiency of oil versus shaft speed

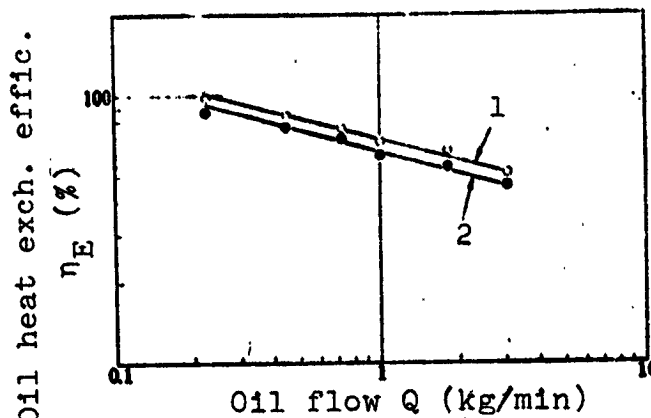


Figure 155. Heat exchange efficiency of oil versus oil flow:
1 — nozzle at unloaded side of inner race); 2 — nozzle at thrust loaded side of inner race

/93

cages, the heat exchange efficiencies are all small, even if there is a large difference in the penetration ratios. Despite the fact that the heat exchange efficiency of #17206 was slightly smaller than #6206 (inner-race-riding cage), its limiting dn value increased greatly, as shown in Figure 128. This again proves, as mentioned in the previous chapter, that it is not possible to talk about the limiting speed simply in terms of the magnitude of the heat exchange efficiency.

6.9. Bearing Friction.

Figure 156 shows the relation between the friction torque and shaft speed for each oil flow from the experimental data in Table 10. The same trend as for #6206 equipped with an inner-race-riding cage in the previous chapter is exhibited. Although the data for #6206 (inner-race-riding cage) go only up to 45,000 rpm, #17206 which goes up to 70,000 rpm also shows that an increase in friction torque due to speed is extremely small.

Figure 157 shows the comparison with #6206 (outer-race-riding cage). As the speed gets higher, the difference in friction torque becomes greater. This large difference in the friction torque characteristics between an inner-race-riding cage and an outer-race-riding cage is, as mentioned in the previous chapter, due to the fact that with an outer-race-riding cage, the sliding friction on the race surface of the cage makes up a large portion

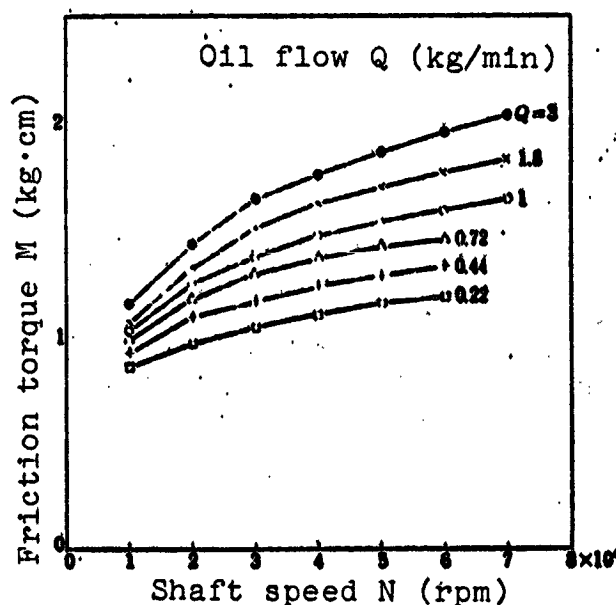


Figure 156. Friction torque versus shaft speed.

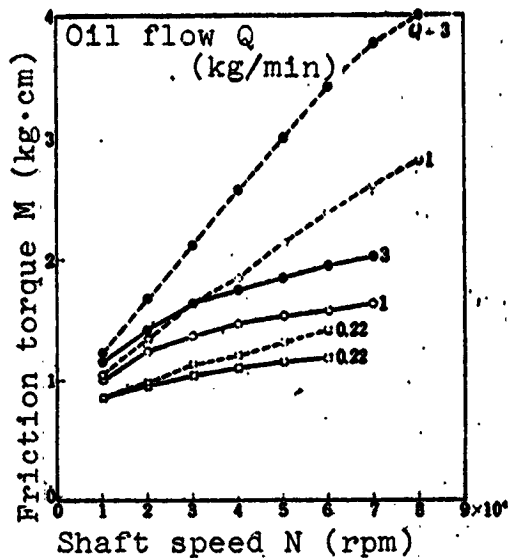


Figure 157. Friction torque versus shaft speed:

— — — #17206; - - - - -
#6206 (outer-race-riding cage)

of the friction torque of the outer race. Figure 158 shows the relation between the shaft speed and the friction power loss obtained from the friction torque, while Figure 159 shows the comparison with an outer-race-riding cage.

When the inlet oil temperature is varied from 30° to 90° C, the relationship of friction torque M with the viscosity at the bearing temperature Z_B , shaft speed N , and oil flow Q in the high speed region can be approximated, just like in the previous chapter, by the following:

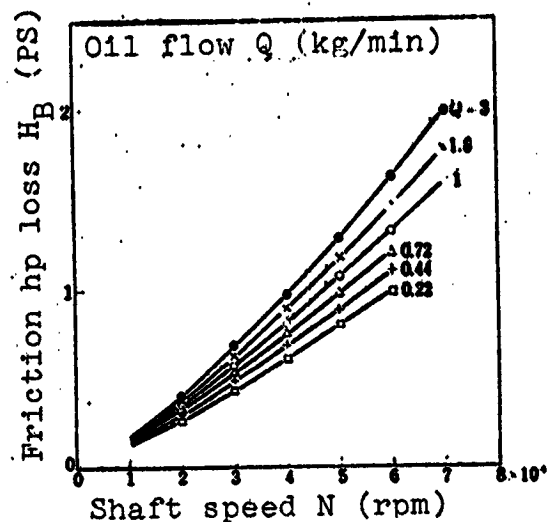


Figure 158. Friction horsepower loss versus shaft speed

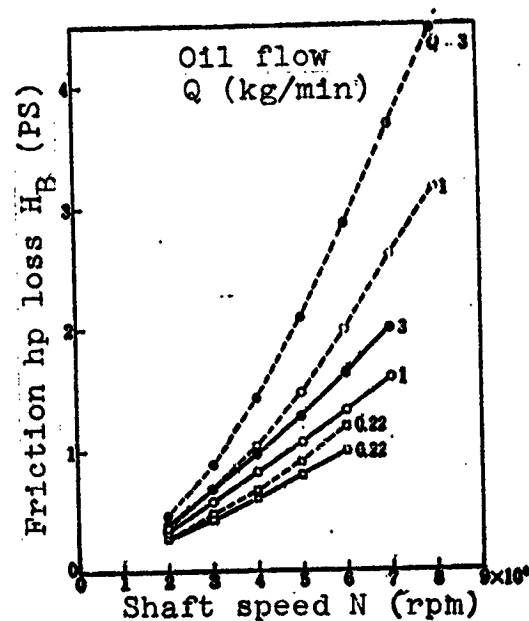


Figure 159. Friction horsepower loss versus shaft speed:

— — — #17206; - - - - -
#6206 (outer-race-riding cage)

$$M \propto Z_B^{0.5} N^{0.4} Q^{0.15}$$

(75) /95

The exponents of each factor in the above equation are similar to those in Equation (51) for #6206 (inner-race-riding cage). For an inner-race-riding cage, the friction torque is governed by a nearly identical equation and, compared to an outer-race-riding cage, the exponents of N and Q are characteristically small.

Figure 160 is a result of correlating Equation (75) with the viscosity at the bearing temperature Z_B for each point in Figure 156, while Figure 161 is similarly correlated with the results under the various thrust loads.

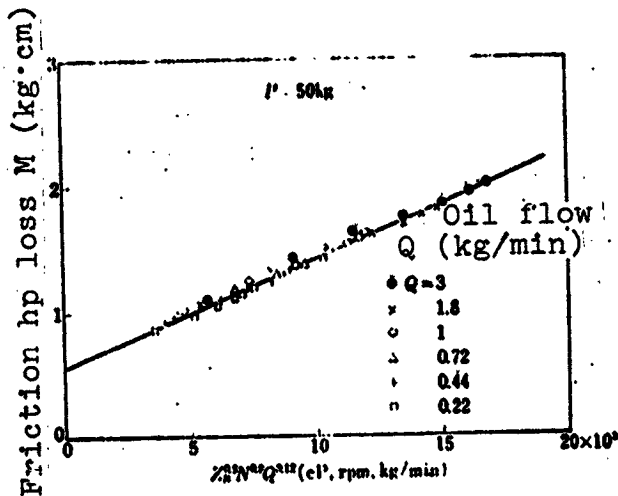


Figure 160. Friction torque, viscosity, shaft speed, and oil flow

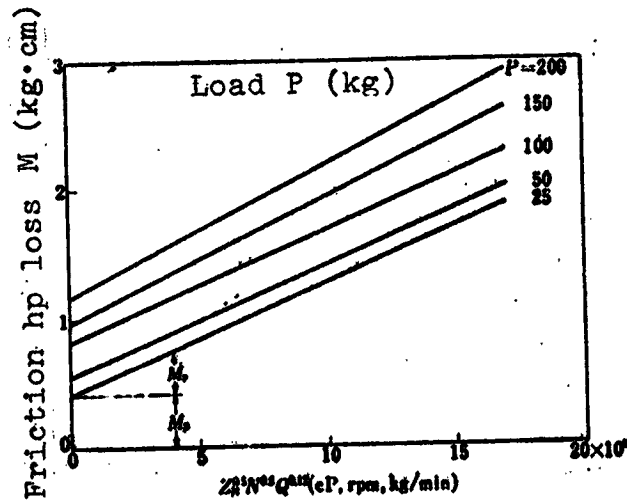


Figure 161. Friction torque, viscosity, shaft speed, and oil flow

Since the non-velocity term M_p of friction torque becomes the following, from Figure 162,

$$M_p \propto P^{0.5} \quad (76)$$

the friction torque M (kg · cm) can be expressed as

$$M = 7.2 \times 10^{-3} P^{0.5} + 8.5 \times 10^{-3} Z_B^{0.5} N^{0.4} Q^{0.15} \quad (77)$$

where P is in kg, Z_B in cP, N in rpm, and Q in kg/min, as before.

The friction power loss H_B (PS) of the bearing is, from Equation (77):

$$H_B = 10^{-6} P^{0.8} N + 1.2 \times 10^{-6} Z_B^{0.5} N^{1.8} Q^{0.12} \quad (78)$$

6.10. Equation for Estimating Bearing Temperature Rise

If the entire friction power loss in Equation (78) is assumed to be carried away by the oil, then the equation for the bearing temperature rise can be obtained similar to the previous chapter. As it cannot be simply calculated as is, a result obtained from an approximation formula for the friction power loss H_B is shown here.

Figure 163 shows the results of correlating the friction power loss in Figure 158 with $Z_B^{0.5} N^{1.8} Q^{0.12}$ in Equation (78). The results similarly correlated for the various loads are shown in Figure 164.

The relation between the friction power loss and load for $Z_B^{0.5} N^{1.8} Q^{0.12}$ of

2×10^8 , 5×10^8 , and 10×10^8 , obtained from Figure 164, is shown in Figure 165. From this, the following approximation can be made:

$$H_B \propto P^{0.8} \quad (79)$$

so that Equation (78) can be approximated as

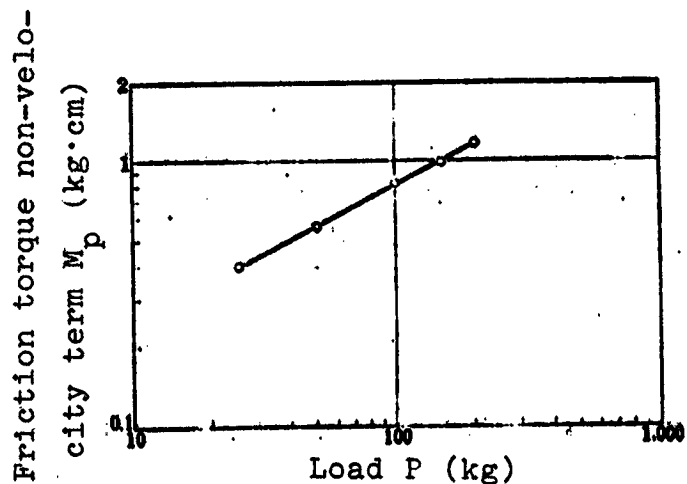


Figure 162. Non-velocity term of friction torque and load

$$H_B = 6.5 \times 10^{-10} Z_B^{0.5} P^{0.8} N^{1.8} Q^{0.12} \quad (80)$$

where Z_B is in cP, P in kg, N in rpm, and Q in kg/min, just as in Equation (78).

In a similar manner to the one used in Chapter 4, the following equations for the bearing temperature rise $T_B - T_I$ can be obtained by using Equations (29) and (30) for the relation between Z_B/Z_I and $T_B - T_I$:

(1) when $T_B - T_I$ is small ($15 - 40^\circ \text{C}$):

$$T_B - T_I = 2 \times 10^{-6} Z_I^{0.33} P^{0.19} N^{1.2} Q^{-0.42} \quad (81)$$

(2) when $T_B - T_I$ is large ($35 - 120^\circ \text{C}$):

$$T_B - T_I = 1.8 \times 10^{-6} Z_I^{0.33} P^{0.19} N^{1.2} Q^{-0.42} \quad (82)$$

Equations (81) and (82) roughly correspond to the experimental equation (69) for the bearing temperature rise, in that the exponents of Z_I , P , N , and Q in the latter equation vary from 0.3 to 0.5, 0.18 to 0.22, 1.0 to 1.38, and -0.41 to -0.57, respectively, depending on the magnitude of $T_B - T_I$.

Figure 166 is a result of correlating the bearing outer race temperature rise in Figure 137 with $Z_I^{0.33} P^{0.19} N^{1.2} Q^{-0.42}$ in Equation

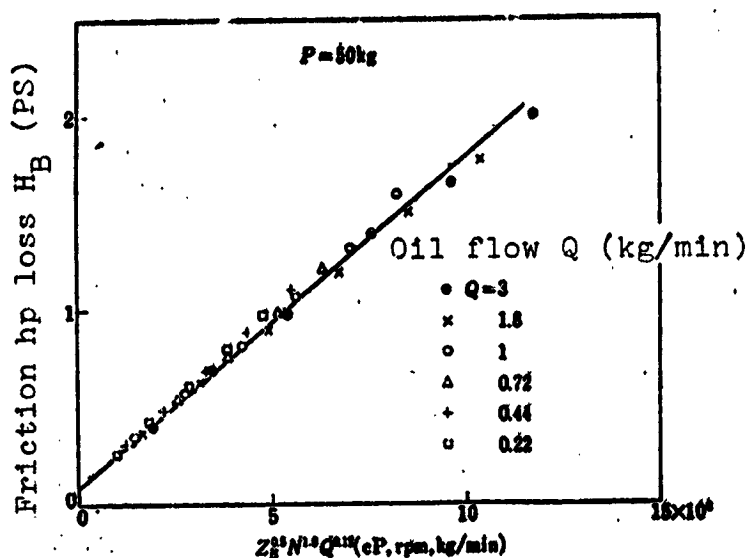


Figure 163. Friction horsepower loss, viscosity, shaft speed, and oil flow

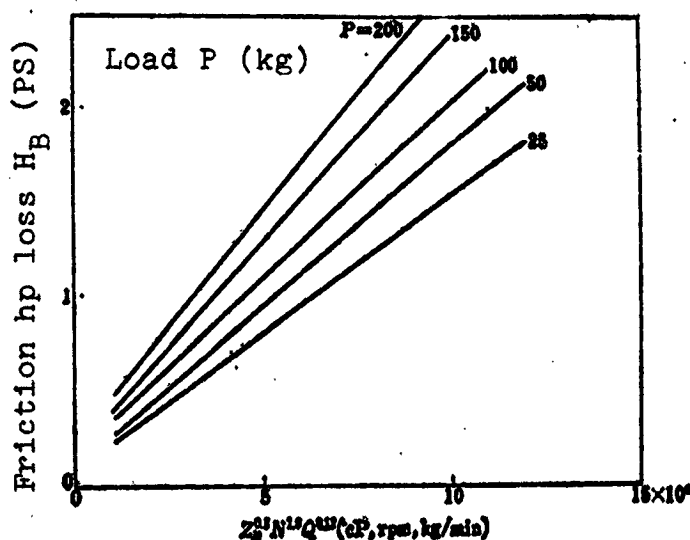
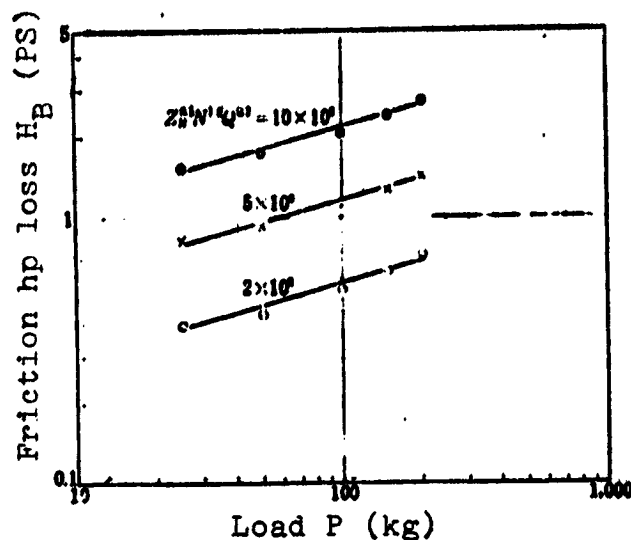


Figure 164. Friction horsepower loss, viscosity, shaft speed, and oil flow

(82), which holds when $T_B - T_I$ is large, i.e., in the high speed region. As Equation (82) holds within the speed range of 10,000 - 70,000 rpm and the 0.22 - 3 kg/min oil flow range, it can be used as an approximation between the low speed to high speed region. Figure 167 is a result of correlating with $Z_I^{0.33}$.

$P^{0.19} N^{1.2} Q^{-0.42}$ in Equation (82) the bearing outer race temperature rise under the various conditions: that is, shaft speed of 10,000 - 70,000 rpm, oil flow of 0.22 - 3 kg/min, thrust load of 25 - 200 kg, and inlet oil temperature of 30 - 90° C. There is a good correspondence between the observed values and Equation (82). An exception is in the region of low speed when the inlet oil temperature is changed. Because the bearing temperature rise is small, and an error is large in this region, it is omitted.

The equation for the bearing temperature rise, calculated from the friction power loss, again agrees very well with the observed data. The fact that the friction of the high speed roller bearing



/98

Figure 165. Friction horsepower loss and load for various values of $Z_B^{0.5} N^{1.8} Q^{0.2}$

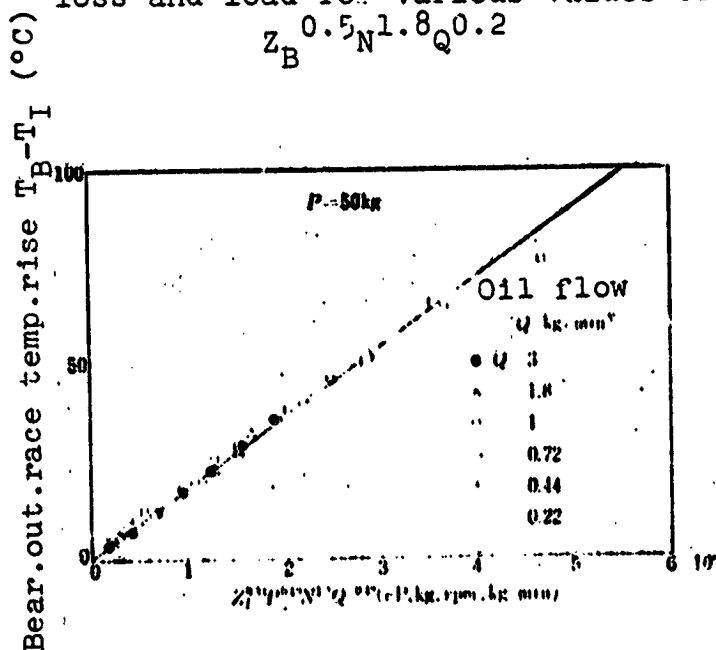


Figure 166. Bearing temperature rise, viscosity, shaft speed, and oil flow

is caused as a whole by a viscous friction remains unchanged.

6.11. Conclusions for Chapter 6

The limiting speed of #17206 angular contact ball bearing, as well as how the bearing temperature rise and the friction torque are affected by speed, thrust load, oil

flow, and other factors are studied and compared to #6206 deep-groove ball bearing. The major conclusions are the following:

(1) The limiting dn value of #17206 angular contact ball bearing appears at 195×10^4 for oil flow of 0.22 kg/min and 0.44 kg/min, 210×10^4 for 0.72 kg/min, and 225×10^4 for 1 - 3 kg/min. For #6206 equipped with the same inner-race-riding cage, its limiting dn value appears in the neighborhood of $150 - 165 \times 10^4$. The fact that the limiting dn value of #17206 is much larger than that of #6206, although both are equipped with an inner-race-riding cage, can be due not only to the difference in the bearing type, but also to the difference in the cage material, since the failure is taking place in both cases on the race riding surface of the cage at the side opposite the nozzle. While the cage material of the deep-groove ball bearing is high-strength yellow brass, the cage material of the angular contact ball bearing is a phenolic resin, and the latter is superior in wear resistance. Although phenolic resin is superior in wear resistance, it is inferior in heat resistance, as it tends to cause carbonization of the race surface of the cage when the temperature rises. By using more heat-resistant and wear-resistant material, it is possible to further raise the limiting dn value, even for an inner-race-riding cage.

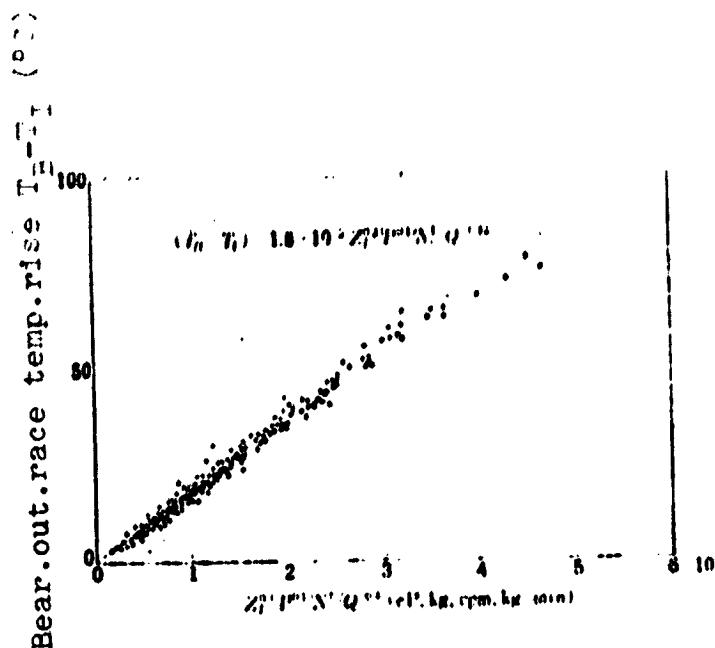


Figure 167. Bearing temperature rise, viscosity, shaft speed, and oil flow

(2) With the angular contact ball bearing, an extremely large difference in the penetration ratios is observed, depending on the nozzle position relative to the direction of the thrust load of the inner race. However, the bearing failure occurs at the identical speed, regardless of the magnitude of the penetration ratio. This is because, with an inner-race-riding cage, even if there is a large difference in the penetration ratio, oil has difficulty reaching the race riding surface of the cage and the side opposite the nozzle, which is most susceptible to failure. That is, as mentioned in the previous chapter, the penetration ratio influences the average temperature of the bearing, but has no direct relation to the failure. The most important thing is to prevent the failure by supplying a large quantity of oil to the race riding surface of the cage at the opposite side of the nozzle, which is most susceptible to failure. In this regard, using two nozzles facing each other 180° apart, with an inner-race-riding cage, can substantially increase the limiting dn value.

(3) The temperature rise from the inlet oil temperature T_I to the bearing outer race temperature T_B in the region with the dn value of $195 - 225 \times 10^4$ can be approximated by

$$(T_B - T_I) \propto Z_I^{0.2-0.3} P^{0.15-0.25} N^{1.0-1.25} Q^{-0.41--0.57}$$

where Z_I is the oil viscosity at the inlet oil temperature, P is the thrust load, N is speed, and Q is oil flow. The smaller values of exponents correspond to the larger value of $T_B - T_I$.

(4) The horsepower absorption by lubricating oil H_0 can be approximated by

$$H_0 \propto Z_I^{0.2-0.3} P^{0.15-0.25} N^{1.1-1.6} Q^{0.25-0.35}$$

The smaller exponents of Z_I , P , and N , and the larger exponent of Q , correspond to the larger value of $T_B - T_I$. Just as for #6206, there is good correspondence with the formula for the bearing temperature

rise. The heat exchange efficiency of lubricating oil η_E (%) can be expressed as a function of oil flow Q (kg/min) as

$$\eta_E = 68Q^{-0.18}$$

It is slightly smaller than #6206 inner-race-riding cage, and all inner-race-riding cages show much smaller values than an outer-race-riding cage type.

(5) As in the previous chapter, the bearing friction consists of viscous friction, on the whole. The friction torque M (kg · cm) and the friction power loss H_B (PS) can be approximated by

$$M = 7.2 \times 10^{-3} P^{0.8} + 8.5 \times 10^{-3} Z_B^{0.8} N^{0.8} Q^{0.18}$$

$$H_B = 10^{-4} P^{0.8} N + 1.2 \times 10^{-3} Z_B^{0.8} N^{1.8} Q^{0.18}$$

where Z_B , the oil viscosity at the bearing temperature, is in cP, P in kg, N in rpm, and Q in kg/min.

Compared to #6206 inner-race-riding cage in the previous chapter, the exponents of each factor are about the same. The big difference in comparing with #6206 outer-race-riding cage is the small exponent of N of an inner-race-riding cage. Whereas the maximum speed of #6206 inner-race-riding cage is 45,000 rpm, the maximum speed of #17206 is 70,000 rpm, and is nearly equivalent to #6206 outer-race-riding cage; this trend is unchanged even in the high speed region.

(6) Assuming all frictional heat is carried away by oil, the following bearing temperature rise ($^{\circ}\text{C}$) can be obtained from the experimental formula for the friction power loss:

$$(T_B - T_I) = 1.8 \times 10^{-3} Z_I^{0.8} P^{0.8} N^{1.8} Q^{-0.48}$$

where Z_I is in cP, P in kg, N in rpm, and Q in kg/min. Thus, the formula for estimating the bearing temperature rise derived from the friction power loss agrees very well with the observed data.

CHAPTER 7. ANGULAR CONTACT BALL BEARING (#30BNT)

7.1. Introduction

The limiting dn value and the bearing performance of the deep-groove ball bearing (#6206) were discussed in Chapters 4 and 5, and those of the angular contact ball bearing (#17206) were discussed in Chapter 6. In all cases, the bearing failure occurred on the race riding surface of the cage at the side opposite the nozzle. Even when oil flow was increased, the highest limiting dn values of these bearings were approximately 285×10^4 for #6206, and 255×10^4 for #17206, and did not reach 300×10^4 .

Thus, to realize the dn value of 300×10^4 , it is necessary to study the new bearing type. For this purpose, #30BNT angular contact ball bearing was made, and the experiments performed. As shown in Figure 19, #30BNT has the shoulder of the inner race dropped, contrary to #17206. When the shoulder of the outer race is dropped, the contact with the outer race track surface becomes unstable due to the centrifugal load at high speeds. Having dropped the shoulder of the inner race, the angular contact ball bearing can also use an outer-race-riding cage, which is advantageous at high speeds. Furthermore, because the inner and outer races are separable, the cage is machined in one piece, thereby increasing the mechanical strength and the manufacturing precision of the cage compared to the rivet assembly for #6206.

Experiments were conducted to study the limiting speed as well as the various performance characteristics, such as the bearing temperature rise and the friction torque of #30BNT, which is considered to be suitable for high speed operation. As a result, it became clear that this type of bearing is best suited for high speed operation, and that the dn value of 300×10^4 is attainable. How the various factors such as oil flow affect the bearing temperature rise and the friction torque for the dn value of up to 300×10^4 was studied and compared with the results in the previous chapter.

/100

7.2. Experimental Conditions

Although already mentioned in Chapters 2 and 3, the conditions used in this experiment are summarized. A single nozzle is placed at the thrust loaded side of the inner race. It is made to face the center of the clearance between the cage and the inner race perpendicularly. The distance between the leading edge of the nozzle and the face of the inner race is 8 mm. The jet velocity is constant at approximately 20 m/s regardless of oil flow.

Unless otherwise specified, the thrust load is constant at 50 kg, and the inlet oil temperature is also constant at 30° C.

7.3. Test Bearing

The test bearing is a SP class #30BNT angular contact ball bearing. It is equipped with an outer-race-riding cage made of high-strength yellow brass. As shown in Figure 168, an oil groove to improve the oil discharge is established around the outside perimeter of the cage. The dimensions of the test bearing are shown in Table 13.

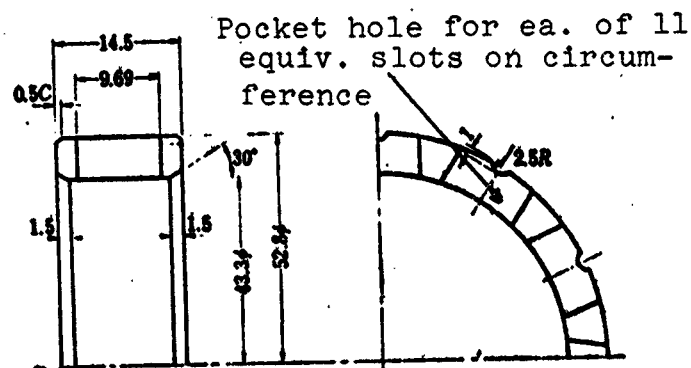


Figure 168. Cage configuration

7.4. Experimental Results

The limiting speed, bearing outer race temperature, outlet oil temperatures at the nozzle side and the bearing transmitted side, friction torque, penetration ratio, and shaft speed under the various oil flow rates, but the constant thrust load of 50 kg and the constant inlet oil temperature of 30° C, are shown in Table 14.

These experimental results, as well as the results obtained by changing the thrust load and the inlet oil temperature, are now discussed.

TABLE 13. TEST BEARING #30BNT (SP)

Diameter of steel ball, mm	9.525 (3/8")
Number of steel balls	11
Percentage of groove radius to steel ball	
Inner race, %	53.5 - 54.5
Outer race, %	51.5 - 52.5
Inside diameter of outer race, mm	53.0
Outside diameter of inner race, mm	40.4
Radial clearance, μm	25 - 35
Cage guide type	Outer-race-riding cage
Guide clearance, mm	0.2 \pm 0 - 0.06
Pocket clearance, mm	0.165 \pm 0.05

TABLE 14. BEARING TEMPERATURE, OUTLET OIL TEMPERATURE, FRICTION TORQUE, PENETRATION RATIO, AND SHAFT SPEED (30° C inlet oil temperature and 50 kg thrust load)

Oil flow Q = 3 kg/min (room temperature 17° C)

Shaft speed, rpm	Bearing outer race temp., °C	Outlet oil temp. (nozzle side), °C	Outlet oil temp. (transm. side), °C	Friction torque, kg·cm	Penetration ratio, %
20,000	38.5	37	37	1.52	68.1
30,000	43	40	41	1.95	58.7
40,000	49	44	47	2.49	50.0
50,000	56.5	48	56.5	3.08	41.9
60,000	67	53.5	68.5	3.46	37.2
70,000	78	60	81.5	3.77	31.5
80,000	90	67.5	96	4.01	27.8
90,000	104.5	74.5	112.5	4.23	24.4
97,000	115.5	80	125.5	4.35	23.7

(Table continued on following page)

TABLE 14 (continued)

Q = 1.8 kg/min (room temperature 15° C)

Shaft speed, rpm	Bearing outer race temp., °C	Outlet oil temp. (nozzle side), °C	Outlet oil temp. (transm. side), °C	Friction torque, kg·cm	Penetration ratio, %
20,000	41	39.5	39	1.42	70.3
30,000	47	44	44	1.80	60.8
40,000	53	49	51.5	2.20	51.3
50,000	62	54.5	62.5	2.63	44.7
60,000	73	61.5	77	3.05	40.4
70,000	86	69	92.5	3.32	35.4
80,000	98.5	75	109.5	3.53	32.4
90,000	115	84.5	129.5	3.69	30.0
100,000	132	93.5	148.5	3.85	29.3

Q = 1 kg/min (room temperature 18° C)

Shaft speed, rpm	Bearing outer race temp., °C	Outlet oil temp. (nozzle side), °C	Outlet oil temp. (transm. side), °C	Friction torque, kg·cm	Penetration ratio, %
20,000	44.5	43.5	42.5	1.30	65.4
30,000	52.5	49.5	49.5	1.61	54.6
40,000	61	56.5	60	1.94	46.1
50,000	71.5	65.5	73.5	2.28	40.8
60,000	86	75.5	92.5	2.52	37.4
70,000	103.5	84.5	111.5	2.71	34.7
80,000	121	92	133	2.83	33.0
90,000	141.5	104.5	154.5	3.00	31.8
100,000	164.5	123	181.5	3.18	29.2

Q = 0.72 kg/min (room temperature 15° C)

Shaft speed, rpm	Bearing outer race temp., °C	Outlet oil temp. (nozzle side), °C	Outlet oil temp. (transm. side), °C	Friction torque, kg·cm	Penetration ratio, %
20,000	48.5	47.5	47.5	1.10	64.7
30,000	58	56.5	56.5	1.42	57.5
40,000	68.5	66	66	1.72	51.7
50,000	80.5	76.5	80	2.06	46.4
60,000	94.5	89	96.5	2.31	41.9
70,000	112.5	101	120	2.50	40.1
80,000	133	111.5	144	2.62	39.2
90,000	155.5	122.5	168	2.72	37.3
100,000	178	138	194	2.80	36.5

(Table concluded on following page)

TABLE 14 (concluded)

Q = 0.44 kg/min (room temperature 17° C)

Shaft speed, rpm	Bearing outer race temp., °C	Outlet oil temp. (nozzle side), °C	Outlet oil temp. (transm. side), °C	Friction torque, kg·cm	Penetration ratio, %
20,000	52	51.5	51	1.07	56.7
30,000	63.5	61.5	60.5	1.29	48.7
40,000	77	74.5	75	1.50	47.2
50,000	92	87	94.5	1.73	43.6
60,000	114	104	119.5	1.93	38.7
70,000	135.5	115.5	143	2.03	36.9
80,000	159	131.5	168	2.14	35.8
85,000	172	141.5	182	2.18	33.5
90,000	failure				

Q = 0.22 kg/min (room temperature 19° C)

Shaft speed, rpm	Bearing outer race temp., °C	Outlet oil temp. (nozzle side), °C	Outlet oil temp. (transm. side), °C	Friction torque, kg·cm	Penetration ratio, %
20,000	58	57	56.5	0.89	50.3
30,000	74.5	71.5	73	1.06	49.2
40,000	92	88	90.5	1.20	49.6
50,000	113.5	108	114.5	1.37	47.7
60,000	137.5	127.5	142.5	1.46	39.1
70,000	162	146	168	1.56	34.8
75,000	179	164	185	1.60	32.5
80,000	196	180	204	1.65	32.1
83,000	failure				

7.5. Allowable Limiting dn Value

Figure 169 shows the relation between the bearing outer race temperature and shaft speed from the results in Table 14. With an oil flow of 0.22 kg/min, the friction torque rapidly increases at 83,000 rpm, and immediately results in a failure. Figure 170 is an exterior view of the inner and outer races and the cage at that time.

The cage face at the opposite side of the nozzle is discolored, indicating a high temperature. As before, the race riding surface of the cage at the opposite side of the nozzle is abraded again, but the track surface of the inner race is most worn out. Because of the centrifugal force, oil is forced to the outer race side, the oil flow becomes small, and the bearing outer race temperature reaches 220°C , leading to the overheating of the bearing, and causing the failure on the inner race track surface, even ahead of the race riding surface of the cage. As mentioned in Chapter 4, #6206 (outer-race-riding cage) had a failure at the bearing outer race temperature of 170°C with an oil flow of 0.22 kg/min . The limiting speed then was suppressed by the abrasion of the race riding surface of the cage rather than the failure on the track surface. Compared to that, #30BNT cage withstands the high speed and the high temperature well. With an oil flow of 0.44 kg/min , the friction torque rapidly increases at $90,000\text{ rpm}$, and failure occurs. Figure 171 shows the exterior view of the

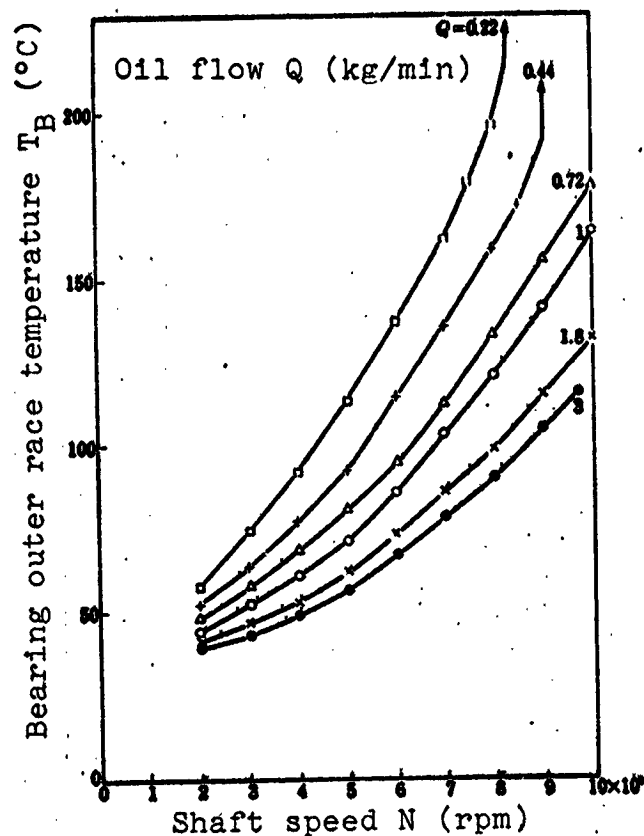


Figure 169. Bearing temperature and shaft speed

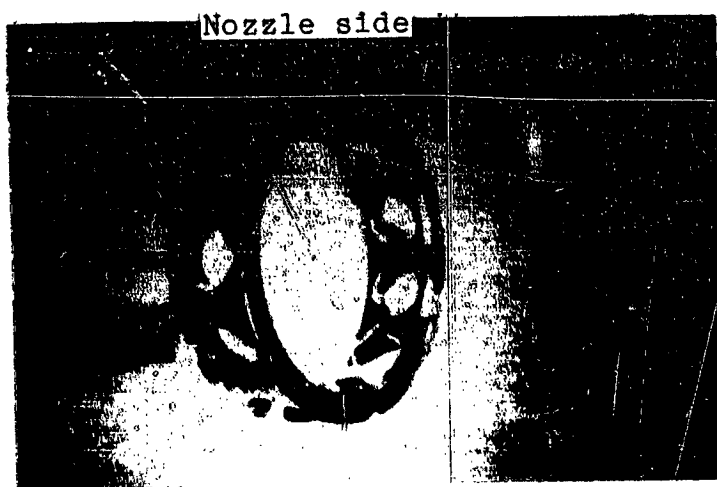


Figure 170. Exterior view of failed bearing

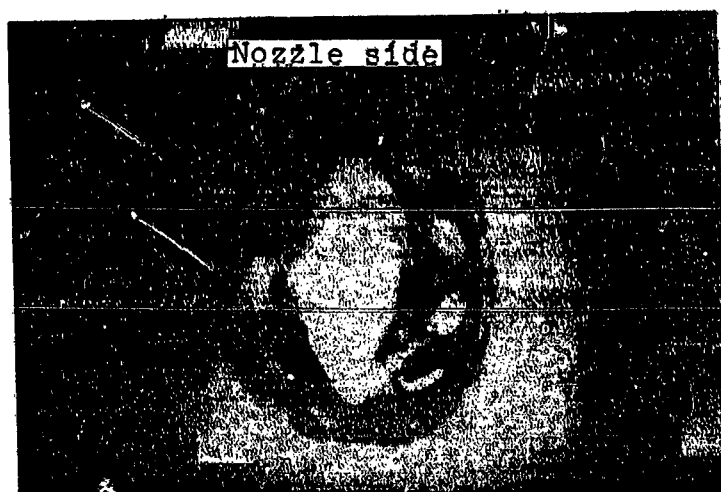


Figure 171. Exterior view of the failed bearing

inner and outer races and cage at that time. When the oil flow is increased to 0.44 kg/min, the track surface of the inner race is not worn out as

much as in the case of 0.22 kg/min oil flow. On the other hand, abrasion on the race riding surface of the cage at the side opposite the nozzle is conspicuous, and the wiping of the cage material and the failure occur on the race riding surface of the outer race facing it. Consequently, in this case, the abrasion and failure of the race riding surface of the cage suppress the limiting speed. With an oil flow of 0.72 kg/min or more, no failure takes place even at 100,000 rpm speed and the dn value of 300×10^4 . The limiting speed must then exist somewhere higher, but because the maximum speed of air turbine was 100,000 rpm, it was not possible to raise the speed further. The reason for the maximum speed of 97,000 rpm with an oil flow of 3 kg/min is that the friction power loss significantly increases at high speed, and 15.5 PS air turbine cannot provide sufficient horsepower. Experiments with dn values greater than 300×10^4 are planned in the future.

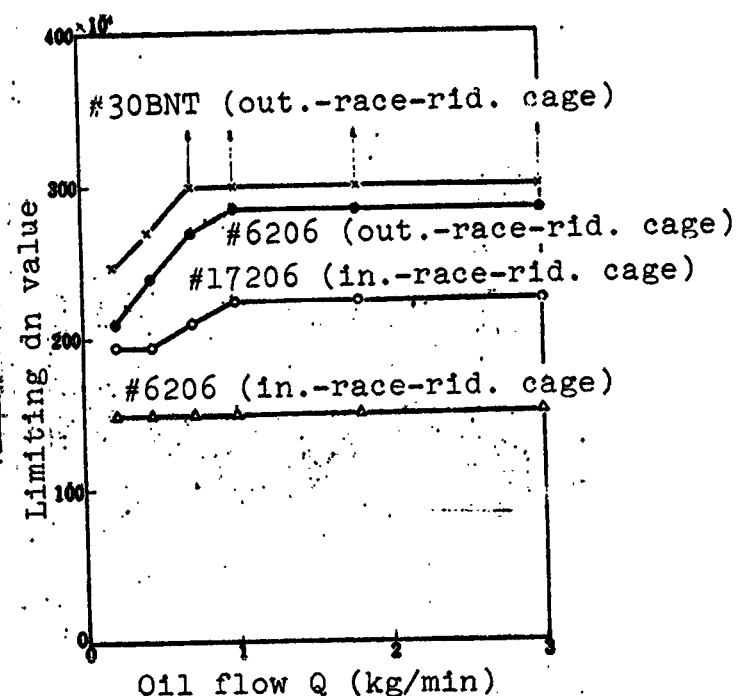


Figure 172. Limiting dn value and oil flow

Figure 172 shows the relation between the limiting dn value and oil flow, together with the previous results. While the limiting dn values of #6206, which is of the same outer-race-riding cage type, are 210×10^4 with an oil flow of 0.22 kg/min, 240×10^4 with 0.44 kg/min, 270×10^4 with 0.72 kg/min, and 285×10^4 with 1 - 3 kg/min, the limiting dn value of #30BNT has increased considerably. As no significant difference can be recognized in their bearing performance characteristics, such as bearing outer race temperature rise, friction torque, and penetration ratio when Tables 3 and 14 are compared, the difference in the limiting dn value is conjectured to be due to the different cage construction technique. That is, the #6206 cage is of the rivet assembly type and is inferior in precision and mechanical strength. On the contrary, since the inner and outer races are separable with #30BNT, a one-piece machined cage can be made, thus raising the precision as well as the mechanical strength. It seems that such a difference appeared as the difference in the limiting dn value. In fact, with #6206 (outer-race-riding cage), when the shaft speed is increased above 80,000 rpm, the friction torque rapidly increases initially and then stabilizes. This can be explained by the local metallic contact and abrasion caused by the inferior manufacturing precision of the sliding friction surface of the cage. On the other hand, with #30BNT, absolutely no such phenomenon was observed up to 100,000 rpm, backing up the above conjecture.

As mentioned previously, aside from the limiting dn value, the bearing performance of #30BNT and #6206 (outer-race-riding cage) are similar. The various characteristics of #30BNT will be briefly mentioned next.

7.6. Bearing Temperature Rise

Figure 173 shows the temperature rise $T_B - T_I$ from the inlet oil temperature T_I (30°C) to the bearing outer race temperature T_B as a function of the shaft speed, using the data in Table 14. The bearing outer race temperature rise $T_B - T_I$ as a function of shaft

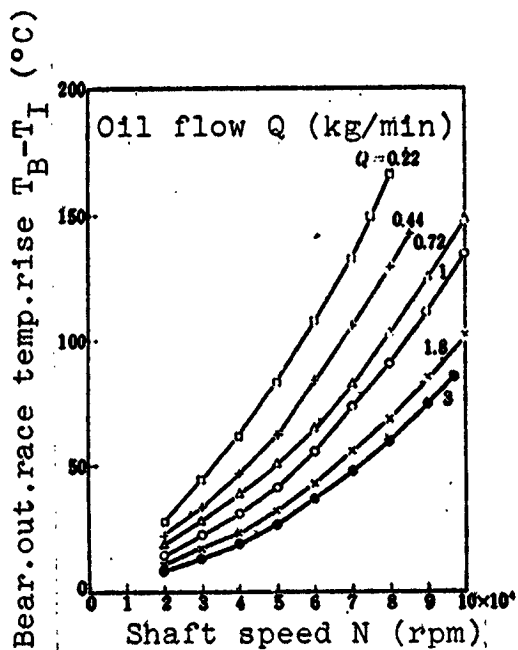


Figure 173. Bearing temperature rise versus shaft speed

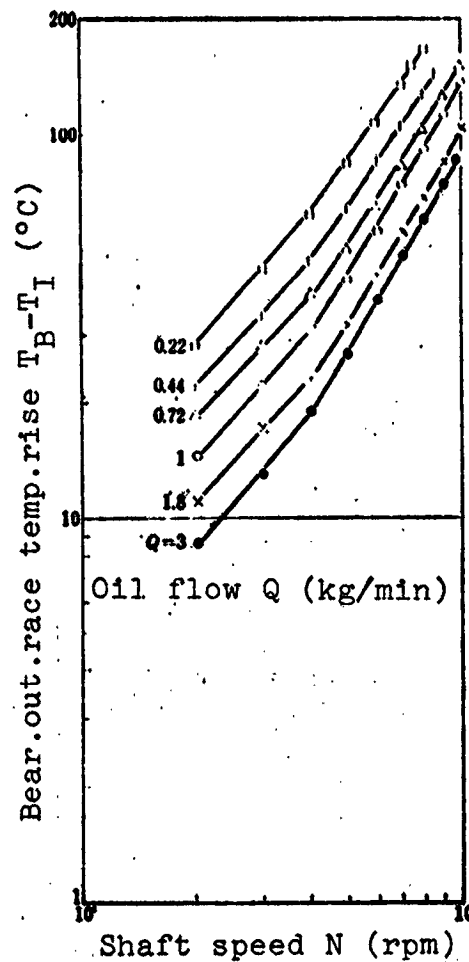


Figure 174. Bearing temperature rise versus shaft speed

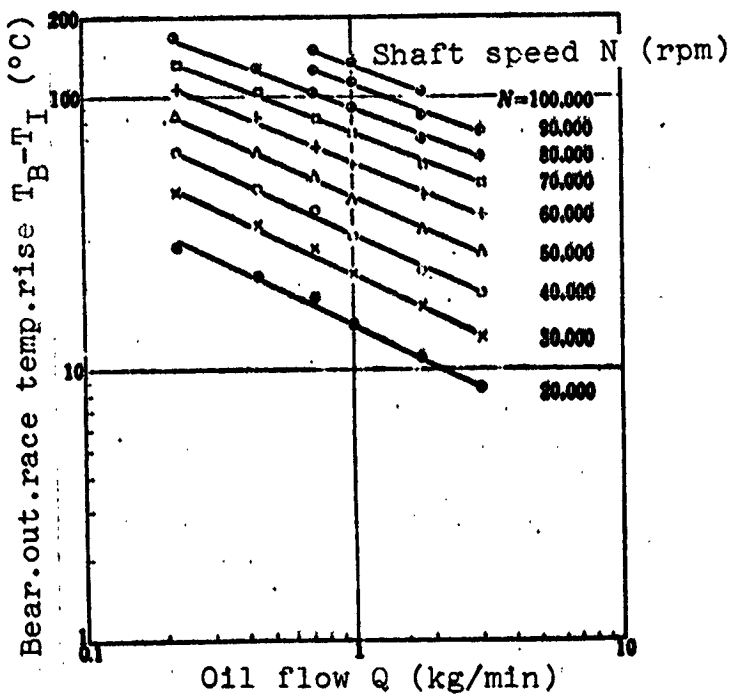


Figure 175. Bearing temperature rise versus oil flow

speed N and oil flow Q are shown in Figures 174 and 175, respectively. The relation between $T_B - T_I$ and N changes at 40,000 rpm, just as with #6206 (outer-race-riding cage). In the high speed region above 40,000 rpm, it can be expressed as

$$(T_B - T_I) \propto N^{0.4-1.0} \quad (83)$$

From Figure 175, $T_B - T_I$ and Q are related by

$$(T_B - T_I) \propto Q^{-0.87-0.8} \quad (84)$$

As before, the smaller exponents of each factor correspond to the larger value of $T_B - T_I$.

The above results are obtained under the constant thrust load of 50 kg and the constant inlet oil temperature of 30° C. When the thrust load is varied from 25 kg to 200 kg, and the inlet oil temperature is varied from 30° C to 120° C, the bearing temperature rise $T_B - T_I$ is related to the load P , and the viscosity at inlet oil temperature Z_I by

$$(T_B - T_I) \propto P^{0.1-0.15} Z_I^{0.25-0.4} \quad (85)$$

The smaller exponents of P and Z_I correspond to the larger value of $T_B - T_I$.

Summarizing the above, the bearing outer race temperature rise in the high speed region can be approximated by

$$(T_B - T_I) \propto Z_I^{0.25-0.4} P^{0.1-0.15} N^{0.4-1.7} Q^{-0.87-0.8} \quad (86)$$

Equation (86) corresponds fairly well to Equation (5) for #6206 (outer-race-riding cage) in Chapter 4, and indicates that, even if the bearing type is different, roughly the same relation holds for the outer-race-riding cages for dn values of up to 300×10^4 .

7.7. Amount of Heat Absorption by Lubricating Oil

Table 15 is a result of calculating the horsepower absorptions by the deflected oil and the transmitted oil, as well as the total horsepower absorption by oil, from Table 14. Figure 176 shows the relation between the total horsepower absorption by oil H_0 and shaft speed N from the data in Table 14. From Figure 177, H_0 and N above

TABLE 15. HORSEPOWER ABSORPTION BY OIL AND SHAFT SPEED
(30° C inlet oil temperature and 50 kg thrust load)

Oil flow $Q = 3 \text{ kg/min}$

Shaft speed, rpm	Horsepower absorption by oil (nozzle side), PS	Horsepower absorption by oil (transmitted side), PS	Total hp absorption by oil, PS
20,000	0.32	0.68	1.00
30,000	0.61	0.94	1.55
40,000	1.02	1.24	2.26
50,000	1.51	1.60	3.11
60,000	2.15	2.08	4.23
70,000	2.94	3.33	5.27
80,000	3.92	2.65	6.57
90,000	4.78	2.86	7.64
97,000	5.36	3.19	8.57

$Q = 1.8 \text{ kg/min}$

Shaft speed, rpm	Horsepower absorption by oil (nozzle side), PS	Horsepower absorption by oil (transmitted side), PS	Total hp absorption by oil, PS
20,000	0.25	0.55	0.80
30,000	0.49	0.75	1.24
40,000	0.81	0.97	1.78
50,000	1.19	1.27	2.46
60,000	1.61	1.65	3.26
70,000	2.20	1.93	4.13
80,000	2.65	2.24	4.89
90,000	3.32	2.81	6.12
100,000	3.89	3.01	6.90

$Q = 1 \text{ kg/min}$

Shaft speed, rpm	Horsepower absorption by oil (nozzle side), PS	Horsepower absorption by oil (transmitted side), PS	Total hp absorption by oil, PS
20,000	0.23	0.41	0.64
30,000	0.44	0.52	0.96
40,000	0.71	0.68	1.39
50,000	1.03	0.87	1.90
60,000	1.41	1.15	2.56
70,000	1.76	1.39	3.15
80,000	2.09	1.69	3.78
90,000	2.52	1.95	4.47
100,000	3.27	2.20	5.47

(Table continued on following page)

TABLE 15 (continued)

Q = 0.72 kg/min

Shaft speed, rpm	Horsepower absorption by oil (nozzle side), PS	Horsepower absorption by oil (transmitted side), PS	Total hp absorption by oil, PS
20,000	0.21	0.39	0.60
30,000	0.39	0.53	0.92
40,000	0.59	0.64	1.23
50,000	0.85	0.80	1.66
60,000	1.19	0.99	2.18
70,000	1.46	1.23	2.69
80,000	1.70	1.54	3.24
90,000	1.99	1.77	3.76
100,000	2.37	2.05	4.42

Q = 0.44 kg/min

Shaft speed, rpm	Horsepower absorption by oil (nozzle side) PS	Horsepower absorption by oil (transmitted side), PS	Total hp absorption by oil, PS
20,000	0.20	0.25	0.45
30,000	0.32	0.32	0.64
40,000	0.50	0.45	0.95
50,000	0.68	0.59	1.27
60,000	0.95	0.72	1.67
70,000	1.15	0.88	2.03
80,000	1.38	1.05	2.43
85,000	1.58	1.08	2.66

Q = 0.22 kg/min

Shaft speed, rpm	Horsepower absorption by oil (nozzle side) PS	Horsepower absorption by oil (transmitted side), PS	Total hp absorption by oil, PS
20,000	0.14	0.14	0.28
30,000	0.24	0.24	0.48
40,000	0.32	0.33	0.64
50,000	0.45	0.45	0.90
60,000	0.65	0.48	1.13
70,000	0.81	0.52	1.33
75,000	0.92	0.52	1.43
80,000	1.07	0.59	1.66

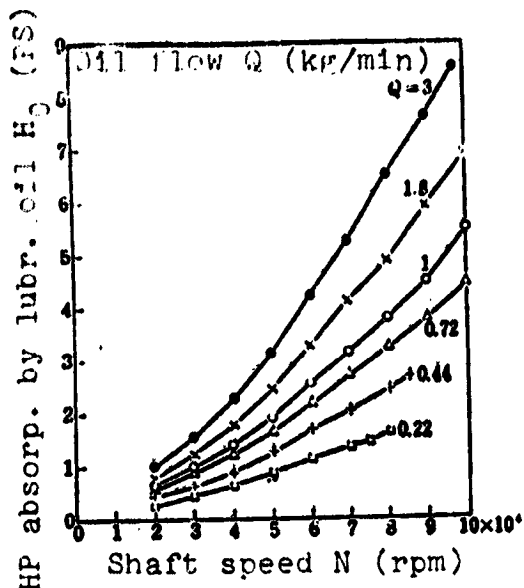


Figure 176. Horsepower absorption by oil versus shaft speed

40,000 rpm are related by

$$H_0 \propto N^{0.8-1.0} \quad (87)$$

From Figure 178, H_0 and Q are related by

$$H_0 \propto Q^{2.8-4.0} \quad (88)$$

The smaller exponent of N and the larger exponent of Q correspond to the larger value of $T_B - T_I$.

The above results are obtained under the constant thrust load of 50 kg and the constant inlet oil temperature of 30° C. When the thrust load is varied from 25 kg to 200 kg, and the inlet oil temperature is varied from 30° C to 120° C, the total horsepower absorption by oil H_0 is related to load P and viscosity at inlet oil temperature by

$$H_0 \propto P^{0.1-0.15} Z_I^{0.5-0.8} \quad (89) \quad /109$$

The smaller exponents of P and Z_I correspond to the larger value of $T_B - T_I$.

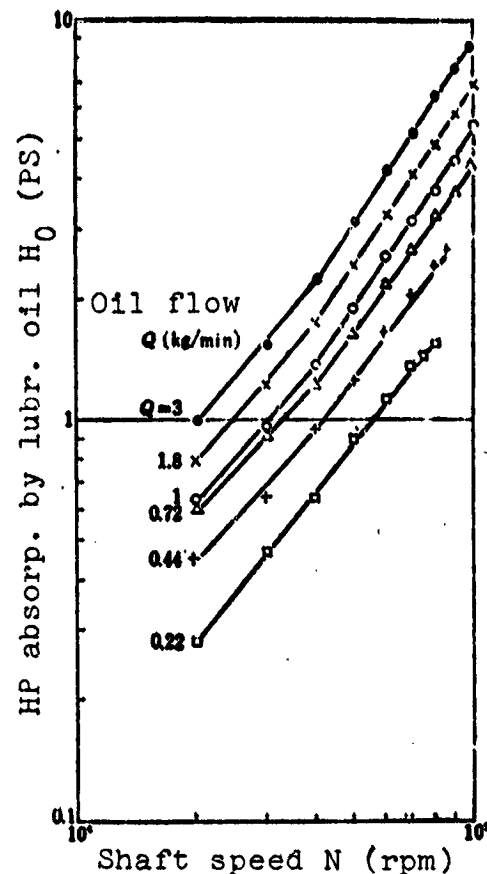


Figure 177. Horsepower absorption by oil versus shaft speed

Summarizing the above, the total horsepower absorption by oil in the high speed region can be approximated by

$$H_0 \propto Z_1^{0.3-0.35} P^{0.1-0.15} N^{0.8-1.0} Q^{0.4-0.5} \quad (90)$$

Equation (90) roughly corresponds to Equation (86) for the bearing outer race temperature rise, as well as to Equation (10) for #6206 (outer-race-riding cage).

As is clear from the comparison of Tables 15 and 4, the percentages of the horsepower absorption are about the same for #30BNT and #6206 (outer race-riding cage), indicating the same trend for the outer-race-riding cage type bearings.

7.8. Heat Exchange Efficiency of Lubricating Oil

Table 16 shows the relation between the heat exchange efficiency of the deflected oil η_R , the heat exchange efficiency of the transmitted oil η_P , and the total heat exchange efficiency η_E and the shaft speed for various oil flow rates calculated from the data in Table 14. Comparing Table 16 with Table 5 for #6206 (outer-race-riding cage), the heat exchange efficiencies are nearly equal. Figure 179 shows the average value of η_E in the high speed region as a function of oil flow Q for #30BNT. From Figure 179, η_E (%) and oil flow Q (kg/min) are related by

$$\eta_E = 83Q^{-0.15} \quad (91)$$

This agrees with Equation (14) for #6206 (outer-race-riding cage).

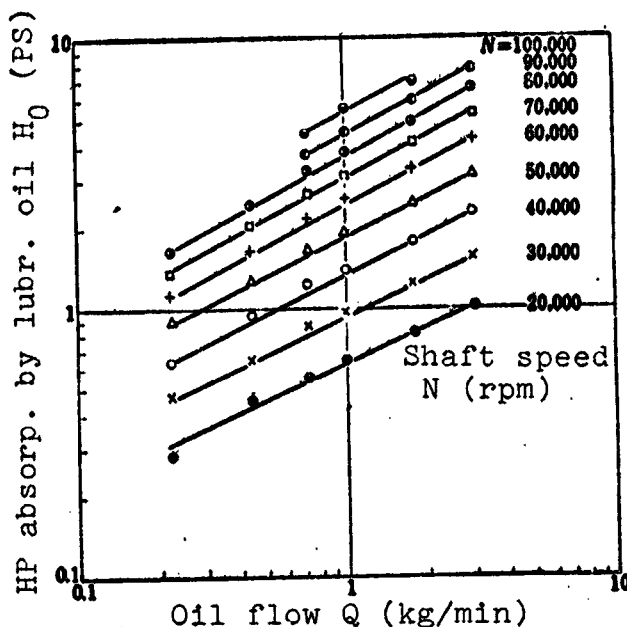


Figure 178. Horsepower absorption by oil versus oil flow

/110

TABLE 16. HEAT EXCHANGE EFFICIENCIES OF OIL η_R , η_P ,
AND η_E AND SHAFT SPEED UNDER VARIOUS OIL
FLOW RATES
(30° C inlet oil temperature and 50 kg thrust load)

Shaft speed rpm	η_R %					
	Oil flow rate					kg/min
	3	1.8	1	0.72	0.44	0.22
20,000	82.4	86.3	93.1	94.6	97.7	96.4
30,000	77	82.3	86.7	94.6	94.0	93.3
40,000	73.6	82.6	85.6	93.5	94.7	93.5
50,000	67.9	76.7	85.6	92.1	91.9	93.4
60,000	63.5	73.3	81.3	91.4	88.1	90.7
70,000	62.5	69.6	74.2	84.8	81.1	90.3
75,000						90
80,000	62.5	65.7	69.2	79.2	78.7	90.1
85,000					78.6	
90,000	59.8	64.1	66.8	74.0		
97,000	58.4					
100,000		62.2	69.1	73.0		

Shaft speed rpm	η_P %					
	Oil flow rate					kg/min
	3	1.8	1	0.72	0.44	0.22
20,000	82.4	81.8	86.2	94.6	93.3	94.6
30,000	84.6	82.3	86.7	94.6	91.0	96.6
40,000	89.5	93.5	96.8	93.5	95.8	97.5
50,000	100	101.5	104.8	99	104	101.3
60,000	104	109.3	111.5	106.3	105.4	104.5
70,000	107.3	111.5	111	109	107	104.5
75,000						104.7
80,000	110	115	113.3	110.6	107	104.9
85,000					107	
90,000	110.7	117	111.7	110.6		
97,000	111.5					
100,000		116.2	112.6	110.6		

(Table continued on following page)

TABLE 15 (CONTINUED)

Shaft speed rpm	PS				%	
	Oil flow rate				kg/min	
	3	1.6	1	0.72	0.44	0.22
20,000	82.4	83.1	88.6	94.6	95.2	95.5
30,000	81.5	82.3	86.7	94.6	92.5	95.0
40,000	81.6	88.2	90.7	93.5	95.2	95.5
50,000	81.4	87.8	93.4	95.3	97.2	97.2
60,000	78.6	87.8	92.6	97.6	94.8	96.1
70,000	76.6	84.4	87.0	94.5	90.7	95.2
75,000						94.8
80,000	75.7	81.7	83.8	91.5	88.8	94.9
85,000					87.5	
90,000	72.2	80.0	81.1	87.6		
97,000	71					
100,000		78	81.8	86.8		

The cooling by oil is thus identical for #30BNT and #6206 (outer-race-riding cage), and the bearing temperature rise is also nearly equal. As mentioned before, the wide difference in the limiting dn value of these two must then be due to the different cage construction technique.

7.9. Bearing Friction

Figure 180 shows the friction torque as a function of speed for various oil flows, from the experimental data in Table 14. Figure 181 shows the friction power loss obtained from the friction torque as a function of speed. The magnitude of each for up to 80,000 rpm is about the same as for #6206 (outer-race-riding cage). In Figure 181, with an oil flow of 3 kg/min, the friction power loss in the neighborhood of 100,000 rpm speed almost reaches 6 PS, indicating how much horsepower is consumed at high speed.

Oil heat exch. effic. η_E (%)

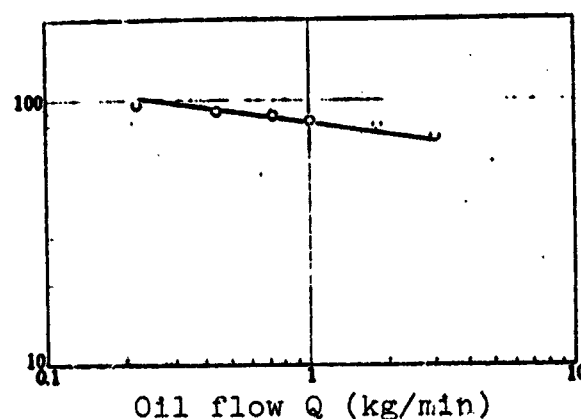


Figure 179. Heat exchange efficiency of oil versus oil flow

/111

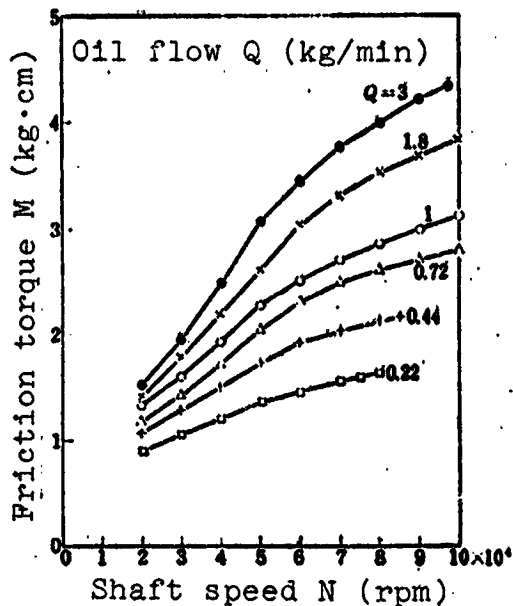


Figure 180. Friction torque versus shaft speed

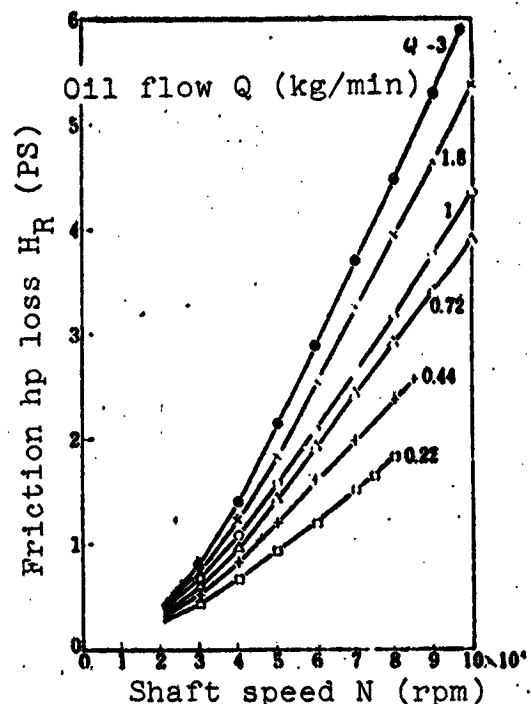


Figure 181. Friction horsepower loss versus shaft speed

When inlet oil temperature is varied from 30° C to 120° C, the relation between the friction torque M and the oil viscosity at the bearing temperature Z_B , shaft speed N , and oil flow Q in the high speed region can be approximated by

$$M \propto Z_B^{0.4} N^{1.2} Q^{0.35} \quad (92)$$

This is roughly the same as for #6206 (outer-race-riding cage). For an outer-race-riding cage, just as for an inner-race-riding cage, the friction torque is governed by nearly the same equation, independent of the bearing type. The friction torque is thus determined by the cage guide type.

Figure 182 is a result of correlating with Equation (92) the viscosity at the bearing temperature Z_B for each point in Figure 180. It is clear that from 20,000 rpm to 100,000 rpm, the friction torque can be expressed by Equation (92). Figure 183 shows the similarly

/113

correlated result under the various thrust loads. Since the non-velocity term M_p of friction torque becomes, from Figure 184,

$$M_p \propto P^{0.5} \quad (93)$$

the friction torque M (kg · cm) can be expressed as

$$M = 7 \times 10^{-3} P^{0.5} + 8.5 \times 10^{-7} Z_B^{0.4} N^{2.3} Q^{0.25} \quad (94)$$

where P is in kg, Z_B in cP, N in rpm, and Q in kg/min.

The bearing friction power loss H_B (PS) is from Equation (95)

$$H_B = 9.8 \times 10^{-7} P^{0.5} N + 1.2 \times 10^{-11} Z_B^{0.4} N^{2.3} Q^{0.25} \quad (95)$$

7.10. Equation for Estimating Bearing Temperature Rise

Although the equation for the bearing temperature rise can be obtained by assuming all friction power loss in Equation (95) is removed by oil, it can be obtained, as in the previous chapter, from the approximation formula for the friction power loss. Figure 185 is a result of correlating

Equation (95) for the friction power loss in Figure 181 with $Z_B^{0.4} N^{2.3} Q^{0.25}$, while Figure 186 is a similarly correlated result for various loads. Figure 187 shows the friction power loss as a function of load for $Z_B^{0.4} N^{2.8} Q^{0.25}$ of 1×10^{11} , 2×10^{11} , 3×10^{11} , and 4×10^{11} , obtained from Figure 186. The friction power loss can then be approximated by

$$H_B \propto P^{0.15} \quad (96)$$

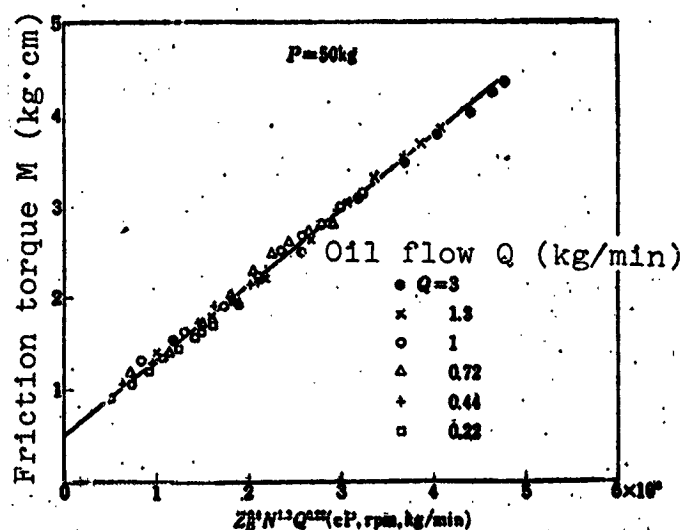


Figure 182. Friction torque, viscosity, shaft speed, and oil flow

where Z_B is in cP, P in kg, N in rpm, and Q in kg/min, just as for Equation (95).

$$H_B = 7.7 \times 10^{-11} Z_B^{0.4} P^{0.11} N^{1.65} Q^{0.45} \quad (97)$$

If the bearing temperature rise is obtained by using the same method as for #6206 (outer-race-riding cage), then from Equations (29) and (30), the following is obtained:

(1) when $T_B - T_I$ is small ($15 - 40^\circ \text{C}$),

$$T_B - T_I = 2.3 \times 10^{-4} Z_B^{0.4} P^{0.11} N^{1.65} Q^{0.45} \quad (98)$$

(2) when $T_B - T_I$ is large ($35 - 120^\circ \text{C}$),

$$T_B - T_I = 2.5 \times 10^{-4} Z_B^{0.4} P^{0.11} N^{1.65} Q^{0.45} \quad (99)$$

The magnitude of exponent of each factor, and the change due to the side of $T_B - T_I$ in Equations (98) and (99) are nearly equivalent to Equation (86), which is the experimental equation for the bearing temperature rise.

Figure 188 is the result of correlating with $Z_B^{0.29} P^{0.11} N^{1.65} Q^{-0.45}$ of Equation (99), which holds in the high speed region or where $T_B - T_I$ is large, the bearing outer race temperature rise and in Figure 173. Although there exists some deviation at the low speed of 20,000 rpm or 30,000 rpm, Equation (99) holds at high speed

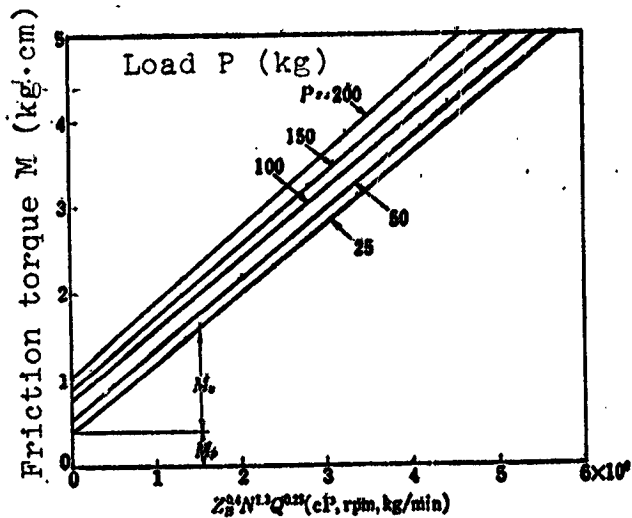


Figure 183. Friction, torque, viscosity, shaft speed, and oil flow under various loads

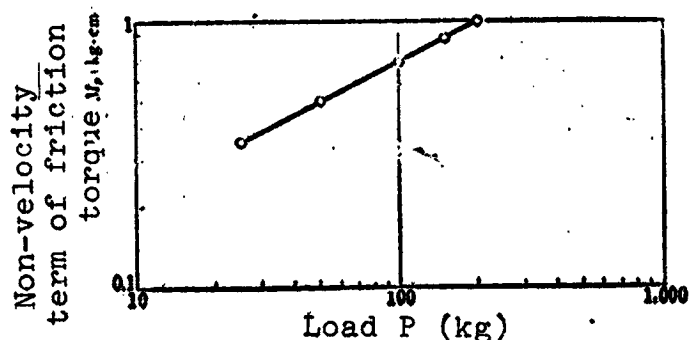


Figure 184. Non-velocity term of friction torque versus load

/115

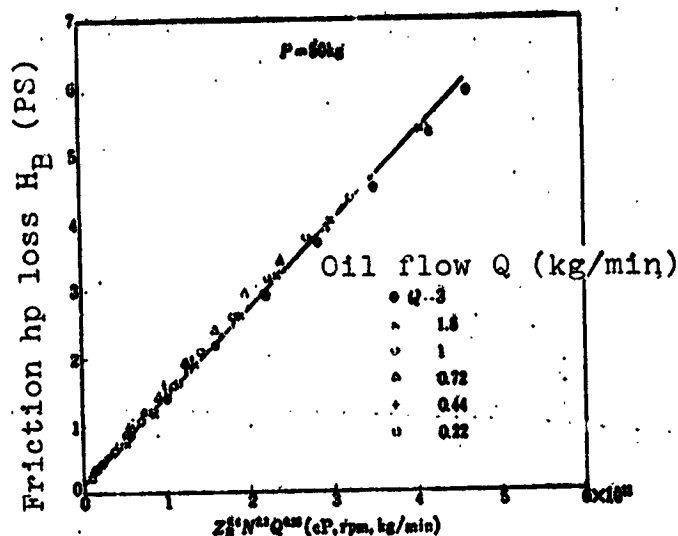


Figure 185. Friction horsepower loss, viscosity, shaft speed, and oil flow

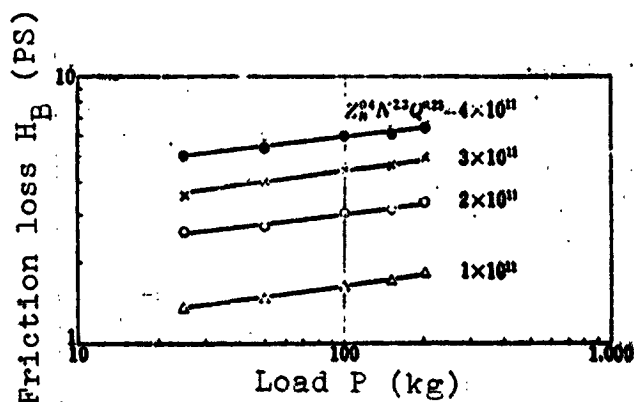


Figure 187. Friction horsepower loss versus load for various conditions

oil temperature from 30° C to 120° C. Equation (99) and the observed data agree very well.

The observed data on the bearing temperature rise agree extremely well with the equation calculated from the friction power loss and the viscous friction law approximately holds for the dn value of up to 300×10^4 . It is important that a certain viscous friction law holds, up to immediately before failure, for the friction of the high

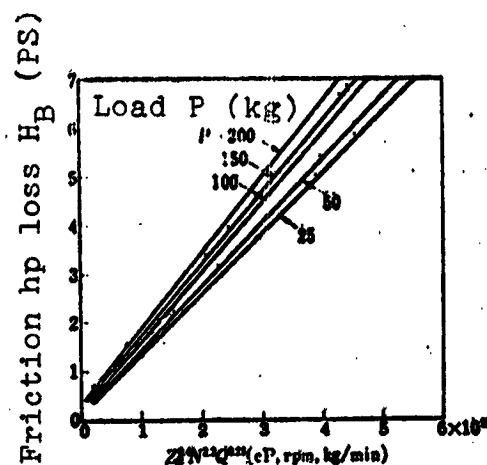


Figure 186. Friction horsepower loss, viscosity shaft speed, and oil flow

of greater than 40,000 rpm. At low speed below 30,000 rpm, it is naturally expected to be governed by Equation (98). Figure 189 is a result of correlating with $Z_I^{0.29} P^{0.11} N^{1.64} Q^{-0.43}$ of Equation (99) /116
the bearing outer race temperature rise $T_B - T_I$ when the speed is varied from 40,000 to 100,000 rpm, oil flow from 0.22 to 3 kg/min, thrust load from 25 - 200 kg, and inlet

speed roller bearing for jet lubrication conditions, despite the severe conditions of high speed and low-viscosity with the dn value of 300×10^4 .

7.11. Conclusions for Chapter 7

The major conclusions on the limiting speed and the bearing performance of the angular contact ball bearing #30BNT are as follows:

(1) With both the deep-groove ball bearing #6206 and the angular contact ball bearing #17206, the failure occurred in the neighborhood of 285×10^4 and 225×10^4 , respectively, and the dn value never reached 300×10^4 , even when the oil flow was increased. On the other hand, with #30BNT, the failure occurs at 83,000 rpm for oil flow of 0.22 kg/min, and at 90,000 rpm for 0.44 kg/min, but above 0.72 kg/min oil flow, the failure did not occur at the dn value of 300×10^4 and the 100,000 rpm speed. This type of bearing is most suitable for high speed operations, because

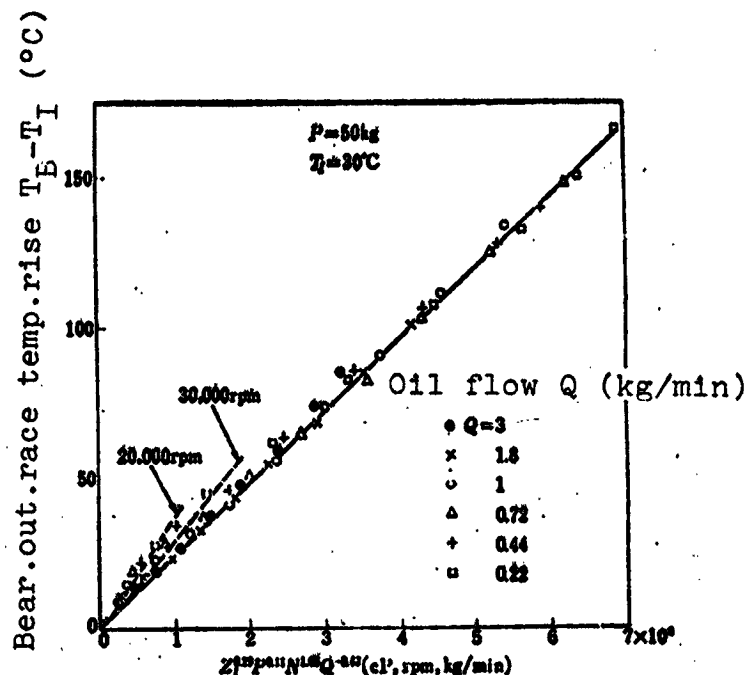


Figure 188. Bearing temperature rise, viscosity, load, shaft speed, and oil flow

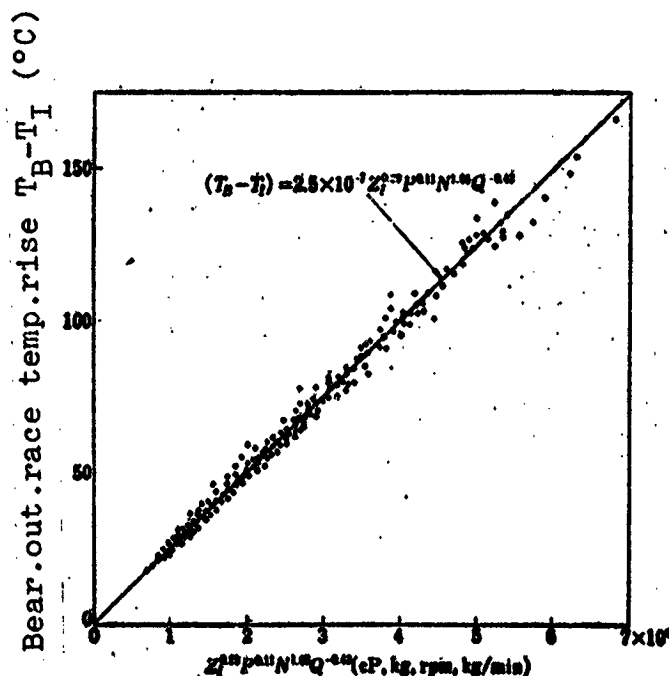


Figure 189. Bearing temperature, viscosity, load, shaft speed, and oil flow

of an outer-race-riding cage and an improved manufacturing precision and large mechanical strength, due to one-piece construction.

(2) Aside from the limiting dn value, the bearing performances of #6206 (outer-race-riding cage) and #30BNT are quite similar. This is because both are of the outer-race-riding cage type, and the bearing performance is roughly determined by the cage guide type.

(3) The temperature rise from the inlet oil temperature T_I to the bearing outer race temperature T_B in the region of up to 300×10^4 dn value can be approximated by

$$(T_B - T_I) \propto Z_I^{0.25-0.4} P^{0.1-0.15} N^{1.4-1.7} Q^{-0.25-0.3}$$

where Z_I is the oil viscosity at an inlet oil temperature, P is thrust load, N is speed, and Q is oil flow. Each smaller exponent corresponds to the larger value of $T_B - T_I$.

(4) The horsepower absorption by lubrication oil H_0 can be approximated by

$$H_0 \propto Z_I^{0.25-0.35} P^{0.1-0.15} N^{1.4-1.7} Q^{0.25-0.3}$$

The smaller exponents of Z_I , P , and N , and the larger exponent of Q , correspond to the larger value of $T_B - T_I$.

The heat exchange efficiency of lubricating oil η_E can be expressed as a function of oil flow Q (kg/min) as

$$\eta_E = 83(Q)^{-0.15}$$

(5) The bearing friction in the region of up to the 300×10^4 dn value consists of viscous friction, on the whole. The friction torque M (kg · cm) and the friction horsepower loss H_B (PS) can be approximated by

$$\begin{aligned} M &= 7 \times 10^{-3} P^{0.1} + 8.5 \times 10^{-3} Z_B^{0.4} N^{1.4} Q^{0.25} \\ H_B &= 9.8 \times 10^{-3} P^{0.1} N + 1.2 \times 10^{-11} Z_B^{0.4} N^{1.4} Q^{0.25} \end{aligned}$$

where Z_B is the oil viscosity in cP at the bearing temperature, P is in kg, N in rpm, and Q in kg/min.

(6) Assuming the entire frictional heat is removed by oil, the bearing temperature rise can be obtained from the experimental formula for the friction power loss as

$$T_B - T_I = 2.5 \times 10^{-4} Z_I^{0.8} P^{0.8} N^{0.8} Q^{-0.8}$$

where Z_I is in cP, P in kg, N in rpm, and Q in kg/min. This estimating equation for the bearing temperature rise agrees very well with the observed data.

CHAPTER 8. SUMMARY

The major conclusions from the experiments conducted to study the limiting speed and the bearing performance of the deep-groove ball bearing #6206 and the angular contact ball bearings #17206 and #30BNT are as follows.

(1) There exist two dominant factors affecting the speed limit of roller bearings. One is the limit in lubrication; in other words, the limit imposed by the failure caused by the piercing of a lubricant film. The other is the strength limit brought about by the shortening of expected life by the centrifugal load of the roller body and the mechanical strength of the cage. From experiment, it was found that bearing failure at high speed always occurred at the sliding friction portions of the race riding surface of the cage at the side opposite the nozzle. Thus, it becomes clear that cage lubrication is the factor which determines the limiting speed today.

(2) The relation between the limiting dn value and oil flow for each bearing type is summarized in Table 17. As the problem at high speed is that of the cage lubrication, the cage guide type, configuration, and material greatly influence the limiting dn value.

As is obvious from Table 17, an outer-race-riding cage is more suitable at high speed than an inner-race-riding cage. Even though both are of the outer-race-riding cage type, the limiting dn value

TABLE 17. LIMITING dn VALUE AND OIL FLOW FOR EACH BEARING TYPE

Oil flow, kg/min	Limiting dn value (mm x rpm)			
	Bearing type			
	#5206 (outer-race-riding cage)	#6206 (inner-race-riding cage)	#17206 (inner-race-riding cage)	#30BNT (outer-race-riding cage)
0.22	310 x 10 ⁴	165 x 10 ⁴	195 x 10 ⁴	310 x 10 ⁴
0.44	240	165	195	270
0.72	270	165	210	300 and above
1	285	165	225	300 and above
1.8	285	165	225	300 and above
3	285	165	225	300 and above

of #30BNT is substantially greater than that of #6206, showing no failure at the dn value of 300×10^4 with an oil flow of 0.72 kg/min, or more. This is because #5206 cage is of the rivet assembly type, whereas #30BNT cage is the one-piece machined type which has high precision and greater mechanical strength. Consequently, #30BNT is best suited for high speed applications.

An inner-race-riding cage is disadvantageous for high speed applications because oil has difficulty reaching the race riding surface of the cage at the side opposite the nozzle, which is most susceptible to failure. Therefore, it is necessary to consider the configuration which easily feeds oil to the race riding surface of the cage and the material possessing the greater resistance to abrasion and failure. For example, the reason for the higher limiting dn value of #17206 than #6206 in Table 17, even though both are of the inner-race-riding cage type, is that the latter uses high-strength yellow brass as the cage material, whereas the former uses phenolic resin, which has a superior wear resistance as cage material. With an inner race-riding cage, it is possible to considerably increase the limiting dn value by setting up two nozzles 180° apart

/117

facing each other, thereby providing oil to the race riding surface of the cage most vulnerable to failure.

(3) The temperature rise $T_B - T_I$ from the inlet oil temperature T_I to the bearing outer race temperature T_B in the region of up to the limiting speed is shown in Table 18 as a function of the oil viscosity at the inlet oil temperature Z_I , thrust load P , shaft speed N ,

TABLE 18. $(T_B - T_I) \propto Z_I^a P^b N^c Q^d$.

Bearing type	a	b	c	d
#6206 (outer-race-riding cage)	0.25~0.5	0.13~0.17	1.44~1.7	0.41~0.55
#6206 (inner-race-riding cage)	0.4~0.5	0.22~0.3	1.3~1.55	0.39~0.55
#17206 (inner-race-riding cage)	0.3~0.5	0.18~0.22	1.0~1.35	0.41~0.57
#30BNT (outer-race-riding cage)	0.25~0.4	0.1~0.15	1.4~1.72	0.37~0.5

and oil flow Q for each bearing type. The smaller exponent of each factor corresponds to the larger value of $T_B - T_I$. Z_I is within the range of 1.5 - 11 cP, P within 25 - 200 kg, and Q within 0.22 - 3 kg/min.

The exponents of Z_I , P , and Q are all similar, an exponent of N for an outer-race-riding cage is greater than for an inner-race-riding cage.

(4) The horsepower absorption by oil H_0 is shown in Table 19 as a function of Z_I , P , N , and Q for each type of bearing. The smaller exponents of Z_I , P , and N , and the larger exponent of Q , correspond to the larger value of $T_B - T_I$. Compared to Table 18, which is an equation for the bearing outer race temperature rise,

Table 19. $H_f \propto Z_I^a P^b N^c Q^d$.

Bearing type	a	b	c	d
#6206 (outer-race-riding cage)	0.24~0.4	0.12~0.18	1.43~1.68	0.47~0.39
#6206 (inner-race-riding cage)	0.35~0.45	0.22~0.3	1.2~1.4	0.44~0.34
#17206 (inner-race-riding cage)	0.3~0.5	0.18~0.25	1.1~1.47	0.36~0.28
#30BNT (outer-race-riding cage)	0.2~0.35	0.1~0.15	1.26~1.45	0.54~0.45

the exponents of Z_I , P , and N are all similar, but the sign of the exponent of Q is reversed and the smaller exponent of Q in the bearing temperature rise, and the larger exponent of Q in the horsepower absorption by oil, correspond to the larger value of $T_B - T_I$, indicating that under jet lubrication almost all of frictional heat generated is carried away by oil. /118

(5) The heat exchange efficiency of lubrication oil η_E (%) as a function of oil flow Q (kg/min) for each bearing type is shown in Table 20. η_E decreases with an increasing oil flow because the percentage of oil flow performing an effective heat exchange by actually getting in contact with the bearing surface decreases when the oil

TABLE 20. HEAT EXCHANGE EFFICIENCY OF OIL η_E

Bearing type	η_E (%)
#6206 (outer-race-riding cage)	$82Q^{-0.15}$
#6206 (inner-race-riding cage)	$70Q^{-0.15}$
#17206 (inner-race-riding cage)	$68Q^{-0.15}$
#30BNT (outer-race-riding cage)	$92Q^{-0.15}$

Q : kg/min

supply is large. In Table 20, η_E is greater for an outer-race-riding cage than for an inner-race-riding cage, due to the greater penetration ratio of an outer-race-riding cage. Consequently, from the standpoint of the cooling of the bearing also, an outer-race-riding cage is superior to an inner-race-riding cage.

Although the bearing outer race temperature rise becomes lower with an increasing η_E , the magnitude of η_E is not necessarily related to the limiting speed, the failure occurring on the race riding surface of the cage at high speed. For example, there are cases in which, even if η_E is increased by changing the nozzle position in an inner-race-riding cage, the limiting speed goes down. Therefore, at high speed, the penetration ratio should be enlarged to increase the heat exchange efficiency of oil and, at the same time, oil should be effectively supplied to the race riding surface of the cage at the size opposite the nozzle, which is most susceptible to failure, so as to reduce the bearing temperature and increase the limiting speed.

(6) Rather than simply being proportional to the product $Z_B N$ of oil viscosity at the bearing temperature Z_B and shaft speed N , as has been considered traditionally, the friction of the roller bearing at high dn values is expressed as a function of Z_B , N , and Q , with certain exponents. Table 21 gives a summary of the experimental equations for the bearing friction torque for each type of bearing. The friction torque formula is approximately determined by the cage guide type. The exponents of P and Z_B are all similar, but the exponent of N is greater for an outer-race-riding cage than for an inner-race-riding cage. As an effect of Q is caused by the churning resistance of oil inside the bearing, the exponent of Q is large when the penetration ratio is large and sufficient churning occurs inside the bearing. The fact that a certain viscous friction law still holds under such a severe high-speed, low-viscosity condition is important.

TABLE 21. EXPERIMENTAL EQUATIONS FOR FRICTION TORQUE

Bearing type	Friction torque M (kg · cm)
#6206 (outer-race-riding cage)	$7 \times 10^{-3} P^{0.6} + 2.5 \times 10^{-6} Z_B^{0.4} N^{0.4} Q^{0.3}$
#6206 (inner-race-riding cage)	$2.3 \times 10^{-3} P^{0.7} + 10^{-6} Z_B^{0.3} N^{0.4} Q^{0.3}$
#17206 (inner-race-riding cage)	$7.2 \times 10^{-3} P^{0.5} + 8.5 \times 10^{-6} Z_B^{0.4} N^{0.4} Q^{0.3}$
#30BNT (outer-race-riding cage)	$7 \times 10^{-3} P^{0.6} + 8.5 \times 10^{-6} Z_B^{0.4} N^{0.4} Q^{0.3}$

Z_B : cP; P: kg; N: rpm; Q: kg/min

As is clear from Table 21, the velocity term of the friction torque becomes extremely large compared to the non-velocity term at high speed. A large influence of shaft speed and an extremely small influence of load on the bearing outer race temperature rise are also caused by this.

(7) If all friction heat is assumed to be removed by oil, the bearing temperature rise can be obtained from the experimental equation for the friction torque. The estimating equations for the bearing temperature rise at the high speed region thus obtained are shown in Table 22. This estimating equation for the bearing temperature rise agrees extremely well with the observed data on the bearing outer race temperature rise under various conditions.

/119

TABLE 22. ESTIMATING EQUATIONS FOR BEARING TEMPERATURE RISE

Bearing type	Bearing temperature rise, $T_B - T_I$ (°C)
#6206 (outer-race-riding cage)	$5.2 \times 10^{-7} Z_I^{0.3} P^{0.5} N^{0.4} Q^{-0.3}$
#6206 (inner-race-riding cage)	$1.8 \times 10^{-6} Z_I^{0.3} P^{0.5} N^{0.4} Q^{-0.3}$
#17206 (inner-race-riding cage)	$1.8 \times 10^{-6} Z_I^{0.3} P^{0.5} N^{0.4} Q^{-0.3}$
#30BNT (outer-race-riding cage)	$2.5 \times 10^{-7} Z_I^{0.3} P^{0.5} N^{0.4} Q^{-0.3}$

Z_I : cP; P: kg; N: rpm; Q: kg/min

Our study has investigated the limiting dn value and the bearing performance of ball bearings with an inside diameter of 30 mm, but it is naturally expected that if the type and the number of the bearing differ, then the results would be different. We would like to further study this area in the future.

In concluding, we extend our deep gratitude to Professor N. Soda of the National Aerospace Laboratory of the University of Tokyo who has guided us in this study. Thanks are also due to the members of the National Aerospace Laboratory, M. Nishimura, K. Usui (now with Marine Research Institute), and T. Hatano (now with Shimada Rikakogyo, Inc.). H. Fujii and M. Takahashi of Fujikoshi, Inc., have contributed greatly to the manufacture of the high speed roller bearing test equipment and the test bearing.

References

1. Soda, N. On the dn Value of Roller Bearings. Kikai no kenkyu, Vol 3, No. 9, 1951, p. 504.
2. Macks, E. F. and Z. N. Nemeth. Lubrication and Cooling Studies of Cylindrical-Roller Bearings at High Speeds. NACA, Report 1064, 1952, p. 143.
3. Anderson, W. J., E. F. Macks and Z. N. Nemeth. Comparison of Performance of Experimental and Conventional Cage Designs and Materials for 75-Millimeter-Bore Cylindrical Roller Bearings at High Speeds. NACA, Report 1177, 1954, p. 1.
4. Soda, N. G. Miyahara and A. Yanagisawa. Study on High-Speed Roller Bearings (First Report). 33rd General Meeting of Nippon Kikai Gakukai, p. 15.
5. Noto, T. Lubrication Characteristics of High Speed Ball Bearings. Bearing Engineer, Vol. 1, No. 1, 1950, p. 8.
6. Hirano, F. Experiments on High-Speed Bearings at NACA. Bearing Engineer, Vol. 4, No. 3, 1954, p. 476.
7. Hirano, F., E. Ohta and T. Fujii. On the Lubrication of Roller Bearings by Nozzle Feeding (First and Second Reports). Nippon kikai gakukai ronbunshi, Vol. 21, No. 102, 1955, pp. 113, 119.

8. Soda, N. Bearing. Iwanami Zensho, 1964, p. 234.
9. Yamada, K. and E. Ohta. Jet Lubrication of High-Speed Cylindrical Roller Bearings. Bearing Engineer, Vol. 8, No. 2, 1959, p. 41.
10. Wilcock, D. F. Turbulence in High-Speed Journal Bearings. Trans. ASME, Vol. 72, No. 6, 1950, p. 825.

Translated for National Aeronautics and Space Administration under contract No. NASw 2483, by SCITRAN, P. O. Box 5456, Santa Barbara, California, 93108